MILD GASIFICATION OF COAL IN A MOVING BED REACTOR

Muthu S. Sundaram*, Peter T. Fallon and Meyer Steinberg
Process Sciences Division
Brookhaven National Laboratory
Upton, New York 11973, U.S.A.

ABSTRACT

The Brookhaven National Laboratory (BNL) tubular moving-bed reactor was used to perform gasification experiments with Wellmore Kentucky No. 8 bituminous coal under mild reaction conditions at two levels of the process variables: temperatures of 550° and 650°C, coal particles residence times of 0.1 min. and 2 min.; and lime addition of 0% and 10% of the coal fed, with inert N_2 as the sweep gas. Using a fractional factorial statistical design, the interactive effects of process variables were evaluated. The highest total hydrocarbon yield of 22.6% (MAF) was obtained at 650°C and 2 min. coal residence time in the presence of 10% lime additive. The gaseous hydrocarbon yield added only another 0.8% to the total hydrocarbon yield under the above conditions.

The effect of coal residence time on total hydrocarbon yield was significant only at the higher temperature level of 650°C and in the presence of the lime additive. In general, increase in residence time, other conditions being equal, tends to decrease the retention of sulfur in char. The presence of lime in the feed had a beneficial effect on the retention of sulfur in the char only at low residence times.

INTRODUCTION

A large body of literature exists on the effects of process variables on product yields from pyrolysis and gasification of coal at high temperatures, often in the range of 900° to 1000°C. However, the independent and interactive influence of factors affecting the mild gasification behavior of coals has not been studied in a systematic manner. Mild gasification is defined as devolatilization at temperatures up to 700°C, and at low pressures, less than 50 psi. The idea is to produce condensible hydrocarbon fuel from coal in a low cost process under mild reaction conditions and use the char for boiler fuel. The effects of temperature, coal particle residence time and lime additive on the yields of products from the mild gasification of Wellmore Kentucky No. 8 bituminous coal are presented herein.

EXPERIMENTAL

Figure 1 shows a schematic of the experimental reactor which consists of two sections. The top section ia a 1-in. I.D. x 11-ft long entrained tubular reactor and the bottom is a 4-in. I.D. x 6-in. long moving bed reactor. The top section can be used under two separate sets of conditions; (1) to obtain short coal particle residence times in the order of a few seconds and (2) to preheat the coal particles to various temperatures for feeding into the moving

bed reactor. A motor-driven vaned agitator keeps the coal moving through the moving bed reactor and empties the char into an unheated collection vessel below. The product gas lines are located between the reactor and liquid condensers in a manner so as to prevent tar accumulation in the ports and the transfer lines. A liquid vythene scrubber is used to scrub the gases to collect any trace hydrocarbon carryover.

An on-line process gas chromatograph is used to measure all the light gases and hydrocarbon products. The condensible liquid products and the char are collected separately. From the elemental analyses of all the products, a complete mass balance is obtained.

The reported experimental yields of coproducts include five categories of hydrocarbons: (1) benzene-toluene-xylene (BTX), (2) hydrocarbon (HC) liquids which consist of all HC liquids heavier than BTX including oxygenates and tars, (3) total liquid HC condensibles, which is the sum of BTX and HC liquids, (4) gaseous HCs mainly CH_4, C_2H_6, and C_2H_4 (CO and CO_2 are analyzed and reported separately, and H_2 and H_2O are determined by difference), and (5) total HCs which is the sum of all liquid and gaseous hydrocarbons. The char collected consists of all the solid non-volatile residue containing no benzene extractable liquids.

RESULTS AND DISCUSSION

A total of eight experimental runs were performed using Wellmore Kentucky No. 8 bituminous coal. The experimental conditions and the yields of the products are shown in Table 1.

In a conventional approach, the value of one process variable is changed at a time, thereby estimating its influence at constant conditions for other variables. This, however, assumes that there is no interaction between the variables. This has a potential of leading to erroneous conclusions. The data in Table 1, on the other hand, provides information on the interactive effects of temperature, residence time and lime addition on the product yields in which more than one variable is changed at a time. In other words, the influence of all variables are estimated throughout the range of each and every variable.

The experimental yields were correlated in accordance with a fractional factorial statistical method. The data from Table 1 can be clearly shown in a three-dimensional box representation in which the interactive effect of all three variables can be represented simultaneously along the three axes of the cube. This is superior to the conventional bivariate plots.

Figure 2 shows the yield of total hydrocarbon products as a function of temperature, residence time and percent lime addition. The circled data are the experimental values at a given condition rounded off to the nearest whole number and the number in parenthesis represents the corners of the cube. The numerical differences in yields at two different conditions are also shown in the figure along the axes with an appropriate sign.

The highest total hydrocarbon products yield was 23.4% (MAF), and it occurred at 650°C in the presence of 10% lime at a 2 min. residence time. At a given residence time, the incremental yield of total hydrocarbon products remained virtually the same at all levels of lime addition tested so far. For example, at all residence times, the total hydrocarbon yield increased by 17 percentage points as a result of an increase in temperature from 550° to 650°C, with 10% lime. Similar effects were noticed when no lime was added to the feed, however, the actual incremental yield is almost halved (17% vs. 9-10%) when compared with the data with 10% lime.

At a given temperature, the effect of residence time and lime addition on total hydrocarbon yield is complex. At 550°C, there is a decrease of 4 percentage points, from 0.1 min. to 2 min. residence in the absence of lime, whereas with 10% lime additive, there is no change in the yield at all. On the other hand, at 650°C, and with 10% lime, there is a marked increase in the total hydrocarbon yield with increase in residence time (8% points).

At higher residence times, there is a slight increase in the yield (3% points) when 10% lime is added (3% vs. 6% at 550°C and 20% vs. 23% at 650°C). At 0.1 min., under identical conditions, a small decrease is seen (7% vs. 6% at 550°C and 17% vs. 15% at 650°C), which corresponds to no change when experimental error is taken into consideration.

The estimates of the individual and interactive effects of the variables can be made via Yate's algorithm, the details of which are available [1,2]. The confounding pattern and Yate's algorithm for the production of total hydrocarbons is shown in Table 2. Figure 3 is a normal probability plot of the estimated effects in Table 2.

Even though the temperature seems to be apparently more effective than any other variable, it should be noted that the observed results can not be explained on the basis of temperature alone. An interactive effect involving the variables, temperature and lime addition, seems to be more significant. At a higher temperature, reactions requiring higher activation energies, which would not otherwise occur at a lower reaction temperature, become more probable. The removal of primary tar via secondary cracking reactions on the surface of the added lime to produce lighter hydrocarbons seems to be favored by an increase in residence time which explains a higher incremental yield of 8 percentage points from 15% (at 650°C, 0.1 min., 10% lime) to 23% (at 650°C, 2 min., 10% lime). This is in agreement with earlier reports on the catalytic effect of inorganic materials on the decomposition of primary tar [3].

The variation in total hydrocarbon condensible product yield with temperature, residence time and lime addition is shown in Figure 4. The effect of the process variables on the liquid hydrocarbon yield is similar to that on the total hydrocarbon (liquid and gas) yield. The yield of gaseous hydrocarbons is much smaller than the liquid hydrocarbon yield. No detectable hydrocarbon or other gases were produced at 550°C. The highest observed gas yield

was 1% at 650°C and 0.1 min. residence time. This indicates that the experimental conditions are much more favorable for the production of liquid hydrocarbons.

At 550°C, the BTX yield was constant at 1.6% MAF and was not affected by residence time or lime additive (Figure 5). At 650°C, the BTX yield varied between 3.1% and 4.4% depending on other conditions. At 650°C, addition of lime increased the BTX yield by 0.4 percentage points both at 0.1 min. and 2 min. residence times; at the same temperature, increase in residence time caused an increase in BTX yield of 0.9 percentage points, both with no lime and with 10% lime addition. From this, it can be inferred that the BTX yield is influenced by an interactive effect involving the variables, temperature and residence time.

From an elemental analysis of the hydrocarbon liquids, the hydrogen to carbon ratio was calculated. The H/C ratio varied between 0.85 to 1.08 (Figure 6). In general, at 550°C, the H/C ratio of the liquid was close to unity (average of 1.03) and at 650°C, the H/C was slightly less than unity (average of 0.93). At 650°C, either addition of lime or increasing the residence time, increased the H/C ratio of the liquid product.

The primary purpose of the addition of lime to the coal feed was to increase the retention of sulfur in the solid residue. The sulfur content of the char was determined via elemental analysis. From a knowledge of the sulfur material balance, the percentage of the sulfur in the feed coal that remained in the char was calculated. The results are pictorially represented in Figure 7 as before. The presence of lime in the feed had a significant effect on the retention of sulfur in the char only at low residence times. For example, at 0.1 min., addition of 10% lime to the feed increased sulfur retention in the char by 12 to 14 percentage points. In general, temperature has slight negative affects and an increase in residence time, other conditions being equal, tends to decrease the retention of sulfur in char. As much as 91% of the original sulfur was retained in the char at 550°C, 0.1 min. residence time and in the presence of lime. However, it should be remembered that the total hydrocarbon yield under these conditions was low at 6.4% (MAF). At conditions of maximum hydrocarbon production (22.6%), sulfur retention in the char was only 79%.

CONCLUSIONS

A summary of the conclusions for the effect of process variables on the Wellmore Kentucky No. 8 coal are as follows:

- The highest total condensible hydrocarbon yield of 22.6% (MAF) was obtained at 650°C and 2 min. coal residence time in the presence of 10% lime additive. The gaseous HC yield adds only another 0.8% to the total HC yield.

- Even though the absolute yields were different, the trend in the total condensible hydrocarbon yield was similar at both residence times of 0.1 and 2 min. For example, at the lower residence time of 0.1 min., increasing the temperature from 550° to 650°C resulted in an 8 to 10 percentage points increase in the hydrocarbon condensible yield, both with and without the lime additive. At the higher residence time of 2 min., the increase in the yield was 16 percentage points, all other conditions remaining the same.

- The effect of coal residence time on total hydrocarbon yield was significant only at the higher (650°C) temperature level and in the presence of the lime additive. For example, at 650°C and in the presence of lime, there was an increase of 8 percentage points in absolute yield which amounts to about a 55% increase in the relative yield (14% MAF to 22% MAF).

- The presence of lime in the feed had a beneficial effect on the retention of sulfur in the char only at low residence times. In general, an increase in residence time, other conditions being equal, tends to decrease the retention of sulfur in char.

- As much as 91% of the original sulfur was retained in the char at 550°C, 0.1 min residence time and in the presence of lime; however, the total HC yield under these conditions was low at 6.4% (MAF). At conditions of maximum condensible hydrocarbon production (22.6%), sulfur retention in the char was only 79%.

- The H/C ratio of the total hydrocarbon condensibles is found to be close to unity (1.0). This indicates the highly aromatic composition of the condensibles.

REFERENCES

1. Sundaram, M. S., Fallon, P. T., and Steinberg, M. Mild Gasification of Coal - First Quarterly Technical Progress Report for Period October 1 - December 31, 1987, Brookhaven National Laboratory, BNL-41050, Jan. 1988.

2. Box, G. E. P., Hunter, W. G., and Hunter, J. S. Statistics for Experiments. An Introduction to Design, Data Analysis and Model Builders, John Wiley and Sons, New York, NY, 1978.

3. Franklin, H. D., Peters, W. A., and Howard, J. B. ACS Fuel Division Prepr., 26 37 (1981).

Table 1. Experimental Yields of Products from Mild Gasification of Coals.
Effect of Process Variables
N_2 Sweep Gas 15 psig

Run No.	Temp. °C	Res. Time (min)	Additive % lime	BTX	Conversion, Wt% MAF Feed Coal			
					HC liquids	Total HC Cond.	Gas	Total
1042	550	0.1	0	1.6	5.4	7.0	0.0	7.0
1047	650	0.1	0	3.1	13.9	17.0	0.2	17.2
1041	550	2.0	0	1.6	4.8	6.4	0.0	6.4
1043	650	2.0	0	4.0	10.2	14.2	0.9	15.1
1040	550	0.1	10	1.6	1.1	2.7	0.0	2.7
1045	650	0.1	10	3.5	15.3	18.8	1.0	19.8
1044	550	2.0	10	1.6	4.5	6.1	0.0	6.1
1027	650	2.0	10	4.4	18.2	22.6	0.8	23.4

Table 2. Yate's Algorithm for the Production of Total HC from Kentucky No. 8.

Run No.	Yield Wt % Coal Feed	(1)	(2)	(3)	Divisor	Estimate	Effect
1042	7.0	24.2	45.7	97.7	8	12.2	Average
1047	17.2	21.5	52.0	53.3	4	13.3	T
1041	6.4	22.5	18.9	4.3	4	1.1	R
1043	15.1	29.5	34.4	1.3	4	-0.3	TR
1040	2.7	10.2	-2.7	6.3	4	1.6	A
1045	19.8	8.7	7.0	15.5	4	3.9	TA
1044	6.1	17.1	-1.5	9.7	4	2.4	RA
1027	23.4	17.3	0.2	1.7	4	0.4	TRA

T = temperature; R = residence time; A = % lime additive.

(1.9)

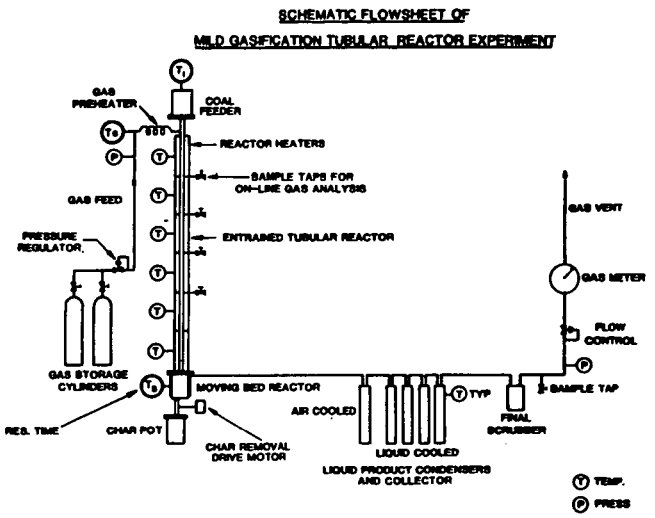

Figure 1. Schematics of Experimental System.

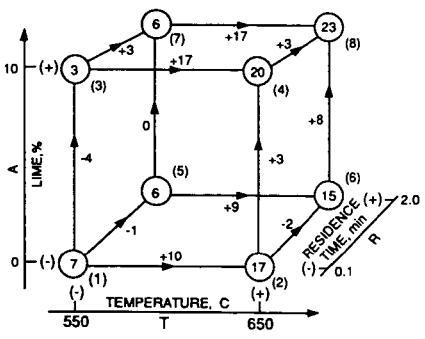

Figure 2. Total Hydrocarbon Yield from Kentucky No. 8 Coal.

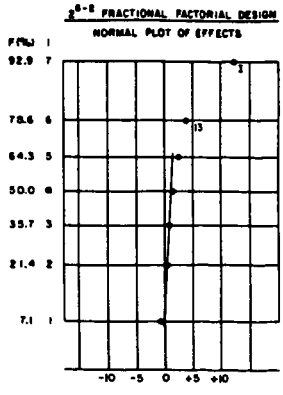

Figure 3. Normal Probability Plot of Total Hydrocarbon Yield Contrasts from Kentucky No. 8 Coal.

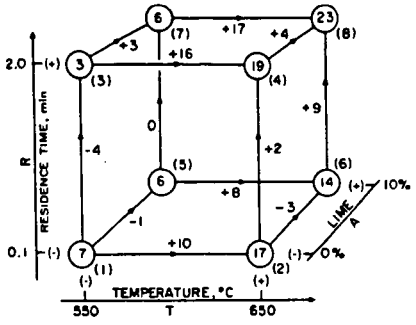

Figure 4. Total Hydrocarbon Condensible Liquid Yield from Kentucky No. 8 Coal.

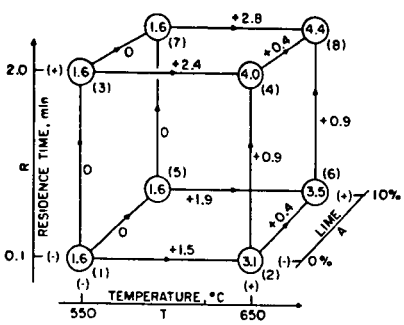

Figure 5. BTX Yield from Kentucky No. 8 Coal.

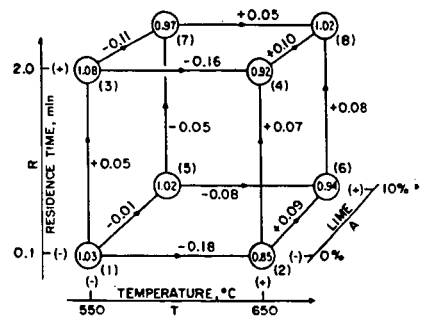

Figure 6. H/C Ratio of Hydrocarbon Liquids from Kentucky No. 8 Coal.

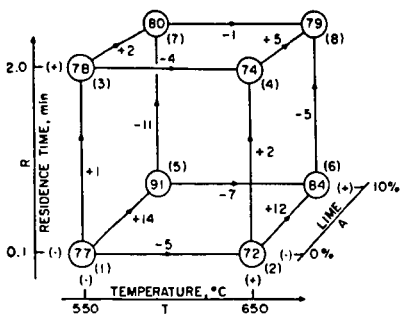

Figure 7. Sulfur Retention in the Char of Kentucky No. 8 Coal.

THE EFFECTS OF MINERALS AND PYROLYSIS CONDITIONS ON CHAR GASIFICATION RATES

M.A. Serio, P.R. Solomon and R. Bassilakis,

Advanced Fuel Research, Inc., 87 Church Street, East Hartford, CT 06108

E.M. Suuberg

Brown University, Box D, Providence, RI 02912

INTRODUCTION

In previous work (1,2), a large set of coals was pyrolyzed under the same conditions, and it was observed that there was a systematic variation in char reactivity with coal rank as indicated by the oxygen content in the raw coal. The current paper extends that study to include the effects of minerals on reactivity differences from these coals. Most of the work concerns reactivity in oxygen, although selected data on reactivity in carbon dioxide are presented.

The previous papers (1-3) have also addressed the effects of pyrolysis conditions (temperature and heating rate) and char physical properties (surface area, resistivity, crystallite size) on char reactivity. The main conclusions were that for low rank coals the reactivity was primarily dependent on the extent of pyrolysis as measured by the char hydrogen (or oxygen) content and relatively independent of the time-temperature history. Based on limited data, it was also noted that the same conclusion with respect to heating rate could not be made for demineralized low rank coals or medium and high rank coals. The current paper revisits the subject of pyrolysis conditions with additional data and also reexamines our previous conclusion that differences in BET surface areas, as measured by CO_2 or N_2 adsorption, are not primarily responsible for large differences in reactivity between chars pyrolyzed under similar conditions.

EXPERIMENTAL

Char Preparation - The chars used in this study were primarily formed from coals in the Argonne premium coal sample bank. The analyses of these coals have been given elsewhere (4). The results for CO_2 reactivity were for coals selected from the Exxon sample bank. These coals are described in Ref. 5. The Argonne samples were 200 x 325 mesh. The Exxon samples were -100 mesh. In addition, a 200 x 325 mesh sample of Zap Indian Head lignite was used for cation loading. The properties of this coal are given in Ref. 1. Chars were prepared at low heating rates (1-200°C/min) by pyrolysis in a Perkin Elmer Model 2 Thermogravimetric Analyzer (TGA) or a Bomem TG/Plus. The TG/Plus couples a Dupont 951 TGA with a Bomem Michelson 100 FT-IR spectrometer (6,7). Chars were prepared at higher heating rates (5000 - 20,000 K/s) in an entrained flow reactor (EFR) or a heated tube reactor (HTR) which have been discussed previously (8).

Coal Modifications - In order to further understand the roles played by the ion-exchangeable cations on char reactivity, a 200 x 325 mesh sieved fraction of Zap Indian Head, demineralized according to the standard Bishop and Ward (9) technique, was subjected to ion-exchange with Ca, Mg, K, and Na using a modification of the procedure by Hengel and Walker (10). The amount ion-exchanged onto the demineralized Zap lignite was controlled by using different molar solutions of the acetate salt. In the case of Ca, 1.5M, 1.0M, 0.5M, 0.3M, 0.1M, and 0.05M acetate salt solutions were employed. In the case of Mg, 1.5M and 0.05M

acetate salt solutions were employed. In the case of K, 1.5M, 0.3M, 0.1M, and 0.04M acetate salt solutions were employed and in the case of Na, 1.5M, 0.3M, 0.1M and 0.05M acetate salt solutions were used. A slurry of 5 grams of demineralized Zap and 125 ml of the desired loading solution was stirred at 57°C for 5 1/2 hours. The solution was allowed to cool to room temperature and stirring was continued for an additional 22 1/2 hours. The slurry was filtered, washed with deionized water and dried at 105°C in a vacuum oven for approximately two hours. The amount of cation exchanged was determined by x-ray analysis.

Reactivity Measurements - Initial char reactivity measurements were made using the isothermal technique developed at Pennsylvania State University (11). In this method, the char is heated in a TGA in nitrogen to the desired temperature, usually 400-500°C. The time for 50% burnoff, $\tau_{0.5}$, is used as the reactivity index. In our char characterization work, we had difficulty applying the isothermal techniques to chars formed over a wide range of conditions. A temperature level selected for one char was inappropriate for another. In order to overcome this difficulty, a non-isothermal technique was developed using a Perkin-Elmer TGA 2 (3). The sample (about 1.5 mg) is heated in air at a rate of 30°C/min until a temperature of 900°C is reached. The TGA records the sample weight continuously and, at the end of the experiment, the weight and derivative are plotted. The temperature (T_{cr}) at which the derivative of the fractional weight loss with respect to time reaches a value of 0.11 wt. fraction/min was chosen as an index of reactivity. This was compared with the $\tau_{0.5}$ values measured by the isothermal technique and a good correlation was observed (3). The value of T_{cr} varies inversely with reactivity. Values of relative reactivity can be calculated by using an activation energy of 34.7 kcal/mole for air (3).

Surface Area Determinations - The surface areas reported in this paper have been obtained at Brown University using a Quantasorb instrument, manufactured by Quantachrome, Inc. The sample cell is immersed in liquid N_2 for N_2 adsorption or a dry ice-acetone bath at -78°C, for CO_2 adsorption. Determinations of surface area from the sorption data have been made using classical BET theory; typically three points have been taken at values of (P/P_0) of 0.1, 0.2, and 0.3.

Swelling Measurements - Solvent swelling measurements were made using the techniques developed by Larson and coworkers (12) to determine the crosslink densities of selected coals and chars.

RESULTS AND DISCUSSION

Reactivity vs Rank - A systematic study of the variation of reactivity with coal rank was performed and reported previously for several of the Exxon coals (1,2). Recently, the same study was done for coals from the Argonne premium sample bank. Figure 1 presents a correlation between the reactivity of char produced in the TGA by heating in nitrogen at 30°C/min to 900°C and the daf oxygen content in the parent coal. The open squares are results obtained for raw coals, the solid triangles show the results for demineralized coals. For raw coals there is a decrease in reactivity with increasing rank, as was found previously for the Exxon coals. In the case of the Exxon coals, the reactivity in CO_2 was also studied for chars which were heated at 30°C/min to 1000°C. These data showed similar trends with rank. This was confirmed by plotting the T_{cr} in CO_2 vs the T_{cr} in air, as shown in Fig. 2.

Jenkins et al. (13) compared the reactivities in air at 500°C of chars from 21 US coals of widely ranging rank which had been prepared by heating at 10°C/min to

1000°C and holding for about two hours. These conditions were significantly more severe than those used in the current study. Nevertheless, the observed trend in reactivity with rank was similar. The range of reactivities they observed was a factor of 170. The range of reactivities observed in the current study was a factor of 380. Besides the fact that their coal set was different, the lower spread in reactivities observed by Jenkins et al. (13) was probably due to the fact that the higher pyrolysis severity causes annealing of the organic part of the char and sintering of the catalytic minerals which tend to even out the differences in reactivity. They were also comparing chars which had been oxidized to higher levels of burnoff than in our own measurements which are done at relatively low burnoff level (~10%). This work at Penn State was later continued to study the reactivity of chars toward CO_2 (14) and H_2O (15). The chars were produced in the same way but the reactivity measurements were done at a higher temperature (900°C). In both cases the observed trends in reactivity with rank were similar to those found in air.

Other major studies of the effects of coal rank on char reactivity in steam have been done in Japan by Takarada et al. (16) and Hashimoto et al. (17). These studies covered coals from all over the world so the results were more scattered, especially for the low rank coals, but the trends with rank were similar. The reactivity ranges found were x 46 and x 170, respectively. In both studies the chars were prepared by heating at a relatively high heating rate.

Effects of Minerals on Low Rank Coals - Since it is known that minerals can have a profound effect on reactivity (11,13-17,19-23) it was decided to repeat the reactivity tests on chars formed from demineralized coals. These results are shown as the solid triangles in Fig. 1. While, the trend for the raw samples is an increase in reactivity (decreasing T_{cr}) with increasing coal oxygen content, the slope for the demineralized samples seems to flatten out at approximately 520°C. Above 10% coal oxygen content, the mineral content of the coal dominates the char reactivity, increasing the char's reactivity (lower T_{cr}) compared to the demineralized samples. The reason for this increase appears to be the catalytic activity of the organically bound alkali metals, particularly the Ca since it is naturally abundant in coals. Below 10% oxygen content, the raw coals have a lower reactivity (higher T_{cr}) than the demineralized samples. Possible reasons for this are discussed below.

In order to ascertain why there is a systematic increase in reactivity with coal oxygen content when reactivity is thought to depend on calcium content, the calcium concentration of coals from the Exxon sample bank were plotted as a function of oxygen concentration in Fig. 3. Above 10% oxygen, there is a systematic increase in Ca with increasing oxygen. Ten percent is about the level at which carboxyl groups appear in coal (18). This suggests that, above 10% oxygen content, there is a systematic increase in the amount of calcium ion-exchanged on the carboxyl groups and it is this calcium component which acts as a catalyst. Other researchers have also observed a relationship between calcium content and reactivity (11,13-17,19-23).

Chars were prepared from the cation loaded coals by heating in N_2 at 30°C/min to 900°C and these were subjected to the non-isothermal reactivity test in air. The char from demineralized Zap coal is far less reactive (higher T_{cr}) than the raw Zap char. As discussed above, this is probably due to the removal of the organically bound alkali metals which are thought to dominate char reactivity in coals possessing more than 10% oxygen. If this is true, then cation loading should result in the restoration of char reactivity.

Plotted in Fig. 4 is the variation of reactivity with the cation loadings. The Ca and Mg loadings effectively restored the reactivity of the demineralized Zap. In the case of Ca, the only significant change in reactivity occurs when the Ca level increases from the 0.01 wt% in the raw demineralized Zap to 1.65 wt% in the 0.05M loading. Further increases in Ca do not cause any marked increases in reactivity. The low Na and K loadings were so effective in promoting the demineralized Zap char reactivity that the loaded samples yielded values of T_{cr} that were 45°C and 30°C respectively less than the T_{cr} of the raw Zap char itself. With higher loadings, however, both Na and K lost their ability to increase char reactivity (lower the T_{cr}) and actually demonstrated hindering effects. The highest Na and K loadings gave values of T_{cr} which were higher by 129°C and 85°C, respectively, than the demineralized Zap sample.

We are not aware of previous work which shows a saturation or hindering effect for ion-exchanged cations, although most of this work has been done in steam or at low loadings in air. For example, the work of Hippo et al. (23) indicated that reactivity in steam increased linearly to relatively high loadings. However, it is possible that these effects may only be evident at the lower temperatures used for the reactivity measurements in air. Surface area measurements were done of the raw and cation-loaded samples in these cases. However, significant differences were not observed. Consequently, the hindering effect must manifest itself either during the char formation process or the gasification process. It is planned to check the first possibility by doing pyrolysis experiments with cation-loaded samples in a reactor which can handle samples which are large enough to allow surface area measurements on the resultant char. The second possibility will be investigated by doing temperature programmed desorption (TPD) experiments on chars produced from raw, cation-loaded and demineralized coals.

A model was developed to predict the intrinsic reactivity (T_{cr}) of char based on calcium content for coals greater than 10% oxygen, while holding the extent of pyrolysis and heating rate constant. For a standard test:

$$T_{cr} = 520 + \alpha \text{ (Ca wt\% - } (\beta * \text{ carbonate))} \qquad (1)$$

where, 520 represents the approximate T_{cr} for demineralized coals, α is the slope from the plot of T_{cr} vs Ca wt% in Fig. 4a, β is a constant and the carbonate value is that obtained from quantitative FT-IR analysis.

Figure 5a displays the correlation between actual T_{cr} and predicted T_{cr} with $\beta = 0$. Since it is the organically bound Ca which is thought to be catalytically active, a much better correlation is obtained when calcite corrections are included in the model (Fig. 5b). Including minerals such as Mg, Na, or K in the correlation did not noticeably improve the predictions.

In order to better understand why the organically bound Ca offers catalytic activity and calcite does not, SEM Ca dot maps were done for a calcium loaded demineralized Zap coal and an Exxon sample which, from FT-IR analysis, was known to be abundant in calcite. The maps indicated that the organically bound Ca is very well distributed throughout the Zap coal while the calcite in the Exxon coal exists in large clusters. This is consistent with the fact that the Ca in the calcite form is not nearly as effective as a catalyst when compared to the ion-exchanged Ca. Radovic et al. (21) have clearly shown the effect of Ca dispersion on reactivity. However, it is also true that even if the calcite were well-distributed, it may not promote gasification reactions.

Effects of Minerals on High Rank Coals - A surprising result from the studies on chars produced from demineralized coals was the fact that the reactivity of the chars from demineralized high rank coals increased (see Fig. 1). This has been observed previously in work at Penn State and elsewhere (13-15, 24-26) and has been explained based on the fact that the demineralization process removes minerals which block pores and increases the accessible surface area of the resultant chars (26). There are data which support this increase in surface area. However, it does not change enough to explain the large differences in reactivity observed for some of the coals. The best example is the Upper Freeport. The difference in T_{cr} of 510°C vs 640°C represents a difference in reactivity of a factor of 25, while surface area differences were only about a factor of 5 (see below). It was also observed that the demineralized Upper Freeport coal was no longer fluid. This suggested that the demineralization process may introduce crosslinks into the coal. A possible reason is the retention of chlorine in the form of HCl from the demineralization process. Previous reports of this phenomena include the work of Macrae and Oxtoby (27-28) who observed that the uptake of small amounts of chlorine by a strongly caking coal completely destroyed its coking properties. They also found that the char produced from the chlorinated coal had a more disordered structure and higher surface area. A separate study by Pichin (29) found that pyrolysis of chlorinated coals does not produce chlorinated tars but only HCl and reduced amounts of volatile matter. Mahajan and Walker (26) cited these two studies as indicating that chlorination will produce a higher surface area and hence higher reactivity char. We believe it is the effect of the chlorine on the molecular order which is ultimately more important.

It was verified that the demineralization process increased the surface area of the resultant char from the Upper Freeport coal when measured by N_2 or CO_2 adsorption. The Upper Freeport char prepared from the raw coal had surface areas of 1.2 and 27 m^2/g for N_2 and CO_2, respectively. The Upper Freeport char prepared from a demineralized coal had surface areas of 3.7 and 134 for N_2 and CO_2, respectively. Assuming that these areas are relevant, they only represent about a factor of five. The other factor of five must be due to differences in the molecular order (active site concentration). It is also true that the BET surface area may overstate the importance of surface area and that the molecular order may be even more important. Of course, it is true, as noted by Walker (30), that the microporosity (which is measured by CO_2 surface area) is intimately related to the molecular order, so it is hard to separate these two effects.

In order to examine the possible role of chlorine on molecular order we heated the demineralized coal at 30°C/min in a TG-FTIR which can monitor the evolution of volatile products. We found evolution of HCl in the temperature range of 250 - 300°C, which was not found for the raw coal. The analyses of chlorine for the Argonne coals also indicated that the Upper Freeport was the only coal in the Argonne set with a zero chlorine content. This is consistent with the fact that the largest increase in reactivity was observed in this coal which would be the most sensitive to chlorine contamination. A third test of this hypothesis was to examine the solvent swelling data for the raw and demineralized Upper Freeport coal and their respective chars produced at 400°C, where maximum swelling is usually observed.

The swelling measurements are somewhat ambiguous on confirmation of crosslinking. The results are shown in Table 1. The raw swelling data are shown as well as the value normalized to the starting coal $(1-X)$. The char produced from the demineralized coal has about the same swelling ratio as the char produced from the raw coal. However, the process of demineralization increased the swelling ratio of

the starting coal, which is why the normalized ratios show a significant reduction in swelling for the char from the demineralized coal relative to the char from the raw coal. These results will require further study. The particle size for the demineralized sample was smaller which may have affected the swelling measurements. It should also be noted that the swelling measurements for the raw coal were done on a sample from the sealed ampoules while the demineralized coal was prepared from a bulk sample received from Karl Vorres which was not subject to the same handling procedures. These measurements will be repeated on raw and demineralized samples prepared from the same starting material.

Besides its possible role in low temperature crosslinking, it has been observed by Macrae and Oxtoby (27-28) that chlorine inhibits the high temperature graphitization process. This would explain the results of Almagro (31) who observed enhanced reactivity for chars from anthracites which had been chlorinated. It is known that impurities can produce dislocations which persist even at very high heat treatment temperatures (32).

The Role of Molecular Order in Char Reactivity - The results for the Upper Freeport, where higher reactivity was associated with loss of fluidity, indicated that further study was needed of the importance of molecular order on reactivity. One method of influencing the molecular order in the case of fluid coals is to change the pyrolysis heating rate. We did a series of experiments where chars were produced by heating at 1, 30 or 200°C/min to 900°C. The chars were then held at 900°C for 2 hours to even out the effects of the amount of time spend at lower temperatures. These results are shown in Table 2. There appears to be a monotonic trend of decreasing reactivity (increasing T_{cr}) with decreasing heating rate in cases 1, 2, and 3. For case #1 and #2 (Zap and demineralized Zap chars) the reactivities at 200°C/min and 30°C/min were unvarying. This was consistent with earlier work on low rank coals which showed no effect of heating rate in the range of 30°C/min to 20,000°C/s. However, the T_{cr} increased by approximately 20°C at 1°C/min. The results for case #3 (Pittsburgh chars) indicated an approximate 13°C increase in T_{cr} as the rate decreased from 200°C/min to 30°C/min and an approximate 10°C decrease as the rate further decreased from 30°C/min to 1°C/min. The latter effect is closest to the reproducibility of the measurements. For case #4 (Rosebud chars), no obvious trends were observed.

Additional results from experiments done over an even wider range of heating rates are shown in Figs. 6 and 7. Figure 6 is the same as Fig. 1 except that additional reactivity data are plotted for chars produced in an entrained flow reactor at 1100°C in which the heating rate was ~10,000 K/s and the total residence time ~0.5 s. This treatment produces a char with nearly the same daf H content as heating in the TGA for 30°C/min to 900°C. The latter treatment is somewhat more severe which may explain some of the observed differences, particularly, for raw low rank coals where reactivity does appear to depend much on heating rate. However, this plot shows significant differences in reactivity for the higher rank coals with heating rate, particularly for the Pittsburgh and Upper Freeport coals which are the most fluid. Figure 7 shows that there is a heating rate effect for demineralized Zap coal at lower extents of pyrolysis but that this appears to be lost as the hydrogen content is reduced below 2%. It is interesting that the demineralized Zap was even less reactive than the average of results for the raw Pittsburgh No. 8 and Kentucky No. 9 bituminous coals indicated by the dashed line.

Summary - The results to date can be summarized as follows: we agree with previous workers (20,26,30,33) that the key factors in determining the reactivity differences between chars produced from various coals under the same conditions

are: 1) the molecular order of the char which determines the active site concentration, 2) the accessibility of reactive gases to the active sites, and 3) the concentration and dispersion of inorganic species present which act as specific carbon gasification catalysts.

However, we would maintain that the emphasis on surface area (20,26,30,33) has often been misplaced and that molecular order is at least as important. This aspect has often been overlooked because the molecular order of the starting coal and the resultant char are directly related to the BET surface area (30). This has resulted in differences in reactivity being attributed to differences in surface area even when the differences in surface area are too small to account for the reactivity differences. In this regard, we would agree that the measurement of active surface area by oxygen chemisorption is more appropriate (34,35) since this measurement incorporates the reactant accessibility and active site concentration into one factor. However, results depend on the conditions used and may not be appropriate for "young" chars with a wide distribution of sites (36).

The molecular order is determined by several factors which can be manipulated: 1) crosslinking by oxygen groups; 2) crosslinking by ion-exchanged cations; 3) heating rate, especially in the case of fluid coals; 4) pyrolysis temperature which causes annealing of the organic and mineral components of the char and an increase in order. The effect of preoxidation (37,38) or chlorination (13-15,24-29) in increasing the reactivity of a highly fluid bituminous coal is a graphic illustration of the importance of molecular order. Supporting evidence is also provided by the significant decline in reactivity with increasing extent of pyrolysis (1-3,13,25,34).

The lack of importance of CO_2 or N_2 surface area as an appropriate normalizing parameter is supported by the fact that these often increase during burnoff at the same time that the observed net reactivity is declining. This is especially true of the N_2 surface area which can increase dramatically at very low levels of burnoff (2).

The role of heating rate is complex. For highly fluid coals, heating at higher rates would result in passing through the plastic stage more quickly and causing more violent gas evolution. This should reduce the order in the char. For lignites, it has been found that heating at high rates causes fluidity which is not observed at low heating rates. However, we have not found much effect of heating rate on reactivity of lignites unless they have been demineralized or heated at very low rates as discussed above. Conversely, heating a fluid coal at very low rates can destroy its fluidity (39) and heating a preoxidized fluid coal at high heating rates can restore its fluidity (38).

The presence of ion-exchanged minerals in low rank coals can affect reactivity in three different ways. One is the well known effect of having a highly dispersed catalytic substance. The second is the fact that the ion-exchanged cations may increase the efficiency of crosslinking based on their significant impact on tar yield (40). Of course, it may also be true that the cations only reduce the volatility of the tar molecules. There is evidence that minerals inhibit high temperature graphitization of the char (32) but also evidence which suggests that the opposite is true (41).

There is some evidence for the effect of cations on molecular order from measurements which we have made on the resistivity and reactivity of chars produced from raw and demineralized coals (2). In three cases for Zap lignite, the

measurements were made from raw demineralized coals produced under the same conditions. In two of the three cases the demineralized chars had a lower resistivity which would indicate a higher degree of order, even though it was shown through measurements on the starting coals that the presence of the minerals did not directly effect the resistivity. In the third case the resisitivities were comparable but this was made for a "young" char. It is true that the presence of even inert but well dispersed minerals would introduce some disorder (32). Other techniques such as NMR and FT-IR can be used to further address this question.

CONCLUSIONS

- For raw coals with greater than 10% oxygen content, the reactivity is determined primarily by the amount of well-dispersed catalytically active minerals.
- For demineralized coals of all ranks the reactivity is determined primarily by the molecular order and the surface area.
- Out of the factor of 380 difference in reactivities between the Argonne coals in air, the following factors result from differences in mineral catalysts, molecular order, and surface area, respectively (15/5/5). These are only estimates which will change as the degree of pyrolysis increases and annealing of the organic and mineral matter begins.
- The molecular order can be affected by crosslinking agents (carboxyl groups, chlorine), crosslinking enhancers (cations), and impediments to crystallite growth (heteroatoms or cations).
- The apparent increase in reactivity for demineralized high rank coals is not only due to a physical effect such as surface area but also results from a decrease in molecular order due to loss of fluidity. This loss of fluidity may result from the ability of residual chlorine to partially crosslink the coal. The chlorine may also affect graphitization of the char.
- For highly fluid coals, the reactivity can be dramatically affected by preoxidation or rapid heating. The previous explanation of these well known effects as primarily a result of increased surface area is probably an overstatement. The effects on molecular order are also important.

ACKNOWLEDGEMENT

This work was supported under contracts DE-AC21-85MC22050 and DE-AC21-86MC23075 from the Morgantown Energy Technology Center of the U.S. Department of Energy.

REFERENCES

1. Best, P.E., Solomon, P.R., Serio, M.A., Suuberg, E.M., Mott, W.R., Jr., and Bassilakis, R., ACS Div. of Fuel Chem. Preprints, **32**, (4), 138, (1987).
2. Serio, M.A., Solomon, P.R., and Suuberg, E.M., 1987 Int. Conf. on Coal Science, (J. Moulijn et al., Eds.) Elsevier Science Publishers, BV Amsterdam, pp. 597-600, (1987).
3. Solomon, P.R., Serio, M.A., and Heninger, S.G., ACS Div. of Fuel Chem. Preprints, **31**, (2), 200, (1986).

4. Vorres, K.S., ACS Div. of Fuel Chem. Preprints, **32**, (4), 221, (1987).
5. Neavel, R.C., Hippo, E.J., Smith, S.E., and Miller, R.N., ACS Div. of Fuel Chem. Preprints, **25**, (3), 246, (1980).
6. Carangelo, R.M., Solomon, P.R., and Gerson, D.G., Fuel, **66**, 960, (1987).
7. Whelan, J.K., Solomon, P.R., Deshpande, G.V., and Carangelo, R.M., Energy and Fuel, **2**, 65, (1988).
8. Serio, M.A., Hamblen, D.G., Markham, J.R., and Solomon, P.R., Energy and Fuel, **1**, 138, (1987).
9. Bishop, M. and Ward, D.L., Fuel, **37**, 191, (1958).
10. Hengel, T.D. and Walker, P.L., Jr., Fuel, **63**, 1214, (1984).
11. Mahajan, O.P., Yarzab, R., and Walker, P.L., Jr., Fuel, **57**, 643, (1978).
12. Green, T.K., Kovac, J., and Larsen, J.W., Fuel, **63**, 925, (1984).
13. Jenkins, R.G., Nandi, S.P., and Walker, P.L., Jr., Fuel, **52**, 288, (1973).
14. Hippo, E. and Walker, P.L., Jr., Fuel, **54**, 245, (1975).
15. Linares-Solano, A., Mahajan, O.P., and Walker, P.L., Jr., Fuel, **58**, 327, (1979).
16. Takarada, T., Tamai, Y., and Tomita, A., Fuel, **64**, 1438, (1985).
17. Hashimoto, K., Miura, K., and Ueda, T., Fuel, **65**, 1516, (1986).
18. Blom, L., Edelhausen, L., and van Krevelen, D.W., Fuel, **36**, (1957).
19. Walker, P.L., Jr., Mahajan, O.P., and Komatsu, M., ACS Div. of Fuel Chem. Preprints, **24**, (3) 10, (1979).
20. Soledade, L.E.B., Mahajan, O.P., and Walker, P.L., Jr., Fuel, **57**, 56, (1978).
21. Radovic, L.R., Walker, P.L., Jr., and Jenkins, R.G., Fuel, **62**, 209, (1983).
22. Johnson, J.L., ACS Div. of Fuel Chem. Preprints, **20**, (4), 85, (1975).
23. Hippo, E.J., Jenkins, R.G., and Walker, P.L., Jr., Fuel, **58**, 338, (1979).
24. Garcia, X. and Radovic, L.R., Fuel, **65**, 292, (1986).
25. van Heek, K.H. and Muhlen, H.J., Fuel, **64**, 1405, (1985).
26. Mahajan, O.P. and Walker, P.L., Jr., Fuel, **58**, 333, (1979).
27. Macrae, J.C. and Oxtoby, R., Fuel, **44**, 395, (1965).
28. Macrae, J.C. and Oxtoby, R., Fuel, **44**, 409, (1965).
29. Pinchin, F.J., Fuel, **37**, 293, (1958).
30. Walker, P.L., Jr., Fuel, **60**, 801, (1981).
31. Almagro, G., Ph.D. Thesis, Penn State University, (1966).
32. Walker, P.L., Jr., Rusinko, F., Jr., and Austin, L.G., Advanced in Catalysis, (D.D. Eley, et al. Eds.), Vol. XI, p. 133, Academic Press, NY (1959).
33. Ashu, J.T., Nsakala, Y.N., Mahajan, O.P., and Walker, P.L., Jr. Fur. **57**, 250, (1978).
34. Radovic, L.R., Walker, P.L., Jr., and Jenkins, R.G., Fuel, **62**, 849, (1983).
35. Khan, M.R., Fuel, **66**, 1626, (1987).
36. Suuberg, E.M., Calo, J.M., and Wojtowciz, M., ACS Div. of Fuel Chem. Preprints, **31**, (3), 186, (1986).
37. Mahajan, O.P., Komatsu, M., and Walker, P.L., Jr., Fuel, **59**, 3, (1980
38. Maloney, D.J. and Jenkins, R.G., Fuel, **64**, 1415, (1985).
39. Hamilton, L.H., Fuel, **59**, 112, (1980).
40. Morgan, M.E. and Jenkins, R.G., Fuel, **65**, 764, (1986).
41. Oya, A., Fukatsu, T., Otani, S., and Marsh, H., Fuel, **62**, 502, (1983).

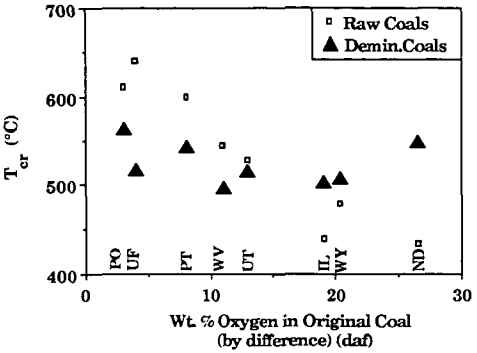

Figure 1. Variation of Reactivity with Coal Oxygen Content for Raw and Demineralized Argonne Coals.

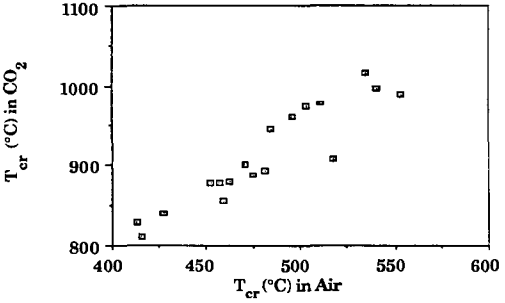

Figure 2. Correlation Between CO_2 and Air Reactivity Parameters for Exxon Coals.

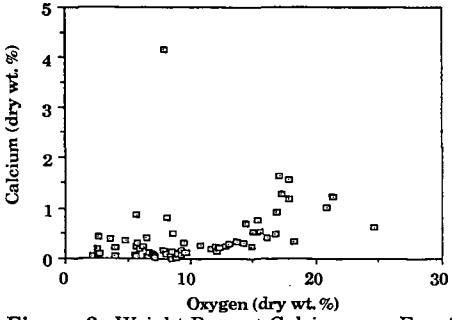

Figure 3. Weight Percent Calcium as a Function of Oxygen in Coal for Exxon Coals.

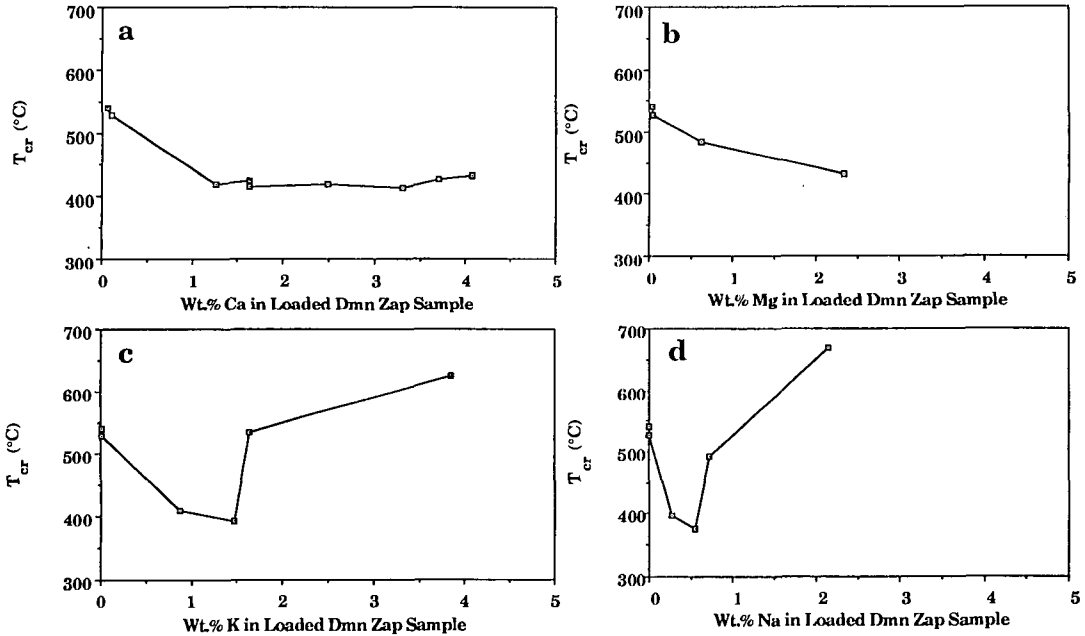

Figure 4. Variation of Reactivity with Cation Loadings for Demineralized Zap Coal. a) Calcium; b) Magnesium; c) Potassium; d) Sodium.

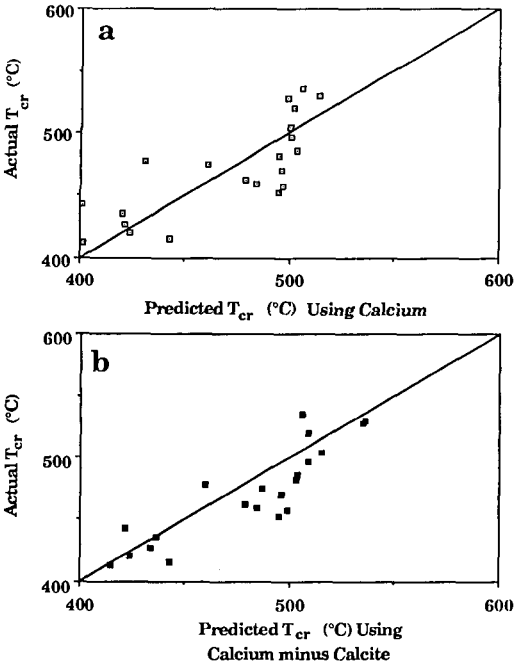

Figure 5. Correlation Between Actual Reactivity and Predicted Reactivity Based on Ca Content. a) with Calcite; b) without Calcite.

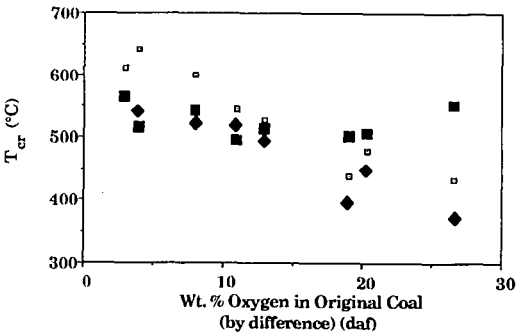

Figure 6. Variation of Reactivity with Coal Oxygen Content for Chars from Raw and Demineralized Argonne Coals Prepared at Low and High Heating Rates. ⊡ Raw Coal Heated at 30°C/min to 900°C; ■ Demineralized Coal Heated at 30°C/min to 900°C; ◆ Raw Coal Heated at ~10,000K/s to 1100°C.

Table 1 - Summary of Volumetric Swelling Measurements on Raw and Demineralized Upper Freeport Coals and Chars.

Sample	Volumetric Swelling Ratio	1 - χ
Upper Freeport (UF)	1.18	---
UF - 400°C Char	2.13	6.28
Demineralized UF	1.80	---
Demin. UF - 400°C Char	2.16	1.45

$$\chi = \frac{VSR_{coal} - VSR_{char}}{VSR_{coal} - 1}$$

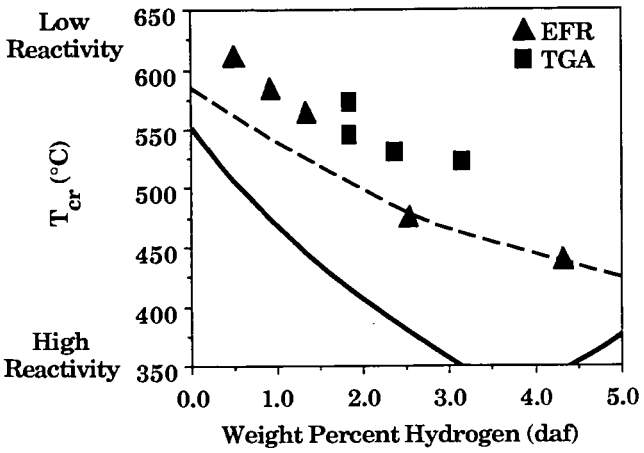

Figure 7. Comparison of Reactivity vs. Hydrogen Content of Chars from Demineralized Zap Lignite (data) with Average Reactivity of Chars from Raw Zap Lignite (solid line) and Average Reactivity of Chars from Two Bituminous Coals (dashed line). The Lignite was Demineralized using the Bishop and Ward (9) Procedure. The Chars were Prepared by Rapid Heating (~10,000°C/s) in an Entrained Flow Reactor (EFR) or Slow Heating (30°C/min) in a TGA.

Table 2

Reactivity Measurements on Chars Produced at Different Heating Rates

Case	#1	#2	#3	#4
Heating Rate	T_{cr}(°C) North Dakota (Zap) Lignite Chars	T_{cr}(°C) HCL, HF Demineralized Zap Chars	T_{cr}(°C) Pittsburgh Seam #8 Chars	T_{cr}(°C) Montana Rosebud Chars
200°C/min	397, 404	553	542, 543	484, 477
30°C/min	402, 408	552	556, 559	483, 493
1°C/min	425	571	567	474

KINETICS OF BROWN COAL GASIFICATION

R. Hegermann, K.J. Hüttinger
Institute of Chemical Technology
University of Karlsruhe, Kaiserstr. 12
Federal Republic of Germany

ABSTRACT

The kinetics of brown coal gasification in CO_2 and steam at various pressures and temperatures were studied by using a fluidized bed reactor. Gasification kinetics are nearly completely controlled by mineral matter, preferentially calcium. At all conditions the gasification behaviour may be described by the following semi-empirical model.

$$r = \frac{2 \cdot Y_{(max)} \cdot X}{X_{(max)}} - \frac{Y_{(max)} \cdot X^2}{X_{(max)}^2} + (a+bX)^{1/2} \cdot (1-X)^{2/3}$$

This equation is based on a particle model ($(1-X)^{2/3}$) which additionally considers a probable catalyst activation or deactivation with progressive gasification ($(a+bX)^{1/2}$) and finally the initially fast coal gasification ($2 \cdot Y_{(max)} \cdot X/X_{(max)} - Y_{(max)} \cdot X^2/X_{(max)}^2$).

INTRODUCTION

Brown coal seems to be an attractive raw material for gasification, because it is believed to be very reactive. The development of gasification processes requires fundamental knowledges about the reactivity in various atmospheres and in view of modern gasification technologies especially at high pressure. Gasification studies were performed at constant temperatures and pressures using a fluidized bed of alumina particles, into which the brown coal was charged. The gasification rates in various atmospheres were measured by on line gas analysis using IR-analyzers and a gaschromatograph. The changes of internal surface area with progressive gasification were determined by carbon dioxide and nitrogen adsorption. For analysis of the gasification mechanism studies with demineralized coal were performed.

EXPERIMENTAL

Three types of Rheinische Braunkohle were used in these studies (1), but only the results of a typical coal will be presented. The analytical data of this coal are given in Table 1. The special property of the coal is that the content of mineral matter merely varies with particle size. The majority of the studies were performed with a particle size fraction ranging from 2 to 3 mm. All samples were carefully dried. For demineralization the coal was treated with conc. HCl/HF (1:1). For further studies calcium was introduced into the demineralized coal by ion exchange using $CaCO_3$.

The experimental equipment used for the gasification studies and the special analytical procedure for an accurate measurement of the gas formation peaks resulting in a batchwise experiment are reported elsewhere (2). Coal samples of 100 to 150 mg were used. Each experiment was done twice.

RESULTS

Gasification kinetics of dry coal

In all experiments the formation rates of all product gases were measured. In the following Figures the carbon conversion to gases, termed as gas yield, are presented as function of the reaction time (series a). The rates of carbon conversion to gases, termed as gasification rate, as function of the normalized gas yield are additionally presented (series b). The latter Figures give further informations about the mode of gasification kinetics (kinetic model). The yields and gasification rates are related on the initial amount of carbon of the coal.
Figs.1 and 2 show the results of gasification with pure CO_2 at four different pressures and at temperatures of 800°C (Fig.1) and 900°C (Fig.2). At both temperatures the gas yields are nearly independent on pressure and amount to roughly 80 %. This means that approximately 20 % of volatiles are formed. The gasification is completed after 1000 to 2000 s (800°C) or 500 to 1000 s (900°C). The pressure influence is anomalous or at least surprising. The rates increase with pressure only up to 0.5 MPa (800°C) or 1.0 MPa (900°C). Fig.3 shows analogous results for gasification with steam by using an argon/steam mixture (1:1) at total pressures of 1.0 and 2.5 MPa. Especially at 800°C the gasification rate is decisively higher than with CO_2, although the steam partial pressure is only 50 % of the CO_2 pressure at each total pressure. The gas yields are similar to those obtained in gasification with CO_2. The anomalous pressure influence can directly be observed at 800°C, at 900°C the rate at 2.5 MPa total pressure (corresponding to pH_2O= 1.25 MPa) is slightly higher than at 1.0 MPa (pH_2O= 0.5 MPa), which also corresponds to the results of CO gasification. It may be expected that the pressure influence becomes negative at 900°C, if the total or partial pressure of pH_2O is further increased.
The reasons for the negative pressure effect at high partial pressure may be (a) a different degassing behaviour at high pressures or (b) a special property of a catalyzed gasification. The explanation will be given in the following chapters.
Fig.4 shows the influence of hydrogen on the steam gasification at 1.0 MPa and 800°C using an $Ar/H_2O/H_2$ mixture (2.5:5:2.5). Hydrogen strongly inhibits the gasification reaction. After 3000 s the gasification rate is nearly zero, although 34 % of the carbon are not yet gasified. Inhibition of non-catalyzed steam gasification is known by numerous studies, but a complete inhibition has not yet been reported.

Changes of internal surface area

The Figures of series b reveal that the gasification of the brown coal does not follow one of the known models (volume, particle,

pore).This still holds, if it is assumed, that the steep increase of the gasification rate at low carbon conversions (Figs. of series b) is a consequence not of the reaction but of the on-line gas analysis, which may be possible. Nevertheless, the changes of the BET surface area with progressive gasification have been determined for some cases.
Fig. 5 shows the BET surface area in dependence on the normalized gas yield for gasifications at 800°C and at pressures of 1.0 and 2.5 MPa. Although it is well known that only the CO_2 adsorption gives reasonable results, the N_2 adsorption was studied for demonstrating the differences between CO_2 and N_2 adsorption kinetics. At both gasification pressures the BET surface area passes through a maximum. A comparison with the Figs. 1b and 2b yields no conformity of the curves. In any case, it may be concluded that the maxima of the BET surface area occur at higher gas yields than the maxima of the gasification rates. This means that the BET surface area obviously has a minor importance for the gasification kinetics.
Fig. 6 shows similar results for the gasification with steam at 1.0 MPa and 800°C using an argon/steam mixture (1:1). The conclusions are the same as drawn for the gasification with CO_2.

Gasification kinetics of 'demineralized' coal

Studies with demineralized coal were performed in order to clarify a possible catalytic effect of mineral matter. By demineralization with HCl/HF the mineral matter could completely be removed from the coal. Gasification studies with such coals were performed at 1.0 MPa and at temperatures of 800°C and 900°C using CO_2 (Figs. 7 and 8) and steam (Fig. 9). The Figs. 7a and b show that the gasification rate of the demineralized coal approaches to zero after 10 % of the carbon are gasified. At 900°C (Figs. 8a and b) the gasification rate is zero after about 2 hours gasification. At that time only 70 % of the carbon are gasified. On the contrary, gasification of the original, non-demineralized coal is already completed after 500 s. These comparison underlines the strong catalytic effect of the minerals. Calcium was believed to be the main active component, because the content of the alkali metals of the coal is negligibly small. By ion exchange 39 % calcium of the original calcium content of the coal could be introduced into the demineralized coal. This doped coal confirms the strong catalytic effect of the calcium, especially at 900°C (Figs. 8a and b).
The steam gasification with demineralized coal yields similar results as found in CO_2 gasification (Figs. 9a and b). Due to the higher reactivity of steam, the effect of demineralization is not as strong as compared to CO_2 gasification. Nevertheless, at 800°C the gasification rate approaches to zero before all carbon is gasified (Fig. 9b).

DISCUSSION

The gasification kinetics of a Rheinische Braunkohle with CO_2 and steam was studied at pressures up to 2.5 MPa and at temperatures of 800°C and 900°C. The gasification rates of steam gasification are higher, but the increase of the gasification rate with partial pressure is limited for both gases. Above 0.5 MPa (800°C) and above

1.0 MPa (900°C) the rates decrease with further increasing pressure. This pressure effect on the gasification rate was unexpected. Gasification studies with demineralized coal show that brown coal or brown coal coke without cations are extremely unreactive. Further studies with a demineralized coal, but doped with calcium (0.5 wt%) envisualized the strong catalytic effect of this element. Therefore, it may be concluded that the high reactivity of the brown coal mainly or exclusively results from the minerals or more precisely from the calcium, because the content of alkali metals is negligibly small.

The gasification kinetics with progressive consumption of coal or coke may be described neither by a volume, pore or particle model (2). This conclusion clearly follows from the plots of the gasification rates versus carbon conversion (normalized carbon yields, Figs. 1b and 2b). It is underlined by the plots of specific surface area versus carbon conversion (Figs. 5 and 6). In fact, the gasification is determined by three processes: (1) Fast gasification of the coal at the beginning, i.e. at low carbon conversions. In this stage the gasification rates may be extremely high. (2) Control of the gasification in the coke gasification stage by catalysis. In this stage the specific surface area should be of minor importance. (3) Increase of the catalyst concentration with progressive gasification. This point may be important, because the initial concentration of calcium is small (1.3 wt%). Instead of a catalyst concentration increase a progressive activation of the catalyst may be operative (steam gasification). The probability of this interpretation is supported by the experimentally observed decreasing activity in the case of the CO_2 gasification. In view of the latter interpretation of the gasification kinetics it is unprobable that the improved accessibility of the internal surface with progressive gasification plays a major role.

In consideration of these processes the following semi-empirical model was derived:

$$r = \underbrace{\frac{2\,Y_{(max)}}{X_{(max)}}\,X - \frac{Y_{(max)}}{X_{(max)}^{2}}\,X^{2}}_{F_3} \cdot \underbrace{(a+bX)^{1/2}}_{F_2} \cdot \underbrace{(1-X)^{2/3}}_{F_1}$$

F1 = particle model; F2 = catalyst activation or deactivation with progressive gasification; F3 = fast coal gasification; $X_{(max)}$ = carbon conversion at highest gasification rate; $Y_{(max)}$ = highest gasification rate.

With this model the gasification kinetics of the coal may be described at all conditions. Examples are given in Figs. 10 and 11.

The differences between the experimental points and the calculated curve at the very low carbon conversions are mainly ascribed to the measurement of the gas formation rates.

REFERENCES

(1) Hegermann, R., Ph. D thesis, University of Karlsruhe, in preparation
(2) Hüttinger, K.J., in: New Trends in Coal Science (Yuda Yürüm,Ed.) (1987), 433 and 453, NATO ASI Series

ACKNOWLEDGEMENT

Financial support by Rheinische Braunkohlewerke AG, Köln, and Federal Ministry of Research and Technology under grant number No. 0326528A3 is gratefully acknowledged.

Table 1 - Elemental analysis and composition of a typical Rheinische Braunkohle (mf); ash content (wt %): 6.7

Elemental analysis (wt %)		ash composition (wt %)	
		Na_2O	0.3
C	60.1	K_2O	0.2
H	4.9	CaO	27.5
N	1.0	MgO	8.6
S	0.9	Fe_2O_3	11.7
O (diff.)	33.1	Al_2O_3, SiO_2	40.0
		SO_3	11.6

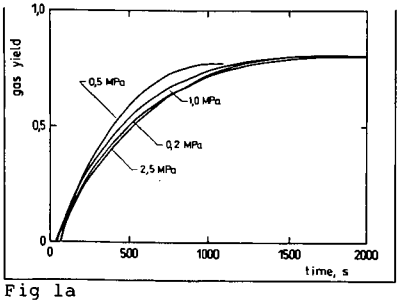

Fig 1a

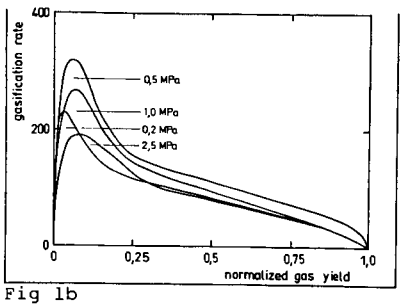

Fig 1b

CO_2 gasification at 800 °C; gasification rates are generally given as $10^5 \cdot mol_{C_{gas}} \cdot mol_{C_o}^{-1} \cdot s^{-1}$

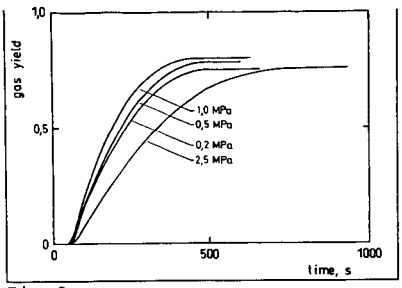

Fig 2a

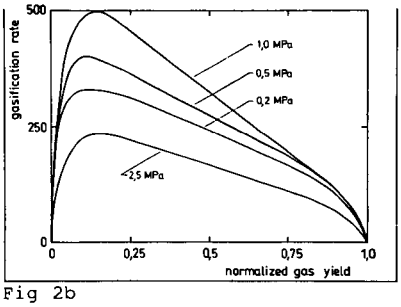

Fig 2b

CO_2 gasification at 900 °C

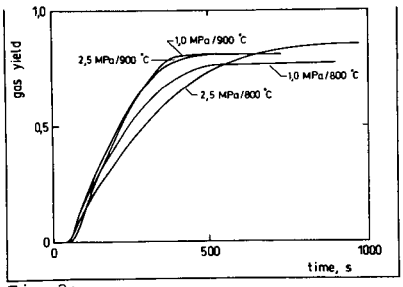

Fig 3a

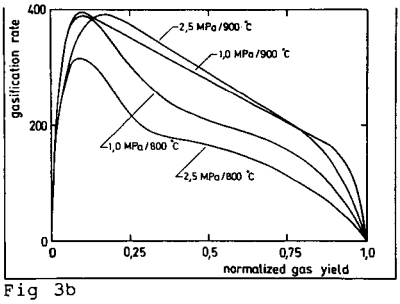

Fig 3b

Steam gasification at 800 °C and 900 °C

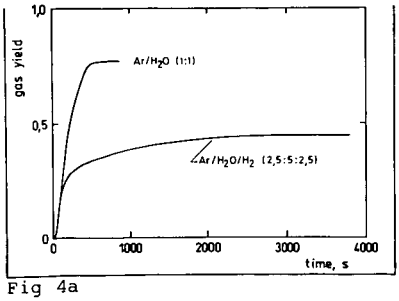

Fig 4a

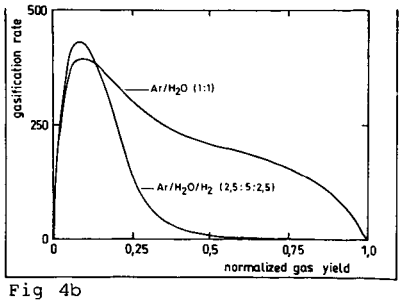

Fig 4b

Steam gasification at 1.0 MPa and 800 °C, influence of hydrogen

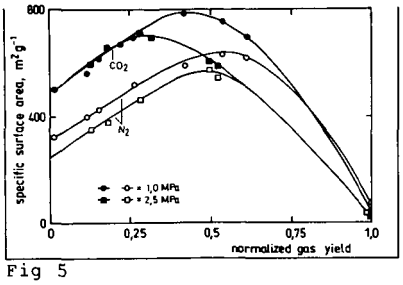

Fig 5

Change of specific surface area during CO_2 gasification at 800 °C

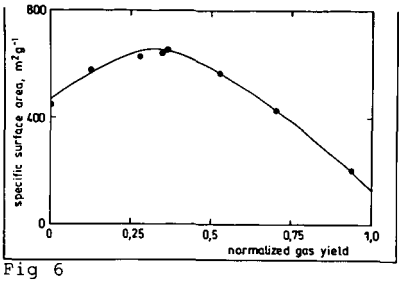

Fig 6

Change of specific surface area during steam gasification at 800 °C

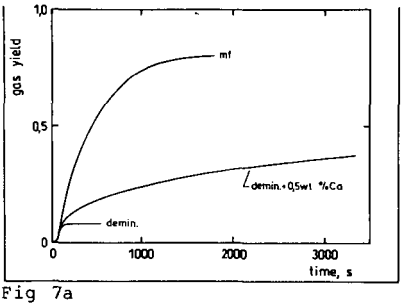

Fig 7a

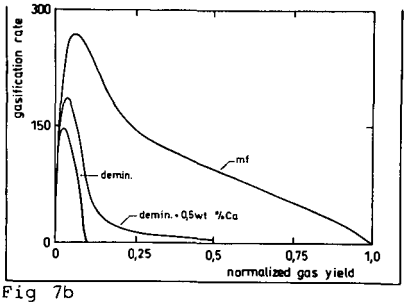

Fig 7b

CO_2 gasification of 'demineralized' coal at 1.0 MPa and 800 °C

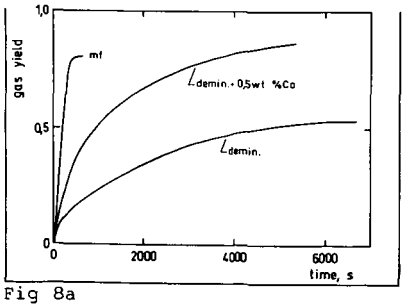

Fig 8a

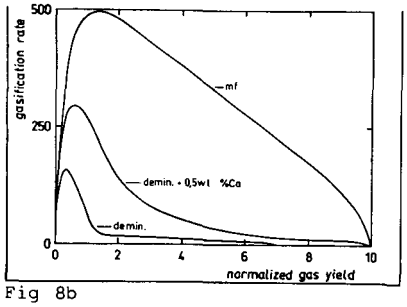

Fig 8b

CO_2 gasification of 'demineralized' coal at 1.0 MPa and 900 °C

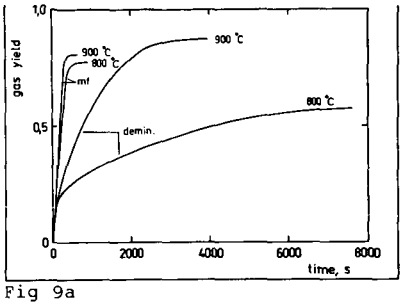

Fig 9a

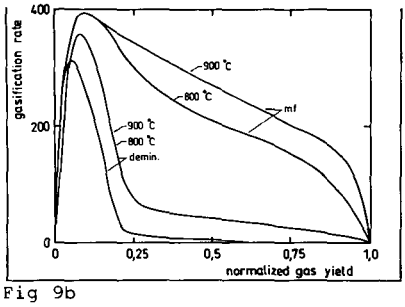

Fig 9b

Steam gasification of 'demineralized' coal at 1.0 MPa

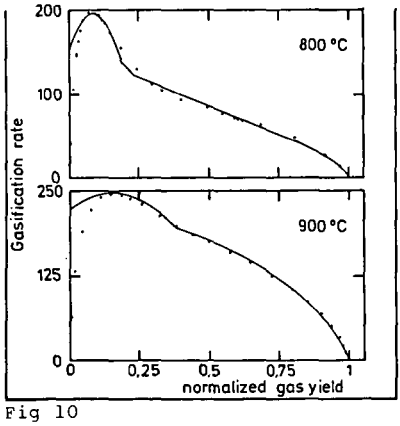

Fig 10

Exemplary check of the semi-empirical equation for CO_2 gasification at 2.5 MPa

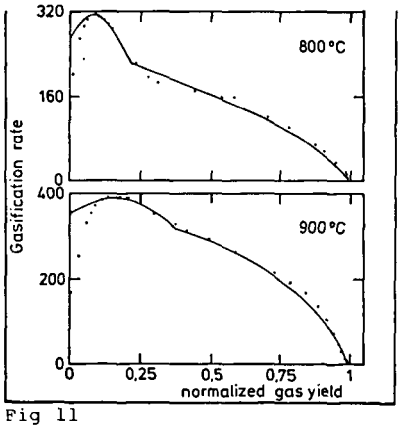

Fig 11

Exemplary check of the semi-empirical equation for steam gasification at 2.5 MPa

THE CATALYTIC EFFECT OF CALCIUM IN AIR GASIFICATION OF A SUBBITUMINOUS COAL CHAR

N.R. Marcilio*, H. Charcosset**, L. Tournayan**, B. Nickel**
and A. Jeunet***
*Fundaçao de Ciência e Tecnologia-Cientec, Porto Alegre-RS, Brazil
**Institut de Recherches sur la Catalyse du CNRS, Villeurbanne, France
***Laboratoire d'Etude Dynamique et Structurale de la Sélectivité,
Domaine Universitaire, Grenoble, France.

INTRODUCTION

Low rank coals contain alkali metals and alkaline-earth metals (especially Ca) which catalyse the gasification by O_2, CO_2 and H_2O.

A great deal of information is still needed concerning the nature and dispersion of the active species, the interaction between these species and organic matter...

A correlation of catalytic activity of CaO, as obtained during pyrolysis performed before gasification, with its dispersion, was observed by Radovic et al. (1).

EXPERIMENTAL

1) Sample preparation

The coal was a brazilian subbituminous coal. It was demineralized by HCl and HF at 333 K, (CD), in order to observe only the catalytic effect of calcium. (CD) was pyrolysed in helium (heating rate : 4 K min^{-1}) up to 1073 K (CD1073). This char was oxidized by HNO_3 15N (CD1073oxi), in order to increase its ion exchange capacity ; the procedure was used by Linares-Solano et al. (2). A cationic exchange was then performed with an 0.1 molar aqueous solution of calcium acetate, as described by Hippo et al. (3) ; drying of the sample (CD1073oxiCa) was carried out under reduced pressure (0.1 Pa) at 383 K. Finally a fraction of this material was pyrolyzed for 2 hrs in helium at 1073 K (CD1073oxiCa1073).

2) Sample characterization

Chemical analysis was used for the organic elements and for Ca. XPS Spectroscopy allowed determination of the surface concentration of Ca ; the depth of analysis was about 1.5 nm. X Ray Diffraction analysis was applied to appreciate the Ca phases. The microtexture was evaluated from the Dubinin-Raduskhevitch (4) method, and assuming a slit shape of the pores from CO_2 adsorption measurements at 273 K. The radical density and the linewidth value were obtained by ESR measurements.

3) Sample reactivity

The gasification experiments were performed under atmospheric pressure of dry air, heating rate 0.8 K min^{-1} and in absence of mass and thermal transfer limitations according to Barthe et al. (5). CO_2 and CO formation was followed by chromatographic analysis.

RESULTS

Table 1 and 2 give the chemical analysis data and the microporous texture data, respectively, for the initial samples CD, CD1073, CD1073oxi and CD1073oxiCa.

Table 3 gives the surface and bulk Ca/C atomic ratios, of the CD1073oxiCa sample either ungasified, or gasified at 30 or 60 %.

We did not detect any crystalline phase of some Ca species in either CD1073oxiCa1073 or in CD1073oxiCa.

Fig.1 shows the gasification versus temperature profiles for the samples CD1073, CD1073oxi CD1073oxiCa and CD1073oxiCa1073. A strong catalytic effect of Ca is apparent from the comparison of the (c) and (d) curves to the (a) and (b) curves.

Table 4 shows the selectivities in CO versus CO + CO_2, which did not vary more than 10 % in course of the gasification experiments. Ca does lower the selectivity in CO.

Table 5 shows the microporous texture data for the CD1073oxi and CD1073oxiCa samples, gasified between 0 % (unconverted materials) and 60 %. The microporous volume, the surface area, and the micropore size are decreased in presence of Ca.

The ESR data are shown in Table 6. The radicals concentration is much smaller in CD1073oxiCa than in CD1073oxi (ungasified samples). That difference tends to cancel out as the burn off increases.

DISCUSSION

Initial sample characterization

The Ca^{++} of the CD1073oxiCa sample are presumed to be selectively exchanged with carboxylic groups of the CD1073oxi sample. In fact, the pH value of the Ca acetate solution was not high enough to allow cationic exchange with hydroxyl groups according to Schafer (6). From the results of surface analysis of Ca (Table 3 ; ungasified sample), Ca should be homogeneously distributed between the surface and the bulk of CD1073oxiCa.

The higher radical concentration of CD1073oxiCa compared to CD1073oxi (Table 6; ungasified samples) may be explained either by quinone reduction into semi-quinone during the Ca acetate solution exchange step, or by a Ca^{++} catalysed adsorption or absorption of O_2 by the demineralized coal (CD). The higher oxygen wt % of CD1073oxiCa compared to CD1073oxi (Table 1) would favour the second hypothesis.

The physico-chemical state of Ca in CD1073oxiCa1073 may not be inferred accurately from the present work ; in particular, no calcium compound could be identified by XRD analysis. The literature data suggest the formation of CaO during the final pyrolysis step at 1073 K, according to Barthe et al. (5).

Reactivity in gasification

The Arrhenius plots for the air gasification reaction of the 4 samples studied are reported in Fig.2. The apparent activation energy is the same, 120 $kJ.mol^{-1}$, in agreement with literature data, Khan (7), Linares-Solano et al (8). The preexponential factor is strongly increased in presence of Ca. A main observation lies in the very similar behaviour of CD1073oxiCa and of CD1073oxiCa1073. Since the evolution of CO, CO_2 from CD1073oxiCa is catalyzed by Ca, already at about 723 K, the Ca carboxylate species should not have to be decomposed into CaO to be catalytically active. The similar catalytic effect of Ca in CD1073oxiCa1073, presumed to consist of CaO/C, indicates the role of the "CaO"/C interface as already mentioned, Linares-Solano et al. (8). It should be considered that the formation of "C-O-Ca" complexes at that interface occurs during the gasification experiment itself. Those active sites composing complexes should be similar to those arising from the Ca carboxylate species of CD1073oxiCa in course of its gasification. Hence a similar reactivity of the Ca exchanged sample and of its repyrolysed derivative; the nature of the Ca catalytically active complexes is not yet established.

Characterization of partially gasified samples

The Ca/C ratios at burn off 30 and 60 % of CD1073oxiCa (Table 3) strongly support the view that gasification takes place in the bulk as well as in the surface of this sample particles. A strongly preferential surface gasification would result in much more enrichment of Ca in the surface, at increased gasification ratios, than is experimentally observed.

It must be pointed out that the microporous volume and area (Table 5) exhibit a drastic decrease as the wt % gasification of CD1073oxiCa becomes equal or superior to 20 % ; this is not observed over the non Ca exchanged sample CD1073oxi. It is possible that the mesoporous area increases in compensation to the decrease of the microporous area, during the gasification of CD1073oxiCa, but it has still to be confirmed.

An increase of the radical concentration was observed following partial gasification of both CD1073oxi and CD1073oxiCa (Table 6). Since the difference

observed between the two samples decreased as the temperature (and therefore the degree of gasification) increased, it may be supposed that kinetic limitations predominate in coal oxidation in the vicinity of room temperature, to be replaced by thermal equilibrium limitations at the higher temperatures of gasification.

CONCLUSION

It is suggested that even at room temperature the calcium exchanged carboxylic groups of coal catalyse the adsorption or absorption of ambient oxygen.

It was shown that thermal decomposition of the Ca carboxylate species into CaO is not a prerequisite to observe a catalytic effect of Ca in the low temperature gasification of C by air.

Partially gasified samples (low temperature air gasification ; Ca carboxylate species as catalyst precursors) show interesting microtextural properties when compared to the blank samples.

ACKNOWLEDGEMENTS

The authors do acknowledge Dr G. Bergeret, Dr J.P. Joly and Prof A. Linares-Solano for helpful discussions.

REFERENCES

(1) L.R. Radovic, P.L. Walker Jr and R.G. Jenkins, Fuel, 62, 209 1983.
(2) A. Linares-Solano, C. Salinas-Martina de Lecea and M. Almela-Alarcon, International Conference on Coal Science, 559-562, Maastricht, Holland, 1987.
(3) E.J. Hippo, PhD Thesis, the effect of cation exchange on the subsequent reactivity of lignite chars to steam, the Pennsylvania state University, 1977.
(4) M.M.Dubinin and L.V.Radushkevish, Proc. Acad. Sci. USSR, 55, (1947) 331.
M.M.Dubinin, Russ.J.Phys.Chem., 39 (1965) 697.
M.Polanyi, Verb.Deutsch.Physik.Ges., 16 (1914)1012.
(5) P. Barthe, H. Charcosset and J.M. Guet, Fuel, 65, 1330, 1986.
P. Barthe, Thèse de Docteur Ingénieur, Lyon 1986.
(6) H.N.S Schafer, Fuel, 49, 197 1970.
(7) M.R. Khan, ACS Division of Fuel Chemistry, 32, N°1, 298 1987.
(8) A. Linares-Solano, E.J. Hippo and P.L. Walker Jr., Fuel, 65, 776, 1986.

Table 1 : Ultimate analysis of the initial samples

Samples	wt (%)					
	C	H	N	O	S	Ca
CD	72.2	4.33	1.46	19.63	0.69	0.04
CD1073	90.4	1.30	1.19	7.04	0.80	0.08
CD1073oxi	73.6	1.80	1.54	24.02	0.56	
CD1073oxiCa	64.0	1.65	1.41	26.10	0.54	3.40

Table 2 : Microporous structure of the initial samples

Samples	Volume (cm^3/g)	Surface (m^2/g)	Diameter (nm)
CD	0.042	90	1.9
CD1073	0.208	370	2.2
CD1073oxi	0.163	329	2.0
CD1073oxiCa	0.131	289	1.8

Table 3 : Atomic ratio Ca/C obtained by ESCA measurements and by ultimate analysis at different conversions of the CD1073 oxi Ca sample

δ (%)	Ca/C (ESCA)	Ca/C (Ultimate Analysis)	$\frac{(Ca/C)\ ESCA}{(Ca/C)Ul.An.}$
0	0.0196	0.0159	1.23
30	0.0212	0.0215	0.99
60	0.0904	0.0397	2.28

Table 4 : Selectivity of CO versus $CO + CO_2$ during gasification

Samples	Selectivity of CO
CD1073	0.24 - 0.26
CD1073oxi	0.11 - 0.13
CD1073oxiCa	0.03 - 0.04

Table 5 : Micropore structure at different conversions of char-air reaction

τ (%)	CD1073oxi			CD1073oxiCa		
	$V(cm^3/g)$	$S(m^2/g)$	$\bar{D}$(nm)	$V(cm^3/g)$	$S(m^2/g)$	$\bar{D}$(nm)
0	0.163	329	2.0	0.131	289	1.8
5	0.206	376	2.2	0.136	304	1.8
15	0.218	395	2.2	0.129	283	1.8
20	0.227	410	2.2	0.140	297	1.9
40	0.213	373	2.3	0.045	82	2.2
60	0.198	349	2.3	0.035	29	2.3

Table 6 : ESR measurements at different conversions of the char-air reaction

τ (%)	CD1073oxi		CD1073oxiCa	
	Hpp(gauss)	R'(spins/g)	Hpp(gauss)	R'(spins/g)
0	3.4	6.5×10^{16}	11.0 and 3.8	1.7×10^{18}
15	3.4	11.0×10^{18}	3.8	8.8×10^{18}
60	4.2	2.4×10^{18}	3.7	12.7×10^{18}

STUDIES OF THE AGGLOMERATION AND REACTIONS OF CA AND K DURING PYROLYSIS AND GASIFICATION

Naresh Shah[1], *Frank E. Huggins*[1], *Anup Shah*[1], *Gerald P. Huffman*[1], *Robert G. Jenkins*[2], *and Andrzej Piotrowski*[3]

[1]University of Kentucky, Lexington, KY 40506
[2]University of Cincinnati, Cincinnati, OH 45221
[3]Penn State University, State College, PA 16802

INTRODUCTION

Efficient catalytic processes are the key to successful and economical coal gasification. With suitable catalysts, gasification rates can be significantly enhanced or the process can be operated at substantially lower temperatures. The importance of alkalies and alkaline earths as catalysts for gasification process is well known (1,2). For over a century alkali additives such as caustic soda and/or lime have been used to promote the reactions of steam and air with coal and charcoal (3). Ca and Na occur naturally in macerals of lignites in a highly dispersed form that is as close to an ideal catalyst dispersion as possible (4,5). Catalytic effects of alkalies on the gasification rates for coal (6,7), char (8,9), graphite (10,11) and wood (12) have been investigated. Enhanced gasification rates of >10 times has been observed with Ca rich lignites compared with base lignite from which Ca has been removed (13). However, the exact role played by these catalysts is not yet clearly understood. Hence there is considerable interest in the structural forms of these catalysts in their dispersed state, after pyrolysis, during gasification and after reaction. Determination of catalyst structures at these various stages has proven difficult because of the high dispersion (often molecular) and relatively very low catalyst concentrations (≈1-2%).

XAFS (X-Ray Absorption Fine Structure) spectroscopy is a powerful structural analysis technique that has unique ability to focus on only one element and provide information about its bonding and the short range structure. It is capable of providing excellent signal to noise ratio at dilute concentrations and at elevated temperatures. It is ideally suited for coal as it can give information on the element of interest at concentrations as low as 100 ppm without elaborate sample preparation (14). In theory, XAFS analysis can be carried out for any element of interest. However, due to X-ray attenuation problems, XAFS has been successful only for elements above S in the periodic table without good vacuum conditions. Thus, even though Na is an important element in coal gasification, it has not been directly analyzed. Ca and K are the two most important elements of interest in coal that have been studied using XAFS analysis.

CCSEM (Computer Controlled Scanning Electron Microscopy) can be used to monitor the physical dispersion of the catalysts in the samples which have undergone advanced stages of pyrolysis and gasification. CCSEM can measure the sizes and compositionss of about 500 particles per hour enabling quantitative measurements of size distributions and weight distributions of inorganic phases in coal and chars (15).

EXPERIMENTAL

XAFS spectroscopy was performed at SSRL during dedicated running conditions. A pure He path to the sample was employed to minimize attenuation of X-rays. Spectra were recorded from ≈100 eV below to ≈500 eV above the K edges of Ca and K in coal using a double crystal Si (111) monochromator. The fluorescent X-rays were measured by a Stern-Heald type detector (16). The in-situ experiments were carried out in a specially designed furnace (17). Data was collected on a PDP 11/23 computer and analyzed on a MicroVax II at the University of Kentucky. Calcite and KCl were used as primary standards for calibration purposes for Ca and K respectively.

Ca loaded chars were prepared and measured for reactivity by Radovic et al. from a Ca rich lignite (Falkirk, ND) and from ion-exchangeable phenol formaldehyde polymer (18). Chars were prepared by slow (up to 1 hr) and rapid (entrained flow reactor, residence time ≈0.3 sec) pyrolysis at 800 and 1000°C in N_2 atmosphere.

RESULTS

As reported earlier, XAFS on lignites without any heat exposure showed that Ca is bonded to carboxyl groups and is molecularly dispersed throughout the lignite macerals (4,5). Fourier transformation of EXAFS provides a radial structure function (RSF) which is closely related to the radial distribution of the shells of neighboring atoms of the central absorbing atom (19,20). Fig. 1 shows several such RSFs. In CaO the nearest neighbor shell of central Ca atom is made up of oxygen atoms at 2.4 Å and then there are shells of Ca, O, Ca, Ca and Ca at about 3.4, 4.0, 4.8, 5.9 and 6.8 Å respectively. These values agree very well with values determined based on NaCl-type structure.

In the Ca-loaded lignite RSF, however, there is only one major peak at approximately 2.4 Å due to the nearest oxygen shell. This is due to non-crystallinity and highly dispersed state of Ca atoms in the lignite macerals. After rapid pyrolysis of this lignite, the RSF does not change significantly. At the temperature conditions used in rapid pyrolysis treatment, the carboxyl groups should be driven off. However, even under such conditions, the nearest neighbor oxygen shell surrounding Ca is virtually unchanged. Moreover, lack of any detectable neighbor shells at longer distances indicate that Ca must still be in a highly dispersed state in the devolatalized, non crystalline char matrix. As the severity of pyrolysis increased (either increasing time or temperature or both), two processes take place: [1] Carboxyl groups start breaking up as the char devolatalizes. In the nearest neighbor shell of Ca, number of O atoms decreases (21). The second shell distance also moves towards that of the Ca-Ca distance in Ca-O and away from the Ca-C distance in the carboxyl groups (22). [2] Ca atoms become more mobile and start agglomeration. This clustering results in longer range order. Thus, as shown in Fig. 1, with slow pyrolysis treatment, the RSF looks increasingly like the CaO RSF as the intensity due to shells of atoms further away increases. Even after slow pyrolysis treatment, there is some Ca left in the dispersed state in the matrix. This is evident in Fig.1D as a major peak of the nearest O shell like that in the untreated coal. Since Ca atoms are no much less dispersed, the effective surface area of the catalytic sites is reduced dramatically. This directly influences the reactivity in the gasification process.

To study the onset of this transformation, in-situ experiments were designed (23). Samples of coal and char loaded with Ca were heated while XAFS spectra were measured. To simulate pyrolysis, initially only He was flowing through the in-situ

furnace. After heating to about 500°C, 90% He - 10% O_2 was introduced to simulate gasification. Unfortunately, due to furnace heater capacity limitations, the samples could be heated only up to 500°C and the experiment could not be carried out to attain the state of slow pyrolysis as mentioned above. Due to this limitation only conditions of very mild pyrolysis were simulated and as expected no major changes in RSF were detected in this type of experiments.

Fig. 2 shows a series of XANES spectra as a function of heating conditions. As the temperature is increased, there is some broadening and loss of resolution of the XANES features. There are no significant peak shifts, peak removal or new peak appearance. Introduction of oxygen into the in-situ cell, to simulate gasification, accelerated these changes only very slightly. A small pre-edge peak intensifies and grows with heat treatment. This peak, presumably, represents a transition of the photoelectron from 1s to a hybridized 3d/2p level formed by Ca to O bonding. The intensity of this peak may, therefore, be indicative of the degree of loss of carboxyl molecules and Ca-O clustering to reach the final stage of CaO. An edge fitting computer program was used to generate the XANES by using the sum of a step and several Lorentzian functions (24). Thus each feature of XANES can be isolated and studied separately. Fig.3 shows the area of this pre-edge peak as a function of heating conditions. The pre-edge feature intensity may vary with the symmetry of the site (25) and it is possible that the Ca site becomes more asymmetric with pyrolysis.

Fig.4 shows a series of XANES spectra of K loaded char at differing heating conditions. Unlike Ca, the XANES spectra of K loaded char indicate a distinct transformation leading to a possibility of phase change. On switching from pyrolysis to gasification conditions, K dispersed in the coal char rapidly agglomerates and forms K_2CO_3 which does not undergo any further transformation under the mild gasification conditions of our experiments.

CCSEM analysis is not well suited for the early stages of pyrolysis and gasification as the catalytic species are very fine and uniformly dispersed. However, in advanced stages of gasification, when the agglomeration of catalysts occurs, CCSEM methods can be used. Presently, we are working with the severely pyrolyzed and ash samples. X-ray mapping feature of CCSEM is very promising. In this way we can directly observe the discrete inorganic particles and the dispersed catalysts in organic phase (26). With pyrolysis and gasification, we can study the agglomeration and reactions of both these phases. Ternary phase diagrams give further insight in this type of reactions (27).

CONCLUSIONS

XAFS spectroscopy is an excellent method to investigate structure of Ca and K catalysts. Ca agglomerates during pyrolysis and gasification at high temperatures. It forms CaO particles under slow pyrolysis conditions. In-situ methods can be used to study this in further detail. Carboxyl-bound K in lignites forms K_2CO_3 during gasification but does not exhibit any major changes under mild pyrolysis and gasification conditions. CCSEM is an excellent tool for analyzing agglomeration and clustering at advanced stages of gasification. X-ray mapping provides direct evidence of presence of bulk discrete mineral phases and dispersed catalytic species in the matrix. Agglomeration and reaction of these phases can be directly observed with this tool.

ACKNOWLEDGEMENTS

This work was supported by the Gas Research Institute. We also acknowledge the U.S. DOE for its support of the Stanford Synchrotron Radiation Laboratory, where the XAFS experiments were performed.

REFERENCES

1. Fuel, special issue on fundamentals of catalytic coal and carbon gasification 62(2), 1983
2. Fuel, special issue on conf. on C and catalysis, 63(8), 1984
3. T. duMotal, British patent 2548 (1887)
4. F.E. Huggins, G.P. Huffman, F.W. Lyttle, R.B. Greegor, Proc. of 1983 Int. COnf. on coal Sc., Pittsburgh, (1983) p.679-682
5. G.P. Huffman, F.E. Huggins, THe chemistry of low rank coals, Ed. H.H. Schobert, ACS, (1984) p.159-174
6. W.P. Haynes, S.J. Gasior, A.J. Forney, ACS, Advances in Chemistry Series, 131, (1974), p.179
7. J.E. Gallagher, C.A. Euker, Energy Research, (1980), p.4
8. N. Kayembe, A.H. Pulsifer, Fuel, 55, (1976), p.211
9. D.W. McKee, C.L. Spiro, P.G. Kosky, E.J. Lamby, ACS Fuel Div. preprints, 27(1),(1982), p.74
10. K. Otto, L. Bartosiewicz, M. Shelef, Carbon, 17, (1979), p.351
11. D. W. McKee, Carbon, 17, (1979), p.419
12. R. A. Ross, P. Fong, Ind. Eng. Chem. Prod. Res. Dev., 21, (1981), p.197
13. E. J. Hippo, R.G. Jenkins, P.L. Walker, Fuel, 58, (1979), p.338
14. J. Wong, C.L. Spiro, D.H. Maylotte, F.W. Lyttle, R.B. Greegor, EXAFS and Near Edge Structure III, Springer Verlag, (1984), 362-367
15. F.E. Huggins, G.P. Huffman, R.J. Lee, ACS Symp. Ser. 205, 'Coal and Coal Products: Analytical characterization techniques' (Ed: E.L. Fuller), (1982), p.239-258.
16. E.A. Stern, S. Heald, Rev. Sci. Instrum., 50, (1979), 1579.
17. Available from the EXAFS Co., Seattle, WA
18. L.R. Radovic, P.L. Walker, R.G. Jenkins, Fuel, 62, (1983), p.209
19. P.A. Lee, P.H. Citrin, P. Eisenberger, B.M. Kincaid, Rev. Mod. Phys., 53, (1981), 769
20. G. S. Brown, S. Doniach, 'Synchrotron Radiation Research, Eds.: H. Winick, S. Doniach, Plenum PRess, (1980), 353-385
21. F.E. Huggins, N. Shah, G.P. Huffman, F.W. Lyttle, R.B. Greegor, Fuel, To be published.
22. F.E. Huggins, G.P. Huffman, N.Shah, R.G. Jenkins, F.W. Lyttle, R.B. Greegor, Fuel, 67, (1988), 938.
23. F.E. Huggins, G.P. Huffman, N. Shah, F.W. Lyttle, R.B. Greegor, R.G. Jenkins, Physica B, to be published.
24. R.B. Greegor, Edgefit computer program.
25. G.A. Waychunas, G. E. Brown Jr., C.W. Ponader, W.E. Jackson, Nature, 332(17), (1988), 251
26. G.P. Huffman, F.E. Huggins, R.W. Shoenberger, J.S. Walker, F.W. Lyttle, R.B. Greegor, Fuel, 65, (1986), p.621-632.
27. G.P. Huffman, F.E. Huggins, N. Shah, these preprints.

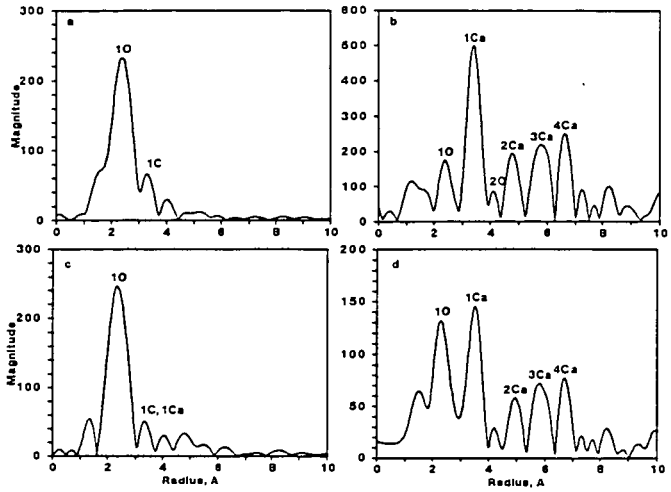

Fig. 1 Radial Structure Function of Ca K-edge EXAFS. (A) Ca loaded Falkirk lignite; (B) CaO; (C) Lignite char after Rapid pyrolysis at 1000C; (D) Lignite char after slow pyrolysis at 1000C.

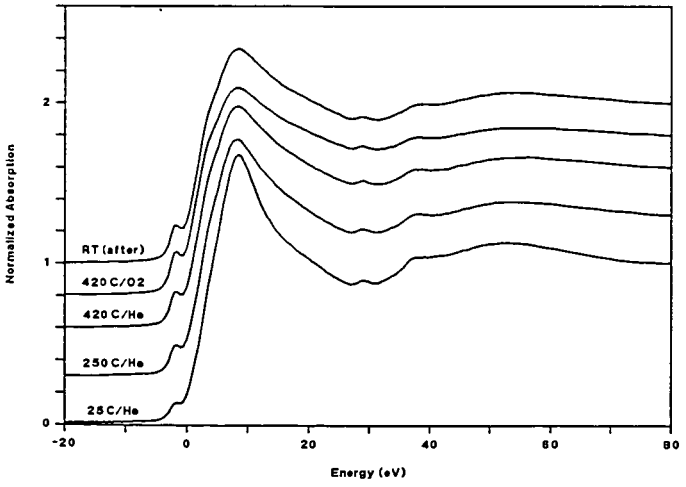

Fig. 2 In-situ XANES spectra of Ca-loaded lignite under He and then 10%O_2-90%He atmosphere at varying pyrolysis/gasification conditions.

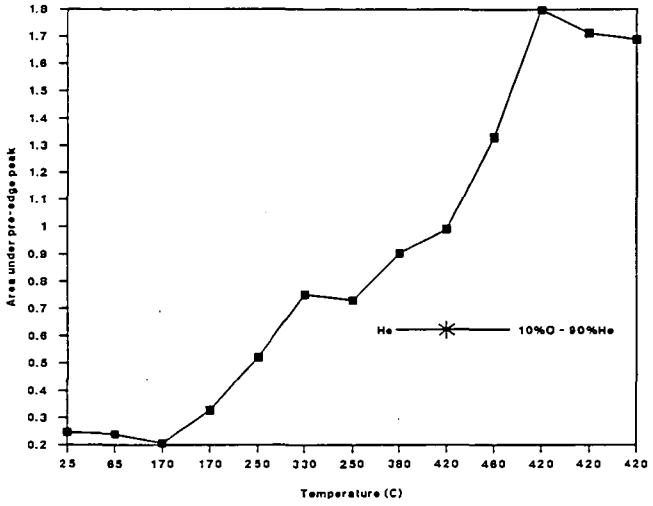

Fig. 3 Area under pre-edge peak of XANES spectra of Ca-loaded lignite at varying pyrolysis/gasification conditions.

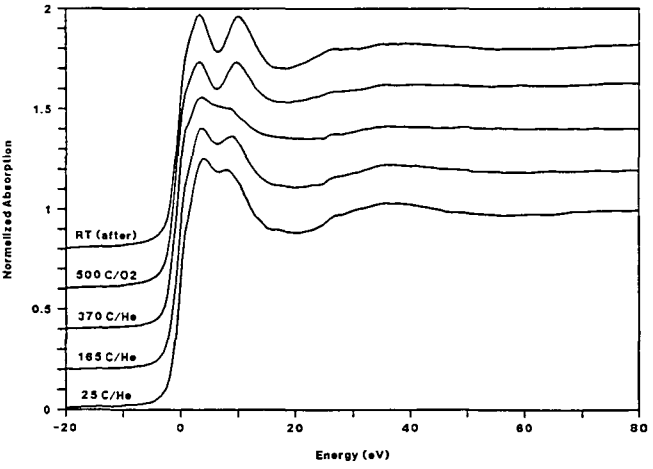

Fig. 4 In-situ XANES spectra of K-loaded lignite under He and then $10\%O_2$-90%He atmosphere at varying pyrolysis/gasification conditions.

CATALYST LOSS AND RETENTION DURING ALKALI CATALYSED CARBON GASIFICATION IN CO_2

R. Meijer, M. Weeda, F. Kapteijn and J.A. Moulijn

Institute of Chemical Technology, University of Amsterdam
Nieuwe Achtergracht 166, 1018 WV Amsterdam, The Netherlands

Abstract

CO_2-chemisorption appears to be a useful method to characterize alkali-metal-oxide clusters. Although after heat treatment the number of catalytic active sites present on the carbon surface decreases significantly, reactivity and stoichiometry of the sites is not affected by reduction and considerable catalyst loss. The amount of alkali metal that can ultimately be stabilised on the carbon surface during alkali catalysed gasification in CO_2 and heat treatment in helium is primarily dependent on the characteristics of the applied carbon.

Introduction

It is well known that addition of alkali metals to carbonaceous materials has a catalytic effect on gasification. Although the detailed mechanism of catalytic gasification is not completely understood, a generally postulated mechanism [1-5] for catalytic gasification consists of an oxidation-reduction cycle in which oxygen is transferred to the carbon matrix through the active alkali-metal-oxide species (1),(2), followed by decomposition of the oxidised carbon site (3), producing CO. The latter step is generally accepted to be the rate determining step in this process, in which [*] and [O-*] represent the 'empty' and oxygen containing alkali metal species active for oxygen transfer to a free carbon site C_f resulting in a surface oxygen complex C(O).

$$CO_2 + * \underset{k_{-1}}{\overset{k_1}{\rightleftharpoons}} CO + O\text{-}* \qquad (1)$$

$$O\text{-}* + C_f \underset{k_{-2}}{\overset{k_2}{\rightleftharpoons}} C(O) + * \qquad (2)$$

$$C(O) \xrightarrow{k_3} CO + C_f \qquad (3)$$

Kinetic measurements have shown that addition of alkali metal enhances the steady state concentration of C(O) complexes, rather than altering the reaction pathway [3,6,7,8]. In many studies published rates of gasification and oxygen-exchange and results of temperature programmed desorption are related to the initial amount of alkali metal present on the sample [2,9]. By heat treatment (TPD or gasification) catalyst can be lost, the amount being dependent on the alkali metal, temperature and nature of the carbon. Therefore the conclusions of studies that do not account for this effect should be considered with caution.

The amount of alkali metal actually present on the carbon surface is therefore an important parameter in the interpretation of rate, chemisorption and desorption data and understanding of the mechanism of catalysed gasification. Loss of active catalyst can be due to several processes: 1) evaporation of alkali metal (oxide); 2) formation of inactive alkali metal species due to reaction with mineral matter; 3) formation of inactive alkali metal carbonate species; 4) diffusion from the reaction surface into the carbon matrix.

The aim of this study was to examine if and to what extent catalyst loss occurs during potassium catalysed gasification in CO_2 of Norit RX1 Extra samples and how this affects the nature and stoichiometry of the remaining catalytic sites. This was achieved by determination of the potassium content after reactivity measurements, CO_2-chemisorption and temperature programmed desorption. The properties of the carbon have been varied by pretreatment in an inert atmosphere (Ar) at temperatures up to 2000 K.

Experimental

I. *Sample preparation*

The activated carbon used in this study is Norit RX1 Extra, an acid washed, steam activated peat char with a high specific surface area (1100 $m^2.g^{-1}$ (CO_2(DR),273 K), 1500 $m^2.g^{-1}$ (N_2(BET),77 K), d_p = 0.25−0.6 mm). Addition of catalyst (0−20 wt% K_2CO_3) to fresh and heat treated (up to 2000 K in argon) carbon samples was performed by pore volume impregnation with an aqueous solution. The initial catalyst loading is expressed as the atomic potassium to carbon $(K/C)_i$ ratio. The alkali metal content was determined (in duplo) by Inductive Coupled Plasma Atomic Emission Spectroscopy (ICP−AES), after acid washing of the samples (2% HNO_3).

II. *Apparati*

The data obtained in this study were generated in a Fixed−Bed flow Reactor (FBR). Experiments in a thermobalance (SETARAM TG 85) were performed for monitoring weight changes during CO_2−chemisorption, Temperature−Programmed−Desorption (TPD) and gasification experiments.

Basically the FBR apparatus [10] consists of two gas mixing sections in which the desired gas mixture can be generated, an oven (T_{max} = 1273 K) containing the carbon sample in a quartz reactor (I.D. = 3 − 5 mm , P_{max} = 0.15 MPa) and a GC (He carrier, TCD detection) and MS (Leybold−Heraeus Q200) for gas analysis. All gases used are of HP or UHP grade and are purified (O_2 and/or H_2O removal) before they are fed to the reactor.

III. *Experimental procedure*

In this study two experimental schemes were applied (figure 1). Resulting in the following seven different procedures (stages between brackets are optional):

type	treatment
1a	SSG
1b	SSG − TPD − SSG
1c	SSG − CO_2-chem. − TPD
1d	SSG − [CO_2-chem.] − TPD − CO_2-chem. − TPD
2a	TPD
2b	TPD − SSG − [TPD]
2c	TPD − CO_2-chem. − TPD

The first step in each experiment was drying *in situ* (T = 473 K, He) of the catalyst/carbon sample (50−100 mg). Partial gasification of the catalyst/carbon sample was performed in 20 μmol $CO_2.s^{-1}$ (T = 1000 K ; P = 0.12 MPa). The steady state gasification rate (SSG) in the FBR is based on either the actual amount of potassium (r_K) or the initial amount of carbon (r_n) present, and expressed as (μmol carbon gasified).(μmol K_a or C_i)$^{-1}$.s^{-1}.

TPD patterns in the FBR are obtained in a flow of 20 μmol $He.s^{-1}$ with a heating rate of 10 $K.min^{-1}$ up to 1200 K, followed by an isothermal period of 30 minutes at 1200 K. The amount of CO and CO_2 released expressed as (μmol CO_x desorbed).(μmol K actually present)$^{-1}$.s^{-1} is plotted as a function of temperature.

After partial (approximately 25% burn−off) gasification in CO_2 (type 1 experiments) the sample was exposed to helium at 1000 K and cooled to 673 K followed by either TPD and gasification (type 1b), CO_2−chemisorption and TPD (type 1c), or a second CO_2−chemisorption and TPD cycle (type 1d).

After TPD of a fresh sample (type 2 experiments) the sample was cooled to either room temperature for potassium analysis (type 2a), to 673−873 K for CO_2−chemisorption (type 2b) or 1000 K for gasification (type 2c), followed by a second TPD.

At the end of each experiment the sample was cooled to room temperature and the potassium content of the residue was determined. The potassium could be quantitatively recovered from the catalyst/carbon residue with an aqueous 2% HNO_3 solution.

Results

Gasification reactivity vs catalyst loading.

The steady state gasification rate for fresh and residual K_2CO_3/Norit RX1 samples is shown in figure 2. For fresh samples (open symbols) the observed gasification rate r_K at 25% burn−off clearly shows a constant value at $(K/C)_a > 0.02$. Over this K/C range investigated the activity per potassium atom is constant. The observed gasification rate r_K of residual samples (closed symbols), independent of the initial loading, corresponds well with rates of fresh samples. Clearly the reactivity per K atom is not affected by extensive potassium loss and repeated heat treatments up to 1200 K.

Figure 3 gives the fraction of catalyst still present as a function of burn−off for samples with different initial potassium loading. It was found that already at low burn−off about 20 to 40 % of the potassium is lost, independent of the initial catalyst loading. This amount remains further fairly constant over the burn−off range investigated (0−60%).

In figure 4 the K/C ratio based on the K actually present (ICP−AES values) is plotted as a function of the K/C ratio calculated from the amount of K initially added. Clearly during TPD extensive potassium loss takes place. During a second heat treatment up to 1200 K no extensive additional catalyst loss occurs. The results show that the amount of alkali metal that can be stabilised on the carbon surface (K/C = 0.018−0.02) during TPD up to 1200 K is nearly independent on the initial alkali metal loading. Furthermore, the amount of alkali metal that ultimately can be stabilised on the carbon surface is strongly affected by the temperature at which the carbon sample has been pretreated (K/C ≃ 0.007 ; $T_{pretreat}$ = 1650−2000 K).

Thermogravimetric measurements show that the amount of oxygen present in the carbon sample decreases with increasing heat treatment temperature.

Outgassing patterns

TPD patterns of fresh carbon/catalyst samples (type 2a,2b,2c) are very reproducible and are fairly similar for all samples investigated. They exhibit a low temperature (400 − 950 K) CO_2 desorption, followed by a two peak CO desorption. The first CO desorption is due to gasification of desorbed CO_2 [11], while the second is ascribed to decomposition of phenolate groups [7,11,12,13,14], the anchors for the alkali−metal−oxide clusters active for alkali catalysed gasification. TPD patterns obtained after gasification in CO_2 at 1000 K and subsequent cooling in helium show only one CO peak. In general the maximum CO desorption shifts to lower temperature with increasing alkali metal loading and the CO/K_a desorption ratio decreases in the same order.

In figure 5a TPD patterns are shown after SSG followed by CO_2−chemisorption at 673 K. The low temperature CO_2−desorption is associated with this CO_2−chemisorption, whereas the high temperature CO desorption is similar as obtained from a TPD after SSG without chemisorption.

TPD patterns after TPD and CO_2−chemisorption at 673 K (type 1d,2c) also show low temperature CO_2 desorption from the alkali metal cluster (figure 5b). The amount of CO or CO_2 desorbed has been corrected for potassium loss during the first TPD. From figure 5b it is clear that independent of the initial potassium loading the TPD patterns are comparable, since the amount of potassium present during this second TPD is about the same for all three samples. However the amount of CO desorbed per K atom present (0.3−0.4) during this TPD (figure 5b) is considerably lower than in a TPD after gasification (0.9, figure 5a).

In figure 6 the outgassing patterns of differently treated samples are compared. A fresh sample shows extensive low temperature CO_2 desorption and only a small amount of high temperature CO desorption. If CO_2−chemisorption is performed at 873 K the total amount of CO/K_a desorbed increases significantly compared with CO_2−chemisorption at 673 K, approaching the CO/K_a ratio desorbed after partial (25% burn−off) gasification at 1000 K (CO/K_a= 0.9). The maximum CO desorption shifts to a temperature comparable to that of desorption of phenolate like species. The amount of CO_2/K_a desorbed decreases with increasing chemisorption temperature (0.33 → 0.22).

Experiments performed in the thermobalance with catalyst/carbon samples show an instantaneous weight increase on CO_2 introduction at 673 K, corresponding to a CO_2/K_a ratio of approximately 0.3, which is in agreement with the TPD results. Pure carbon shows no weight change, thus the assumption that the weight increase can be attributed to CO_2 in the alkali−metal−oxide cluster is justified.

Discussion

The fact that during alkali catalysed gasification, using pore volume impregnated catalyst/carbon samples, catalyst loss at low burn−off is substantial (figure 3) was also found by Sulimma et al. [15] in the case of steam gasification. They furthermore observed a substantial increase in catalyst loss with increasing burn−off.

Our results concerning the amount of alkali metal that can ultimately be stabilised by the carbon surface are consistent with results reported in literature. Shadman et al. [16] reported K/C = 0.002 after complete reduction in nitrogen at 1073 K for an alkali−carbonate/Carbopack B sample (graphitized carbon , S_a = 100 $m^2.g^{-1}$).

The fact that potassium shows interaction with the carbon, resulting in an amount that can be stabilised on the carbon at high temperature was already observed by Tromp and Cordfuncke [17]. They also concluded that pretreatment of a catalyst/activated carbon sample at higher temperature resulted in an decrease in alkali carbon interaction. Saber et al. [18] concluded that after heat treatment in an inert atmosphere at 1350 K the amount of potassium loss by volatilization increases with decreasing oxygen content of the carbon. This is consistent with our data which show that after heat treatment of the carbon sample (1650−2000 K) the K/C ratio that can ultimately be stabilised by the carbon surface at 1200 K is considerably lower than for unpretreated samples (K/C = 0.007 vs. 0.018).

Gasification of K_2CO_3/Norit RX1 residues which have undergone considerable catalyst loss, shows that the observed gasification rate per μmol potassium present (r_K) is similar to that of fresh samples with the same $(K/C)_a$ ratio. Sams et al. [19] concluded that independent of initial loading and heat treatment time the rate is an unique function of the $(K/C)_a$ ratio with the restriction that the K/C value is below the saturation level.

The percentage and rate of potassium loss during alkali catalysed gasification or heat treatment in an inert atmosphere reported in literature differ enormously [8,14,15,16,18,19]. The amount of alkali metal that can ultimately be stabilised on the carbon surface is dependent on the characteristics of the applied carbon (oxygen content and heat treatment temperature). The rate at which potassium is lost is however strongly dependent on the experimental conditions (apparatus, *T*, *P*, flow rate, gas phase) and the method of impregnation [15].

Outgassing patterns

TPD patterns of fresh and partial gasified alkali−carbonate/Norit RX1 Extra samples are in good agreement with earlier reported patterns by Kapteijn et al. [11]. From figure 5a it can be seen that CO_2−chemisorption at 673 K after partial gasification produces the same CO desorption pattern as with direct outgassing after gasification. Samples with different initial catalyst loading still show distinct differences in outgassing pattern. A second outgassing with the same sample (figure 5b) shows that, as expected from the alkali metal measurements, the CO_2 and CO outgassing patterns have become rather independent of the initial catalyst loading; it is also clear that the amount of CO desorbed (CO/K_a = 0.3−0.4) is considerably lower than after gasification or CO_2−chemisorption at 873 K (CO/K_a = 0.9).

CO_2−chemisorption after TPD shows a distinct difference in CO desorption pattern with increasing chemisorption temperature (figure 6). From the absence of high temperature CO desorption it is concluded that at low CO_2−chemisorption temperature (673 K) it is not possible to restore all catalytic sites active for gasification. This indicates that, although CO_2 is chemisorbed at 673 K inside the alkali−metal−oxide cluster, only a small amount of oxygen is built in with direct interaction with the carbon. Ratcliffe [12] showed that on outgassing of a K_2CO_3/Spherocarb sample after $^{13}CO_2$−chemisorption at 333 K , ^{13}CO desorption as a result of $^{13}CO_2 + C_f \longrightarrow {}^{13}CO + C(O)$ was detected between 700 and 800 K. This ^{13}CO desorption was followed at higher temperature by ^{12}CO release, with a maximum at 1030 K due to desorption of the oxidized carbon sites. This was also reported by Kelemen and Freund [8] and corresponds to the outgassing patterns in figure 5b in which clearly two ^{12}CO desorption peaks can be observed. The first is due to decomposition of chemisorbed CO_2, the second can be described to two processes: a minor desorption of oxidised carbon sites ($C(O) \rightarrow CO$), and a major decomposition of 'phenolate' groups ($C-O-K \rightarrow CO + K$), being the anchors for the catalytic active alkali−metal−oxide species.

Although CO_2−chemisorption at 673 K after TPD shows a low CO/K_a ratio (±0.3) the same CO_2/K_a ratio (±0.3) is found as after gasification.

These values are in good agreement with CO_2-chemisorption results reported by Mims and Pabst [4], Ratcliffe and Vaughn [13], Cerfontain [20] and Koenig [21], indicating that the alkali metal cluster even after reduction and considerable catalyst loss, can chemisorb one CO_2 molecule per every 3 to 4 potassium present on the surface.

Conclusions

The most important conclusions that arise from this study are:

* The amount of potassium that can ultimately be stabilised on the carbon surface is primarily dependent on the oxygen content of the carbon. This can be reduced by heat treatment of the applied carbon.
* Although the number of active sites present on the carbon surface decreases significantly during TPD or gasification, the intrinsic reactivity and stoichiometry of the sites under gasification conditions is not affected.
* CO_2-chemisorption below 700 to 800 K is not capable of completely restoring the 'phenolate' groups that act as the anchors of the catalytic active alkali-metal-oxide sites. Above this temperature clearly these groups are formed.
* The catalytic active potassium (oxide) cluster is capable of chemisorbing one CO_2 molecule per every 3 to 4 potassium atoms present. This seems to be generally valid.

Acknowledgement

These investigations have been executed within the framework of the Dutch National Coal Research Programme (NOK), which is managed by the Project Office for Energy Research (NOVEM) and financed by the Ministry of Economic Affairs.

References

[1] Kapteijn, F., and Moulijn, J.A., *Fuel*, 62, 221 (1983)
[2] Cerfontain, M.B., Meijer, R., and Moulijn, J.A., *Proc. Int. Congress on Coal Science, Sydney, 277 (1985)*
[3] Kapteijn, F., Peer, O., and Moulijn, J.A., *Fuel*, 65, 1371 (1986)
[4] Mims, C.A., and Pabst, J.K., *J. Catal.*, 107, 209 (1987)
[5] Moulijn, J.A., Cerfontain, M.B., Kapteijn, F., *Fuel*, 63, 1043 (1984)
[6] Freund, H., *Fuel* 64, 656 (1985)
[7] Cerfontain, M.B., and Moulijn, J.A., *Advances in Coal Chemistry (ed. N.P. Vasilakos Theophrastus Publ. Co., Athene, Greece,* 233-263 (1988)
[8] Kelemen S.R., and Freund, H., *J. Catal.*, 102, 80 (1986)
[9] Sams, D.A., and Shadman, F., *Fuel*, 62, 880 (1983).
[10] Meijer, R., Kapteijn, F., and Moulijn, J.A., to be published.
[11] Kapteijn, F., Abbel, G., and Moulijn, J.A., *Fuel* 63, 1036 (1984)
[12] Ratcliffe, C.T., *Proc. Int. Congress on Coal Science, Sydney, Australia*, 281 (1985)
[13] Ratcliffe, C.T., and Vaughn, S.N., *Prep. Am. Chem. Soc. Div. Fuel Chem.*, 30, 304 (1985)
[14] Mims, C.A., and Pabst, J.K., *Fuel*, 62, 176 (1983)
[15] Sulimma, A., Mühlen, H.-J., and van Heek, K.H., *Proc. Int. Congress on Coal Science, Maastricht, The Netherlands*, 551 (1987)
[16] Shadman, F., Sams, D.A., and Punjak, W.A., *Fuel*, 66, 1658 (1987)
[17] Tromp, P.J.J., and Cordfunke, E.H.P., *Thermochim. Acta*, 81, 113 (1984)
[18] Saber, J.M., Falconer, J.L., and Brown, L.F., *Fuel*, 65, 1356 (1986)
[19] Sams, D.A., Talverdian, T., and Shadman, F., *Fuel* 64, 1208 (1985).
[20] Cerfontain, M.B., Meijer, R., Kapteijn, F., and Moulijn, J.A., *J. Catal.*, 107, 173 (1987)
[21] Koenig, P.C., Squires, R.G., and Laurendeau, N.M., *J. Catal.*, 100, 228 (1986)

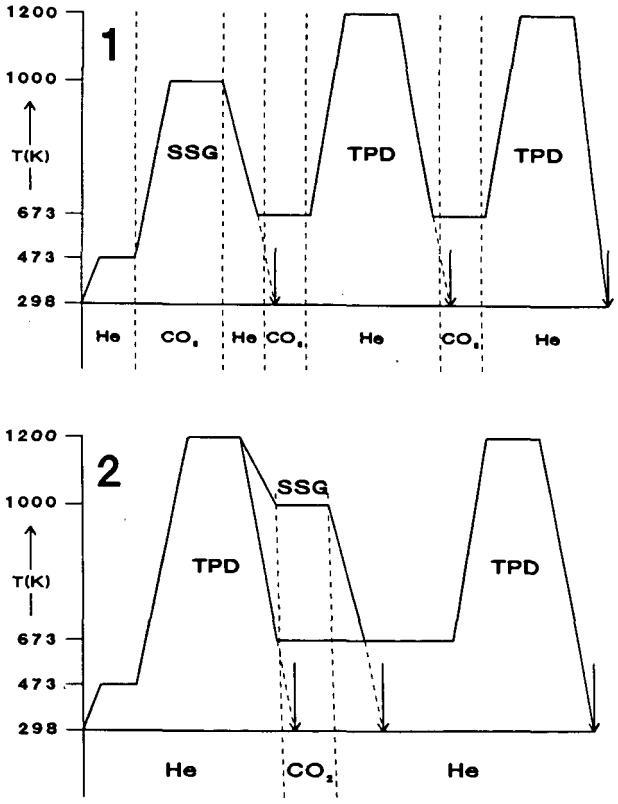

Figure 1 : Experimental procedures: type 1 (upper part) and type 2 (lower part). SSG and TPD refer to Steady State Gasification and Temperature Programmed Desorption.
The arrows indicate the points in the experiments at which alkali metal determinations were performed.

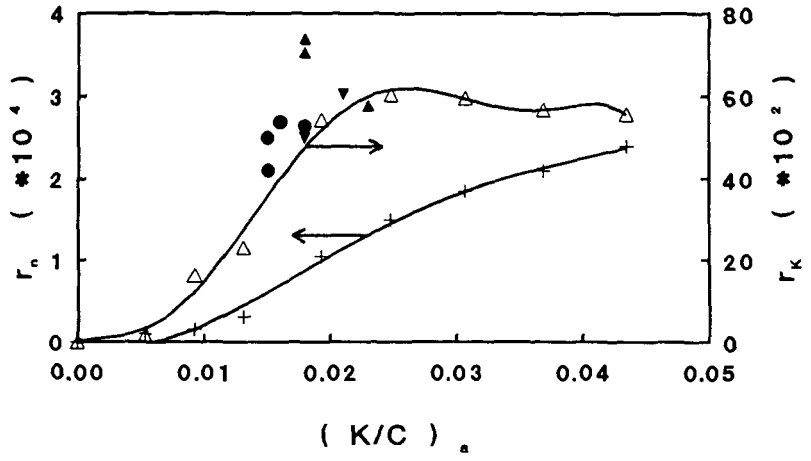

Figure 2 : Steady state gasification rate (T=1000 K, P=0.12 MPa) of fresh (open symbols) and residual (closed symbols) K_2CO_3/Norit RX1 samples as a function of the actual K/C ratio (+ - r_n ; △ - r_K ; ● $(K/C)_{initial}$ = 0.019; ▼ $(K/C)_{initial}$ = 0.031; ▲ $(K/C)_{initial}$ = 0.043).

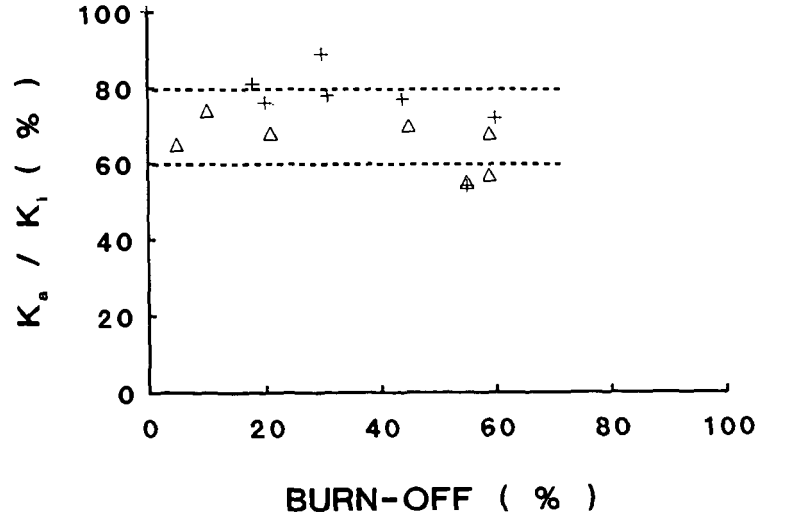

Figure 3 : Catalyst loss (K_a/K_i)as a function of burn-off during alkali catalysed gasification in CO_2 (T=1000 K, P=0.12 MPa).
+ $(K/C)_{initial}$ = 0.019
△ various loadings: $(K/C)_{initial}$ = 0.0054 - 0.0435

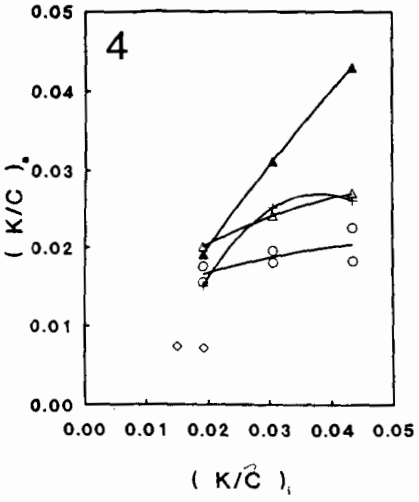

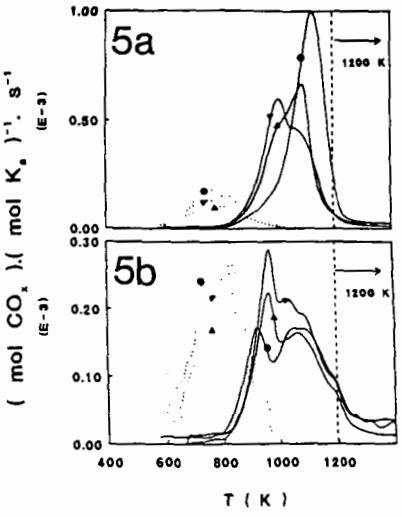

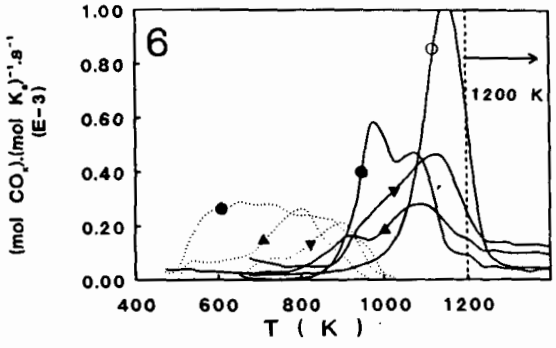

Figure 4 : Actual (K/C) ratio as a function of the initial (K/C) ratio after different treatment: ▲ no treatment; + TPD; △ SSG and TPD; ○ second TPD; ◇ TPD heat treated carbon samples.

Figure 5 : First(5a) and second(5b) TPD patterns after CO_2-chemisorption at 673 K (type 1d experiment) of samples with varying initial potassium loading. (----- = CO_2 ; ——— = CO ; ● $(K/C)_{initial}$ = 0.019 ; ▼ $(K/C)_{initial}$ = 0.031 ; ▲ $(K/C)_{initial}$ = 0.043)

Figure 6 : TPD patterns for K_2CO_3/Norit RX1 Extra $(K/C)_{initial}$ = 0.019 samples (---- = CO_2 ; ——— = CO).
- ● fresh sample
- ▲ after TPD and CO_2-chemisorption at 673 K
- ▼ after TPD and CO_2-chemisorption at 873 K
- ○ after partial gasification (CO_2 , 1000 K) to approximately 25 % burn-off.

A MODEL OF NICKEL-CATALYZED GASIFICATION

M. E. Vincett, C. R. F. Lund, and J. Tsamopoulos
Chemical Engineering Department
SUNY-Buffalo, New York, 14260

ABSTRACT

The diffusion of carbon through a spherical nickel catalyst particle has been modeled using a finite elements approach. A steady-state model (applicable to gasification of carbons which do not lead to catalyst deactivation) is capable of explaining reported variations in reaction rate with catalyst particle size. The model uses reported values for the diffusion coefficient and solubility of carbon in nickel, and the necessary rate constants are determined from available rate data. This has the benefit of producing a model with few adjustable or empirical constants. An unsteady-state model has also been developed and can be used to explain observed deactivation with this catalyst system.

INTRODUCTION

The gasification of carbons and coals using transition metal catalysts is well-studied experimentally, but there are several observed phenomena which are still not fully understood. With nickel catalysts for example, it has been observed that the apparent activation energy for the reaction changes as the temperature increases (1,2). Also with nickel catalysts and certain carbons there is a continuous deactivation of the catalyst as reaction proceeds (2,3,4). Recently studies have been made wherein the combined diffusion and reaction phenomena have been modeled in an attempt to explain the observed behavior of transition metal catalysts during carbon gasification (5,6). In these studies a major focus has been the explanation of the dependence of the rate of gasification upon the size of the catalyst particle. The controlled-atmosphere electron microscopy (CAEM) technique has provided a wealth of rate versus particle size data (7-9).

The present study also involves the formulation of a model which includes both diffusion and reaction phenomena occurring within and on a single catalyst particle. Previous models have used cubic (5) and cylindrical (6) particle shapes and have considered channeling along the surface of a graphite basal plane. Spherical particles tunneling inside the carbon matrix have been modeled in this study. Consequently, the results are not influenced by the channel depth. In addition to the dependence of the rate of particle movement (i. e. the rate of gasification) upon particle size, temperature effects have also been examined. This has been done in two different ways. First the shape of the rate versus particle size curve has been computed at a number of temperatures in the range of practical gasification conditions. Additionally, for a single, representative particle size the dependence of the rate of particle movement has been calculated as a function of temperature.

METHODS

Nickel was chosen as the catalytic material to be modeled. Nickel is very active at low temperatures, and low temperature operation is desirable for thermodynamic reasons if methane is the desired product. Nickel remains

metallic under most gasification conditions, but it does deactivate (4). Additionally, the properties of carbon-nickel alloys are readily available due to the importance of these materials in steelmaking. The carbon was assumed to be isotropic and to be essentially free of impurities which would poison the catalyst.

Figure 1 depicts a spherical nickel particle as it catalyzes the gasification of carbon. The particle has one hemispherical surface which is in immediate contact with the carbon, and another which is exposed to the gas phase. As the carbon is gasified, the particle moves through the carbon creating a tunnel (or if it is on a basal plane surface of graphite it would create a channel like those which have been observed by CAEM). A spherical co-ordinate system centered on the particle center is shown in the figure. In this system r is the distance from the center of the particle and θ is the angle measured from a line along the tunnel centerline.

It is assumed that the problem will be symmetric about the tunnel axis, and that carbon will dissolve into the particle along the leading hemisphere (from $\theta = \pi/2$ to $\theta = \pi$). The carbon is assumed to diffuse through the particle to emerge on the surface of the trailing hemisphere (from $\theta = 0$ to $\theta = \pi/2$). Finally the carbon reacts with oxygen atoms adsorbed on this surface producing the gasification products.

A material balance on the carbon within the particle at steady-state requires that

$$D \cdot \nabla^2 C = 0 \qquad (1),$$

where D is the diffusion coefficient and C is the concentration of dissolved carbon in the metal. As discussed by Tsamopoulos et al. (6) the boundary condition imposed at the leading hemisphere is that the flux in the direction of tunneling is constant, and this flux is chosen such that the particle is just saturated with carbon at the leading point $\theta = \pi$. Additionally it is assumed that there is no flux in the θ direction at $\theta = 0$ and at $\theta = \pi$. Finally on the trailing hemisphere the flux of carbon is set equal to the rate of reaction.

The form of the rate expression used on this surface was derived by assuming that the gas phase composition in the vicinity of the particle is constant and that a pseudo-equilibrium is established between gas phase H_2O and H_2 and surface oxygen. This gives a rate expression of the form

$$r = k \cdot \theta_C \cdot (1 - \theta_C) \qquad (2),$$

where r is the reaction rate, k is a combination of rate constants, the pseudo-equilibrium constant and H_2O and H_2 partial pressures, and θ_C is the fractional surface coverage of carbon. In the present study the bulk concentration at the surface has been converted to a fractional surface coverage by simply preserving the ratio of carbon to nickel atoms. That is, no surface enrichment or bulk enrichment has been accounted for.

The Galerkin/finite elements approach was used to solve equation (1) subject to these boundary conditions. Published values of the solubility of carbon in nickel and the diffusion coefficient of carbon in nickel were used (10-12).

The value of the constant k in equation (2) was found using a particle size of 6 nm, a rate of 0.252 mmol C/(min mg_{Ni}), and a temperature of 825 K. A second value of k, at 975 K, was similarly found using a rate of 1.70 mmol C/(min mg_{Ni}). These values for the rate and average particle size were measured experimentally by Wigmans and Moulijn (2). To find these values of k, equation (1) was solved varying k until the predicted carbon gasification rate matched the experimental rate.

The constant k in equation (2) was then assumed to vary with temperature according to the Arrhenius expression, $k = k_0 \cdot \exp(E_A/RT)$. Thus from these two data points the only "missing" constants in equation (1) and its boundary conditions were found. It is then possible to use the model to predict the rate behavior for any particle size and at any temperature.

RESULTS AND DISCUSSION

Using the procedure described in the preceding section, the activation energy for the surface rate constant was found to equal 7.18 kcal/mol. This value is very low, probably due to the assumption made in relating the bulk concentration to the fractional surface coverage. This is discussed further later in this section.

Equation (1) was then solved for a number of particle sizes and temperatures. The results are plotted in Figure 2 as a family of curves of tunneling rate versus particle size. For each temperature, the rate is plotted relative to a 10 nm particle at that same temperature. In the figure it is seen that as the temperature increases the rate becomes less dependent upon the particle diameter. This is because the rate of diffusion of carbon through the metal increases rapidly with temperature, and at the higher temperatures shown in the figure, the surface reaction has become the rate-limiting step. Indeed, in these cases the solution of equation (1) shows that the particle is essentially saturated with carbon everywhere.

In the original CAEM work reported by Baker and Sherwood (8) a very strong dependence of rate upon particle size was observed at 1150 °C. However in the present modeling study virtually no dependence upon particle size is predicted at this temperature. Subsequent work by Baker et al. (9) indicates that in fact nickel metal is active at much lower temperatures than suggested in (8). Based upon the present results, it might be possible that in the original study (8) the catalyst was nickel oxide and not the metal. If the diffusion coefficient for carbon in nickel oxide was available, equation (1) could be solved to see if a dependence of rate upon particle size would be expected; we could find no values for that diffusion coefficient. It does not seem unlikely, however, that the diffusion coefficient for carbon in nickel oxide would be several orders of magnitude smaller than that for carbon in nickel metal, and consequently a strong dependence of rate upon particle size would be expected for nickel oxide catalyst at 1150 °C.

Equation (1) was solved for a 6 nm particle at a number of temperatures, and the results are plotted in the form of an Arrhenius plot in Figure 3. The two triangles represent the two data points which were used to find E_A and k_0 in the Arrhenius expression. This plot is remarkably similar to the experimental data reported by Wigmans and Moulijn (2) which show an Arrhenius behavior where below ca. 825 K the apparent activation energy is equal to 40.6

kcal/mol, an abrupt change is seen in the apparent activation energy at ca. 825 K, and above this temperature an apparent activation energy of 20.3 kcal/mol is measured. These authors (2) attributed the decrease in activation energy to the onset of mass transfer limitations at the higher temperatures.

When an apparent activation energy is calculated from the slope of Figure 3 in the high temperature region, a value of 16.8 kcal/mol results. A similar calculation in the low temperature region gives an apparent activation energy of 46.0 kcal/mol. These results are remarkably close to those reported by Wigmans and Moulijn. However, the present modeling study shows that in fact the gasification reaction is mass-transfer-limited in the low temperature region, and that the limiting mass transfer is that of carbon through the metal, not that of the gas phase either from the bulk gas to the carbon surface nor of the gas in the pore structure of the carbon.

This is contrary to the traditional situation in catalysis where as the temperature rises mass transfer from the flowing gas to the surface of the solid material can become rate-limiting. Indeed, the apparent activation energy in the high temperature region, 20.3 kcal/mol, is quite high to be assigned to a mass transfer coefficient. Furthermore, the high activation energy at lower temperatures nearly equals the activation energy for the diffusion coefficient of carbon in nickel.

The solution of equation (1) at the higher temperatures reveals that the particle is essentially saturated with carbon throughout its volume. Under these conditions the rate of the reaction will be determined by the rate of the surface reaction as expressed in equation (2). We have assumed that the fractional surface coverage of carbon, θ_C, equals the carbon to nickel ratio in the bulk. At bulk carbon concentrations which are significantly less than saturation this assumption should be reasonably accurate, however, as the bulk concentration approaches saturation it will not be so. Specifically, as the bulk concentration just equals saturation, it would be expected that the fractional surface coverage would just approach 1.0 (then as the bulk concentration surpasses saturation, multi-layer carbon precipitation would ensue). Thus, in a regime where the particles are nearly saturated it would be expected that θ_C would approach 1.0 regardless of the temperature, and this, in turn would mean that the two terms θ_C and $(1 - \theta_C)$ would show very little dependence upon temperature. Then all temperature dependence would be reflected in the surface rate constant, k, and the apparent activation energy would equal the activation energy of the surface reaction rate constant.

Using the assumption that the fractional surface coverage equals the bulk carbon to nickel ratio will result in a value of θ_C which is less than unity, and further, it will result in a value of θ_C which varies with temperature the same way that the carbon solubility does. In this case, the overall temperature dependence will be reflected in the product of the surface rate constant and the fractional surface coverage, and the apparent activation energy would nearly equal the sum of the activation energy of the solubility of carbon in nickel (9.7 kcal/mol (12)) and the activation energy of the surface rate constant.

Hence, if a more reasonable method of relating the surface coverage to the bulk concentration is employed, it is expected that the value of the activation energy for the surface reaction step will increase from the present

value of 7.18 kcal/mol to a value approximately equal to the experimentally observed high temperature value of 20.3 kcal/mol. We are presently pursuing these calculations.

Finally, Kelemen (13) has recently reported that the activation energy for the surface reaction equals 31 to 32 kcal/mol on Ni(111). The present study indicates that the maximum value expected for the activation energy is of the order of 20 kcal/mol. This perhaps suggests that the surface of the active catalyst particles does not resemble a Ni(111) surface.

CONCLUSIONS

The steam gasification of carbon using nickel catalysts appears to be a reaction in which the rate-limiting step changes from diffusion of carbon through the metal at low temperatures to surface reaction kinetics on the metal at high temperatures. This results in a particle size dependence of the rate of gasification which changes as the temperature changes.

REFERENCES

1. Bernardo, C. A., and Trimm, D. L., *Carbon* **17**, 115 (1979).

2. Wigmans, T., and Moulijn, J. A., in "New Horizons in Catalysis," (*Proc. 7th Int. Congr. Catal.*), Seiyama and Tanabe, eds., vol. 7A, p. 501. Elsevier, New York, 1981.

3. Colle, K. S., Kim, K., and Wold, A., *Fuel* **62**, 155 (1983).

4. Lund, C. R. F., *J. Catal.* **95**, 71 (1985).

5. Choi, A. S., Devera, A. L., and Hawlay, M. C., *J. Catal.* **106**, 131 (1987).

6. Tsamopoulos, J., Dandekar, H. W., and Scholtz, J., submitted to *J. Catal.*

7. Baker, R. T. K., *Catal. Rev. - Sci. Eng.* **19**, 161 (1979).

8. Baker, R. T. K., and Sherwood, R. D., *J. Catal.* **70**, 198 (1981).

9. Baker, R. T. K., Chludzinski, J. J., Jr., and Sherwood, R. D., *Carbon* **23**, 245 (1985).

10. Kovenskiy, I. I., *Fiz. Metal. Metalloved.* **16**; 613 (1963).

11. Massaro, T. A., and Petersen, E. E., *J. Appl. Phys.* **42**, 5534 (1971).

12. Lander, J. J., Kern, H. E., and Beach, A. L., *J. Appl. Phys.* **23**, 1305 (1952).

13. Kelemen, S. R., *Appl. Surf. Sci.* **28**, 439 (1987).

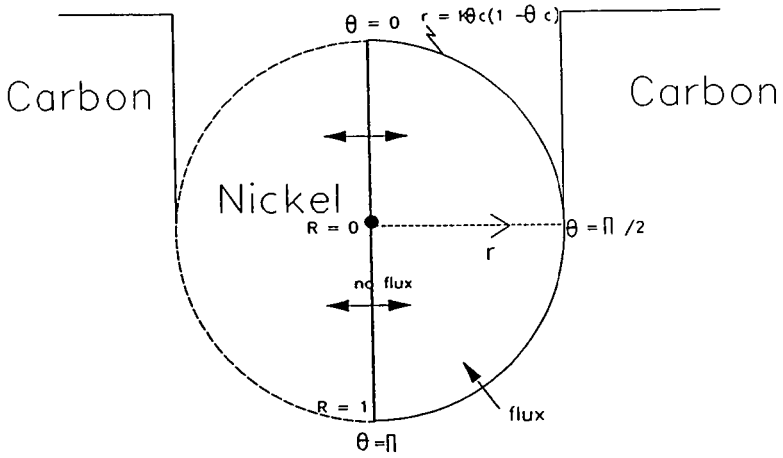

Figure 1. A schematic representation of the catalyst particle during gasification.

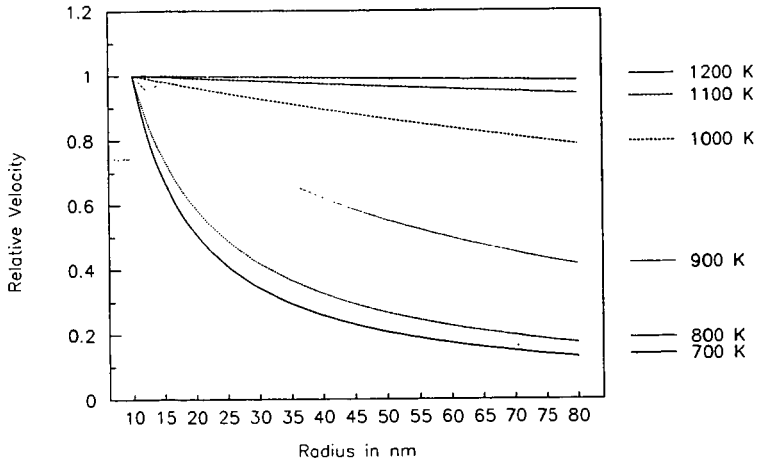

Figure 2. The dependence of the rate of gasification upon the particle size as a function of reaction temperature. At each temperature the rates are normalized to the rate of a 10 nm particle at that temperature.

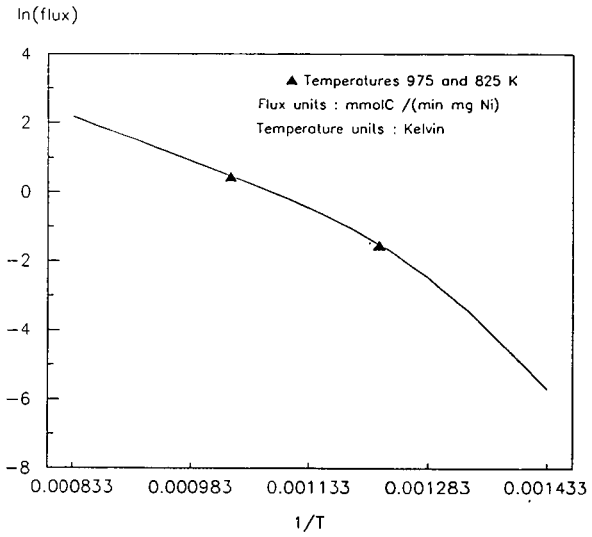

Figure 3. An Arrhenius plot of the rate of gasification computed using the model. The two points represent the experimental data used to find the surface reaction rate constant as described in the text.

IRON GROUP METAL CATALYZED HYDROGASIFICATION IN THE PRESENCE OF SUPPORTED HYDROGENATION NICKEL CATALYST

Shiro Matsumoto

Government Industrial Research Institute, Kyushu
Shukumachi, Tosu, Saga, 841 Japan

INTRODUCTION

The catalytic hydrogasification of "coal" is successfully carried out by Tomita[1] and Hüttinger[2] and their co-workers using nickel and iron as catalysts. On the other hand, hydrogasification of coal char and carbon has attracted a little attention because of strong thermochemical suppression at higher temperature and low gasification rate compared with the gasification by H_2O or CO_2 and also because only noble metals such as platinum show high catalytic activity. But, it is known that iron group metals iron, cobalt and nickel also have catalytic activity for hydrogasification of carbonaceous materials like graphite. The activity and reaction mechanism are well studied using controlled atmosphere electron microscopy[3].

This study shows the reactivity of iron, cobalt and nickel catalyzed char gasification with hydrogen at atmospheric pressure, and that the mixing of supported nickel catalyst with metal loaded char remarkably increases hydrogasification rate.

EXPERIMENTAL

Most experiments here were performed in a micro flow reactor at one atmospheric pressure. The effluent gas was analyzed using gaschromatography. Yallourn brown coal from Australia was used as starting material because of low ash and sulfur content. Coal was first crushed in 32-60 mesh and demineralized with hot HCl. Metals were loaded on demineralized coal by wet impregnation of aqueous metal nitrate solution and then heat treated to char in high purity argon at various temperatures. Supported nickel catalyst is a commercial hydrogenation catalyst in which about 45% of nickel is supported on diatomite and the particle size is under 150 mesh.

RESULT AND DISCUSSION

KINETICS

Fig. 1 shows the hydrogasification profiles of metal loaded and demineralized Yallourn chars heat treated at 1123K for 30 minutes. Catalytic effect of iron group metals is apparently shown. The catalytic activity decreases in the order of Co > Ni > Fe at this temperature and at this catalyst loading levels. One of the characteristics of the profiles is that the initial low reactivity is observed for all the catalyst loaded chars. Then gasification rates gradually increase with time to a steady

state. The time of this initial low reactivity was less than 30 minutes at 1173K in TGA analysis of heat treated chars at 1173K for 1 hour and became longer with temperature decreasing and lasted over 300 minutes at temperatures below 1043K. XRD study showed that all the catalysts were almost reduced to metallic phase during heat treatment of coals. These observations indicate that the initial low reactivity is due to poisoning of very small amount of sulfur which strongly chemisorbs on the catalyst surface.

Fig. 2 shows the catalytic activity of chars at 993K when mixed with the same weight of supported hydrogenation nickel catalyst. Despite no methane evolves at this temperature without supported nickel catalyst, higher reactivity is observed for all chars than the results in Fig. 1. Although supported nickel catalyst increases the gasification rate of demineralized char, the effect is distinguishing for metal loaded chars. And the time of initial low reactivity becomes short and almost negligible for Co loaded char. Gasification profile of catalyst loaded char is as follows; there is short and low reactivity at the initial stage and then after the gasification rate reaches a maximum, it decreases gradually. The decrease in rate is probably due to deactivation of supported nickel catalyst at high temperatures. The supported hydrogenation nickel catalyst not only increases the gasification rate catalyzed by iron group metals, but decreases the time of initial low reactivity, that is, removes the chemisorbed sulfur from catalyst surface. The decreasing order of catalytic activity is again Co > Ni > Fe.

Further two experiments were done to check the effect of supported nickel catalyst on catalyzed char hydrogasification. First, reaction temperature was changed. Methane formation was observed at 943K for Fe loaded char and even at 843K for Co loaded char. The gasification rate of Co loaded char at 843K is about 0.4 mg/g/min and the value of activation energy is 23.2 Kcal/mol in the temperature range between 843 and 993K.

Next, the amount of catalyst loading was changed. The results are depicted in Fig. 3. The chars in this experiment were heat treated at 1173K for 1 hour and a maximum gasification rate was employed. The gasification rate increases by only about 0.1% catalyst loading for all catalysts. However, the increase in gasification rate becomes small at the catalyst loading level over 0.2% and a leveling-off in the rate is observed for Fe. This rate-loading relation is the same as the relation observed for the gasification rate without supported nickel catalyst at higher temperature. This observation suggests that supported nickel catalyst increases gasification rate by enhancement of the catalytic activity of iron group metals.

MECHANISM

There are some ideas for the reason that supported hydrogenation nickel catalyst enhances the catalytic activity of iron group metals. One of the ideas is a bimetallic effect, that

is, nickel on the supported catalyst makes alloy with the iron group metals during gasification. To examine this idea, the same amount of iron and nickel was loaded on Yallourn coal and gasification rate was measured after charring. No methane was formed at 993K. This means that the enhancement of catalytic activity of supported nickel catalyst is not due to the bimetallic effect. It is supposed that some catalytic activities of supported nickel catalyst enhance the activity of Fe, Ni and Co for hydrogasification

It is well known that nickel catalyst for hydrogenation adsorbs hydrogen, where it dissociates to atomic hydrogen and also hydrogen atoms spill over to neighboring materials.[4] On the other hand, it is proposed that the rate controlling step of catalytic hydrogasification is the formation of atomic H.[5] Supported nickel catalyst is mixed with catalyst loaded char only mechanically in this study. However, supported nickel catalyst is very fine particles and there is a possibility that nickel catalyst contacts with iron group metals on the char. So, hydrogen atom can spill over to the catalyst species on char as illustrated in Fig. 4 and consequently supported nickel catalyst enhances the catalytic activity of iron group metals.

The mechanism mentioned above is only reasonable idea so far. But, there is another idea that hydrogen atom in supported nickel catalyst spills over to carbon directly and promotes the cleavage of C-C bond. In fact, supported nickel catalyst enhances the reaction rate of demineralized Yallourn char as depicted in Fig. 2. However, demineralized char contains a small amount of iron and iron shows hydrogasification activity at its low loading level as shown in Fig. 3. Therefore, the effect of supported nickel catalyst on demineralized char is mainly due to a trace of iron in the char and atomic H in the catalyst species is a very important factor on catalytic hydrogasification.

CONCLUSION

Iron, cobalt and nickel show catalytic activity for C-H_2 reaction. The hydrogenation nickel catalyst adsorbs hydrogen, and dissociated hydrogen atom spills over to catalyst species and consequently enhances the catalytic activity of those metals.

REFERENCE

1. Ohtsuka, Y., Tamai, Y. and Tomita, A., J. Energy & Fuels, 1, 32(1987)
2. Hüttinger, K. J. and Krauss, W., Fuel, 60, 93(1981)
3. Baker, R. T. K., Chludzinski, J. J. Jr., and Sherwood, R. D., Carbon, 23, 245(1985)
4. Conner, W. C., Jr., Pajonk, G. M. and Teichner S. J., Advances in Catalysis(Edited by D. D. Eley, H. Pines and P. B. Weistz), Vol.34, pp.1-79, Academic Press, New York(1986)
5. McKee, D. W., Chemistry and Physics of Carbon(Edited by P. L. Walker, Jr. and P. A. Thrower), Vol.16, pp.1-118, Marcel Decker, New York(1981)

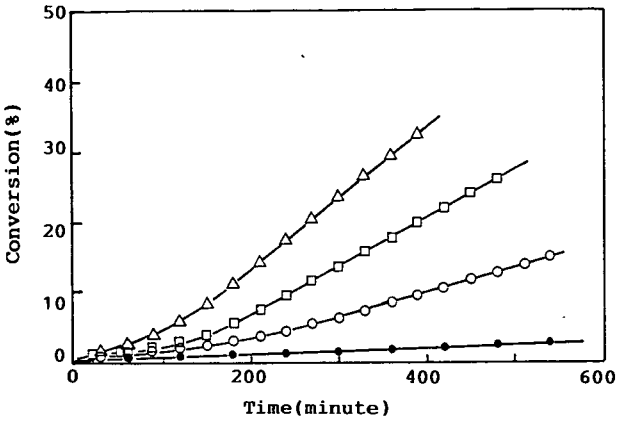

○;0.80%Fe, △;0.92%Co, □;0.83%Ni, ●;Demineralized

FIGURE 1. HYDROGASIFICATION YALLOURN CHARS AT 1093K

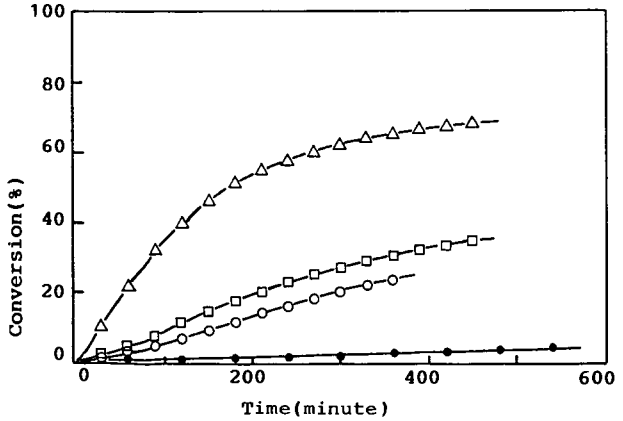

○;0.80%Fe, △;0.92%Co, □;0.83%Ni, ●;Demineralized

FIGURE 2. HYDROGASIFICATION OF YALLOURN CHARS AT 993K WHEN MIXED WITH SUPPORTED HYDROGENATION NICKEL CATLYST

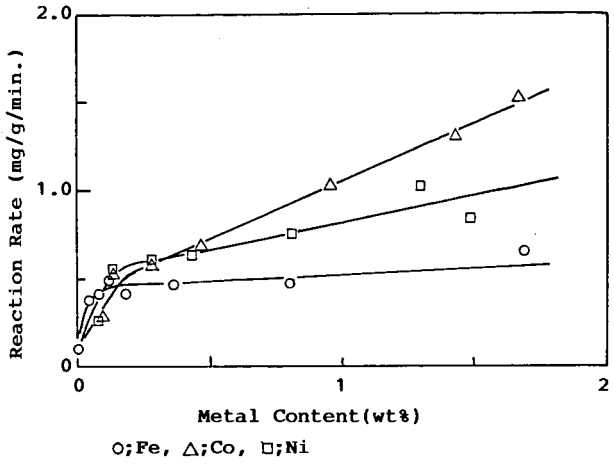

FIGURE 3. CATLYTIC ACTIVITY OF IRON GROUP METALS FOR HYDROGASIFICATION AT 973K WHEN MIXED WITH SUPPORTED HYDROGENATION NICKEL CATALYST

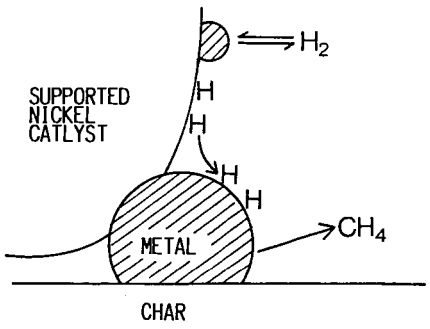

FIGURE 4. SCHEMATIC DIAGRAM OF HYDROGEN ATOM SPILL OVER IN THE SUPPORTED NICKEL CATALYST AND METAL LOADED CHAR SYSTEM

MECHANISMS OF STEAM GASIFICATION AND THE ROLE OF HYDROGEN INHIBITION

K. J. Hüttinger
Institut für Chemische Technik, Universität Karlsruhe
Kaiserstrasse 12, D-7500 Karlsruhe, FRG

ABSTRACT

Mechanism(s) of the carbon/steam reaction as published in literature are critically discussed. For this purpose, the various surface reactions are divided into primary and secondary reactions. Primary reactions involve a free active site:

$$C_f + H_2O \rightleftharpoons C(O) + H_2 \quad (1)$$
$$C_f + H_2 \rightleftharpoons C(H_2) \quad (2)$$
$$C_f + 1/2\ H_2 \rightleftharpoons C(H) \quad (3)$$

Secondary reactions are consecutive reactions of the intermediate surface complexes:

$$C(O) \longrightarrow CO + C_f \quad (4)$$
$$C(O) + H_2O \longrightarrow CO_2 + H_2 + C_f \quad (5)$$
$$C(H_2) + H_2 \longrightarrow CH_4 + C_f \quad (6)$$

The probability of each reaction is examined in view of recent results in literature and own experimental observations, mainly based on TPD studies. Hydrogen inhibition reactions (1) to (3) are specially treated. The rate laws derived from eqs.(1) to (6) are tested by experimental studies. Hydrogen inhibition mainly results from reaction (3) and additionally from reaction (1).

INTRODUCTION

The mechanism(s) and kinetics of the carbon/steam reaction are not yet fully understood (1-3), and this conclusion also holds for the strongly inhibiting effect of hydrogen as one of the reaction products (3-6).

The oldest and the most often used mechanisms for describing the carbon/steam reaction are the oxygen exchange mechanism A and the hydrogen inhibition mechanism B (1-3).

Mechanism A

$$C_f + H_2O \underset{k_{-1}}{\overset{k_1}{\rightleftharpoons}} C(O) + H_2 \quad (1)$$
$$C(O) \xrightarrow{k_2} CO + C_f \quad (2)$$

Mechanism B

$$C_f + H_2O \xrightarrow{k_1} C(O) + H_2 \quad (3)$$
$$C(O) \underset{k_3}{\overset{k_2}{\rightleftharpoons}} CO + C_f \quad (4)$$
$$C_f + H_2 \underset{k_{-3}}{\overset{}{\rightleftharpoons}} C(H_2) \quad (5)$$

In mechanism A the hydrogen inhibition results from the equilibrium of reaction (1), in mechanism B from the equilibrium adsorption of hydrogen according to eq. (5). Both mechanisms yield formally equal surface reaction rate r_S.

Mechanism A

$$r_S = \frac{c \cdot k_1 \cdot P_{H_2O}}{1 + \frac{k_1}{k_2} \cdot P_{H_2O} + \frac{k_{-1}}{k_2} P_{H_2}} \quad (6)$$

Mechanism B

$$r_S = \frac{c \cdot k_1 \cdot P_{H_2O}}{1 + \frac{k_1}{k_2} \cdot P_{H_2O} + \frac{k_3}{k_{-3}} \cdot P_{H_2}} \quad (7)$$

Only GIBERSON and WALKER (5) reported already in 1966 that the hydrogen inhibition is caused by dissociative chemisorption of hydrogen. In this case, eq.(5) of mechanism B has to be changed as follows:

$$C_f + \frac{1}{2} H_2 \underset{k_{-3}}{\overset{k_3}{\rightleftharpoons}} C(H) \quad (8)$$

Eqs. (3), (4) and (8) lead to mechanism C. The resulting surface reaction rate is:

$$r_S = \frac{c \cdot k_1 \cdot P_{H_2O}}{1 + \frac{k_1}{k_2} \cdot P_{H_2O} + \frac{k_3}{k_{-3}} \cdot P_{H_2}^{0.5}} \quad (9)$$

Mechanism C has recently been confirmed by YANG and YANG (6). The difference between mechanisms A or B and mechanism C is very important, because the inhibiting effect at low hydrogen partial pressures is much stronger if hydrogen is chemisorbed by dissociation.

All three mechanisms A, B and C have the same disadvantage. They are only applicable to the water gas reaction:

$$C + H_2O \rightleftharpoons CO + H_2 \quad , \quad (10)$$

whereas steam gasification of carbon is a complex reaction which includes at least two consecutive reactions, namely the carbon monoxide shift reaction

$$CO + H_2O \rightleftharpoons CO_2 + H_2 \quad , \quad (11)$$

and the methane formation by methanation of carbon monoxide

$$CO + 3\ H_2 \rightleftharpoons CH_4 + H_2O \quad , \quad (12)$$

or the methane formation by hydrogasification

$$C + 2\ H_2 \rightleftharpoons CH_4 \quad . \quad (13)$$

Modern gasification technologies use total pressures of at least

2 MPa, which favours the consecutive reactions. For such conditions, rate equations have been proposed for instance by BLACKWOOD (7) and MÜHLEN (8). Both authors use the adsorption term of mechanism A or B.

The present paper is concerned with an analysis of the probable mechanism(s) of the carbon/steam reaction with special consideration of the hydrogen inhibition. The analysis is based on informations given in literature and own experimental results.

ANALYSIS OF THE CARBON/STEAM REACTION

The surface reactions in the carbon/steam reaction may be devided into primary and secondary reactions. Primary reactions are such ones in which a free active site is involved:

$$C_f + H_2O \rightleftharpoons C(O) + H_2 \qquad (14)$$

$$C_f + H_2 \rightleftharpoons C(H_2) \qquad (15)$$

$$C_f + \tfrac{1}{2} H_2 \rightleftharpoons C(H) \qquad (16)$$

Secondary or consecutive reactions are thus reactions of the intermediate carbon surface complexes:

$$C(O) \longrightarrow CO + C_f \qquad (17)$$

$$C(O) + H_2O \longrightarrow CO_2 + H_2 + C_f \qquad (18)$$

$$C(H_2) + H_2 \longrightarrow CH_4 + C_f \qquad (19)$$

Many further surface reactions may be assumed, for instance instead of eq.(14):

$$C_f + H_2O \rightleftharpoons C(OH) + \tfrac{1}{2} H_2 \qquad (20)$$

$$2\,C_f + H_2O \rightleftharpoons C(OH) + C(H) \qquad (21)$$

or instead of eq.(19)

$$C(H_2) + H_2O \longrightarrow CH_4 + CO + C_f \qquad (22)$$

In the following the eqs.(14) to (19) will be examined only. At a first view they seem to be the most probable ones. The experimental results show that some of these are probably less whereas other ones are more important.

Eq.(14) is the decisive primary reaction. It is assumed to be an equilibrium reaction. This is in accordance with mechanism A. C(O) surface complexes may easily be reduced by hydrogen. In gasification with H_2O/H_2 mixtures their concentration depends on the H_2O to H_2 ratio. Both conclusions result from extensive TPD measurements, whereby carbon monoxide desorption was measured after quenching the samples from gasification to room temperature (9,10). YANG and YANG (6) also assume that eq.(14) is an equilibrium reaction but they do not consider this conclusion in deriving the rate equation.

The non-dissociative and dissociative chemisorption of hydrogen according to the eqs.(15) and (16) are parallel reactions of eq.(14). Both sorption mechanisms are discussed in literature (mechanisms B and C). Hydrogen desorption from the $C(H_2)$ complex, i.e. from aliphatically bound hydrogen, occurs at about 600 °C. Hydrogen desorption from the C(H) complex or of aromatically bound hydrogen requires temperatures above 800 °C (9,10). TPD measurements show hydrogen desorption at about 600 °C only in the case of low temperature chars after gasification in H_2O/H_2 mixtures. High temperature chars or carbons desorb hydrogen nearly exclusively above 800 °C, even if the gasification is performed with H_2O/H_2 mixtures. With such carbons methane formation is small. $C(H_2)$ complexes are assumed to be the decisive intermediates in methane formation (11). If methane formation is negligible, the rate of eq.(15) must be zero (equilibrium). This is the case for eq.(16) under all conditions.

In summarizing eqs.(14) to (16) hydrogen may inhibit the gasification reaction in different ways and to different extents. According to the TPD measurements eq.(15) should be of less importance. Strongest inhibition doubtless results from dissociative chemisorption (eq.(16)). because the majority of carbon edge atoms is saturated by aromatically bound hydrogen (10). Hydrogen inhibition by dissociative chemisorption also follows from the results of kinetic studies by GIBERSON and WALKER (5) and YANG and YANG (6), which are very convincing. This conclusion leads to the question whether the equilibrium of eq.(14) has to be considered additionally. One case may be gasification at high hydrogen partial pressures.

The secondary reactions are based on the reactions of the C(O) surface complex and the $C(H_2)$ surface complex. The dissociation of the C(O) surface complex (eq.(17)) obviously is irreversible as assumed in all mechanisms. The reaction of the C(O) complex with steam (eq.(18)) is a competition reaction to the direct desorption of the C(O) surface complex. If the desorption of the C(O) complex represents the rate limiting step of gasification, which is assumed by most authors, the carbon dioxide formation according to eq.(18) represents an important reserve for increasing the gasification rate. High steam partial pressures favour carbon dioxide formation. The stability of the C(O) complex represents the decisive point. Stability increases with increasing heat treatment temperature of the char. Therefore, carbon dioxide yields increase with increasing heat treatment temperature of the char.

The reaction of the $C(H_2)$ surface complex with hydrogen is the decisive methane formation in hydrogasification (11), possibly also in steam gasification at high hydrogen partial pressures. At high steam partial pressures and small hydrogen partial pressures, methane formation according to eq.(22) is more probable. This conclusion leads to the question whether eq.(15) is important under these conditions.

Nevertheless, for a first approach eqs.(14) to (19) seem to be a useful basis for deriving rate equations of carbon gasification with steam, which have to be examined by experimental studies.

MECHANISMS AND KINETICS

For formulating mechanisms, the sequence of eqs.(14) to (19) will be changed. The following sequence is used:

Eq.(14): eq.(1), eq.(17): eq.(2), eq.(15): eq.(3), eq.(16): eq.(4), eq.(18): eq.(5), eq.(19): eq.(6). This rearrangement of equations is useful for an improved clarity of the mechanisms and kinetic equations.

For the water gas reaction, the new eqs.(1) to (4) have to be considered. The rates of eqs.(3) and (4)are zero (equilibrium adsorption). This assumption leads to the following rate equation:

$$r_S = \frac{c \cdot k_1 \cdot P_{H_2O}}{1 + \frac{k_1}{k_2} P_{H_2O} + \frac{k_{-1}}{k_2} P_{H_2} + \left[1 + \frac{k_{-1}}{k_2} P_{H_2}\right]\left[\frac{k_3}{k_{-3}} P_{H_2} + \frac{k_4}{k_{-4}} P_{H_2}\right]^{0.5}} \qquad (23)$$

At low hydrogen partial pressures some terms may be neglected, whereby the rate equation of mechanism C is finally resulting.(eq.(9)). This equation is confirmed by the works of GIBERSON and WALKER (5) and YANG and YANG (6). The equilibrium constant of dissociative hydrogen chemisorption at graphite edge atoms was determined by YANG and YANG (6):

$$K_4 = \frac{k_4}{k_{-4}} = 2 \cdot 10^{-3} \cdot \exp(21650/RT), \text{ bar}^{-0.5} \qquad (24)$$

Eq. (24) yields remarkably high values, at 800 °C: 53, at 1000 °C: 10.

In the case of remarkable carbon dioxide formation the set of surface reactions has to be extended by the new eq.(5). The resulting rate equation is:

$$r_S = \frac{c \cdot k_1 \cdot P_{H_2O} \cdot \left[1 + \frac{k_5}{k_2} \cdot P_{H_2O}\right]}{1 + \frac{k_1 + k_5}{k_2} P_{H_2O} + \frac{k_{-1}}{k_2} P_{H_2} + \left[1 + \frac{k_5}{k_2} P_{H_2O} + \frac{k_{-1}}{k_2} P_{H_2}\right]\left[\frac{k_3}{k_{-3}} P_{H_2} + \frac{k_4}{k_{-4}} P_{H_2}\right]^{0,5}} \qquad (25)$$

This equation may also be simplified. As far as the steam conversion and thus the partial pressure of hydrogen are small, the following equation may be used:

$$r_S = \frac{c \cdot k_1 \cdot P_{H_2O} \left[1 + \frac{k_5}{k_2} \cdot P_{H_2O}\right]}{1 + \frac{k_1 + k_5}{k_2} P_{H_2O} + \left[1 + \frac{k_5}{k_2} P_{H_2O}\right] \frac{k_4}{k_{-4}} P_{H_2}^{0.5}} \qquad (26)$$

Experimental results at steam partial pressures up to 0.8 MPa could

well be described by eq.(26). However, an improved fit was obtained by neglecting the term $(k_2+k_5)\cdot P_{H_2O}\cdot k_2^{-1}$. This means that the dissociative chemisorption of hydrogen may represent the dominating, inhibiting process.

The rate equation of the water gas reaction with simultaneous formation of methane may be derived by using the new eqs.(1) to (4) plus eq.(6). The rate equation is as follows:

$$r_S = \frac{c\left[k_1\cdot P_{H_2O}\cdot C_2 + \frac{k_3}{k_{-3}}\cdot k_5\cdot P_{H_2}^2\cdot C_1\right]}{\frac{k_1}{k_2}\cdot P_{H_2O}\cdot C_2 + \frac{k_3}{k_{-3}}\cdot P_{H_2}\cdot C_1 + \left[1+\frac{k_4}{k_{-4}}P_{H_2}^{0.5}\right]\cdot C_1\cdot C_2} \qquad (27)$$

$$C_1 = 1 + \frac{k_{-1}}{k_2}P_{H_2}\ ; \qquad C_2 = 1 + \frac{k_5}{k_{-3}}P_{H_2}$$

An experimental test of eq.(27) is extremely difficult because 8 constants have to be determined. A more promising way to prove eq.(27) would be an examination of pure hydrogasification. As follows from the general discussion of the single steps of gasification it is obvious that this gasification is also inhibited by dissociative chemisorption of hydrogen.

RESULTS AND DISCUSSION

The detailed results of experimental studies are given in another paper (12). For determination of the rate constants the initial reaction rates were used. They are obtained by plotting the gas formation or gasification rates versus the degree of carbon conversion X at X = 0. Initial reaction rates are independent of any changes of porosity, internal surface area or particle size.

The experimental results show that the dissociative chemisorption of hydrogen plays a dominating role in steam gasification and it probably represents the main inhibiting effect. From the present results it can not yet be decided whether the equilibrium of the dissociation reaction of steam according to eq.(1) has an additional inhibiting effect or not. This question is investigated in recent studies. In any case, it may be concluded that the non-dissociative chemisorption of hydrogen plays no role and it may therefore be neglected.

REFERENCES

(1) Walker, P.L.Jr., Rusinko, F.Jr., Austin, E.L., Adv. Catalysis 11, 133 (1959)
(2) Laurendeau, N.M., Prog.Energy Combust. Sci. 4, 211 (1978)
(3) Hüttinger, K.J., Chemiker-Zeitung 112, 149 (1988)
(4) Hüttinger, K.J., Carbon 26, 79 (1988)
(5) Giberson, R.C., Walker, P.L.Jr., Carbon 3, 521 (1966)
(6) Yang, R.T., Yang, K.L., Carbon 23, 537 (1985)

(7) Blackwood, J.D. et al., Aust. J. Chem. 11, 16 (1958; ibida 12, 533 (1959)
(8) Mühlen, H.-J., Dissertation, Universität Essen (1983)
(9) Hermann, G., Hüttinger, K.J., Carbon 24, 705 (1986)
(10) Nill, J.-S., Dissertation, Universität Karlsruhe, in preparation
(11) Shaw, J.T., Proc.Intern. Conf. on Coal Science, Düsseldorf (1981), Glückauf 209
(12) Hüttinger, K.J., Lietzke, G., EKEP 41 (1988), in press.

ACKNOWLEDGEMENT

Financial support of this study by the German Research Foundation (DFG) is gratefully acknowledged.

APPLICATION OF COMPUTER MODELING TECHNIQUES TO THE KINETICS OF THE REACTION OF CARBON WITH OXYGEN

S. Ahmed and M.H. Back
Ottawa-Carleton Chemistry Institute,
University of Ottawa Campus, Ottawa, Canada K1N 6N5
and
J.M. Roscoe
Department of Chemistry,
Acadia University, Wolfville, Nova Scotia B0P 1X0

ABSTRACT

Computer modeling techniques are applied to the kinetics of the reaction of carbon with oxygen. The rates of disappearance of oxygen, of formation of CO, CO_2 and the surface complex, measured over the temperature range 748-1173 K and the pressure range 0.5-400 Pa may be described by a mechanism involving adsorption of oxygen, formation of the strongly-bound complex, desorption of the complex and reaction of the complex with a gas-phase molecule of oxygen. The latter is shown to be an important source of CO_2 at low temperatures and higher pressures of oxygen. An important feature of the mechanism is the existence of at least two distinct types of active sites for the binding of the complex on the carbon surface, each with a characteristic reactivity. Most of the results on which the model is based were obtained using thin films of pyrolytic carbon, but some results from the oxidation of graphon are also consistent with the mechanism.

INTRODUCTION

The purpose of the present study is to illustrate the application of computer modeling techniques to the reaction of carbon with oxygen. The kinetics of this reaction have been studied over a period of several decades (1,2) with most emphasis placed on steady-state solutions leading to an interpretation of the order and activation energy of the over-all rate. The importance of the strongly-bound surface complex in the oxidation process was first recognized by Walker and colleagues (3). The properties of the complex have been extensively studied (4,5,6) but its role in the various elementary surface processes involved in oxidation is not understood in detail.

The development of computer modeling techniques has opened the way for the testing and evaluation of mechanisms with far more sensitivity than is possible with steady-state methods. A major requirement in the use of these techniques is the availability of reliable measurements for the rates of the elementary processes in the mechanism. Recently, kinetic studies of the reaction of oxygen with carbon in a static system (7), involving a complete analysis of the time course of the reaction in terms of the depletion of oxygen and carbon and of the formation of carbon monoxide and carbon dioxide, led to an estimate of the concentration of adsorbed species on the surface and of the values

of some of the rate constants for the elementary processes in the reaction. Using these results a mechanism for the reaction has been developed and tested using computer modeling techniques. The present paper reviews the development of the mechanism from the results of the reaction in the temperature range 748 - 898 K and pressures of oxygen of 90 - 133 Pa, where the product was almost entirely carbon dioxide (8), and then describes the extension of the mechanism to results obtained at temperatures up to 1073 K, where carbon monoxide was a major product. Finally, the model was applied to results obtained by Laine, Vastola and Walker, (LVW), (3) at 898 K and at pressures of 0.1 Pa.

EVALUATION OF THE ELEMENTARY PROCESSES IN THE OXIDATION

Details of this interpretation have been described previously (8) and will be reviewed only briefly. The number of active sites, C_F, on the carbon surface used in the experiments, was obtained by measurement of the active surface area, as defined by LVW (3). Adsorption of oxygen was assumed to occur in two steps

(1) $C_F + O_2 \rightarrow C(O_2)$

(2) $C_F + C(O_2) \rightarrow 2(CO)_C$

where C_F is a free carbon site and $C(O_2)$ refers to an adsorbed molecule before formation of the strongly-bound complex, $(CO)_C$, takes place. An estimate of k_1 was obtained from the initial rapid decrease in pressure of oxygen observed in experiments below about 848 K, and was calculated from the expression,

$$-d[O_2]/dt = k_1 C_F^0 [O_2]^0$$

The activation energy for k_1 was about 40 kJ mol^{-1}. It was assumed that k_2 was substantially less than k_1 and the ratio k_2/k_1 was set at 0.1 in the low temperature region.

The rate of desorption of the complex

(3) $(CO)_C \rightarrow CO(g) + C_F$

was estimated from the results of temperature-programmed desorption measurements. Because the rate was slow compared to the measured rate of the reaction below about 900 K, a new type of reaction was proposed (7) involving reaction of the complex with gaseous oxygen, giving carbon dioxide.

(4) $C_F + (CO)_C + O_2 \rightarrow CO_2 + (CO)_C + 2C_F$

Estimation of the rate constant for reaction (4) required values for the concentration of each complex on the surface, $C(O_2)$ and $(CO)_C$, as well as the concentration of free sites, C_F, at any time. The concentration of the strongly-bound complex, $(CO)_C$, was obtained, at any stage of the reaction, by removing reactants, products and $C(O_2)$ by evacuation, leaving only $(CO)_C$ on the surface. Temperature-programed desorption to 1223 K, with measurement of the carbon monoxide and carbon dioxide evolved, gave directly the number of moles of $(CO)_C$.

$(CO)_C = CO + 2CO_2$

Since CO was not a product of the reaction at these temperatures the difference between the measured pressure at any time and the

initial pressure was related to the concentration of both $C(O_2)$ and $(CO)_C$ as follows,

$P_t - P_0 = -\Delta O_2 = 2(CO)_C + C(O_2)$

allowing an estimate of the quantity of $C(O_2)$. The concentration of free sites at any time, C_F, was given as the difference between the initial value, C_F^0, and the sum of sites occupied by $C(O_2)$ and $(CO)_C$.

$$C_F = C_F^0 - [(CO)_C + C(O_2)]$$

The rate constant for reaction (4) was estimated from the following expression for the rate of disappearance of oxygen, after the initial stage of the reaction.

$$-d[O_2]/dt = k_1 C_F [O_2] + k_4 C_F [(CO)_C] [O_2]$$

The values of the rate constants and their Arrhenius parameters are given in Table 1. The concentration of all reactants were expressed as total mol in the particular reaction system, since this allows a direct relation between gas phase and adsorbed molecules, although the values are not transferable to other systems. The calculations used a computer program which has been employed in previous studies (9). It uses the popular DIFSUB integrator and has provision for first order sensitivity analysis and automatic adjustment of kinetic parameters to fit experimental yield-time date.

DEVELOPMENT OF THE MODEL

A. TEMPERATURES BELOW 898 K

The reactions described formed the starting point for the development of the mechanism, but, as expected, were not sufficient to describe the yields of products and consumption of reactants over the complete course of the reaction. Only by introducing two types of active sites, C_A and C_B, with different reactivities and a certain amount of interconversion, was agreement obtained between the calculated and observed results. Because of the different reactivities not all the reactions were important for each type of site. The following set, which includes several variations of reaction (4), represents the minimum number required for quantitative agreement.

1A	CA	+	O_2	→	$C(O_2)_A$					
1B	CB	+	O_2	→	$C(O_2)_B$					
2A	CA	+	$C(O_2)_A$	→	$2(CO)_{CA}$					
3B	$(CO)_{CB}$	→	CO	+	CB					
4B(a)	CB	+	$(CO)_{CB}$	+	O_2	→	CO_2	+	$(CO)_{CB}$	+ 2CB
4B(b)	CB	+	$(CO)_{CB}$	+	O_2	→	CO_2	+	$(CO)_{CB}$	+ CB
4B(c)	CB	+	$(CO)_{CA}$	+	O_2	→	CO_2	+	$(CO)_{CB}$	+ CA
5A	CB	+	$C(O_2)_A$	→	$(CO)_{CA}$	+	$(CO)_{CB}$			

The mechanism was tested at temperatures of 748, 798, 848 and 898 K and an example of the results is shown in Figure 1a. In the Figures the points represent the experimental measurements and the lines represent the calculated values. The rate constants giving the best fit at each temperature were further adjusted to conform

to an Arrhenius temperature dependence and the final values are those given in Table 1.

From this mechanism the following picture of the reaction emerges. The sites designated C_A adsorb oxygen rapidly and are quickly saturated, while the sites C_B adsorb oxygen more slowly and participate in other reactions. The very different nature of adsorption on C_B sites is reflected in the larger activation energy for reaction 1B compared to 1A. Reactions which are kinetically described by reaction (4), with the variations listed as (a), (b) and (c), can account for the formation of carbon dioxide, but at these temperatures appear to occur mainly on B sites. Nevertheless interconversion of the sites through reaction (5) was important. Reaction (3) is included here but makes little contribution at these temperatures. It should be noted that several other types of surface processes involving both $(CO)_C$ and $C(O_2)$ were initially included in the mechanism, but, using reasonable values for rate constants, were not found to contribute significantly.

B. TEMPERATURES ABOVE 898 K

While the simple mechanism, with rate constants conforming to an Arrhenius dependence, gave reasonable agreement with the measurements up to 898 K, it became clear that further reactions were needed to describe the reaction at higher temperatures. One desorption reaction was no longer adequate and desorption of carbon monoxide from A sites was included, using a higher activation energy and frequency factor than for desorption from B sites. Above about 1000 K adsorption on and reaction with the carbon surface became important for both products, carbon monoxide and carbon dioxide. Also at these temperatures the A sites began to dominate the reaction. The following reactions were added, using the rate constants given in Table 1.

2B $\quad C_B + C(O_2)_B \rightarrow 2(CO)_{CB}$

3A $\quad (CO)_{CA} \rightarrow CO + C_A$

7A $\quad C_A + CO_2 \rightarrow (CO)_{CA} + CO$

8B $\quad C_B + CO \rightarrow (CO)_{CB}$

9A $\quad CO + (CO)_{CA} \rightarrow CO_2 + C_A$

9B $\quad CO + (CO)_{CB} \rightarrow CO_2 + C_B$

An example of the calculated and measured yields of products and consumption of reactants is shown in Figure 1b.

C. COMPARISON OF THE MODEL WITH THE RESULTS OF LVW

The model presented provided a reasonably quantitative description of the results obtained from a study of the reaction of oxygen with pyrolytic carbon in the form of a thin film on the surface of a quartz reactor. To test the generality of the mechanism the model was applied to the results of LVW obtained from a study of the reaction with Graphon at 898 K and pressures of oxygen of ~0.1 Pa. By introducing two alterations to the mechanism good agreement was obtained between predicted and observed results. First, the rate constants in reactions 2A and 3A were increased by factors of

14 and 120 respectively, reflecting the high reactivity of Graphon. Secondly, a new type of adsorption site, designated C_{AA}, was introduced, which rapidly but loosely binds oxygen, reaction (10), and provides a new route to the formation of $(CO)_{CA}$, reaction (11).

10 $\quad C_{AA} + O_2 \rightarrow C(O_2)_{AA}$

11 $\quad C_A + C(O_2)_{AA} \rightarrow (CO)_{AA} + (CO)_{CA}$

The rate of reaction (10) is the key factor in reproducing the decay curves of oxygen observed by LVW (3). The new type of site binds a single oxygen atom particularly strongly, and may give the very stable complex suggested by LVW. The results calculated from the revised mechanism are compared with the results of LVW in Figure 2a and in Figure 2b the previous mechanism (without reaction (10) and (11)) is compared with the results of ref (7) at the same temperature.

DISCUSSION

The most significant features of the model are the existence of at least two distinct types of active sites on the carbon surface, with different reactivities, and the introduction of the general type of reaction given by equation (4), where a gas-phase molecule of oxygen reacts with the chemi-sorbed complex. Although rate constants for these reactions were based on measurements made in a particular system with a particular type of carbon, the basic features of the mechanism should be generally applicable to the reaction of oxygen with carbon.

The idea that the carbon surface may contain more than one type of active site has been suggested many times, based on results from a variety of studies. The model clearly shows the difference in reactivities of the A and B sites, not only in the rate constants for reactions 1 and 2 but in reaction 3 and the subsequent reactions. The relative values for these rate constants as well as the relative concentrations of the sites may change with different types of carbon and indeed the modifications to the mechanism to provide agreement with the results of Laine, Vastola and Walker were essentially of this sort.

Reaction (4) and its variations account for the fact that carbon dioxide is a primary product of the reaction and that its rate remains dependent on the pressure of oxygen even at high pressure. Furthermore these reactions will undoubtedly have activation energies lower than that of direct desorption and will be important at temperatures where the latter is still slow.

The model also shows that the role of the complex resembles that of active sites in a catalytic process. The complex is a reaction intermediate, even though new carbon atoms are continuously involved in its formation, and, as suggested previously (7), the rate may be expressed as a turn-over number, based on the concentration of complex on the surface. Rates from a variety of studies, for which the number of active sites had been measured, were in reasonable agreement when expressed in this way.

REFERENCES

1. P.L. Walker, F.J. Vastola and P.J. Hart, in "Fundamentals of Gas-Surface Interactions" eds. H. Saltsburg, J.N. Smith and M. Rogers, Academic Press, New York (1967) p. 307
2. H. Marsh, Chem. Soc. Spec. Pub. no. 32. p. 13 London (1978)
3. N.R. Laine, F.J. Vastola and P.L. Walker, J. Phys. Chem. 67 2030 (1963)
4. C. Morterra, M.J.D. Low and A.G. Severdia, Carbon 22 5 (1984)
5. G. Tremblay, F.J. Vastola and P.L. Walker, Carbon 16 35 (1978)
6. R.T. Yang in "Chemistry and Physics of Carbon", ed. P.A. Thrower, vol 19, p. 163, Marcel Dekker, New York (1984)
7. S. Ahmed and M.H. Back, Carbon 23 513 (1985)
8. S. Ahmed, M.H. Back and J.M. Roscoe, Comb. Flame 70 1 (1987)
9. J.M. Roscoe and M. Thompson, Int. J. Chem. Kin. 17 967 (1985)

TABLE 1

Rate constants used in obtaining the results in Figures 1 and 2.

Reaction	k_{748}	k_{898}	k_{1073}	unit
1A	3.51×10^{2}	1.35×10^{3}	4.01×10^{3}	$mol^{-1}s^{-1}$
2A	7.45×10^{2}	1.43×10^{4}	1.58×10^{5}	$mol^{-1}s^{-1}$
3A	0	3.76×10^{-4}	3.51×10^{2}	s^{-1}
5A	2.61×10^{2}	2.51×10^{4}	1.03×10^{6}	$mol^{-1}s^{-1}$
7A	0	0	8.83×10^{5}	$mol^{-1}s^{-1}$
9A	0	0	1.50×10^{9}	$mol^{-1}s^{-1}$
1B	0.105	17.3	1.10×10^{3}	$mol^{-1}s^{-1}$
2B	0	0	1.00×10^{5}	$mol^{-1}s^{-1}$
3B	0	0	5.04×10^{-2}	s^{-1}
4B(a)	2.14×10^{8}	1.20×10^{10}	3.18×10^{11}	$mol^{-2}s^{-1}$
4B(b)	7.17×10^{5}	1.01×10^{9}	3.69×10^{11}	$mol^{-2}s^{-1}$
4B(c)	1.61×10^{8}	3.90×10^{8}	8.02×10^{8}	$mol^{-2}s^{-1}$
8B	0	0	6.00×10^{2}	$mol^{-1}s^{-1}$
9B	0	0	1.28×10^{6}	$mol^{-1}s^{-1}$

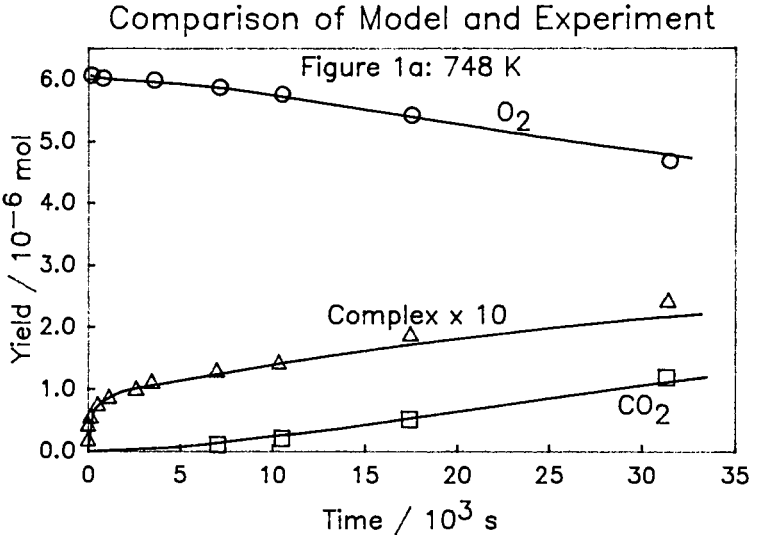
Comparison of Model and Experiment
Figure 1a: 748 K
O_2
Complex x 10
CO_2
Yield / 10^{-6} mol
Time / 10^3 s
0.0
1.0
2.0
3.0
4.0
5.0
6.0
0
5
10
15
20
25
30
35

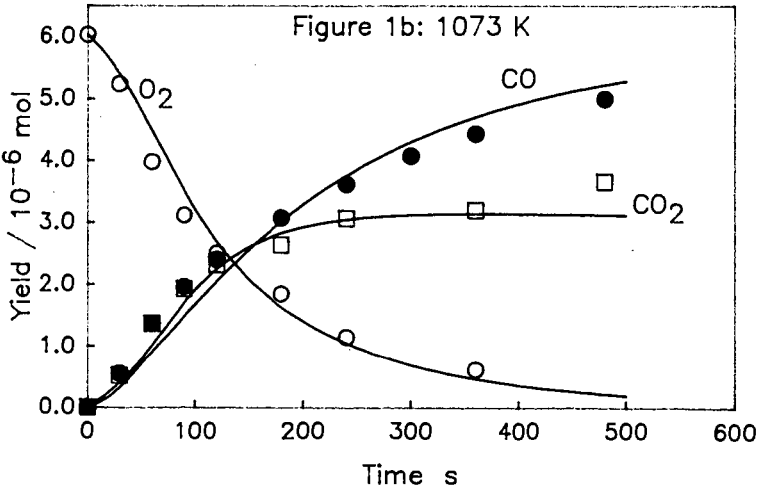
Figure 1b: 1073 K
O_2
CO
CO_2
Yield / 10^{-6} mol
Time s
0.0
1.0
2.0
3.0
4.0
5.0
6.0
0
100
200
300
400
500
600

Comparison of Model and Experiment at 898 K

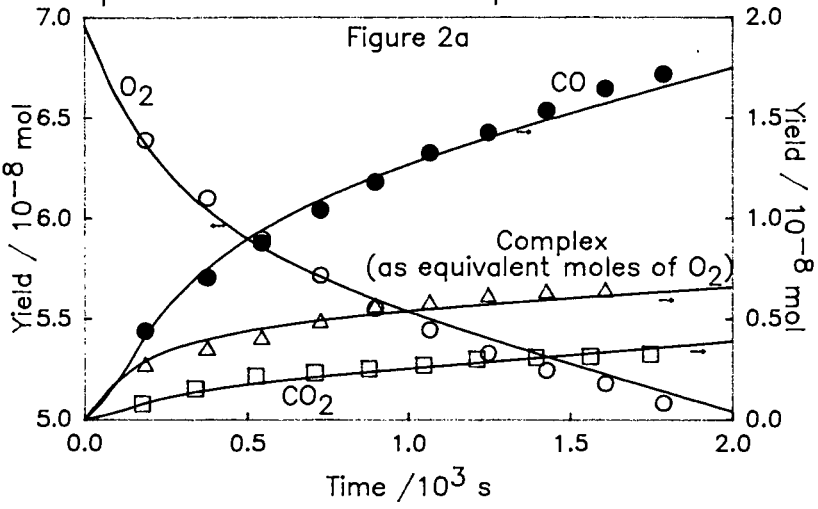

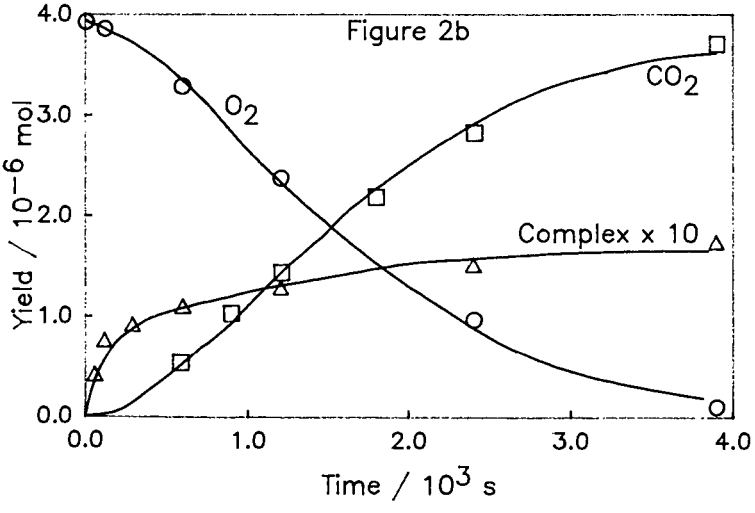

A Mathematical Model of Temperature Programmed Desorption of Oxygen Complexes From Porous Chars and Carbons

J.M. Calo and P.J. Hall
Chemical Engineering Program
Division of Engineering
Brown University
Providence, Rhode Island 02912

Introduction

Temperature programmed desorption/mass spectrometry (TPD/MS) has become a popular technique for investigating the nature and behavior of oxygen surface complexes on carbons and chars (e.g., see [1-3]). Such studies have been generally useful in establishing certain qualitative aspects of the behavior of these surface complexes. We have been applying this technique in our laboratory as a probe of the energetic heterogeneity of coal char surfaces [4]. In Figure 1 are presented typical TPD spectra for CO and CO_2 obtained in our laboratory for a Pittsburgh #8 coal char sample gasified to 27.3% in oxygen. As can be seen, the spectra consist of two small, relatively broad CO_2 peaks, and a large CO peak with a high temperature shoulder. It is noted that these spectra are remarkably similar to those reported for other significantly different carbons (e.g., see [1-3]). We have interpreted the origins of these features in another publication [5]. Essentially, it appears that the first CO_2 peak at 600K is most probably due to intrinsic CO_2-liberating complexes, such as lactones and/or carboxylic anhydrides [2,3]; while the first CO peak is most probably due to intrinsic CO-liberating complexes, such as carbonyls and/or semi-quinones [2,3].

We have shown [6], however, that the second CO_2 peak, centered at about 900K, is at least partially due to CO_2 produced in the secondary reaction:

$$CO(g) + [CO] \text{ <===> } CO_2(g) + C_f, \qquad [R.1]$$

where [CO] is a surface complex with a single oxygen molecule, and C_f is a "free active site." The importance of this reaction was discovered in a series of experiments employing a number of coal chars over a large variation in heating rate. For those chars that exhibited significant porosity, it was noted that the total integrated amount of CO_2 exhibited a broad maximum at a heating rate ca. 100K/min, while the total oxygen balance (i.e., $CO+2CO_2$) remained invariant. The high temperature shoulder on the primary CO peak, evident in Figure 1, is hypothesized to be primarily due to re-adsorption of free CO(g) evolved during the course of the TPD [5]. This was determined from TPD experiments in which a previously "thermally cleaned" char surface was exposed to CO at low temperatures for a prolonged period of time. Subsequent TPD revealed a high temperature CO peak precisely at the location of the high temperature shoulder in Figure 1 [5]. This conclusion is also supported by the CO chemisorption results of Marchon et al. [7].

Recently, we have been directing our efforts at quantifying the information available from such desorption chromatograms. As one of the tools in this endeavor, we have developed a mathematical model. In the current paper, we present the essentials of this model and some sample results. We then compare some model predictions to experimental TPD observations. In this manner, we demonstrate the utility of the model and highlight areas where work remains to be done.

The Model

Even though there seems to be general qualitative agreement as to the basic features present in TPD spectra of surface oxides from carbonaceous solids, there is still very little actually known about the mechanisms involved in producing these features. Therefore, any model formulated at this time will almost certainly have to be modified to take into account new discoveries as we learn more about the processes that occur during TPD. Even so, we demonstrate here that even a rudimentary model is still a useful tool even at this stage of development to aid in the elucidation of the relevant mechanisms. It is in this spirit in which we present our work here.

One of the most elementary forms of the current model is based on the assumption of two distinct types of complexes on the carbon surface: (1) intrinsic CO_2-liberating complexes (e.g., lactones, carboxylic acids, carboxylic anhydrides); and (2) intrinsic CO-liberating complexes (e.g., semi-quinones and carbonyls). It is further assumed that the population of active sites at which these complexes are formed is distributed energetically, but that there is a finite number that is conserved during the course of the TPD experiment; i.e., the total concentration of active sites, C_t, is a constant. Based upon our previous work [5,6], we also allow for the secondary interactions [R.1], which interconvert the free oxides of carbons once they are produced within the char porosity.

In addition to the preceding, the model also allows for transport resistance. More specifically, in the version of the model presented here, we focus on a microporous char such that the primary resistance to transport lies in microporous regions; i.e., the larger pores present no transport resistance to the evolved gases. It is assumed, for the sake of simplicity, that the microporous regions are spherical with a characteristic radius, R. It is further assumed that the transport is activated. In any case, it is noted that this particular view is not necessary in order to predict the TPD spectra for non-transport limited conditions, and that different carbons and chars will obviously exhibit different transport characteristics. Consequently, it is expected that the model will have to be tailored appropriately in order to account for the actual conditions that obtain.

With the preceding assumptions in mind, the following dimensionless mass balances can be formulated for four species; i.e., two surface complexes and the two oxides of carbon, CO and CO_2:

$$\partial u_1/\partial\tau = g_1\nabla^2 u_1 + \phi_{d1}\,\theta_1 - \phi_1\,u_1\,\theta_1 + \phi_2\,u_2\,(1-\theta_1-\theta_2)$$

$$\partial u_2/\partial\tau = g_2\nabla^2 u_2 + \phi_{d2}\,\theta_2 + \phi_1\,u_1\,\theta_1 - \phi_2\,u_2\,(1-\theta_1-\theta_2)$$

$$d\theta_1/d\tau = -\,\phi_{d1}\,\theta_1 - \phi_1\,u_1\,\theta_1 + \phi_2\,u_2\,(1-\theta_1-\theta_2)$$

$$d\theta_2/d\tau = -\,\phi_{d2}\,\theta_2$$

where: $u_1 = \varepsilon\,C_{co}/C_t$ $\quad \theta_1 = [CO]/C_t$ $\quad \tau = t/t_d$

$u_2 = \varepsilon\,C_{co2}/C_t$ $\quad \theta_2 = [OCO]/C_t$ $\quad t_d = R^2/D_{1,0}$

$g_1 = \exp(-E_{1d}/RT)$ $\quad g_2 = (D_{2,0}/D_{1,0})\ \exp(-E_{2d}/RT)$ $\quad r = r'/R$

$D_{1,0}$, $D_{2,0}$ pre-exponentials for the diffusivity for θ_1 and θ_2

C_t = mol active sites/cm^3 microparticle

ε = void fraction of char microporous region

$\phi_{d1} = t_d\,k_{d1,0}\exp[-E_{d1}/RT]$, the desorption rate constant for θ_1

$\phi_{d2} = t_d\,k_{d2,0}\exp[-E_{d2}/RT]$, the desorption rate constant for θ_2

$\phi_1 = t_d\,k_{1,0}\exp[-E_1/RT]\,C_t/\varepsilon$, forward rate constant for reaction [R.1]

$\phi_2 = t_d\,k_{2,0}\exp[-E_2/RT]\,C_t/\varepsilon$, reverse rate constant for reaction [R.1]

The linear heating regimen provides the relationship between time and temperature: $\Theta = 1 + \Omega\,\tau$; where $\Omega = Bt_d/T_0$, $\Theta = T/T_0$, B is the heating rate, and T_0 is the initial temperature. Surface heterogeneity is modeled using activation energies that are functions of surface coverage:

$$E_{d1} = E_{d1,0} - \alpha\,\theta_1;\ E_{d2} = E_{d2,o} - \beta\,\theta_2;\ E_1 = E_{1,0} - \gamma\,(\theta_1+\theta_2);\ E_2 = E_{2,o} + \delta\,(\theta_1+\theta_2)$$

The corresponding boundary conditions for a typical TPD experiment are:

$u_1 = u_2 = 0$ @ $r = 1$ (i.e., no external mass transfer resistance)

$\partial u_1/\partial\tau = \partial u_2/\partial\tau = 0$ @ $r = 0$ (symmetry condition)

The initial conditions are:

$$\theta_1 = \theta_{1,0};\ \theta_2 = \theta_{2,0};\ u_1 = u_2 = 0 \text{ @ } \tau = 0$$

Since a TPD spectrum represents the *rate* of gas evolution *vs* temperature (or time), the dimensional

evolution rate from the char is determined by the flux at the exterior of the microporous regions, J:

$$\text{Rate} = (A_p/V_p)\, J = -(3\, C_t/\varepsilon\, t_d)\, (\partial u_1/\partial \tau)_{r=1};\ \text{mol/cm}^3\ \text{s},$$

where A_p, V_p are the exterior surface area and the volume of the microporous regions, respectively (for spherical geometry, $A_p/V_p = 3/R$). The resultant model was solved using the code PDECOL [8].

Results and Discussion

In Figure 2 are presented results of the model for three heating rates under conditions where there is a single activation energy for the desorption of each of the surface species. As can be observed, the peak maximum is quite sensitive to heating rate, moving to higher temperatures with heating rate, as expected for first order desorption processes. In order to match the peak temperatures of 600K and 1000K evident in the data in Figure 1 at 100K/min, the required activation energies are 38.8 and 66.7 kcal/mol, respectively. It is also noted that the two peaks are relatively narrow.

In Figure 3, model results are presented which incorporate surface heterogeneity, modeled as presented above, *plus* secondary reactions via [R.1], for the same three heating rates used in Figure 2. As can be ascertained from this figure, save for the high temperature shoulder on the CO peak (an effect which is not included in the model), these results are quite similar to the experimental spectra presented in Figure 1, especially, of course, the one calculated for a heating rate of 100K/min. Obviously, surface heterogeneity broadens the features considerably. Also, the sensitivity to heating rate is still evident.

Our experimental TPDs do not exhibit as much sensitivity to heating rate as those shown in the model results of Figures 2 and 3. Some sample experimental TPDs are presented in Figures 4 and 5. Although Figure 4 for the Stockton-Lewiston coal char does exhibit some variation of the major CO peak temperature with heating rate, the Pittsburgh #8 coal char shows practically none. Therefore, at this point we are still unsure as to whether surface heterogeneity can entirely account for this experimentally observed behavior, and/or whether the fundamental assumption concerning first order desorption is in error.

In any case, the major striking feature of Figure 3 is the appearance of a second CO_2 "reflection" peak under the major CO desorption peak, which is obviously due to secondary reaction via the forward step of [R.1]. In fact, in all our extensive experimental TPD data on porous coal chars, we have never observed a CO peak ca. 1000K without also observing a "reflection" CO_2 peak. The "reflection" peak in Figure 3 decays with significantly greater "tailing" than the CO peak. That this "tailing" is not due to diffusional resistance is evident by comparison with the first CO_2 peak which does not "tail" very much at all, under the conditions assumed. It is also noted that in order to produce the "reflection" peak, the reverse step of [R.1] must also be included. If this is not done, the rate of conversion to CO will increase much more rapidly with temperature since the rate constant is assumed to be Arrhenius temperature dependent. Under these conditions, the conversion of CO will continue unabated until all the surface complex is exhausted. The reverse reaction is also required by the principal of microscopic reversibility.

Figure 6 presents model results obtained by varying the diffusion time, t_d. As can be seen, increasing the diffusion time over the range examined, by increasing t_d from 2 to 200 s, does not appreciably increase "tailing" of the "primary" CO_2 and CO peaks. However, the degree of secondary reaction is quite sensitive to the diffusion time. The higher the diffusion time, the greater the conversion of free CO to CO_2 via [R.1], as manifested by a decreasing "primary" CO peak, and an increasing "secondary" CO_2 peak; by t_d = 200s, the "secondary" CO_2 peak is *greater* than the "primary" CO peak in this calculation. In addition, it is interesting to note that the "secondary" CO_2 peak progressively shifts to lower temperature, while the primary CO peak shifts to higher temperature with increasing degree of secondary reaction. In fact, for t_d = 200s, the "secondary" CO_2 peak crosses the "primary "CO peak. This type of behavior has also been noted experimentally in our coal char TPDs. One such representative set of results for Wyodak coal char is shown in Figure 7.

The enhancement of secondary reaction with increasing t_d is due, of course, to the fact that increased intrapore residence time favors the conversion of free CO to CO_2 via [R.1]. The degree of secondary reaction is primarily dependent on three variables: the concentration of intrapore CO; [CO] surface complex coverage; and intrapore residence time. Although we have not yet shown it with the model, we believe that the maximum in net CO_2 production with heating rate [4] is a manifestation of this effect. That is, at low heating rates the amount of CO_2 increases with heating rate, as occurs in Figure 6, since higher temperatures are achieved at high enough intrapore concentrations to enhance CO_2 formation via [R.1]. However, at some point, the intrapore residence time becomes low enough due to the large intrapore gradients induced by rapid desorption, and perhaps enhanced by rapid activated diffusion, that intrapore concentrations begin to progressively decrease by the time the appropriate temperature range is attained in the course of the TPD. The resultant effect is to decrease the net amount of CO_2 produced beyond this point - hence the maximum.

Conclusions

The preceding has shown that a numerical model of the TPD behavior of surface oxygen complexes is a very useful tool for aiding in the interpretation of experimental TPD data. The fact that secondary reaction via [R.1] contributes significantly to the spectra, in terms of CO_2 "reflection" peaks and diminution of the primary CO peak, shows that it becomes a very important consideration under the appropriate conditions. The fact that the degree of secondary reaction has been found to be very sensitive to the kinetic parameters, energetic heterogeneity via the activation energy variation with surface coverage, and the diffusion time may help explain the significant *quantitative* variations in TPD spectra obtained by different workers on various chars and carbons. In fact, it may be possible to develop the sensitivity of secondary reaction to intrapore diffusivity into a technique for measuring transport rates. Diffusional resistances of the order-of-magnitude examined here do not seem to contribute appreciably to "tailing" and broadening of the primary desorption peaks; surface heterogeneity seems to be primarily responsible for the latter. This result will be used to obtain a measure of the energetic heterogeneity of coal chars under varying conditions. The model will be the primary tool in this regard. Recently, we have also begun to incorporate CO re-adsorption onto high-energy sites during the course of TPD, in order to model the high temperature shoulder, which, under certain circumstances, we have observed develop into a separate CO peak, the appearance of which varies considerably depending on various conditions. This mechanism represents another secondary interaction effect with the char surface that occurs during TPD that must be taken into account in order to properly deconvolute TPD spectra of oxygen complexes from coal chars.

Acknowledgement

This paper resulted from work under contract number DE-AC21-87MC232384 from the Morgantown Energy Technology Center of the U.S. Department of Energy.

References

1. Tremblay, G., Vastola, F.J., and Walker, P.L., Jr. *Carbon* **16**, 35 (1978).
2. Otake, Y., *Ph.D. Dissertation,* The Pennsylvania State University, 1986.
3. Marchon, B., Carrazza, J., Heinemann, H., and Somorjai, G.A. *Carbon* **26**, 507 (1988).
4. Calo, J.M. and M.T. Perkins,*Carbon* **25**, 395 (1987).
5. Hall, P.J., and Calo, J.M., submitted to *Energy and Fuels,* 1988.
6. Hall, P.J., and Calo, J.M., *Proc. Int. Carbon Conf., Carbon '88,* B. McEnaney and T.J. Mays, eds., p. 77, IOP Publishing Co., Bristol, U.K., 1988.
7. Marchon, B., Tysoe, W.T., Carrazza, J., Heinemann, H., and Somorjai, G.A. *J. Phys. Chem.* (1988).
8. Madsen, N.K., and Sincovec, R.F. *ACM Trans. Math. Software,* **5**, 326 (1979).
9. Debelak,K., DOE Final Technical Report for METC Contract No., DE-AC21-81MC16053-F, August,1983.
10. Strange, J.F., and Walker, P.L., Jr., *Carbon* **14**, 345 (1976).

Table I. "Base case" parameter values.

$k_{1d,0}$, $k_{2d,0}$	kT/h	s^{-1}
k_{10}	3.14×10^{18}	$cm^3/mol\ s$
$k_{2,0}$	1.25×10^{22}	$cm^3/mol\ s$
$E_{1d,0}$, α	73.0,10.0	kcal/mol
$E_{1d,0}$, β	41.0,100.0	kcal/mol
$R^2/D_{1,0}$	2(1)	s
$D_{2,0}/D_{1,0}$	7(1)	-
E_{d1}, E_{d2}	2(1)	kcal/mol
C_t	2.5×10^{-5}	mol/cm^3 (2)
ε	0.3	-
B	1.67	K/s
$E_{1,0}$, γ	74.0(3),20.0	kcal/mol
$E_{2,0}$, δ	99.0(3),10.0	kcal/mol

(1) Estimated from Ref. [9].
(2) mol active sites/cm^3 of microporous carbon region.
(3) Obtained from Ref. [10].

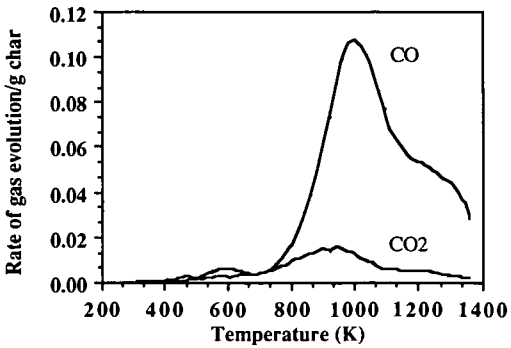

Figure 1. Experimental TPD spectra of Pittsburgh #8 coal char gasified to 27.3% burn-off in 0.1MPa of oxygen at 723K; taken at 100K/min.

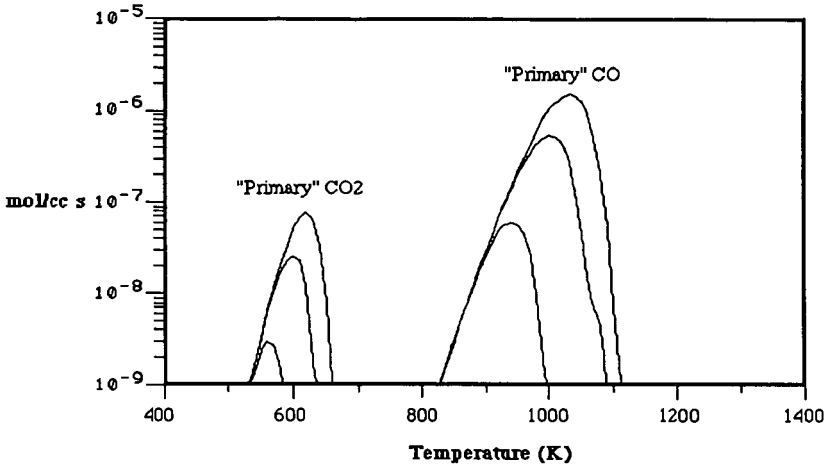

Figure 2. Model TPD spectra for two types of homogeneous complexes (i.e.; CO_2- and CO-liberating), at three heating rates: 300K/min; 100K/min; and 30K/min. The higher heating rate corresponds to the larger peak in each case. The activation energies for the 600K and 1000K peaks are 38.3 and 66.7 kcal/mol, respectively. The logarithmic ordinate scale is used to present all three cases conveniently on one plot.

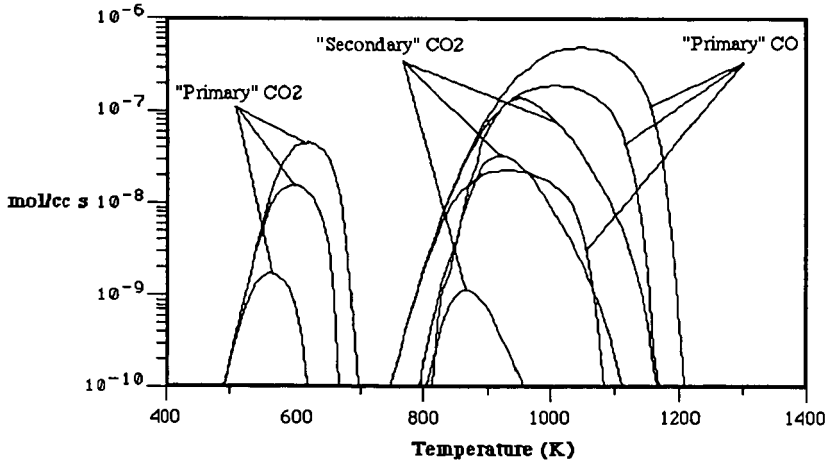

Figure 3. Model TPD spectra, including surface heterogeneity and secondary reaction via [R.1], for the "base case" parameter set listed in Table I, for three heating rates: 300K/min; 100K/min; and 30K/min. The higher heating rate corresponds to the larger peak in each case. The logarithmic ordinate scale is used to present all three cases conveniently on one plot.

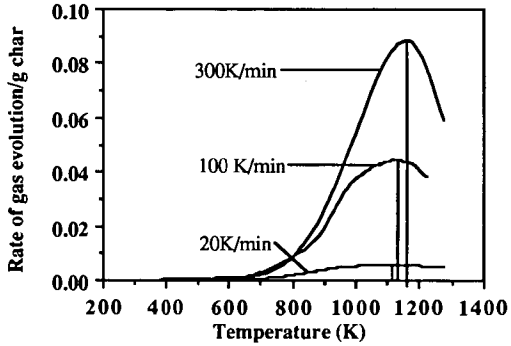

Figure 4. Experimental CO TPD spectra for Stockton-Lewiston coal char after chemisorption for twelve hours in 0.1MPa of oxygen at 523K at heating rates of 300K/min, 100K/min, and 20K/min.

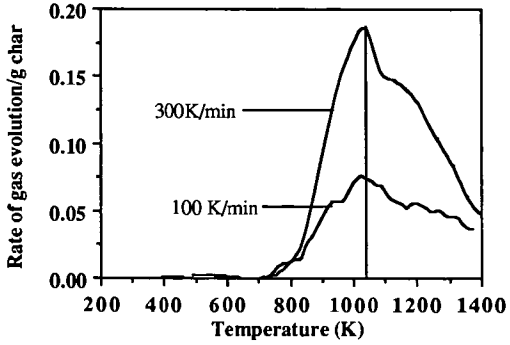

Figure 5. Experimental CO TPD spectra for Pittsburgh #8 coal char gasified to 10% burn-off in 0.1MPa of oxygen at 823K at heating rates of 300K/min and 100K/min.

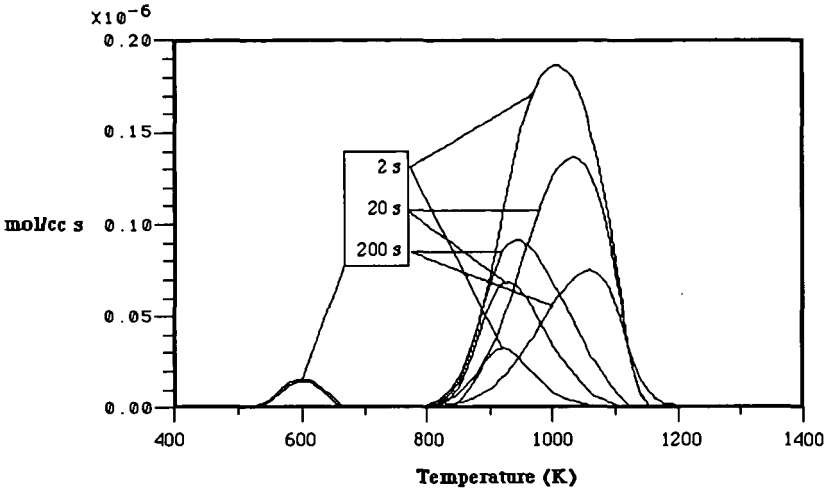

Figure 6. Model TPD spectra, including surface heterogeneity and secondary reaction via [R.1], for the "base case" parameter set listed in Table I with diffusion times of 2, 20, and 200 s.

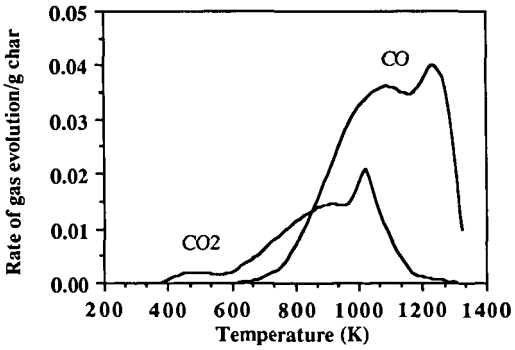

Figure 7. Experimental TPD spectra of ungasified Wyodak coal char exposed to 0.1MPa of oxygen at 573K for twelve hours; taken at 100K/min.

TRANSIENT KINETIC STUDIES OF CHAR GASIFICATION IN CARBON DIOXIDE

Hong Jiang and Ljubisa R. Radovic
Department of Materials Science and Engineering
Fuel Science Program
The Pennsylvania State University
University Park, PA 16802

INTRODUCTION

The rate (R) of a heterogeneous gas/solid reaction (e.g., char gasification) at a given level of solid conversion (X_s) and at constant reactant gas pressure can be expressed in the following form [1,2]:

$$R \equiv \frac{1}{1-X_s}\frac{dX_s}{dt} = kC_s \qquad (1)$$

In Equation 1, C_s is the "concentration" of the solid. It is conventionally identified with the total surface area (TSA) of the solid. Two parameters are of primary practical and fundamental interest here: the rate constant (k) and the time (t) necessary to achieve complete solid (char) conversion.

The rate constant for char (carbon) gasification expressed per unit TSA is very much dependent on the origin and/or thermal history of the char [1,3,4]. The rate constant expressed per unit ASA was found to be a function of temperature only, within a factor of 2-3 [1,3].

At constant reactant gas pressure, the complete char consumption time is determined from the following expression:

$$t = \frac{1}{k}\int_0^1 \frac{dX_c}{C_c(1-X_c)} \qquad (2)$$

It is seen that the integration of this expression requires the knowledge of the conversion dependence of the char concentration term, i.e., $C_c = f(X_c)$. Laine et al. [5] were successful in determining this functional relationship for the gasification of a graphitized carbon black with oxygen; they determined the unoccupied active surface area (UASA) by taking into account the inhibiting effect of the stable complex formed during the low-pressure reaction. Attempts to determine UASA using the same [6] or analogous [7] approach for less ordered carbons such as coal chars have not been successful, however. A satisfactory correlation was not found between the total active surface area (ASA), measured by low-temperature oxygen chemisoprtion, and rate variations with conversion [6,7]. The consequences of this finding can best be analyzed by noting that the rate is proportional to the number of reactive sites, i.e., sites at which the carbon-oxygen intermediate forms (at reaction temperature) and decomposes to form gaseous reaction products. These should be distinguished from the sites that give origin to a "stable" complex which inhibits, at least temporarily, the formation of the reaction intermediate [5]. Therefore, Equation 1 can be rewritten as:

$$R = k\,(TSA)\left(\frac{ASA}{TSA}\right)\left(\frac{RSA}{ASA}\right) \qquad (1a)$$

Very few, if any, studies of carbon and char gasification kinetics have attempted the direct determination of the reactive surface area (RSA). In practically all existing kinetic models, for example, the assumption is made that RSA/TSA is constant and the gasification reactivity profiles (reactivity variations with conversion) are thus interpreted on the basis of TSA variations with conversion. More often than not, however, this assumption is not valid [2]. In our experience, the useful simplifying assumption that RSA/ASA is constant is most often valid to within a factor of 2-3 [1,8]. When a more precise comparison of reactivities of different chars is needed or when Equation 2 needs to be solved for a given char, this assumption needs to be relaxed and tested.

The technique of transient kinetics has often been used in heterogeneous catalysis [9]. It has the virtue of being able to provide separately the rate constant and the (re)active site density (RSA). Only recently has its use been suggested [10] and reported [11,12] for providing new insights into carbon (char) gasification kinetics. In this paper, we discuss its application to char gasification in carbon dioxide.

EXPERIMENTAL

Three chars were used in this study: a relatively pure Saran char, prepared from the corresponding copolymer [1]; a bituminous coal char, with a significant quantity of noncatalytic inorganic constituents, obtained from a high volatile A bituminous coal (PSOC 1098) [13]; and a lignite char, with the catalytically active calcium (Dem+Ca) loaded by ion exchange onto the demineralized lignite (PSOC 246) [3,13]. More detailed char characterization is given elsewhere [14].

Figure 1 gives the schematic representation of the experimental system. A char sample (20-70 mg, <75 μm) is reacted in a differential fixed-bed flow reactor (1 cm, ID) and the products are continuously monitored by nondispersive infrared analysis (Beckman, model 864). All samples were heated to 1173 K under flowing N_2 (99.999% purity), and then cooled to the gasification temperature (in the range 950-1130 K, chosen to obtain comparable char reactivities). After partial gasification, the flow of CO_2 (200 cm^3/min, STP) was interrupted and switched back to that of N_2 (200 cm^3/min, STP) at the same reaction temperature. The steady-state and transient response of CO concentration vs. time were monitored by the infrared analyzer.

Preliminary runs were carried out to determine the reaction conditions of temperature, sample size, particle size, and gas flow rate to eliminate mass transfer limitations [14].

RESULTS AND DISCUSSION

Figure 2 shows the steady-state rate variation with conversion (or time) for the bituminous coal char gasified in 1 atm CO_2 at different temperatures. A monotonically increasing specific gasification rate (in g char reacted per hour per unit mass of unreacted char) is observed in all cases. Figure 3 shows the Arrhenius plot for the same char. The activation energy was found to be 60 ± 2 kcal/mol and constant over the entire conversion range; this indicated the absence of transport limitations.

Figure 4 shows typical transient responses observed when the flow or reactant gas (CO_2) was replaced, at a particular conversion level, by that of the inert gas (N_2). The time scale for the achievement of baseline concentration levels of the product (CO) was of the order of minutes for all samples. With no sample in the reactor (blank experiment), this time scale was of the order a few seconds.

The well known and generally accepted [15] mechanism of the reaction, involving free carbon (re)active sites (C_f), was assumed:

$$C_f + CO_2 \leftrightarrow C\text{-}O + CO \qquad (3a)$$

$$C\text{-}O \rightarrow CO + C_f \qquad (3b)$$

The reaction rate is equal to the rate of decomposition of the C-O intermediate. The integrated area under the transient response curve, such as shown in Figure 4, gives the concentration of C-O intermediates (i.e., RSA) at the conversion level at which the steady-state reaction was interrupted.

Figures 5-7 show the results of transient kinetic experiments for the three chars used in this study. In all cases both the reaction rate and RSA monotonically increase with conversion. The reactive surface area of the lignite char, in which CaO acts as an efficient CO_2 dissociation center (catalyst) [3], is seen to be almost an order of magnitude higher than the RSA of the Saran and bituminous coal chars, in which CO_2 dissociation occurs predominantly on the carbon (re)active sites. It is interesting to note that RSA of the latter two is one order of magnitude smaller than their ASA (low-temperature oxygen chemisorption capacity) [1]. It is two orders of magnitude higher, though, than the relatively low value obtained by Freund [11] for a Carbosieve, also a highly disordered carbon, gasified in CO_2 at 850-980 K.

In complementary studies [7,16], we have found that the amount of stable complex (remaining on the char surface after partial gasification and subsequently removed at higher temperatures by temperature-programmed desorption) on these chars also increases monotonically with conversion, by a factor of about 3-4. The oxygen chemisorption capacity (ASA) of the bituminous coal char, on the other hand, exhibited a maximum value at an intermediate conversion level, therefore indicating that RSA/ASA varies with conversion. Two practical consequences of these findings have emerged [1,16]:
(1) For a quantitative explanation of char reactivity profiles, direct measurements of RSA are necessary; the amount of stable complex on the char surface can also be used, at least qualitatively, because it seems to correlate well with RSA.
(2) For a quantitative explanation of reactivity differences among different chars, ASA is good to within a factor of 2-3; the amount of stable complex on the chars surface cannot be used because it is very sensitive to the reaction temperature and its value decreases with increasing temperature.

From a fundamental standpoint, two issues need further discussion: (1) the reason for the apparent existence of a qualitative correlation between RSA and the amount of stable complex on the surface of a char at a given temperature; (2) the existence of a turnover frequency for char gasification. The former is discussed in some detail elsewhere [16,17]; suffice it to say here that "stable" complex formation should be regarded not only as a temporarily inhibiting process [5], but also as an intermediate step in the mechanism of gasification, particularly for disordered carbons and at relatively high pressures.

Figure 8 shows excellent linear relationship between reactivity and RSA for the three chars analyzed in this study. Thus obtained rate constants (see Equation 1a), or turnover frequencies [18], are seen to be independent of conversion. Their values are 20.8 h^{-1} (1133 K), 14.4 h^{-1} (1093 K), and 4.0 h^{-1} (953 K) for the Saran char, bituminous coal char and Dem+Ca lignite char, respectively. These are, not unexpectedly, relatively low values compared to the commonly encountered catalyst turnover frequencies of 1 s^{-1} [18]. It is also interesting to compare the turnover frequency for the Dem+Ca lignite char obtained here with that obtained for a similar char gasified with O_2 [19]; the latter value (about 0.3 s^{-1}) is several orders of magnitude higher, as expected. A comparison of turnover frequencies of the Saran char and the bituminous coal char at

the same temperature is also interesting. At 1103 K, these are 9.8 h^{-1} and 16.8 h^{-1}, respectively [14]. This suggestion of possible structure sensitivity [18,20] of char gasification is being investigated further in our laboratory.

SUMMARY AND CONCLUSIONS

The analysis of char gasification in CO_2 using the transient kinetic approach gives a direct measurement of the reactive surface area of chars. The use of this technique has also provided the heretofore elusive quantitative experimental explanation of reactivity variations with conversion. It was found that the ratio of the reactive surface area of a bituminous coal char to its active surface area is not constant, but varies as a function of conversion. Turnover frequencies for char gasification in CO_2 have been determined. Preliminary experiments suggest that char gasification may be a structure-sensitive reaction.

ACKNOWLEDGEMENTS

Initial support of this work by the Minerals Research Institute and the Cooperative Program in Coal Research at Penn State University is gratefully acknowledged. Further support was provided by the Gas Research Institute, Contract No. 5086-260-1419. The coal samples were obtained from the Penn State/DOE Coal Sample Base.

REFERENCES

1. Radovic, L.R., Walker, P.L., Jr. and Jenkins, R.G. Fuel 62, 849 (1983).
2. Radovic, L.R., Lizzio, A.A. and Jiang, H. Carbon, submitted (1988).
3. Radovic, L.R., Steczko, K., Walker, P.L., Jr. and Jenkins, R.G. Fuel Process. Technol. 10, 311 (1985).
4. Smith, I.W. Fuel 57, 409 (1978).
5. Laine, N.R., Vastola, F.J. and Walker, P.L., Jr. J. Phys. Chem. 67, 2030 (1963).
6. Taylor, R.L. and Walker, P.L., Jr. Extended Abstracts, 15th Biennial Conference on Carbon, Philadelphia, PA, 1981, p. 437.
7. Radovic, L.R. and Lizzio, A.A. Proceedings of the 4th Annual Pittsburgh Coal Conference, 1987, p. 440.
8. García, X. and Radovic, L.R. Fuel 65, 292 (1986).
9. Biloen, P. J. Mol. Catal. 21,17 (1983).
10. Kapteijn, F. and Moulijn, J.A. "Carbon and Coal Gasification," (J.L. Figueiredo and J.A. Moulijn, Eds.), NATO ASI Series, E 105, Martinus Nijhoff Publishers, 1986, p. 219.
11. Freund, H. Fuel 65, 63 (1986).
12. Adschiri, T., Zhu, Z.-B. and Furusawa, T. International Conference on Coal Science, Elsevier, 1987, p. 515.
13. PennState/DOE Coal Data Base, The Pennsylvania State University.
14. Jiang, H. M.S. Thesis, The Pennsylvania State University, 1989.
15. Laurendeau, N.M. Prog. Energy Combust. Sci. 4, 221 (1978).
16. Lizzio, A.A. and Radovic, L.R. ACS Preprints (Div. Fuel Chem.), Dallas, 1989.
17. Radovic, L.R., Lizzio, A.A. and Jiang, H. Extended Abstracts, 19th Biennial Conference on Carbon, University Park, PA, 1989.
18. Boudart, M. and Djéga-Mariadassou, G. "Kinetics of Heterogeneous Catalytic Reactions," Princeton University Press, 1984.
19. Radovic, L.R., Walker, P.L., Jr. and Jenkins, R.G. J. Catal. 82, 382 (1983).
20. Carberry, J.J. J. Catal. 107, 248 (1987).

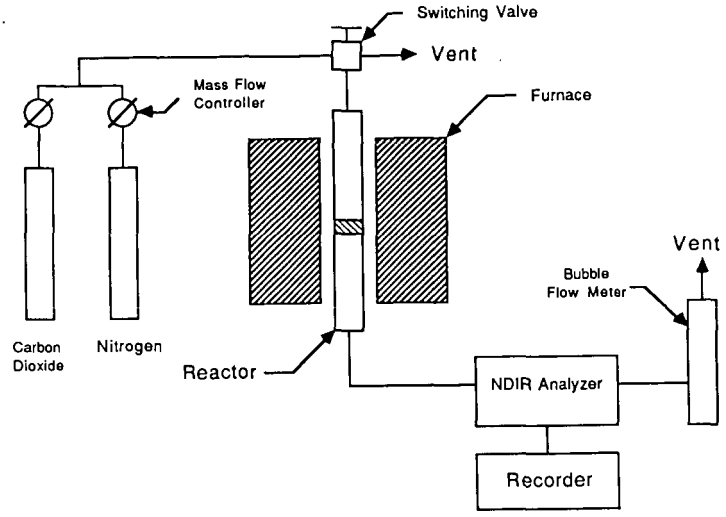

Figure 1. Schematic representation of the experimental system for transient kinetic studies.

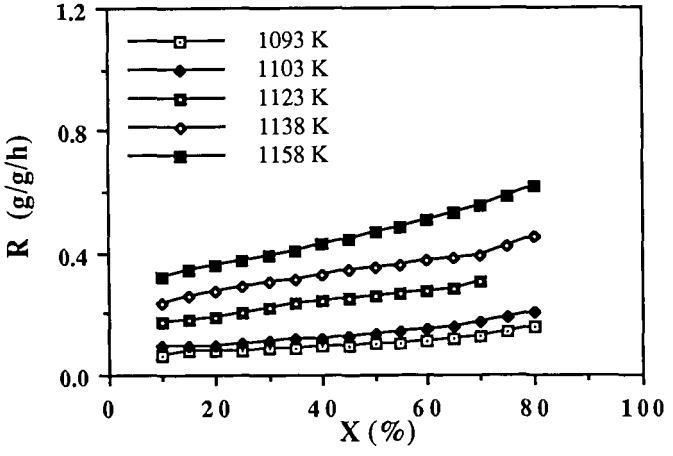

Figure 2. Typical steady-state responses of the experimental system: specific rate vs. conversion for the gasification of bituminous coal char in 1 atm CO_2.

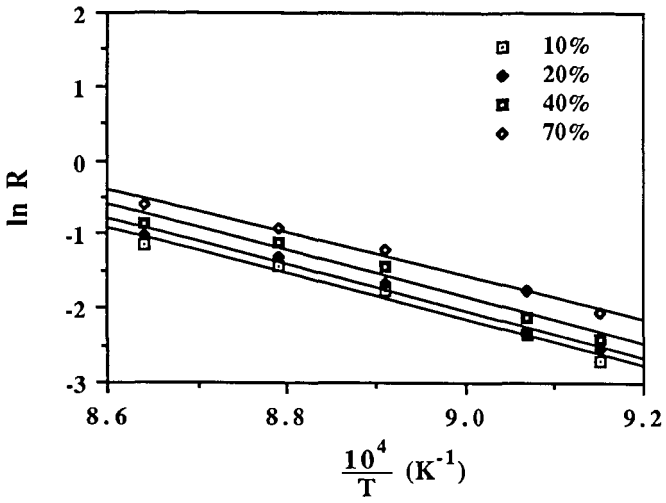

Figure 3. Arrhenius plot for the gasification of bituminous coal char in 1 atm CO_2.

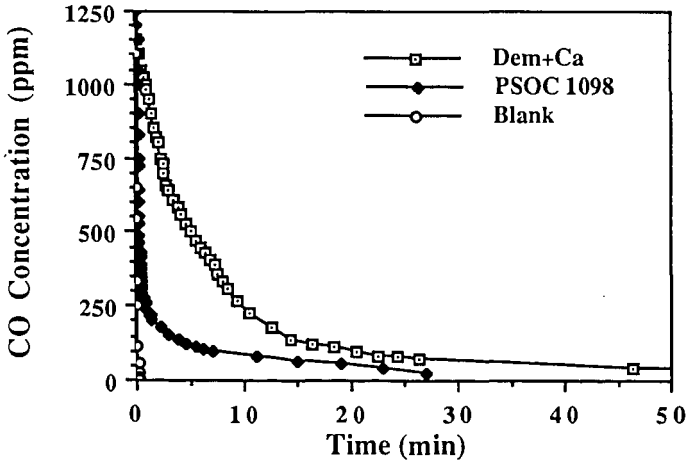

Figure 4. Typical transient responses of the experimental system.

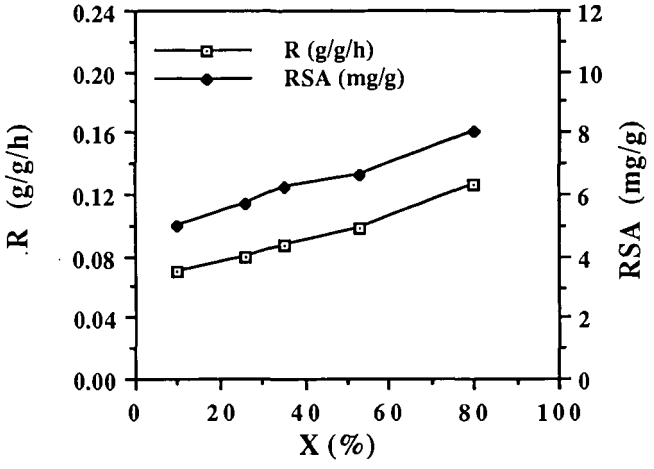

Figure 5. Specific rate and reactive surface area vs. conversion for the bituminous coal char gasified in 1 atm CO_2 at 1093 K.

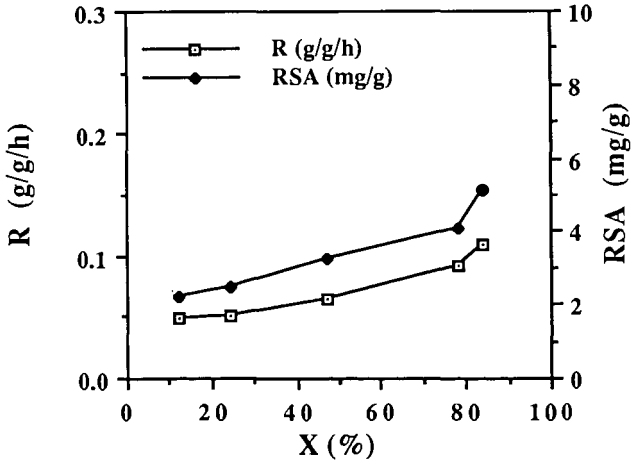

Figure 6. Specific rate and reactive surface area vs. conversion for Saran char gasified in 1 atm CO_2 at 1133 K.

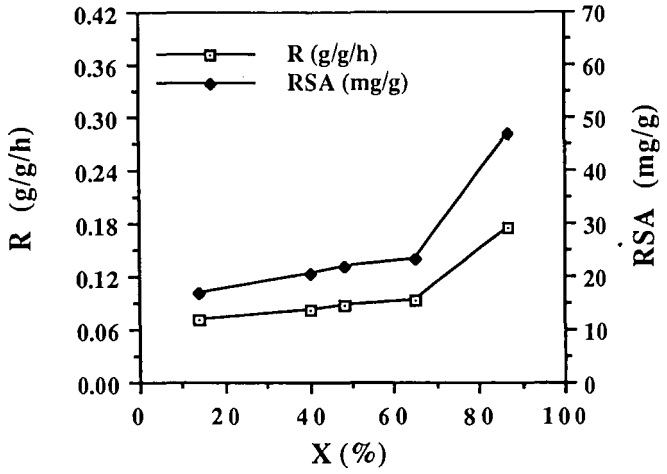

Figure 7. Specific rate and reactive surface area vs. conversion for Dem+Ca char gasified in 1 atm CO_2 at 953 K.

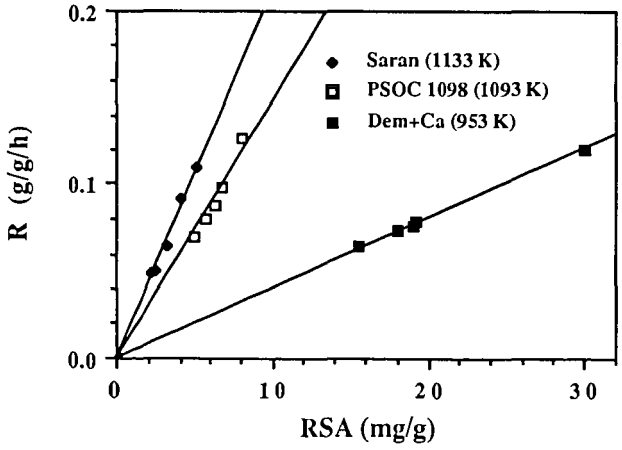

Figure 8. Determination of turnover frequency for the gasification of chars in 1 atm CO_2.

CHARACTERIZATION OF COAL CHAR REACTIVITY BY THE NUMBER OF ACTIVE SITES DURING CO_2 GASIFICATION

Z-B, Zhu
Department of Chemical Engineering
East China Institute of Technology
May Road, CHINA

T.Furusawa, T.Adschiri and T.Nozaki
Department of Chemical Engineering
The University of Tokyo
7-3-1 Hongo, Bunkyo-ku, 113 JAPAN

ABSTRACT

The present authors modified the transient kinetics method for the evaluation of the number of working active sites. The method was effectively used for the unified interpretation of both the reactivity and its dynamic change with increased conversion of nine different chars which are different in nature and origin. This method was developed furthermore for the evaluation of elemental reaction rate constants.

INTRODUCTION

Gasifier performance significantly depends on the coal char reactivity which are largely different among different chars. Thus the rational design and analyses of coal gasifier require the prediction of coal char reactivity as well as the sound understanding of gas-solid contact. Previous workers have tried to interpret the difference of the gasification rate by introducing various parameters including surface area(1) and the amount of metals in ash. Present authors have developed the new method to count the mol numbers of carbon atoms during gasification for the evaluation of char reactivity by transient kinetics experiment(2,3). The objective of the present study is the further development of this method for the evaluation of the elemental reaction rate constants.

EXPERIMENTAL

The experiments were conducted in a horizontal quartz tube reactor(i.d. 6 mm). The amount of chars of 15-85 mg was loaded in the middle part of the reactor tube. The reactor was heated up to the gasification temperature at the heating rate of 5 K/min in the pure nitrogen stream(2 m/s). The temperature of the bed was measured by a clomel-alumel thermocouple placed within the bed. The temperature difference trough the bed was within 1 K at 1173K.

The nitrogen stream was switched over to carbon dioxide stream(2 m/s). The concentration of carbon monoxide produced was analyzed by FID after methanation. The variation of carbon monoxide concentration was followed intermittently at intervals of several seconds. The gasification rate of chars at atmospheric pressure are evaluated from the concentration of carbon monoxide, as follows.

$$\frac{dX}{dt} = \frac{C\ F}{2\ 0.025}\ \frac{0.012}{W_0} \quad [s^{-1}] \qquad (1)$$

where conversion of char was evaluated from the integrated amount of carbon monoxide produced. Then the carbon dioxide stream was switched over to nitrogen stream and the transient decay of carbon monoxide concentration was followed intermittently. After the concentration of carbon monoxide became so low as to be ignored, carbon dioxide were introduced again. This procedure was repeated several times to cover the whole range of conversion.

RESULTS AND DISCUSSION

Outline of our previous results and unified interpretation of char reactivity by number of working active sites

The number of working active sites was defined as the integrated amounts of carbon monoxide evolved after shutting off the carbon dioxide stream, as follows.

$$n = \int_0^t \frac{C\ F}{0.025}\ \frac{0.012}{W_0}\ dt \qquad (2)$$

Previous investigation proved that the effects of both the backmixing of gases in the system on the number of active sites are negligible under the present experimental condition(2).

Figure 1 demonstrated that sixty times differences among the gasification rates of chars were fairly well interpreted by the difference in the number of working active sites at the temperature of 1173 K(3). The gasification rates normalized by the number of working active sites, dX/dt/n, decrease slightly with increased conversion but remain mostly constant during gasification, as shown in Fig.2(3). Thus evaluated results were plotted against reciprocal temperature in Fig.3. The result indicated that the rate per unit number of working active sites is the function of temperature alone. The activation energy of the reaction is around 125kJ/mol. Similar results of the rate normalized by surface area, dX/dt/S(X), were obtained in our previous study(2,3).

Thus the present results support our previous results that surface area is an available parameter for the interpretation of both the difference and the dynamic change in gasification rate with increased conversion. Evaluated number of working active sites may be closely related to the number of intermediate species, such as surface oxide complex.

Development of new method

The rate constant of carbon monoxide desorption, K_d, after terminating gasification were also evaluated. The typical results of the desorption of carbon monoxide was shown in Fig.4. The results indicated that the partial pressure of carbon dioxide affects the number of working active sites but does not the desorption rate constant, K_d. The number of working active sites increased but the increasing rate decreased with increased partial pressure of carbon dioxide, as shown in Fig.5. The number of working active sites will be saturated at higher

pressure. Saturation mechanism is discussed later.

Figure 6 shows the typical dynamic change of carbon monoxide concentration, C(t), after introducing carbon dioxide at the temperature of 1123 K for Taiheiyo coal char. Steady state concentration, $C_{st}(t)$, in the early period were evaluated by extrapolation of C(t) over the latter period. The dynamic change of $[C(t)-C_{st}(t)]$ are shown in Fig.7. The rate constants, K, were evaluated over the range of carbon dioxide partial pressure from 15kPa to 100kPa. The dependency of the evaluated rate constant, K, on carbon dioxide partial pressure shown in Fig.8 can be described as follows.

$$K = L + J\,P_{CO2} \tag{3}$$

The intercepts, I, are found to be almost the same as the desorption rate constants, K_d.

The following mechanism proposed by Ergun(3) and accepted widely can be used to interpret the above results.

$$C + CO_2 = C(O) + CO \tag{4}$$
$$C(O) = CO \tag{5}$$

The first step is the dissociative adsorption of carbon dioxide which produce the surface oxide complex and the second step is the desorption of surface oxide complex to produce carbon monoxide.

The dynamic response of carbon monoxide after introducing carbon dioxide, C(t), can be expressed as

$$C(t) = \frac{0.025}{F}\,\frac{I_1P_{CO2}N}{I_1P_{CO2}+I_3}\,\frac{W_0}{0.012}\,[2I_3+(I_1P_{CO2}-I_3)\exp(-(I_1P_{CO2}+I_3)t)] \tag{6}$$

The steady state concentration of carbon monoxide, C_{st} is

$$C_{st} = \frac{0.025}{F}\,\frac{2I_1P_{CO2}I_3N}{[I_1P_{CO2}+I_3]}\,\frac{W_0}{0.012} \tag{7}$$

The the difference of the concentration, $C(t)-C_{st}$, is

$$C(t)-C_{st} = \frac{0.025}{F}\,\frac{2I_1P_{CO2}I_3N}{I_1P_{CO2}+I_3}\,\frac{W_0}{0.012}\,(I_1P_{CO2}-I_3)\exp(-(I_1P_{CO2}+I_3)t) \tag{8}$$

The rate constant of variation of $[C(t)-C_{st}]$ is $(I_1P_{CO2}+I_3)$ which is consistent with the P_{CO2} dependence of the rate constant shown in Fig.8. Thus the intercept in the figure is I_3, according to the above mechanism.

The dynamic change of carbon monoxide after shutting off the carbon dioxide is explained by the reaction of the second step, namely the desorption of surface oxide complex.

$$C_d(t) = 0.025n_0(W_0/0.012)\exp(-I_3t)/F \tag{9}$$

Thus, the consistence of K_d and L evaluated above can be also interpreted.

The number of working active site is related to the partial pressure of carbon dioxide and the total number of active site, N, as

$$1/n = 1/N + (1/N)I_3/I_1P_{CO2} \qquad (10)$$

The reciprocal number of working active site, (1/n), is plotted against $1/P_{CO2}$ in Fig.9. The pressure dependence of the number of working active site, n, can be explained by Eq.(10). The slope of this figure is almost the same as the ratio of I_3 and I_1P_{CO2} which were evaluated above. The intercept is 1/N and thus the total number of active sites can be also evaluated.

CONCLUSION

The present authors has developed the new method to evaluate the number of working active sites during gasification. The difference of the reactivity among nine chars which are different in nature and origin could be fairly well interpreted by the number of working active sites. Dynamic change of reactivity with increased conversion could also be explained by the change of the number of working active sites.

The pressure dependency of working active site was investigated. The transient kinetics method was developed furthermore for the evaluation of elemental reaction rate constants and total number of active sites.

NOMENCLATURE

C	concentration of carbon monoxide	[-]
C_{st}	steady state concentration of carbon monoxide	[-]
F	gas flow rate	[$m^3 s^{-1}$]
I	rate constant	[s^{-1}]
J	rate constant	[$s^{-1}atm^{-1}$]
K	rate constant	[s^{-1}]
K_d	rate constant	[s^{-1}]
L	rate constant	[s^{-1}]
N	total number of active site	[$mol_{carbon}\ mol^{-1}_{initial\ carbon}$]
n	number of working active site	[$mol_{carbon}\ mol^{-1}_{initial\ carbon}$]
P	partial pressure	[atm]
S	surface area	[$m^2 kg^{-1}_{carbon}$]
T	absolute temperature	[K]
t	time	[s]
W_0	initial weight of carbon	[kg]
X	conversion	[-]

REFERENCES

1) Adschiri, T. and Furusawa, T., Fuel, 65, 927(1986)
2) Zhu, Z-B, Adschiri, T., Furusawa, T., Proceedings of Int. Symp. Coal Science 1987, pp515-518
3) Zhu, Z-B, Adschiri, T. and Furusawa, T., Proceedings of the 2nd Japan-China Symposium on Coal and C_1 Chemistry, 51
4) Ergun, S., J. Phys. Chem. 60, 480(1956)

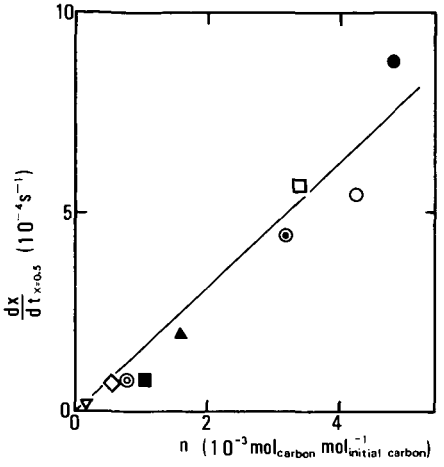

Figure 1. Relationship between the gasification rates and the number of working active sites.

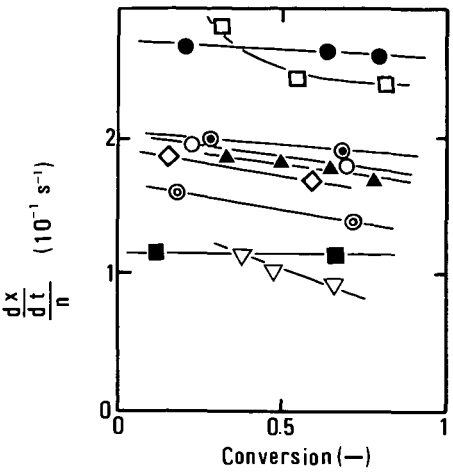

Figure 2. Gasification rates per unit number of working active sites.

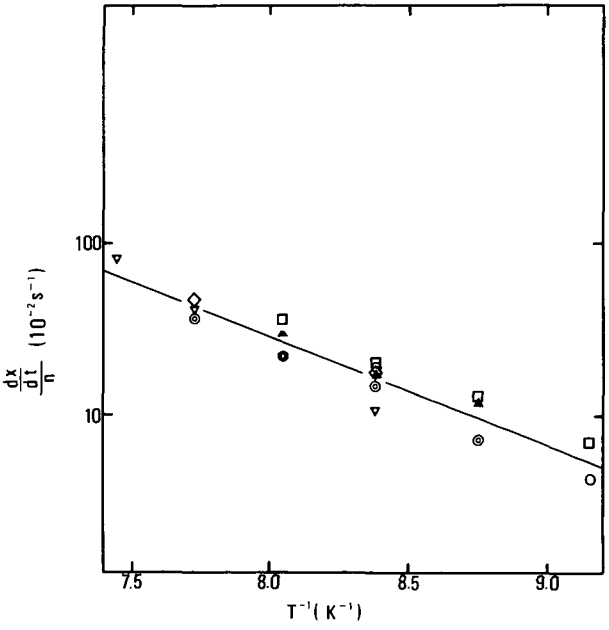

Figure 3. Arrhenius plot of gasification rates per unit number of working active sites.

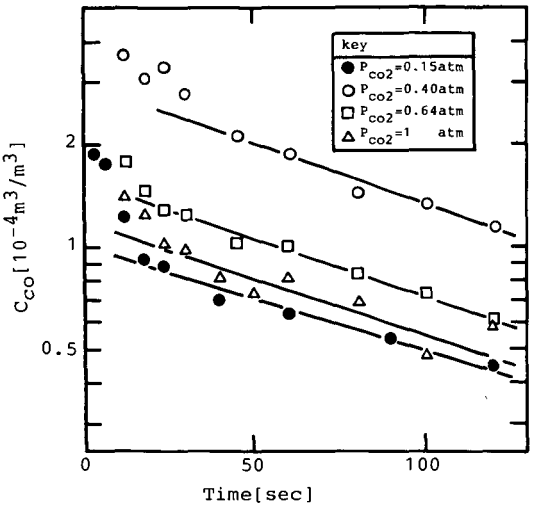

Figure 4. The typical disorption of carbon monoxide.

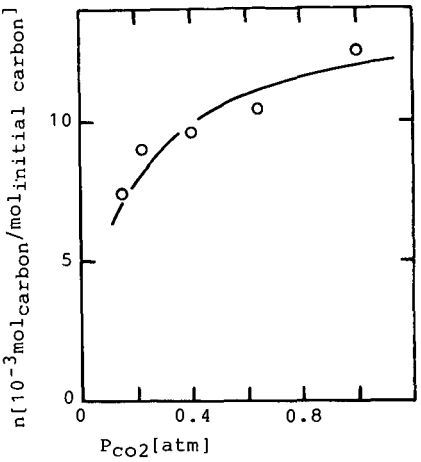

Figure 5. The number of working active sites Vs. partial pressure of carbon dioxide.

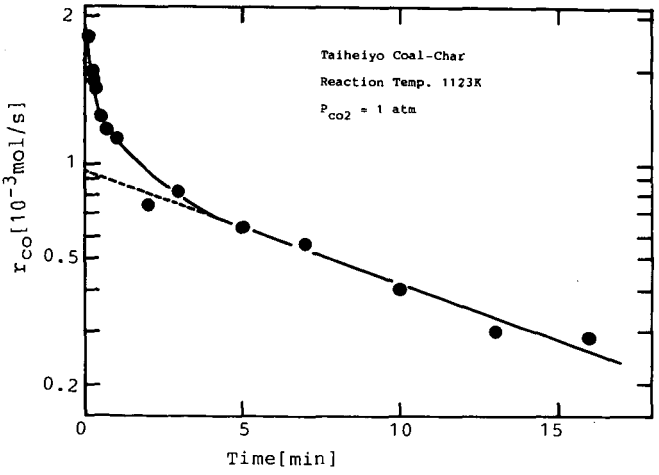

Figure 6. The typical dynamic change of carbon monoxide concentration.

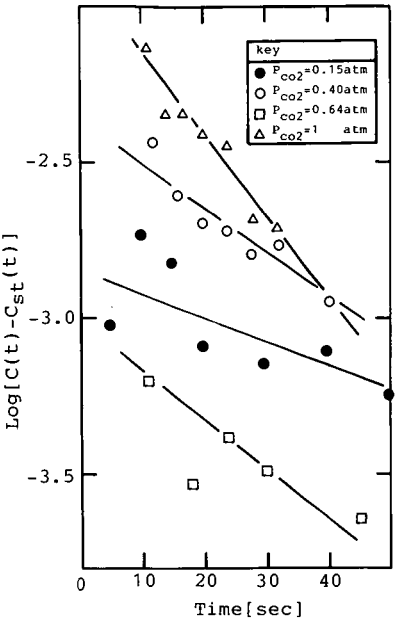

Figure 7. The dynamic change of [C(t)-C_{st}(t)].

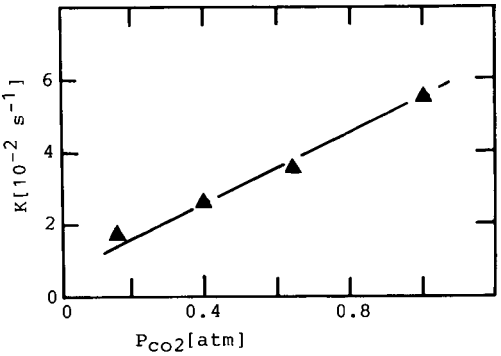

Figure 8. The rate constant K Vs. partial pressure of carbon dioxide.

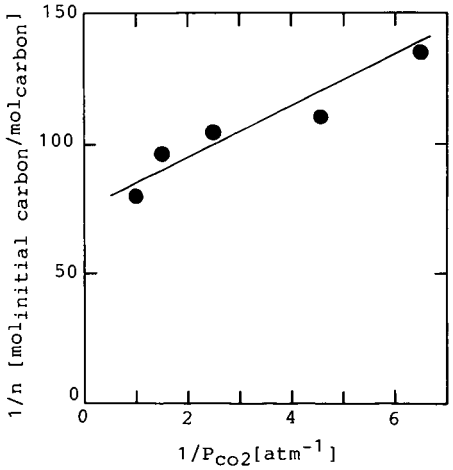

Figure 9. Relationship between the number of working active sites and the partial pressure of carbon dioxide.

INTRINSIC REACTIVITY OF COKE AND CHAR TO CARBON DIOXIDE

David J. Harris and Ian W. Smith
CSIRO Division of Coal Technology
PO Box 136, North Ryde, N.S.W., 2113, Australia

INTRODUCTION

Petroleum coke and coal derived cokes and chars find widespread use in metallurgical and gasification processes. During aluminium smelting, carbon electrodes are consumed not only by the desired electrolytic reactions but also by undesirable means, such as gasification by carbon dioxide and oxygen from the surrounding air. In ferrous and non-ferrous blast furnace processes, metallurgical coke is often excessively consumed by reaction with carbon dioxide which may lead to degradation of coke strength, and hence reduce furnace permeability. Further, due to the endothermic nature of the reaction, excessive reaction of coke with CO_2 may lead to disturbance of the desired blast furnace temperature profile and heat balance. Coal chars find widespread use as a source material in gasification processes and in activated carbon manufacture. Chars derived from Australian brown coals are particularly suited to the latter application as they contain only very small quantities of mineral matter.

In order to devise means of suppressing wasteful consumption of carbon and energy in metallurgical processes and to optimise the utilisation of coal chars in other processes it is necessary to have a quantitative understanding of the factors which control the rate of carbon gasification. The rate of reaction of coke or char with CO_2, in common with other gas-solid reactions, is controlled by three main factors [1]: (a) the rate of reactant gas transport to the coke or char surface; (b) the combined effects of the rate of diffusion of the gas through the pore structure of the material and the rate of chemical reaction of the gas with the carbonaceous components of the coke or char; and (c) the rate of chemical reaction alone.

The reaction conditions selected for the present study were such that any significant influences of factors (a) and (b) were eliminated in order to allow the intrinsic chemical reactivity of the selected materials to the reaction $C_{(s)} + CO_{2(g)} = 2CO_{(g)}$ to be evaluated.

EXPERIMENTAL

Three materials were considered in this study. They were (1) an experimental metallurgical coke produced from Queensland coking coal in a small scale (7 kg) laboratory coke oven; (2) a sample of petroleum coke used in the production of anodes for a commercial aluminium smelter and previously studied in this laboratory [2], and (3) a sample of char produced from a Victorian brown coal. Chemical analyses of these materials are given in Table 1.

The experimental apparatus is illustrated in Figure 1. This apparatus and the procedures adopted are a modification of a system previously developed at CSIRO [2,3]. It allows the reaction rate, order in CO_2 concentration and activation energy to be determined from a single experiment.

The rate of carbon loss (dW/dt) was determined directly from the flow-rate and carbon monoxide content of the reactor exit gas stream which was continuously measured with a non-dispersive infra-red CO analyser. The specific reaction rate, ρ [g/min.g], was then calculated according to Equation (1):

$$\rho = \frac{1}{W}\left(\frac{dW}{dt}\right) \qquad [g/min.g] \qquad (1)$$

where W is the weight of sample remaining at any time, t.

It is known that the product carbon monoxide can have a retarding effect on the rate of reaction [4]. The present investigation was carried out with carbon monoxide levels always below 1% v/v, at which value the retardation effect can be ignored [5].

During an experiment, step changes were made in the concentration of carbon dioxide in the reactant gas stream. This was achieved by alternating between the two reactant streams indicated as streams A and B in Figure 1. Hence the reaction rate of individual samples was determined at several carbon dioxide concentrations (approximately 30, 50, 75 and 100% v/v) in a single experiment. The reaction order thus determined was corrected, using the experimentally determined activation energy (see below), for any temperature variation brought about by the change in gas composition and is independent of changes in the pore structure of the sample.

At the conclusion of a test, the furnace was switched off and the activation energy of the reaction calculated from an Arrhenius plot of the rate data obtained during cooling of the reaction system. The weight loss of the materials was very small (less than 1%), and the pore structure therefore assumed to remain unchanged, during this period.

The total surface area, A_g, of the sample residue was then measured and the intrinsic reaction rate, ρ_s, calculated according to Equation (2).

$$\rho_s = \frac{\rho}{A_g} \qquad [g/m^2.min] \qquad (2)$$

The kinetic data, obtained at a common extent of reaction, are expressed as

$$\rho = A_g \, C_g^{\,m} B \exp(-E/RT) \qquad [g/min.g] \qquad (3)$$

where R is the gas constant, m is the order of reaction in CO_2 concentration, C_g, E is the activation energy, and B is a pre-exponential or frequency factor.

The observed values of E and m in Equation (3) only represent their respective true values when neither external transport nor pore diffusion effects have any significant effect on the observed reaction rate. Preliminary experiments revealed that the reaction rate, ρ, was independent of the reactant gas flowrate (between 500 and 1000 ml/min) and of coke or char particle size (between 0.2 and 1.7 mm) and that particle density decreased linearly during gasification. These observations confirm that mass transfer processes do not exercise a significant influence on the reaction rate under the conditions selected for the present work.

RESULTS

The results of a typical experiment are shown in Figures 2 and 3. In Figure 2, the reaction rate, ρ, at 890°C, of a bed of 0.9 mm metallurgical coke particles is plotted as a function of the fractional weight loss of the coke. The response to sudden changes in the inlet gas composition can be clearly seen. The reaction order, m, was calculated at these step changes and is shown, in the upper portion of Figure 2, to remain approximately constant during reaction (average value = 0.68). The activation energy, E (239 kJ/mol), was determined from the Arrhenius diagram of Figure 3, a plot of the data over the declining temperature period depicted in the final portion of Figure 2.

The results of a series of experiments using all three materials are summarised in Table 2 and Figure 4. The overall activation energy of the reaction is similar for all three materials examined here and values in the range 185-245 kJ/mol were found. The kinetic data determined for the petroleum coke in this study are in general agreement with the results of a previous investigation using this material [2].

It appears that E increases during reaction of the brown coal char, however the range of this variation is not large and further work is required to determine the significance of this trend. Similar behaviour was not apparent for the other materials where variations in E between experiments are not considered significant given the heterogeneous nature of the materials (particularly the metallurgical coke).

The order of reaction with respect to CO_2 partial pressure was approximately constant for all of the materials as the extent of gasification increased. The average values of m for the three materials are summarised in Table 2. Similar values of m (0.65-0.68) were found for the petroleum and metallurgical cokes while reaction of the brown coal char showed a slightly lower dependence on CO_2 partial pressure (m = 0.57). Values of m in the range 0.55-0.60 were also found during a number of experiments using different particle sizes of brown coal char.

It is apparent in Figures 2 and 4 that the rate of reaction of the metallurgical and petroleum cokes increases during reaction. The brown coal char demonstrated an apparent decline in reaction rate in the initial period of reaction, up to approximately 6% weight loss (Figure 5), beyond which the rate increased strongly with further gasification (Figure 6). The reasons for the initial decrease in the observed reaction rate of this material are not yet explained but it is possible that this initial evolution of CO is the result of desorption of oxygen containing species which are present initially on the char surface and were not dislodged by heating to reaction temperature in nitrogen.

The subsequent increase in the reaction rate of the char and the increase in ρ during reaction of the two cokes is thought to be due, at least in part, to alteration of the surface area of the materials. The relatively high initial surface area of the brown coal char (Table 2) may also account for its high values of ρ relative to the coke samples (Fig. 4).

Surface areas of coke and char residues at various extents of gasification are presented in Table 2 and Figure 7. The surface areas of the brown coal char and metallurgical coke increase greatly during reaction with CO_2 while that of petroleum coke, despite a measurable increase, remains very low.

The intrinsic reaction rate of each of the materials was calculated from the rate and surface area data of Figures 4 and 7 respectively, according to Equation (3) and is shown in Figure 8. The main features of Figure 4 remain evident, however the relative reactivities of the materials change greatly when allowance is made for the changing surface area of the materials. Despite their vastly different total surface areas, the brown coal char and the metallurgical coke are seen to display similar reactivities per unit surface area (Figure 8). At all temperatures, the petroleum coke was far more reactive, per unit surface area, to CO_2 than the coal derived materials. As the reaction proceeds and the surface area increases, the intrinsic reactivity, ρ_s, of all the materials decreases. This behaviour has not yet been explained and will be considered in future work. An attempt to determine the reasons for the high intrinsic reactivity of petroleum coke relative to the coal derived materials will also be made.

CONCLUSIONS

Measurements have been made of the intrinsic reactivity of a petroleum coke, a metallurgical coke and a brown coal char to carbon dioxide over the temperature range 650-900°C and at carbon dioxide partial pressures between 0.3 and 1 atm.

The order of reaction with respect to carbon dioxide concentration remained constant during reaction up to 42% weight loss at approximately 0.65 for petroleum coke and metallurgical coke and 0.55-0.60 for brown coal char. The activation energy of reaction was similar for all materials and was in the range 185-245 kJ/mol. The surface area of the materials varied widely and increased during reaction (up to 42% weight loss) by factors of approximately 5, 100 and 25

for the petroleum coke, metallurgical coke and brown coal char respectively. The intrinsic reaction rate per unit surface area decreased during gasification of each of the materials.

REFERENCES

1. Walker, P.L. Jr., Rusinko, F. Jr. and Austin, L.G., Advances in Catalysis, 11, 133 (1959).

2. Tyler, R.J. and Smith, I.W., Fuel, 54, 99 (1975).

3. Tyler, R.J., Wouterlood, H.J. and Mulcahy, M.F.R., Carbon, 14, 271 (1976).

4. Turkdogan, E.T. and Vinters, J.V., Carbon, 8, 39 (1970).

5. Turkdogan, E.T. and Vinters, J.V., Carbon, 7, 101 (1969).

TABLE 1: Chemical Analysis of Cokes and Char (% w/w)

Material	Ash	C	H	N	S	O
Metallurgical Coke	12.1	85.0	0.4	1.9	0.6	0.0
Petroleum Coke	0.5	96.7	0.2	1.6	1.0	0.0
Brown Coal Char	2.4	94.9	0.6	0.5	0.1	1.5

TABLE 2: Summary of Reactivity Data for 0.9 mm Particles

Material	weight loss (%)	E (kJ/mol)	m (average)	A_g (m^2/g)
Petroleum coke	0	-	-	0.6
	6	231	nd	0.9
	31	214	0.65	3.1
	42	218	0.65	2.4
Metallurgical coke	0	-	-	0.9
	9	239	0.68	54.9
	38	216	0.66	98.6
Brown coal char	0	-	-	39.1
	6	185	0.57	358.7
	18	214	nd	464.4
	41	244	nd	986.9

nd = not determined

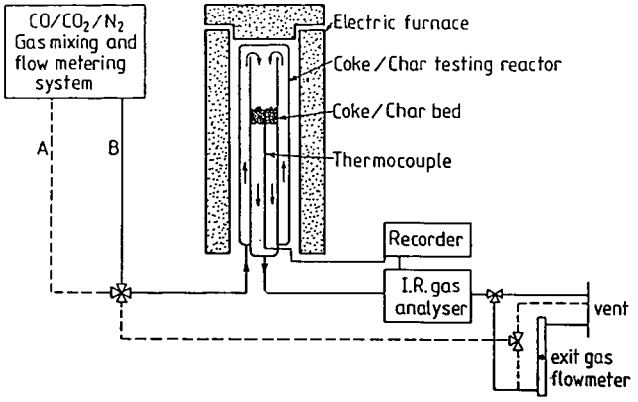

Figure 1 Schematic representation of experimental apparatus

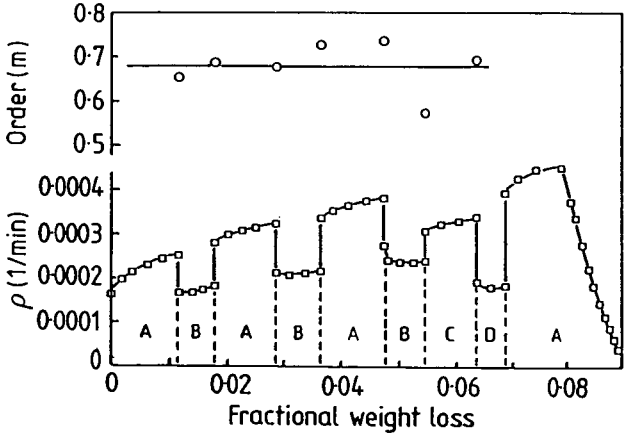

	A	B	C	D
CO_2(%)	100	50	77	30

Figure 2 Reaction rate (●) and order (○) for metallurgical coke (0.9 mm) reacted in CO_2/N_2 mixtures at 890°C.

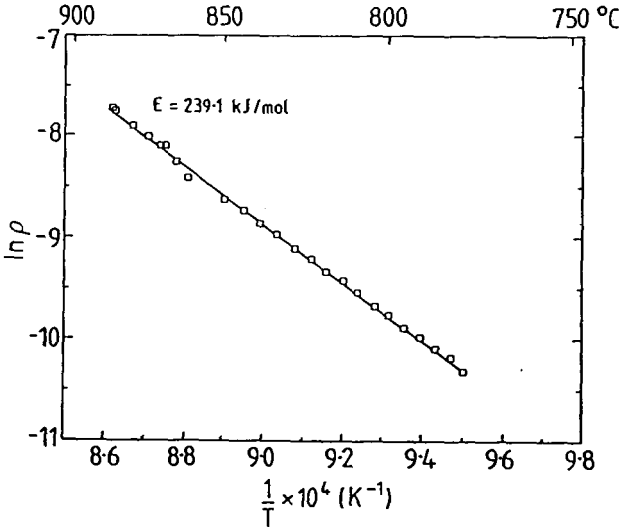

Figure 3 *Reaction rate, ρ (g/min.g), during cooling of coke sample as depicted in final portion of Figure 2.*

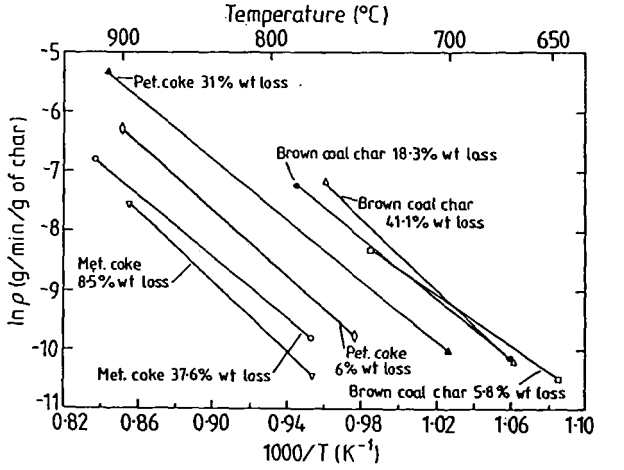

Figure 4 Relation between reaction rate, ρ (g/min.g), and temperature for brown coal char, metallurgical coke and petroleum coke. (p_{CO_2} = 1 atm).

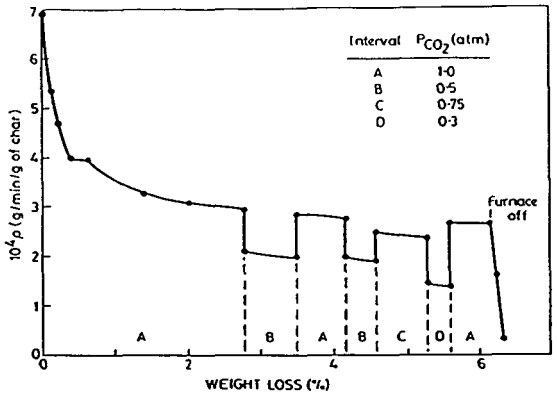

Figure 5 Reaction rate of brown coal char (0.9 mm) during the initial period of reaction at 740°C.

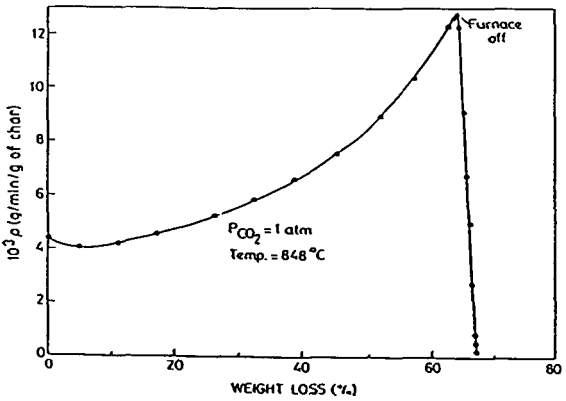

Figure 6 Reaction rate as a function of the extent of gasification of char at 848°C.

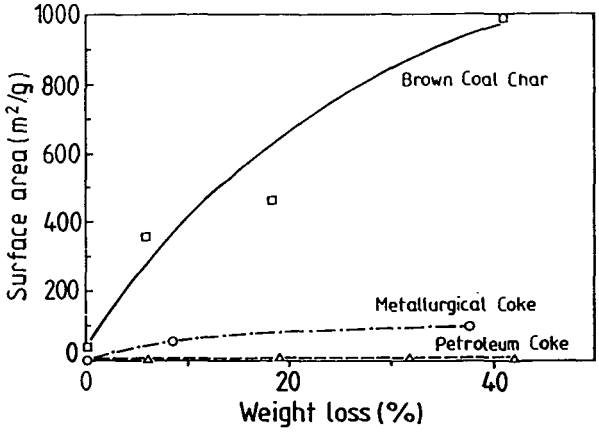

Figure 7 Effect of reaction on total (N_2, BET) surface area.

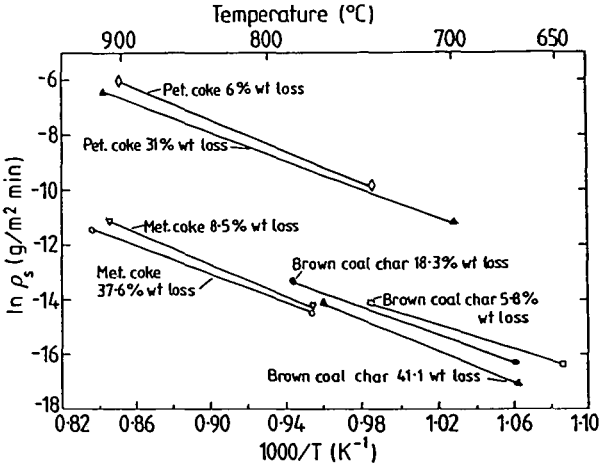

Figure 8 Intrinsic reaction rate, ρ_s (g/min.m^2) of brown coal char, metallurgical coke and petroleum coke. (p_{CO_2} = 1 atm).

TEMPERATURE-PROGRAMMED DESORPTION STUDIES OF COAL CHAR GASIFICATION

Anthony A. Lizzio and Ljubisa R. Radovic
Department of Materials Science and Engineering
Fuel Science Program
The Pennsylvania State University
University Park, PA 16802

INTRODUCTION

In recent years, it has become increasingly clear that the understanding of char gasification kinetics requires more detailed information about the nature of the surface intermediates (carbon-oxygen complexes) formed during reaction. The first step in char (carbon) gasification is the dissociative chemisorption of reactant gas molecules (O_2, CO_2, H_2O) on the active sites of carbon, located at the edges of, and imperfections within, the turbostratic carbon crystallites [1]. A distribution of activities is known to exist among these carbon active sites [2,3]; some sites are more active than others. The sites which are important for predicting gasification rates are thought to be the ones that have intermediate activity, i.e., the ones that are sufficiently active to chemisorb dissociatively the reactant gas, but not to the extent that a stable C-O complex is formed [4,5]. Temperature-programmed desorption (TPD), an experimental technique widely used in the field of heterogeneous catalysis [6] and recently applied in coal char gasification studies [7-10], may be used to discern the nature of this distribution. TPD spectra provide useful information not only on the extent [11,12] but also on the energetics of desorption of C-O complexes from the char surface. In order to gain new insights into char gasification kinetics, it should prove beneficial to analyze TPD spectra, both qualitatively and quantitatively, with respect to factors which are known to significantly influence rates of gasification, e.g., nature of reactant gas, level of conversion (or extent of reaction), and the presence of inorganic impurities. The main objective of this study is to characterize the energetic heterogeneity of surfaces of coal chars, and carbons in general, and to relate it to their observed catalyzed and uncatalyzed gasification behavior in O_2 and CO_2.

EXPERIMENTAL

The coals used in this study include a high volatile A Illinois #6 bituminous coal (PSOC 1098) and a North Dakota lignite (PSOC 246) [13]. Demineralized coal samples (Dem) were obtained by washing the raw coal with HCl and HF; essentially all the inorganic constituents were removed. The demineralized lignite was subsequently ion-exchanged with Ca^{+2} (designated as PSOC 246 Dem Ca sample) using a 1.5 M solution of calcium acetate [4]. All coal chars were prepared under identical pyrolysis conditions (900 °C, 10 °C/min, 0.5 h). A polymer-derived carbon, Saran char [4], and a graphitized carbon black, Graphon [3], both extensively studied in the literature, were also used.

Temperature-programmed desorption experiments were carried out in a flow-thru, fixed-bed reactor system. A quadrupole mass spectrometer (Dycor, model M100) was used to continuously monitor the evolution of CO, CO_2, H_2O, H_2 and O_2. Direct sampling of the effluent stream from a quartz reactor, operated at atmospheric pressure, was done through a 50 μm ID capillary tube. The partial pressure data were collected by an IBM PC and stored in a Lotus 1-2-3 worksheet for future analyses. A typical TPD experiment began with *in situ* partial gasification of the char in 1 atm air or 1 atm CO_2. Relatively low reaction temperatures were chosen to ensure uniform, kinetically controlled rates (typically, 0.01-0.05 h^{-1}). After reaching the desired conversion, the sample (200-400 mg) was cooled in the reactant gas to a temperature at which no significant gasification occurred, e.g., 120 °C.

The reactant gas was flushed from the system with high-purity argon (99.9995%). Once the concentrations of O_2, CO and CO_2 returned to baseline levels, the sample was heated in flowing argon (47 cm^3/min) at a constant heating rate of 5 °C/min to a final temperature of 1000 °C. This temperature was held for 2 h, in most cases, to achieve complete desorption of CO and CO_2 from the char surface. After each TPD experiment, the mass spectrometer was calibrated to permit a quantitative analysis of the partial pressure data. All TPD spectra were expressed per unit weight of carbon (200 mg) to allow direct comparison of peak heights.

RESULTS

Typical TPD spectra are shown in Figure 1. In all figures, the units on the ordinate and the abscissa are ppm and °C, respectively. In all figures and Table 1, the samples are designated by their name, reactant gas used, gasification temperature (°C), and level of conversion (X_C) achieved. The parameters obtained by analyzing the TPD spectra include the absolute amount of oxygen adsorbed on the char surface (wt % O), the relative amounts of CO and CO_2 evolved, given as the CO/CO_2 ratio, and the CO and CO_2 peak temperature(s), Tp_{CO} and Tp_{CO2} (°C). Table 1 lists the values of these parameters for all the TPD spectra referred to in this paper.

Effect of Reactant Gas. Figure 2 and Table 1 show that significantly more C-O complexes are formed during gasification in air than in CO_2. Table 1 also shows that the chars in Figure 2 adsorbed about the same amount of oxygen after partial gasification in air; however, significant differences in the amount of adsorbed oxygen are observed after partial gasification in CO_2. In comparison with gasification in air, peak temperatures are seen to increase by about 300 °C after partial gasification of the PSOC 1098 and Saran chars in CO_2; on the other hand, Tp_{CO} and Tp_{CO2} do not change as much for the PSOC 246 Dem Ca char. It is interesting to note that the amount of CO_2 evolved from the PSOC 1098 and Saran chars after partial gasification in CO_2 (see Figures 2b,d) is significantly smaller than that evolved from the PSOC 246 Dem Ca char (see Figure 2f).

Effect of Conversion Level. Figures 3 and 4 show the TPD spectra for the three chars reacted in air and CO_2, respectively, to three levels of conversion. In all cases the amount of adsorbed oxygen increases with conversion (see Table 1 and Figure 5). In addition, Table 1 shows that the CO/CO_2 ratio decreases monotonically with conversion in air, particularly for the PSOC 1098 and Saran chars.

Effect of Inorganics. Figures 6 shows the effect of mineral matter on the TPD spectra of the partially gasified bituminous coal char. It is seen that some of the peaks disappear upon demineralization and can thus be assigned to the presence of inorganics in the chars. For comparison, Figure 7 shows the TPD spectra of partially gasified Graphon and Saran char. Both are known to be essentially free from the catalytic effects of inorganic impurities. Figure 8 shows the effect of inorganics (i.e., discrete minerals as well as cations, and Ca in particular) on the TPD spectra of the partially gasified lignite char.

DISCUSSION

Before interpreting the TPD spectra in terms of the extent of adsorption on, and energetics of desorption from, the char surface, experimental artifacts and possible complicating effects (such as mass transport limitations and secondary reactions) need to be considered. It should be noted that a mass 28 fragment of CO_2 (about 5% of the mass 44 signal) was always produced in the mass spectrometer. The TPD spectra shown in this paper were not corrected for this. Therefore, extraneous peaks appear in CO evolution profiles when the concentration of CO_2 is very large (e.g., see Figures 1a and 3b,c,i). In addition, the frequent appearance of a small shoulder in the CO spectra of coal chars at 1000 °C is an experimental artifact due to the rather abrupt halt in the temperature rise upon reaching

the final desorption temperature. The possibility of interparticle diffusional limitations was investigated by varying the sample size (100-1500 mg) and the carrier gas flow rate (10-100 cm^3/min); peak temperatures for CO and CO_2 evolution varied by no more than 10 °C. The possibility of intraparticle diffusional effects and/or secondary reactions of desorbed species was not tested directly. However, Otake [14] has shown that a heating rate of 5 °C/min is satisfactory for resolving the CO and CO_2 desorption peaks in a TPD spectrum of a microporous char. In addition, he provided evidence that the rates of CO and CO_2 desorption were governed solely by the decomposition of C-O complexes on the surface and not also by secondary reactions involving the desorbed species. Hall et al. [10] have recently interpreted the observed effect of heating rate variations (20-300 °C/min) on the relative amounts of CO and CO_2 desorbed from some coal chars in terms of secondary reactions of desorbed species. One of their arguments favoring this interpretation is the decreasing CO/CO_2 ratio with increasing conversion of a subbituminous coal char in air. An alternative interpretation of this behavior, also observed in our study (see Figure 3 and Table 1) and elsewhere [15], is that the probability of formation of CO_2, through interaction of adjacent and/or mobile C-O complexes, increases with increasing surface coverage. Furthermore, at our relatively low heating rate, the concentration of CO in the pores should be sufficiently low to prevent significant occurrence of secondary reactions. The TPD spectra obtained in this investigation are thus considered to be representative of the original state of C-O complexes on the char surface.

Char Reactivity and TPD Spectra. It is well known that the low-temperature oxygen chemisorption capacity of an unreacted char is a good index of its gasification reactivity, particularly for the purpose of comparing chars whose reactivities differ by more than a factor of 2-3 [4]. However, this concept has failed to explain the gasification behavior of partially reacted chars [5,15]. A quantitative interpretation of reactivity profiles, i.e., of variations in rate with conversion for a given char, was recently concluded to require not only the knowledge of the extent of chemisorption of oxygen but also an understanding of the energetic heterogeneity of the char surface [5,16]. It should be realized that the total amount of C-O complex evolved in a TPD experiment includes the "stable" complex as well as the reactive surface intermediate [17]. The concept of "stable complex" as an inhibitor of carbon gasification, shown to be valid at low pressures [18], is an oversimplification when applied to gasification at higher pressures [19-21]. In fact, the monotonic increases in the amount of oxygen adsorbed with conversion, well substantiated here and elsewhere [15, 21-23], correlate well with the often observed increasing specific gasification rate with conversion [16,17,24]. This correlation is thought to be the result of the fact that some C-O complexes are reaction intermediates. It can also be interpreted as a result of (a) a decrease in the desorption activation energy with increasing surface coverage [14,20], (b) an "activating" effect of the complex on the surrounding carbon atoms [21], or (c) the increase in the ratio of edge (active or reactive) carbon atoms to basal-plus-edge (total number of) carbon atoms in the turbostratic structure of the char as gasification proceeds [16]. Ultimately, however, reactivity profiles are probably best understood by measuring directly the reactive surface area of the chars [16,24].

In this study, an attempt was also made to correlate the reactivity of each char with the amount of oxygen adsorbed during gasification. Figures 2a,c,e and Table 1 show that, even though the three chars have vastly different reactivities in air (the catalyzed reaction of PSOC 246 Dem Ca being the fastest and the uncatalyzed reaction of Saran char being the slowest [4]), these differences cannot be explained using the total amount of C-O complexes formed during gasification (the majority of which is known to be the "stable" complex). Figures 2b,d,f and Table 1 show that a better qualitative correlation exists between the total amount of C-O complex and reactivity for these chars partially gasified in CO_2; similar results were obtained by Kyotani et al. [8] for various coal chars gasified in steam. It is interesting to note [18] that as much as 85% of the total C-O complex formed on the surface of Saran char after partial gasification in CO_2 is the reactive surface intermediate.

A comparison of TPD spectra obtained after partial gasification in air, at relatively low temperatures, and in CO_2, at higher temperatures, is also useful (see Figure 2). After partial gasification in CO_2,

only relatively stable C-O species, which decompose above 700 °C and yield predominantly CO, remain on the surface, in agreement with the findings of Keleman and Freund [25] for a glassy carbon. The fact that greater amounts of oxygen on the surface are observed after gasification in air is consistent with the view that the C-O_2 reaction is much faster than the C-CO_2 reaction because of a more facile dissociation step [26]. Ahmed and Back [22] have observed a decrease in the amount of surface oxygen with increasing temperature after partial gasification (and subsequent low-temperature oxygen chemisorption) in the same gas (O_2); they have attributed this to a "minor variation in the procedure for preparation" of their carbon films. In fact, having in mind that low-temperature oxygen chemisorption provides little additional surface coverage for chars previously gasified in O_2 [5], this effect is indeed expected [27].

Catalysis and TPD Spectra. A comparison of the TPD spectra of the as-received bituminous and lignite chars, together with those of the relatively pure carbon materials (chars prepared from the demineralized coals, Saran char and Graphon), may provide useful information about the effect of inorganics on the energetic heterogeneity of coal char surfaces.

The amount of oxygen adsorbed on partially oxidized Graphon is about an order of magnitude lower and Tp_{CO} and Tp_{CO2} are about 100 °C higher than for the much more reactive Saran char (see Figures 7a,b and Table 1). The significantly smaller CO/CO_2 ratio for Saran char (see Table 1) is attributed to the fact that a relatively larger portion of its total surface is covered with C-O complexes, thus favoring CO_2 formation. From Figures 6a,b, the appearance of a clearly resolved high-temperature peak in the CO desorption spectrum and a low-temperature peak in the CO_2 desorption spectrum of the as-received bituminous coal char is seen to be due to the presence of inorganics, even though they have no catalytic effect [28] (see also Figures 1a, 2a, 3a-c). Hall et al. [10] recently observed similar behavior for a subbituminous coal char reacted in O_2, but attribute it to the "catalytic effect of the mineral matter." It is interesting to note the remarkable similarities in the TPD spectra of the demineralized bituminous coal char, Saran char and Graphon (see Figures 6b and 7).

The relatively high gasification reactivity of lignite chars compared to those obtained from higher-rank coals has been attributed to the catalytic effect of highly dispersed CaO on the char surface [29]. Figures 8a-c suggest that the catalytic effect of CaO in air cannot be clearly detected in TPD spectra. Demineralization of the lignite and subsequent Ca^{+2} exchange result in no significant difference in the CO and CO_2 desorption spectra or the amounts of oxygen on the surface. Figure 3 shows, however, differences in the evolution of CO and CO_2 spectra with increasing conversion for the catalyzed (3g-i) vs. the noncatalyzed (3a-c and 3d-f) reaction.

Figures 8d-f show quite a different situation for the lignite char gasified in CO_2. The CO desorption spectrum of the demineralized sample (see Figure 8e) exhibits only one peak, typically found in spectra of uncatalyzed chars (see Figures 2b,d, 4a-c). Two CO peaks are observed for the Ca-exchanged sample (see Figure 8f), in agreement with the results of Kapteijn et al. [30]. It is tempting to attribute the lower-temperature peak to the interaction of the adsorbed oxygen with the catalytic sites and the higher-temperature peak to its interaction with the carbon active sites [30]. A very sharp intermediate CO peak appears in the spectrum of the as-received lignite char (see Figure 8d); it may be tentatively attributed to a catalytic species other than Ca, e.g., Na or K [8]. The sharp CO_2 peak (see also Figures 2f, 4g-i), not observed after partial gasification of uncatalyzed chars in CO_2, is attributed to the decomposition of $CaCO_3$ [8].

SUMMARY AND CONCLUSIONS

Temperature-programmed desorption was used to determine the extent and energetics of desorption of carbon-oxygen complexes from coal char surfaces; an attempt was made to relate this to their observed gasification behavior. The potential usefulness of this technique stems from the fact that

stable complex formation is considered to be not only an inhibiting process but also an intermediate step in the mechanism of carbon gasification. Very significant differences in the extent of oxygen adsorption and the CO and CO_2 desorption spectra were found depending on the reactant gas used, level of conversion achieved and the presence of inorganic impurities. In general, a better qualitative correlation between the extent of oxygen adsorption and the kinetics of both catalyzed and uncatalyzed gasification was observed after partial gasification in CO_2. The establishment of better quantitative correlations is being sought by further analysis and possible deconvolution of the TPD spectra.

ACKNOWLEDGEMENTS

This work is supported by the Gas Research Institute, Contract No. 5086-260-1419. The coal samples were obtained from the Penn State/DOE Coal Sample Base.

REFERENCES

1. Essenhigh, R.H. "Chemistry of Coal Utilization," 2nd Suppl. Vol. (M.A. Elliott, Ed.), Wiley, 1981, p. 1153.
2. Magne, P. and Duval, X. Carbon 11, 475 (1973).
3. Tremblay, G., Vastola, F.J. and Walker, P.L., Jr. Carbon 16, 35 (1978).
4. Radovic, L.R., Walker, P.L., Jr. and Jenkins, R.G. Fuel 62, 849 (1983).
5. Radovic, L.R. and Lizzio, A.A. Proc. Annual Conf. Coal Sci., Pittsburgh, PA, 1987, p.440.
6. Falconer, J.L. and Schwarz, J.A. Catal. Rev. - Sci. Eng. 25, 141 (1983).
7. Kyotani, T., Karasawa, S. and Tomita, A. Fuel 65, 1466 (1986).
8. Kyotani, T., Zhang, Z.-G., Hayashi, S. and Tomita, A. Energy & Fuels 2, 136 (1988).
9. Zhang, Z.-G., Kyotani, T. and Tomita, A. Energy & Fuels 2, 679 (1988).
10. Hall, P.J. and Calo, J.M. Proc. Int. Conf. Carbon (B.McEnaney and T.J. Mays, Eds.), IOP Publishing, Bristol, UK, 1988, p. 77.
11. Causton, P. and McEnaney, B. Fuel 64, 1447 (1985).
12. McEnaney, B. and Wang, J. Proc. Int. Conf. Carbon (B.McEnaney and T.J. Mays, Eds.), IOP Publishing, Bristol, UK, 1988, p. 564.
13. Penn State/DOE Coal Data Base, The Pennsylvania State University.
14. Otake, Y. Ph.D. Thesis, The Pennsylvania State University, 1986.
15. Taylor, R.L. and Walker, P.L., Jr. Extended Abstracts, 15th Biennial Conf. Carbon, Philadelphia, PA, 1981, p. 437.
16. Radovic, L.R., Lizzio, A.A. and Jiang, H. Carbon, submitted (1988).
17. Radovic, L.R., Lizzio, A.A. and Jiang, H., Extended Abstracts, 19th Biennial Conf. Carbon, University Park, PA, 1989.
18. Laine, N.R., Vastola, F.J. and Walker, P.L., Jr. J. Phys. Chem. 67, 2030 (1963)
19. Vastola, F.J., Hart, P.J. and Walker, P.L., Jr. Carbon 2, 65 (1964).
20. Chen, C.-J. and Back, M.H. Carbon 17, 495 (1979).
21. Ahmed, S. and Back, M.H. Carbon 23, 513 (1985).
22. Su, J.-L. and Perlmutter, D.D. AIChE J. 31, 1725 (1985).
23. Lizzio, A.A., Piotrowski, A. and Radovic, L.R. Fuel 67, 1691 (1988).
24. Jiang, H. and Radovic, L.R. ACS Preprints (Div. Fuel Chem.), Dallas, 1989.
25. Keleman, S.R. and Freund, H. Energy & Fuels 2, 111 (1988).
26. Keleman, S.R. and Freund, H. Carbon 23, 723 (1985).
27. Laine, N.R., Vastola, F.J. and Walker, P.L., Jr. Proc. 5th Carbon Conf., Vol.II, Pergamon Press, 1963, p. 211.
28. Lizzio, A.A. M.S. Thesis, Polytechnic University, 1988.
29. Radovic, L.R., Walker, P.L., Jr. and Jenkins, R.G. J. Catal. 82, 382 (1983).
30. Kapteijn, F., Porre, H. and Moulijn, J.A. AIChE J. 32, 691 (1986).

Table 1

Quantitative Analysis of TPD Spectra

Fig.	Char, Gas, ^{o}C, X_c	wt% O	CO/CO_2	T_{PCO}	T_{PCO2}
1a	PSOC 1098, O_2, 350, 0.75	30.7	1.9	640,830	520,680
1b	Saran, O_2, 388, 0.72	25.3	3.1	640	560
2a	PSOC 1098, O_2, 350, 0.20	13.8	2.4	670,820	490,650
2b	PSOC 1098, CO_2, 865, 0.20	2.8	9.6	910	640,810
2c	Saran, O_2, 388, 0.20	12.9	5.9	640	540
2d	Saran, CO_2, 860, 0.20	0.3	——	910	——
2e	PSOC 246 Dem Ca, O_2, 315, 0.20	14.4	2.0	730	460,600
2f	PSOC 246 Dem Ca, CO_2, 680, 0.20	7.6	3.1	720	700
3a	PSOC 1098, O_2, 350, 0.06	8.9	2.8	830	480,650
3b	PSOC 1098, O_2, 350, 0.54	23.8	2.4	640,840	500,670
3c	PSOC 1098, O_2, 350, 0.93	37.0	1.0	620,810	510
3d	Saran, O_2, 388, 0.05	5.5	7.0	660,810	530
3e	Saran, O_2, 388, 0.38	20.5	4.8	640	540
3f	Saran, O_2, 388, 0.90	26.8	2.8	630	590
3g	PSOC 246 Dem Ca, O_2, 315, 0.05	9.1	2.0	810	480,610
3h	PSOC 246 Dem Ca, O_2, 315, 0.50	20.1	2.0	710	540,650
3i	PSOC 246 Dem Ca, O_2, 315, 0.85	41.2	1.5	700	580,690
4a	PSOC 1098, CO_2, 865, 0.13	2.0	9.1	880	610,790
4b	PSOC 1098, CO_2, 865, 0.42	4.7	17.7	920	630,820
4c	PSOC 1098, CO_2, 865, 0.73	8.2	16.3	950	680,850
4d	Saran, CO_2, 860, 0.13	0.3	——	890	——
4e	Saran, CO_2, 860, 0.47	0.4	——	910	——
4f	Saran, CO_2, 860, 0.85	0.9	——	900	——
4g	PSOC 246 Dem Ca, CO_2, 680, 0.05	5.6	3.3	770	680
4h	PSOC 246 Dem Ca, CO_2, 680, 0.40	10.4	2.7	730,870	730
4i	PSOC 246 Dem Ca, CO_2, 680, 0.72	15.5	1.7	770,890	760
6a	PSOC 1098, O_2, 350, 0.30	17.8	2.4	640,850	490,660
6b	PSOC 1098 Dem, O_2, 350, 0.33	15.6	4.6	640	480,640
7a	Graphon, O_2, 580, 0.82	1.3	13.3	720	640
7b	Saran, O_2, 388, 0.26	13.5	5.2	640	530
8a	PSOC 246, O_2, 315, 0.33	13.3	2.0	720,800	610
8b	PSOC 246 Dem, O_2, 315, 0.37	16.5	2.5	750	460,610
8c	PSOC 246 Dem Ca, O_2, 315, 0.35	17.1	2.3	720	490,630
8d	PSOC 246, CO_2, 680, 0.42	8.8	2.3	720,770,850	720
8e	PSOC 246 Dem, CO_2, 680. 0.36	6.4	4.4	860, 860	670
8f	PSOC 246 Dem Ca, CO_2, 680, 0.40	10.4	2.7	730, 870	730

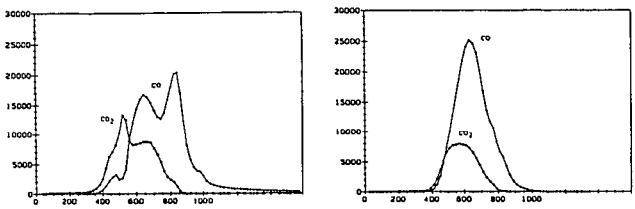

Figure 1. Typical TPD Profiles for the Bituminous Coal Char and Saran Char Reacted in 1 atm Air.

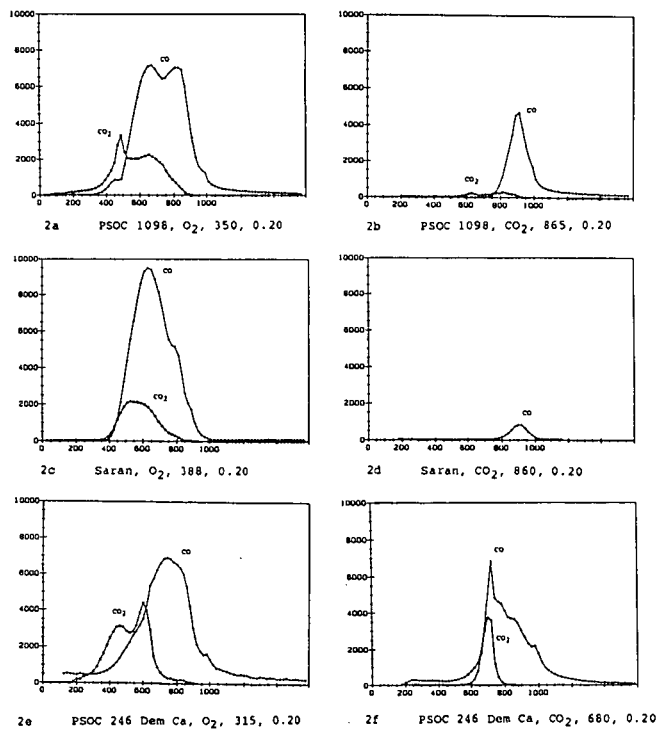

Figure 2. Effect of Reactant Gas on TPD Profiles of Chars Reacted in 1 atm Air and 1 atm CO_2 to 20 % Conversion.

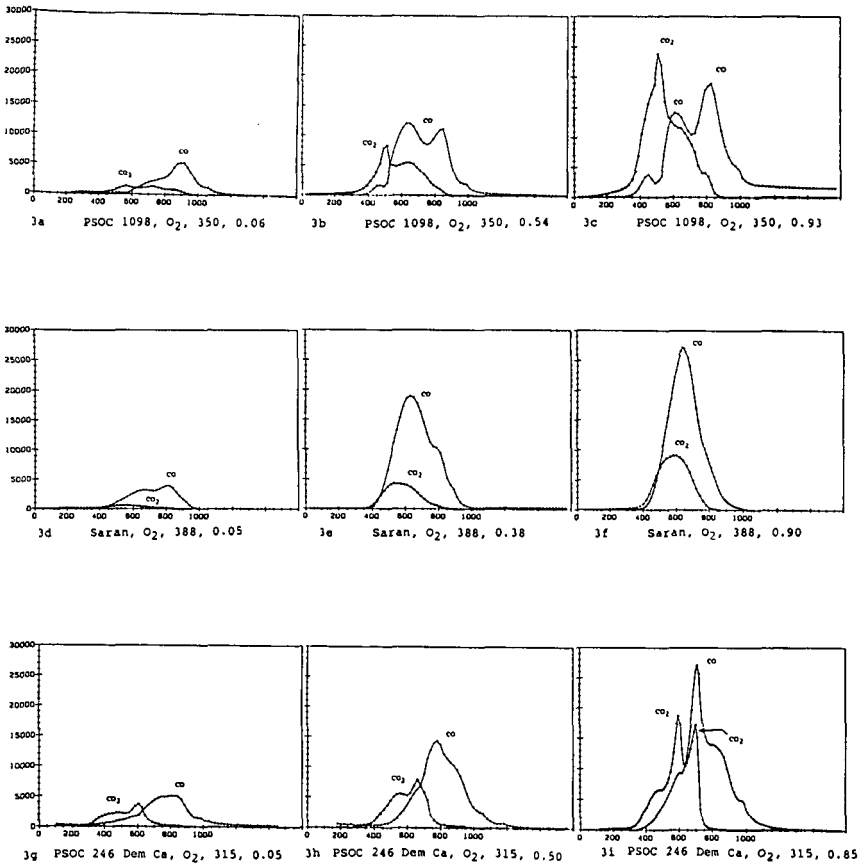

Figure 3. Effect of Conversion Level on TPD Profiles of Chars Reacted in 1 atm Air.

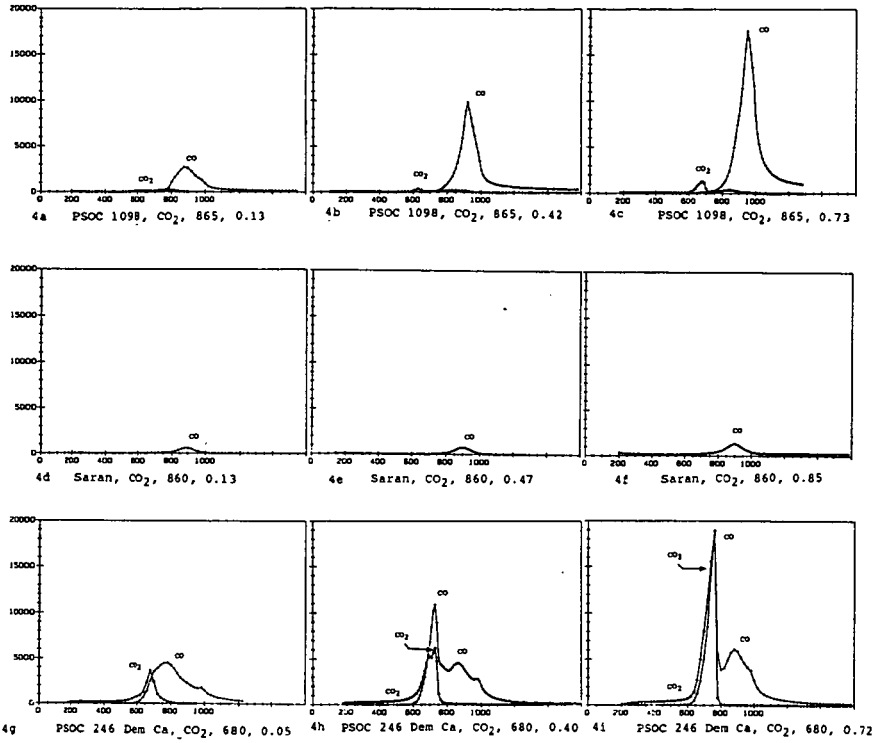

Figure 4. Effect of Conversion Level on TPD Profiles of Chars Gasified in 1 atm CO_2.

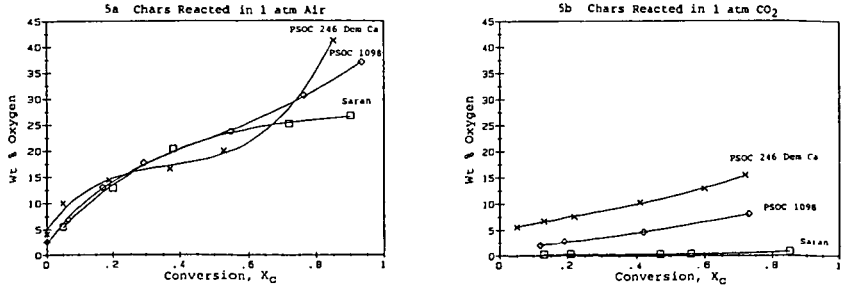

Figure 5. Effect of Reactant Gas and Conversion Level on Oxygen Uptake by Chars Partially Gasified in 1 atm Air and 1 atm CO_2.

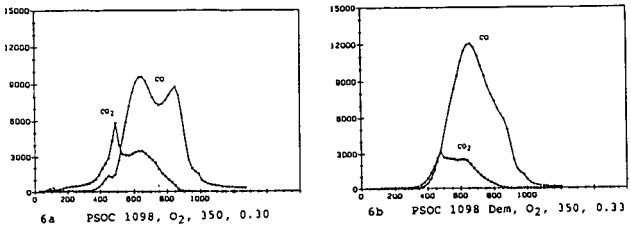

Figure 6. Effect of Mineral Matter on TPD Profiles of the Bituminous Coal Char Reacted in 1 atm Air.

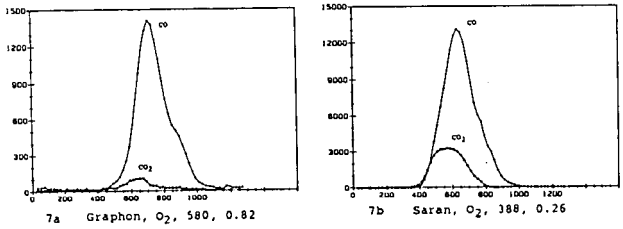

Figure 7. Representative TPD Profiles For Uncatalyzed Chars Reacted in 1 atm Air.

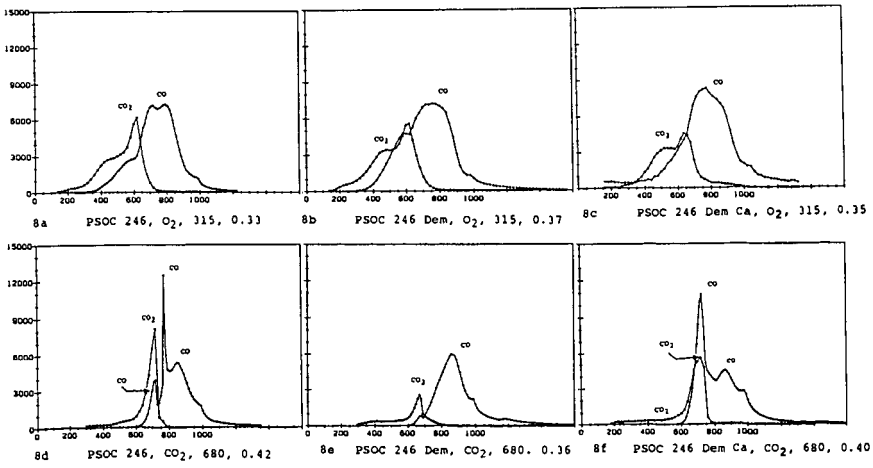

Figure 8. Effect of Mineral Matter and Calcium on TPD Profiles of a Lignite Char Reacted in 1 atm Air and 1 atm CO_2.

The Nature of Carbon-Oxygen Complexes Produced by Different Oxidants: Towards a Unified Theory of Gasification?

P. J. Hall, J. M. Calo, H. Teng, E. M. Suuberg, J. A. May and W. D. Lilly.
Chemical Engineering Program
Division of Engineering
Brown University
Providence, R.I. 02912

Introduction

There have been relatively few studies directly comparing the nature of surface carbon-oxygen complexes produced by the oxidation of carbon by different oxidizing agents. However, such studies as there are suggest, for the most part, a strong similarity between the chemical nature of such complexes, thereby potentially providing a unifying basis for the gasification of carbon by oxidizing species. In one such study, Marchon *et al.* [1] chemisorbed O_2, CO_2 and H_2O onto polycrystalline graphite at different temperatures, performed linear temperature programmed desorption (TPD) at a heating rate of 50 K/min, and compared the resulting desorption spectra. The principal TPD features were large CO desorption peaks at 973, 1093 and 1253K. They tentatively assigned these features to semi-quinone functional groups. It was concluded that the activation energy for adsorption was determined by the local surface environment of the group, the surface coverage, and the nature of the adsorbing molecule itself. Marchon *et al.* [1] also proposed a general mechanism of gasification, in which oxidizing species with the general formula RO, formed a semi-quinone group which could either be desorbed as CO or could be further oxidized to give a CO_2-producing lactone group. While generally plausible, this mechanism still leaves open the question of why one oxidizing agent should be more reactive than another for a particular carbon; e.g., why oxygen should be more reactive than NO, which is, in turn, more reactive than CO_2, when compared at the same gas phase concentration and temperature.

The present paper has two principal objectives: to further test the theory of the universal nature of oxygen complexes by comparing the TPD spectra of a char oxidized in O_2, CO_2, NO, HNO_3 and H_2O_2; and the reactivity question, which is approached by analysing TPD data, and reactivity and surface area measurements for a gasified char.

Experimental

The TPD apparatus has been described previously [2]. A heating rate of 100K/min was used in the current work because this yielded reasonable gas evolution rates and peak resolution. The carrier gas was ultra-high purity helium, and the typical TPD sample size was 10 mg. The results are presented with arbitrary rate and total gas units, but the scales are directly comparable from one graph to another. Char produced from Pittsburgh # 8 coal, obtained from the Argonne Premium Coal Sample Bank, was used in this set of experiments, because this coal goes through a fluid phase on carbonisaton in which most of the original porosity is lost. Therefore, essentially all the porosity is developed via gasification. The nitrogen BET surface area of the ungasified char resulting from heat treatment at 1273K for 2 hours was 3 m^2/g.

Oxidation by the gaseous oxidants and reactivity measurements were made in a TGA in the corresponding atmosphere at 0.1MPa. O_2 and CO_2 gasification were conducted in flowing gas, and NO gasification in a batch mode. Oxidations by HNO_3 were performed by stirring the char in a 15N solution at room temperature for 15 min. The same procedure was followed for H_2O_2 in a 30% solution. Nitrogen surface areas were determined from adsorption at 77K in a flow BET apparatus. Where appropriate, CO_2 surface areas were determined at 195K. No attempt was made to collect gaseous products of gasification during oxidation, so the total extents of oxidation by the different methods cannot be computed.

Results and Discussion

The TPD spectra for Pittsburgh # 8 coal char oxidized by O_2, CO_2, NO, HNO_3 and H_2O_2 are shown in Figures 1 through 5, respectively. As can be seen, there are certain features that are common to all the spectra, with two desorption peaks for CO_2 at about 600K and 920K and two desorption peaks for CO at 1000K and 1250K. The higher temperature CO peak is displaced to higher temperatures for low surface coverages and certain peaks may be absent for specific oxidants and/or gasification temperatures. These desorption peaks occur at similar temperatures for the different oxidants, and the principal differences between the spectra in Figures 1 through 5 lie in the intensity of the peaks. The general features of TPD spectra have been discussed by Hall and Calo [3], and are most clear for the O_2 oxidized char. The low temperature CO_2 peak appears to be at least partially the desorption of intrinsic CO_2-producing groups, most probably lactones and/or acid anhydrides [1, 4]. The higher temperature CO_2 peak has been shown to be at least partially due to secondary reactions of CO (gas) with non-desorbed surface complexes by via the reaction:

$$CO + [C\text{-}O] <=> CO_2 + C_f \qquad [R.1]$$

where [C-O] is a surface oxygen complex and C_f is an unoccupied active site. The 1000K CO

peak seems to be the result of intrinsic CO-producing groups such as carbonyls or semi-quinones. The origin of the 1250K peak (visible as a shoulder on the main CO peak in Figure 1) has been speculated to be at least partially due to the re-adsorption of CO to form a more stable CO surface complex [3].

The question that naturally arises then is whether the apparent uniformity in the chemical nature of functional groups can be used as a basis for a unified model of carbon gasification. At least part of the answer may be provided by a comparison of the relative reactivities, TPD spectra and surface area measurements of the same char gasified by NO, O_2, and CO_2.

Table 1 shows degree of burn-off, reactivity, total amount of oxygen present as stable complex (i.e., $CO + 2CO_2$) desorbed during TPD, and the corresponding N_2 BET surface area of the resulting chars for the O_2, NO and CO_2 gasified chars.

There are a number of obvious differences between the oxidation behaviour of O_2 and NO. O_2 is more reactive than NO, and the rate of increase of reactivity of O_2 with temperature in the low temperature range (< 900K) is also greater. For comparable O_2 and NO reactivities, (i.e., NO at 1123K and O_2 at 723K), the O_2 gasification surface area is over 20 times greater than the NO gasified surface area. This is indicative of significant porosity development in O_2 and that the reaction is restricted to "external"surface area in NO. This is confirmed by the CO_2 surface areas being lower than, or of the order of, the N_2 surface areas. The fact that the O_2 gasification surface area at 723K is also greater than the 723K NO gasification surface area implies that this is not simply a thermal effect. Further evidence for this comes from the fact that the N_2 surface area, and the amount of stable complex, as determined by the TPD experiments, does not vary with degree of NO gasification at 723K. Table 1 shows that both surface area and amount of stable complex are strong functions of degree of burn-off for O_2 gasification.

Another significant difference between the O_2 and NO-gasified chars can be discerned from the TPD spectra of the chars in Figures 6 and 7, respectively. The higher temperature CO peak is more intense than the 1000K peak for all of the NO-gasified chars, which may be interpreted as suggesting that there are few surface carbonyl or semi-quinone groups, or, at least, that they are of a different nature than those formed by O_2. There is also evidence for a 1000K shoulder for the 723K gasified chars, but, in the case of the 10% gasified char, this appeared following over 50 hours of exposure to NO. Only the mildest oxidation conditions, (e.g., chemisorption of NO at 523K), shown in Figure 3, produces a resolved low temperature CO peak. Conversely, the 1000K

peak is generally stronger than the 1250K peak for the O_2-gasified chars, and only for the 823K gasified chars are the peaks of comparable intensity.

Based upon the available evidence thus far, the absence of the less stable carbonyl or semi-quinone oxygen complexesin NO gasification may be accounted for by a fast reaction such as "stripping":

$$NO + C[O] \rightarrow CO_2 + 1/2\ N_2 \text{ (or C-N)} \qquad [R.2]$$

The limiting step in NO gasification could then be the formation of surface complexes by NO, which would tend to make the reaction first order with respect to NO. Indeed, first order kinetics have been reported for this reaction in a number of studies [5]. The NO "stripping" reaction can explain the origin of CO_2 in NO oxidation, which has previously been attributed to surface complex stripping by CO [5]. Vastola *et al.* [6] and Hall and Calo [3] have shown that the latter reaction does not take place appreciably under isothermal conditions. The higher temperature CO peak can be explained by the re-adsorption of bulk phase CO product from the reaction, since the gasification was conducted in a batch mode.

The preceding discussion still begs the question as to whether there is a causal relationship between the apparent absence of carbonyl or semi-quinone oxygen and the absence of porosity. An answer to this is necessarily speculative but, if indeed the gasification is adsorption-limited (due to relatively fast NO stripping and slow formation of complexes), then the equilibrium concentration of surface complexes would be less than for the corresponding O_2 gasification. The effectiveness of R.2 would also mean that NO has a low probability of significantly developing porosity. The result is that gasification would tend to proceed more in a "shrinking sphere" mode. For oxygen gasification, the situation is more complex. A larger fraction of the surface is covered by stable complex because there is no obvious "stripping" mechanism, and one molecule of O_2 can produce two complexes. Such effects as changes in the surface energetic heterogeneity with coverage, due to lateral complex-complex interactions, and limited accessibility of active sites result in more complex kinetics.

CO_2 has a much lower reactivity than NO, and Figure 2 shows that the principal desorption product after gasification at 1133K is high temperature CO. There is also, however, some evidence for 1000K CO. Unlike NO, CO_2 gasification develops measurable porosity in the Pittsburgh # 8 char. The absence of significant 1000K CO is most easily explained by the high gasification temperature (i.e., the high thermal decomposition rate of the resultant complexes) since, presumably, the 1000K sites are those directly involved in gasification. Results on other coal chars and carbons ([1, 2]) of non-gasifying CO_2 chemisorption show that both 1000K and

higher temperature CO are desorption products under these conditions. The generally low reactivity of chars in CO_2 can be explained by the hypothesis that upon dissociation, the products are a carbonyl or semi-quinone group and CO, both of which form stable complexes, thereby tending to stabilize the surface. The primary difference between O_2 and CO_2 gasification in the context of this qualitative model is that in O_2 adjacent carbonyl groups can interact to form less stable groups [4], whereas in CO_2 there is a significantly lower probability of having adjacent carbonyl or semi-quinone groups.

Conclusions

The theory of the unified nature of carbon-oxygen complexes seems to be qualitatively corroborated by the current work with different oxidizing agents. It has also been shown that commonality of functional groups, although of significance, is not sufficient to explain differences in reactivity or the manner in which gasification develops porosity. In particular, the rate of oxidant adsorption, the thermal stability of the dissociation products, and, in the case of NO oxidation, the possibility of oxygen stripping reactions, must also be taken into account. The use of an essentially non-porous char has shown that different oxidants can develop porosity quite differently in chars. The same may not be possible for some porous carbons due to the possibility that a relatively small degree of burn-off can produce significantly disproportionate porosity by opening previously inaccessible pores.

Acknowledgements

This work was conducted under contract DE-AC21-87MC23284 with the Morgantown Energy Technology Center and grant DE-FG22-87PC79929 from the University Coal Research Program of the DOE.

References

1. Marchon, B., Carrazza, J., Heinemann, H. and Somorjai, G.A. *Carbon*, **28**, 507, 1988.
2. Hall, P.J. and Calo, J.M. *Proc. Int . Carbon Conf. Carbon '88*, p.77, (McEnaney, E. and Mays, T.J., eds) IOP Publishing Co. Bristol, UK, 1988.
3. Hall, P.J. and Calo, J.M. submitted to *Energy and Fuels.*, 1988
4. Otake, Y. PhD Thesis, The Pennsylvania State University, 1986.
5. Chan, L.K., Sarofim, A.F. and Beer, J.M. *Combustion and Flame*, **52:37-45**, 37, 1983.
6. Vastola, F.J., Hart, P.J. and Walker, P.L., Jr, *Carbon*, **2**, 65, 1965.

Table 1, Reactivity and surface areas of Pittsburgh # 8 coal char in various oxidants

Oxidant	Gasification Temperature, K	% Burn-off	Reactivity (g/g hr)	Total oxygen	N_2 Surface Area (m^2/g)
O_2	723	10	0.28	0.282	91
O_2	723	25	0.28	0.366	150
O_2	773	27	0.65	0.251	69
O_2	823	25	2.58	0.115	--
NO	723	5	$3.3x10^{-3}$	0.195	10
NO	723	10	$3.2x10^{-3}$	0.198	10
NO	923	10	$3.5x10^{-2}$	0.123	3
NO	1123	10	0.43	0.078	2
CO_2	1133	9	0.18	0.086	72

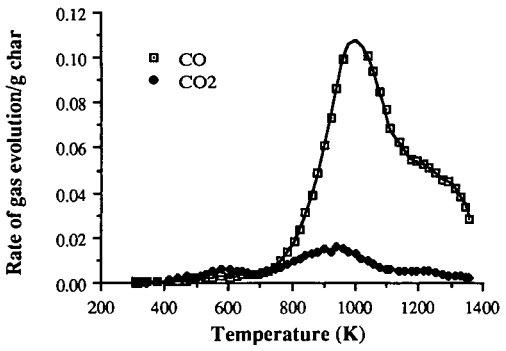

Figure 1. 100K/min TPD spectra of Pittsburgh # 8 coal char following gasification in 0.1 MPa of O_2 at 723K to 25% burn-off.

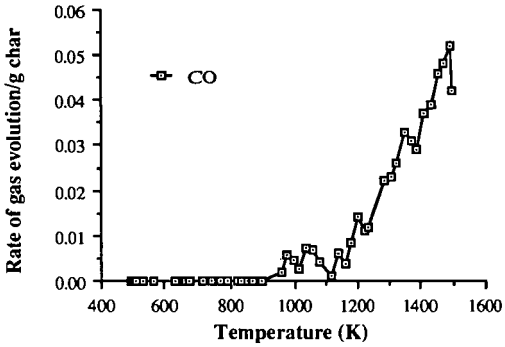

Figure 2. 100K/min TPD spectrum of Pittsburgh # 8 coal char following gasification in 0.1 MPa of CO_2 at 1133K to 9% burn-off.

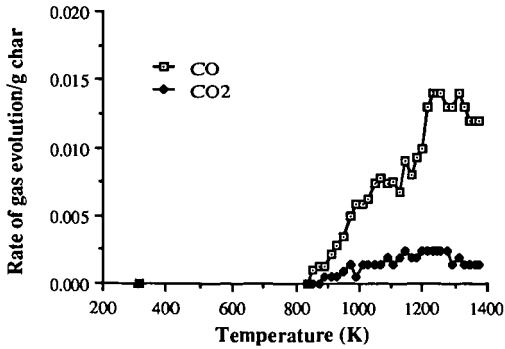

Figure 3. 100K/min TPD spectra of Pittsburgh # 8 coal char following chemisorption in 0.1 MPa of NO for 35 hours at 523K.

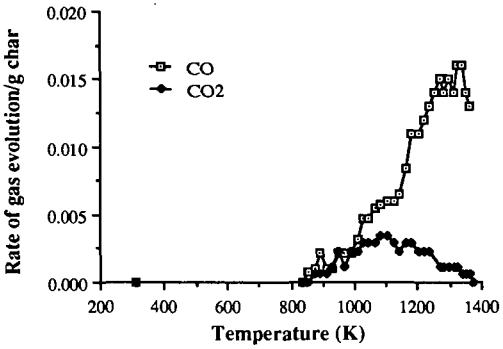

Figure 4. 100K/min TPD spectra of Pittsburgh # 8 coal char following oxidation in 15N HNO_3 for 0.5 hours at 323K.

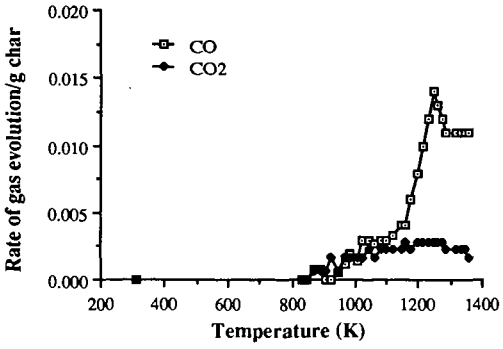

Figure 5. 100 K/min TPD spectra of Pittsburgh # 8 coal char following oxidation in H_2O_2 for 2 hours at 290K.

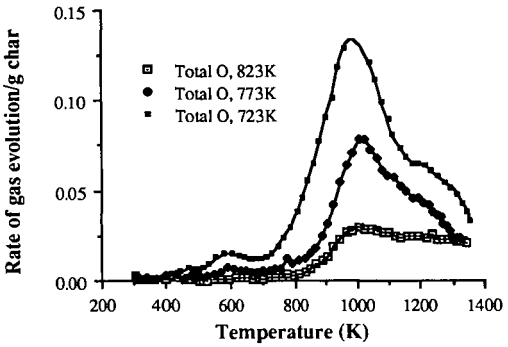

Figure 6. **100K/min TPD spectra of Pittsburgh # 8 coal char following gasification in 0.1 MPa O_2 to 25% burn-off at varying temperature.**

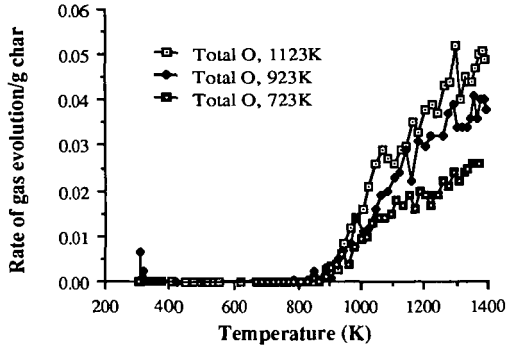

Figure 7. 100K/min TPD spectra of Pittsburgh # 8 coal char following gasification in 0.1 MPa NO to 10% burn-off at varying temperature.

CATALYTIC GASIFICATION OF GRAPHITE AND CHARS

Heinz Heinemann, G.A. Somorjai, Pedro Pereira, Jose Carrazza
Center for Advanced Materials
Materials and Chemical Sciences Division
Lawrence Berkeley Laboratory
and Department of Chemistry
University of California
Berkeley, California U.S.A.

INTRODUCTION

In earlier papers [1-5] we have reported on the low temperature catalytic gasification of carbonaceous materials with steam. The use of catalysts is necessary if the process is to be carried out at temperatures below 1000 K. While alkaline or alkaline-earth hydroxides and carbonates have been studied by many investigators, they show catalytic activity only at temperatures above 1000 K. Transition metals, in particular nickel and iron, are able to catalyze the process at temperatures as low as 750 K but they deactivate very fast. These transition metal catalysts are active only if the reaction conditions permit their presence in the metallic state.

In our earlier work we have described catalysts which are mixtures of potassium hydroxide and nickel oxide and have demonstrated that they showed the highest activity of all the systems previously studied at below 1000K. We also showed that this catalyst mixture formed a relatively low melting eutectic that can wet the surface of the carbon substrates forming a liquid film which attacks the carbonaceous material by edge recession mode rather than by a channeling mode which prevails for potassium hydroxide alone and nickel alone.

A disadvantage found with the potassium-nickel catalysts is that they have a tendency to deactivate over a period of time when used on chars due to an interference or poisoning by ash components in the char. The present paper presents information on the role of ash components on catalytic gasification and describes another type of catalyst, namely a mixture of alkali and earth alkali oxides such as K_2O-CaO, which is almost as active and is less sensitive to poisoning than the potassium-nickel composition.

EXPERIMENTAL

Four chars ranging from lignite to bituminous coal char have been gasified along with graphite in the presence of various catalysts. The chars and their composition are summarized in Table 1.

The graphite used was spectroscopic grade graphite (Ultra Carbon Corp., type UCP-2, 325 mesh) having a BET surface area of $47 m^2/g$.

The carbonaceous samples were impregnated by incipient wetness methods with solutions of KOH, KNO_3, $Ca(NO_3)_2$, or $Ni(NO_3)_2$ respectively. The atomic ratio of K/M^{2+} was equal to 1 and the ratio of K/C = 0.01. The samples were dried at 920 K for one hour and the nitrates were decomposed. In some experiments with char the catalyst was prepared first by mixing aqueous solutions of KNO_3 and $Ni(NO_3)_2$ or $Mg(NO_3)_2$ and drying. The solid catalyst was then finely ground with the char in the correct proportions.

The experimental setup of the flow reactor is shown in Fig. 1. The reactor is a 3.7 mm ID 316 stainless steel tube. Between 0.5 and 1.0 g of sample is deposited between two alumina wool plugs. Passing steam through the system in the absence of a sample does not give any reaction. The reaction temperature can be adjusted to $\pm 1^{o}C$ of the desired value. Steam is produced by pumping water with a Harvard Compact Infusion pump, Model 975, through heated lines with an inlet temperature to the reactor of 450 K. At water flows of less than 0.1cc/min total pressure in the reactor is 15 psig ± 1 psig. A liquid rate of .06cc/min was selected as a standard flow, equivalent to 270 cc/min of steam at 850 K. Steam leaving the reactor is condensed by volume expansion. Gas produced is measured and analyzed by gas chromatography and liquid water is measured to permit a mass balance.

A thermal detector with a column of 100/120 carbosieve S-II, 10' x 1/8", supplied by SUPELCO is used for the analysis of H_2, CO, CO_2, and CH_4. Water is eluted from the column at a flow rate of 30 ml/min He carrier gas, a column temperature of 425 K for 9 min, followed by a rise to 500 K achieved at a rate of 25^{o}/min and maintained at 500 K for 12 min.

The flow reactor test is standardized as follows: The reactor containing the carbon plus catalyst mixture is heated to 725 K at a rate of 125^{o}/hr in a 5cc/min helium flow. The temperature of 725 K is maintained for 2 hours to assure complete decomposition of the catalyst nitrates and their conversion to oxides. Water flow is then started and the temperature is raised at a rate of about 10^{o}/min to the desired reaction temperature, usually 900 K.

RESULTS

Potassium-nickel catalysts which show high activity at gasification temperatures in the 600-900K range deactivate as a function of time, apparently due to interaction with ash components of chars.

In a search for catalysts which would be likely to show less deactivation by ash components and which would also be less expensive than nickel, it was found that alkali-earth alkali combinations are of considerable interest. Potassium-calcium oxide mixtures were only slightly less active than potassium-nickel.

Activation energies for the potassium-nickel and potassium-calcium catalysts were determined on graphite and are not appreciably different on various chars (Table 2).

In general graphite and chars exhibit the same gasification mechanism as evidenced by similar activation energies: kinetic rate = $p^{n}(H_2O)p^{n}(H_2)$, $0<n<1$ and $\Delta E=\sim 63$ Kcal.

The ease of gasification increases in the order: graphite < bituminous < subbituminous < lignite chars. Table 3 illustrates this behavior. While K-Ca is more active for lignite and subbituminous chars than K-Ni, the reverse is true for bituminous chars.

No difference in gasification was observed between catalyst prepared by impregnation of char or by physical mixing of catalyst and char.

In kinetic studies of steam gasification of a number of chars impregnated with 1% of equimolar potassium and nickel oxides or of K-Ca oxides, it was found that the predominant gas composition is H_2 and CO_2. It was observed that the CO/CO_2 ratio of gases produced varies with different chars. Thus, the ratio is .8 for Illinois #6 char and .08 for North Dakota lignite char, which has a much higher ash content. It was also found that impregnation with potassium hydroxide alone results in much higher CO/CO_2 ratios than K/Ni and therefore, in less hydrogen. Thus, Illinois #6 char with potassium alone produces a 3.5 CO/CO_2 ratio compared to .8 for K/Ni. Essentially no CH_4 was found.

The rate of hydrogen production as a function of catalyst loading increases rapidly in the case of the North Dakota char. This is shown in Table 4. Gasification at 890 K resulted in an almost 5-fold increase in the hydrogen production rate when the loading was 2.5% rather than 1% with an additional increase of 20% when the loading was 3.2%.

Catalytic activity of ash components in the char was observed in a number of cases and particularly for the North Dakota char. In the absence of a catalyst, initial gasification was observed (Fig. 2) until a total of about 30% of the char was gasified. The rate of hydrogen production per minute declined rapidly and eventually died. When the remaining 70% of the char was impregnated with 1% Ni/K, gasification resumed at a good rate and with only a slight decline in hydrogen production (Fig. 3). The North Dakota char was demineralized by HF/HCl treatment to an ash content of less than 2%. The demineralized char showed no activity in the absence of added catalysts. This proves that the previously observed gasification activity of the native char was due to a catalytic action of the ash.

After impregnation of the demineralized char with Ni/K rapid gasification occurs as shown in Fig. 4. The rate of gasification of the demineralized char promoted by Ni/K is almost an order of magnitude higher than that observed for the steam deactivated char with the same catalyst (Fig. 3). The gas product distribution is the same, namely mostly CO_2 and hydrogen with small amounts of CO and with almost negligible CH_4 production. The decline in hydrogen production shown in Fig. 4 at the end of gasification is due to the relatively small amounts of char remaining in the reactor after about 75% carbon conversion.

A comparison of the rate of char conversion for alkali-alkali earth (K-Ca) catalysts and for alkali-transition metal catalysts (K-Ni) is shown in Fig. 5 for a subbituminous char (Rosebud). The superiority of the K-Ca catalyst over the K-Ni catalyst is apparent. When the char is first demineralized, the K-Ni catalyst shows better gasification than the raw char, while the K-Ca catalyst looses some activity when used in the demineralized char. This indicates that ash components poison the K-Ni catalyst but enhance the activity of the K-Ca catalyst.

An important finding toward proposing a reaction mechanism is the fact that the catalysts used in this work can dissociate water at reaction conditions in the absence of carbon. With a K-Mg catalyst the activation energy for H_2 production from water was 132 Kcal/mol. It has also been noted that while the stoichiometric ratio of H_2/CO_2 in carbon gasification should be 2, it is slightly higher than 2 during the first 50% of gasification and lower than 2 during the second half. This indicates sorption of CO or CO_2 on the char in

early stages of gasification and desorption in the later states. Breaking of C-C bonds is probably the rate controlling step. Figure 6 shows the ratios of H_2/CO_2 produced at various stages of gasification.

CONCLUSION

Graphite and chars can be gasified at 800-900°K by treatment with steam in the presence of catalysts comprising mixtures of potassium and nickel salts or potassium and calcium salts. The ease of gasification increases graphite < bituminous < subbituminous < lignite. The catalysts must be wetting the carbonaceous material and gasification proceeds by edge recession. Potassium-nickel catalysts, while slightly more active, are more subject to poisoning by ash components than potasssium-calcium catalyts. An important first step in the gasification mechanism appears to be water dissociation that is catalyzed by all the active catalysts.

ACKNOWLEDGEMENT

This work was supported by the Assistant Secretary for Fossil Energy, Office of Management and Technical Coordination, Technical Division of the U.S. Department of Energy under Contract Number DE-AC03-SF00098, through the Morgantown Energy Technology Center, Morgantown, WV 26505.

REFERENCES

1. J. Carrazza, W. Tysoe, H. Heinemann, and G.A. Somorjai, J. Catal., 96, 234 (1985).

2. J. Carrazza, J.J. Chludzinski, H. Heinemann, G.A. Somorjai, and T.K. Baker, J. Catal., 110, 74 (1988).

3. J. Carrazza, G.A. Somorjai, and H. Heinemann, Am. Chem. Soc, Fuel Div. Preprints, 31, #3, 158 (1986).

4. B. Marchon, J. Carrazza, H. Heinemann, and G.A. Somorjai, Carbon, 26, 507 (1988).

5. F. Delanay, W.T. Tysoe, H. Heinemann, and G.A. Somorjai, Carbon, 22, 401 (1984).

Table 1..PROXIMATE, ULTIMATE, AND INORGANIC CHEMICAL ANALYSES OF COALS USED IN GASIFICATION TESTS

Seam	N.Dakota		OH Pitt No. 8	
Mine	Lignite	Rosebud	Franklin	
125 KY No. 13				
Proximate Analysis, wt%				
Moisture	3.4	23.1	2.5	9.8
Volatile Matter	71.6	28.5	38.6	32.2
Ash	25.0	11.3	7.5	7.3
Fixed Carbon	-.	37.1	51.4	50.7
Total	100.0	100.0	100.0	100.0
Ultimate Analysis, wt% (dry basis)				
Ash		14.66	7.68	8.08
Carbon		62.78	74.47	73.74
Hydrogen		4.40	5.24	4.82
Sulfur		1.29	3.21	1.40
Nitrogen		0.99	1.50	1.85
Oxygen (by difference)		15.88	7.90	10.11
Total		100.00	100.00	100.00
Ash Composition, wt%				
SiO_2	26.1	48.8	41.6	58.5
Al_2O_3	13.7	23.55	20.9	26.9
Fe_2O_3	6.6	7.02	31.7	8.1
TiO_2	0.6	0.12	1.02	0.87
P_2O_5	0.2	0.25	0.07	0.16
CaO	22.4	7.16	1.14	0.90
MgO	8.1	2.57	0.36	1.21
Na_2O	1.8	0.09	0.35	0.24
K_2O	.6	0.36	0.98	2.94
SO_3	18.1	9.91	1.00	0.80
Total	98.2	99.78	99.2	100.62
Ash Content (as ashed for analysis of ash, dry basis)			7.7	8.2
Basic Ash Constituents, wt%		19.22	35.2	13.4
Dolomite Ratio, wt%		56.6	4.3	15.8
SiO_2/Al_2O_3 Ratio		2.1	2.0	2.2
Forms of Sulfur, wt% (dry basis)				
Pyritic		0.76	2.37	0.40
Sulfate		0.015	0.21	0.10
Organic		0.52	0.97	1.03
Total		1.28	3.56	1.53

Forms of Iron (dry basis)	wt%	% of Fe	wt%	% of Fe	wt%	% of Fe
Pyritic	1.32	62*	2.07	96	0.35	70
HCl-Soluble	0.12	6	0.08	4	0.15	30
Total of HCl Sol + Pyritic	2.13*	100	2.15	100	0.50	100
Acid-Insoluble	0.69	--	<0.10	--	<0.1	
Pyritic, % of total Fe**		--		97		54

*Based on total iron including 0.69 wt% HCl-insoluble
**Of 1/4-inch-top-size coal after storage

Table 2: Arrhenius Analysis for Gasification

Catalyst and Char	Activation Energy Kcal/mol
K-Ni Graphite	~61.0
K-Ca Rosebud Char	58.8
K/Ca Franklyn Char	64.4
K-Ca Franklyn Char demineralized	63.1
K-Ni Franklyn Char	54.1

Table 3: Relative Gasification Conversion of Chars

Catalyst Activity	Char Class	% Conversion at 900K After 1000 Min
K-Ca > K-Ni	Lignite	100
K-Ca > K-Ni	Subbituminous	90-100
K-Ni > K-Ca	Bituminous	45-50

Table 4. Rate of H_2 Production as Function of Catalyst Loading Ni/K = 1.0.

Ni/C	H_2 rate ml/min	m mol/H_2/mol Ni/min
1.0×10^{-2}	0.5	49
2.5×10^{-2}	2.48	97
3.2×10^{-2}	2.90	89

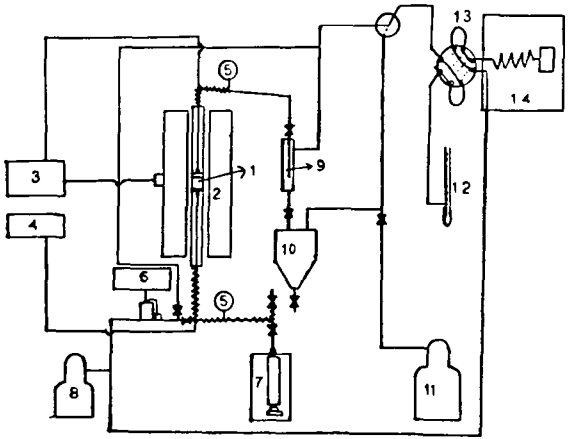

Figure 1. Experimental Setup

1.	Sample	8.	He 99.99% bottle
2.	Oven	9.	Expander
3.	Temperature control	10.	Meter recipient
4.	Temperature indicator	11.	Callibrating mixture for G.C.
5.	Pressure gauges	12.	Bubble flowmeter
6.	Mass flow controller	13.	Gas sample valve
7.	Syringe pump	14.	Gas chromatograph

⋈ : Valve
∿∿ : Wire heater

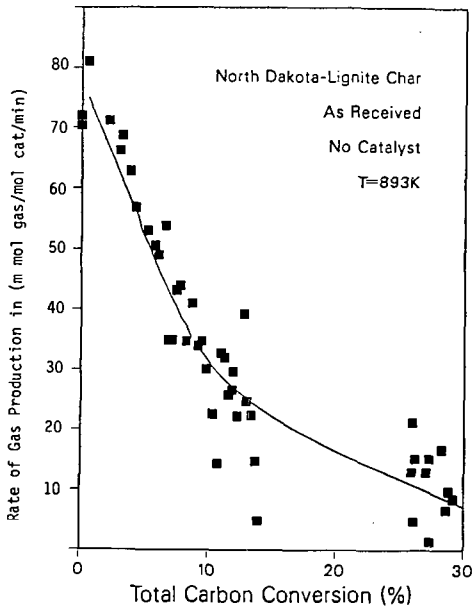

Fig. 2. Variations of the rate of carbon gasification by steam at 893 K, with total carbon conversion, for North Dakota-lignite char, as received, without addition of any catalyst.

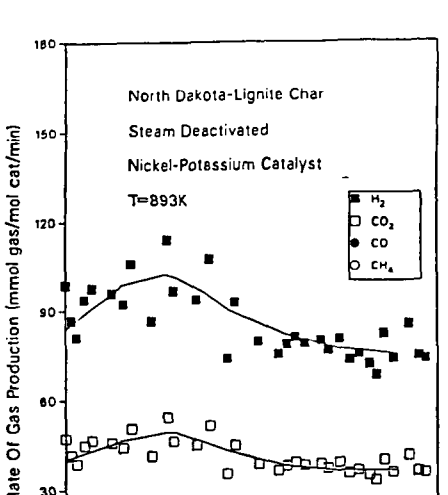

Figure 3. Rate of gas production, as a function of carbon conversion, for all the gases formed on the steam gasification of deactivated char at 893 K, catalyzed by the nickel-potassium mixture. The molar ratio of nickel to potassium was equal to 0.9, and the catalyst loading was equal to 2.0 mmol cat/g char. The initial weight of char was 0.6 g.

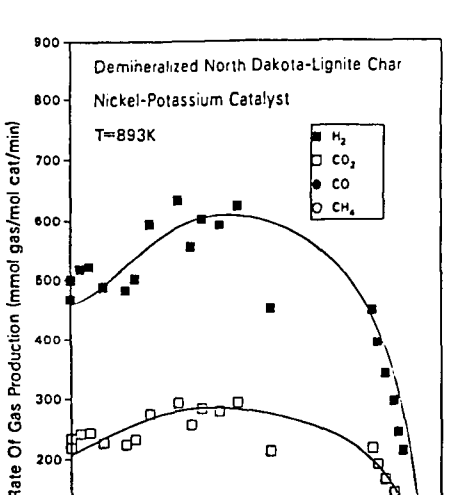

Figure 4. Rate of gas production as a function of carbon conversion, for all the gases formed from the steam gasification of demineralized char at 893 K, catalyzed by the nickel-potassium mixture. The molar ratio of nickel to potassium was equal to 0.9, and the catalyst loading was equal to 2.0 mmol cat/g char. The initial weight of char was 0.5g.

Fig. 5. Rosebud Char Steam Gasification
K-Ca and K-Ni Compared

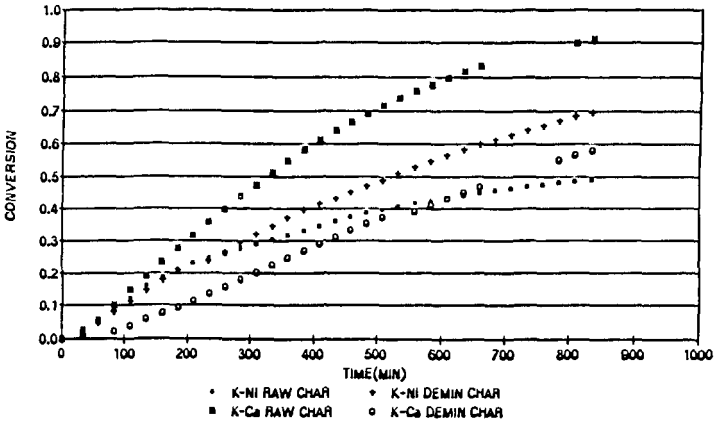

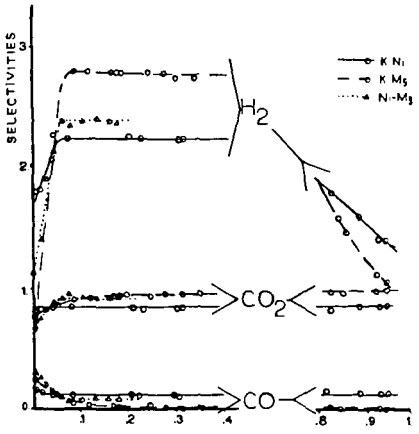

Fig. 6. Selectivity vs. Conversion for Steam Gasification of North Dakota Char Demineralized.

A KINETIC MECHANISM OF THE WATER–GAS–SHIFT REACTION OVER K_2CO_3/CARBON

R. Meijer, M. Sibeijn, M.R.B. van Dillen, F. Kapteijn and J.A. Moulijn

Institute of Chemical Technology, University of Amsterdam
Nieuwe Achtergracht 166, 1018 WV Amsterdam, The Netherlands

Abstract

Kinetic data of the alkali catalysed WGS reaction can be described by a two step oxygen–exchange mechanism and an additional CO_2–chemisorption step. The Water–Gas–Shift reaction rate is dependent on both the partial pressure of the reducing and the oxidizing agent. In the presence of CO_2 in the gas phase reactivity is low, or decreases significantly if CO_2 is added to a CO,H_2O mixture.

Introduction

The Water–Gas–Shift reaction (1) is not only of importance for hydrogen production on industrial scale, but also as a side reaction in steam gasification.

$$CO + H_2O \rightleftarrows H_2 + CO_2 \qquad (1)$$

Many investigators have studied the kinetics of the WGS reaction over iron, copper, chromium and cobalt–molybdenum catalysts [1–8], but few studies have been made on the role of the WGS reaction in alkali catalysed steam gasification [9–13]. In this study results are presented of a kinetic study on the WGS reaction catalysed by K_2CO_3/activated carbon at temperatures (650–950 K) where gasification and methanation do not occur.

The kinetics of the WGS reaction have been described [9] as a set of two oxygen–exchange reactions (2),(3), similar to the oxidation–reduction cycle in the mechanism for alkali catalysed gasification in CO_2 and H_2O.

$$H_2O + * \underset{k_{-1}}{\overset{k_1}{\rightleftarrows}} H_2 + O\text{-}* \qquad (2)$$

$$CO + O\text{-}* \underset{k_{-2}}{\overset{k_2}{\rightleftarrows}} CO_2 + * \qquad (3)$$

Hüttinger et al. [9] have studied the CO,H_2O oxygen–exchange rate. Their kinetic data are fitted by a power–law rate equation (4) assuming differential reactor behaviour. They concluded that addition of H_2 to the feed does not affect the oxygen–exchange rate, addition of CO_2 was not investigated.

$$r = k\ pCO^{0.5}\ pH_2O^{0.4} \qquad (4)$$

Based upon substantial evidence [11,14–16] Cerfontain et al. [14] have proposed an extended model for describing oxygen–exchange in CO,CO_2 mixtures: a CO,CO_2 oxygen–exchange (8), preceded by a CO_2–chemisorption step. This CO_2–chemisorption is nearly temperature and pressure independent and CO_2 easily exchanges with gas phase CO_2. Furthermore the amount of chemisorbed CO_2 per amount of metal initially present correlated with the oxygen–exchange rate.

It is plausible that in the presence of CO_2 in the gas phase, CO_2–chemisorption in the alkali–metal cluster also plays a role in the alkali catalysed WGS reaction. The two step model (2),(3) is therefore extended with additional chemisorption steps (5),(6),(7) and other routes for CO,CO_2 exchange (5),(6) or (6),(7),(8).

$$CO + O\text{-}* \underset{k_{-3}}{\overset{k_3}{\rightleftarrows}} CO_2\text{-}* \qquad (5)$$

$$CO_2\text{-}* \quad \underset{k_{-4}}{\overset{k_4}{\rightleftarrows}} \quad CO_2 + * \qquad (6)$$

$$CO_2 + O\text{-}* \quad \underset{k_{-5}}{\overset{k_5}{\rightleftarrows}} \quad CO_3\text{-}* \qquad (7)$$

$$CO_2 + CO_2\text{-}* \quad \underset{k_{-6}}{\overset{k_6}{\rightleftarrows}} \quad CO_3\text{-}* + CO \qquad (8)$$

A possible mechanism for CO,CO_2 oxygen−exchange, in which a CO_2−* intermediate is present, is a combination of steps (5) and (6). In order to establish a kinetic model of the alkali catalysed WGS reaction the influence of catalyst loading, partial pressures of reactants and products on the forward− (H_2O + CO →) and backward− (CO_2 + H_2 →) oxygen exchange rate have been studied.

Experimental

WGS experiments were performed in a Fixed−Bed flow reactor described in detail elsewhere [17,18]. Basically it consists of a gas mixing section, an oven (T_{max} = 1273 K , P_{max} = 2.5 MPa) containing the carbon sample in a quartz tube (I.D. = 3 − 7 mm) and a gas chromatograph (HP 5190 A) for product analysis (dual column, He carrier, TCD detection). All experiments were performed in a ceramic (0.2−1.6 MPa) or quartz (0.15 MPa) reactor.

The activated carbon used in this study is Norit RX1 Extra, an acid washed, steam activated peat char with a high specific surface area (1100 $m^2.g^{-1}$ (CO_2(DR),273 K), 1500 $m^2.g^{-1}$ (N_2(BET),77 K), particle size 0.25−0.6 mm, 3 wt% ash). Addition of catalyst was performed by pore volume impregnation with an aqueous M_2CO_3 (M= Na,K,Cs) solution. The catalyst loading is expressed as a molar M/C ratio.

A reproducible sample for each WGS experiment was obtained by drying *in situ* (T= 473 K, He) followed by isothermal gasification (T = 1000 K, P_t = 0.15 MPa, F_t = 140 $\mu mol.s^{-1}$, pH_2O or pCO_2 = 0.05 MPa, balance He) to a steady gasification level (20−30 wt% burn−off). Subsequently the sample is cooled to 673 K and a WGS experiment is started. The WGS oxygen−exchange rate r_{ox} is measured in a temperature cycle (673−950(833)−673 K), in which temperature is varied stepwise, and expressed as (μmol oxygen exchanged).(μmol carbon initially present)$^{-1}.s^{-1}$. The oxygen exchange rate of a particular reactant mixture is referred to as r_{ox} (reactant molecules), e.g. the forward shift as $r_{ox}(CO,H_2O)$.

CO,H_2O oxygen−exchange experiments were performed with a feed consisting of CO,H_2O and a balance of helium in which the reactant ratio in the feed (q = $(pCO/pH_2O)_{feed}$) was varied from 0.15 to 5.0 (P_t = 0.15 MPa, F_t = 140 $\mu mol.s^{-1}$).

CO_2,H_2 oxygen−exchange experiments were performed with variation of total pressure (0.15−1.6 MPa) and reactant ratio (q' = $(pH_2/pCO_2)_{feed}$ = 0.14 − 7.0).
For each q and q' value a fresh sample was used. Inhibition effects of products on oxygen−exchange rates were studied by (partially) replacing the helium in the feed (P_t = 0.15 MPa) by a product.

Results

In figure 1 WGS rate data ($r_{ox}(CO,H_2O)$) and CO_2− and H_2O−gasification data (r_n) are shown. Clearly in all three cases the same dependency on the K/C ratio is observed. The carbon itself hardly showed any oxygen−exchange reactivity. It is found that $r_{ox}(CO,H_2O)$ is dependent on both the partial pressure of the reducing and the oxidizing agent. As shown in figure 2 addition of H_2 to a feed, containing CO and H_2O, does not affect the measured CO conversion, whereas CO_2 strongly inhibits.

$r_{ox}(H_2,CO_2)$ is predominantly dependent on the H_2 partial pressure. Figure 3 shows that with increasing pH_2 (q' constant; open vs. closed symbols) $r_{ox}(H_2,CO_2)$ increases. With increasing pCO_2 (pH_2 constant; open and closed symbols) a decrease in $r_{ox}(H_2,CO_2)$ is observed. From figure 4 it can be seen that addition of H_2O decreases the measured CO_2 conversion significantly,

whereas addition of CO only has a small effect.

Discussion

The WGS reaction, like $^{12}CO,^{13}CO_2$ [14] and D_2,H_2O [19] oxygen−exchange, takes place in the alkali−metal−oxide clusters present on the carbon surface. Furthermore oxygen−exchange rates exhibit the same dependency on the K/C ratio as gasification reactions. In contrast to reported D_2,H_2O and $^{12}CO,^{13}CO_2$ oxygen−exchange rates, $r_{ox}(CO,H_2O)$ is dependent on both the partial pressure of the reducing and the oxidizing agent. With a two step oxygen−exchange mechanism (2),(3), kinetic data from CO,H_2O exchange experiments could be adequately described. However addition of CO_2 to the CO,H_2O reactant mixture and the CO_2,H_2 exchange data showed a poor correlation with this model. This is probably caused by a strong CO_2−chemisorption under these conditions.

Therefore the kinetic model for best describing the WGS reaction consists of a CO,CO_2 oxygen exchange via a chemisorbed CO_2 intermediate (steps 5 and 6), whereas the H_2,H_2O exchange is believed to proceed via (2).

Direct proof for the existence of CO_2−chemisorption is obtained from thermogravimetric experiments [20] with catalyst/carbon (M= Na,K,Cs) samples. Introduction of CO_2 at 650 K to a gas phase containing CO,H_2O or H_2,H_2O shows an instantaneous weight increase. If the total weight gain is ascribed to CO_2−chemisorption in the alkali metal cluster (pure carbon shows no weight change), this corresponds to a CO_2/M ratio of approximately 0.3 for all three alkali metals investigated. Removing CO_2 from the gas phase only shows a slow isothermal (650 K) desorption rate. The chemisorbed CO_2 can be completely removed on heating in argon to 850 K.

Mims and Pabst [11] have studied the oxygen−exchange rate in various mixtures and observed a rate order which is in good agreement with this study: $r_{ox}(D_2,H_2O) >> r_{ox}(H_2O,CO) > r_{ox}(CO_2,H_2) > r_{ox}(CO,CO_2)$

All oxygen−exchange rates (especially D_2,H_2O) are several orders of magnitude higher than the matching gasification rates. Addition of CO_2 to a D_2,H_2O mixture surpresses the oxygen−exchange rate to a level similar to that of CO_2,H_2 exchange. This difference in oxygen−exchange reactivity can be explained by a different state of the alkali cluster, depending on the amount of CO and/or CO_2 which is present in the gas phase. From this and other studies [9,11,14,19] a summary of the order and pressure dependencies of oxygen−exchange rates can be made (table 1).

At present more work is in progress on determination of the rate parameters by modeling the whole data set, CO,H_2O, CO_2,H_2 and product inhibition data, taking CO_2 chemisorption into account.

Conclusions

- The WGS oxygen exchange takes place in the alkali−metal−oxide cluster and shows the same rate dependency on the alkali metal loading as gasification reactions.
- The WGS oxygen−exchange is, in contrast to D_2,H_2O [19] and $^{12}CO,^{13}CO_2$ [14] oxygen−exchange, dependent on both the partial pressure of the reducing and the oxidizing agent.
- The oxygen−exchange rate in the presence of CO_2 is low or decreases significantly if CO_2 is added to a CO,H_2O mixture.
- In the presence of CO_2 in the gas phase, CO_2−chemisorption in the alkali−metal−oxide cluster takes place.
- Kinetic data of the alkali catalysed WGS reaction can be described by a two step oxygen−exchange mechanism and an additional CO_2−chemisorption step

Acknowledgement

These investigations have been executed within the framework of the Dutch National Coal Research Programme (NOK), which is managed by the Project Office for Energy Research (NOVEM) and financed by the Ministry Of Economic Affairs.

References:

[1] Newsome, D.S., *Catal. Rev.–Sci. Eng.*, 21(2), 275 (1980)
[2] Kodama, S., Mazume, A., Fukuba K., and Fukui, K., *Bull. of the Chem. Soc. of Japan*, vol 28, No.5, 318 (1955)
[3] Bohlbro, H., *Acta Chemica Scandinavica*, 15, 502 (1961)
[4] Tinkle M., and Dumesic, J.A., *J. Catal.*, 103, 65 (1987)
[5] Rethwisch, D.G., and Dumesic, J.A., *Applied Catlysis*, 21, 97 (1986)
[6] Salmi, T., Bostrom, S., and Lindfors, L.–E., *J. Catal.*, 112, 345 (1988)
[7] Chinchen, G.C., and Spencer, M.S., *J. Catal.*, 112, 325 (1988)
[8] Campbell, C.T., and Daube, K.A., *J. Catal.*, 104, 109 (1987)
[9] Hüttinger, K.J., Masling, B., and Minges, R., *Fuel*, 65, 93 (1986)
[10] Wigmans, T., Elfring, R., and Moulijn, J.A., *Carbon*, 21, 1 (1983)
[11] Mims, C.A., and Pabst, J.K., *J.* Catal., 107, 209 (1987)
[12] Kapteijn, F., Niamut, H.F.A., and Moulijn, J.A., *Proc. Carbon 86*, 537 (1986)
[13] Tone, S., Kimura, S., Hino, Y., and Otake, T., *J. of Chem. Eng. of Japan*, 18, 131 and 225 (1985)
[14] Cerfontain, M.B., Meijer, R., Kapteijn, F., and Moulijn, J.A., *J. Catal.*, 107, 173 (1987)
[15] Ratcliffe, C.T., and Vaughn, S.N., *Prep. Am. Chem. Soc. Div. Fuel Chem.*, 30, 304 (1985)
[16] Koenig, P.C., Squires R.G., and Laurendeau N.M., *J. Catal.*, 100, 228 (1986)
[17] Kapteijn, F., Peer, O. and Moulijn, J.A., *Fuel*, 65, 1371 (1986)
[18] Kapteijn, F., and Moulijn, J.A., *Final Report NOK–UGS* project no. 4351–5, nov 1985
[19] Mims, C.A., and Pabst, J.K., *Am. Chem. Soc., Div. Fuel. Chem., Prepr.*, 25(3), 258 (1980)
[20] Meijer, R., Kapteijn, F., and Moulijn, J.A., to be published

Table 1 : Order and pressure dependencies of oxygen exchange rates.

order of oxygen-exchange rates	effect on the exchange rate		
	↑	≈	↓
D_2, H_2O	D_2	H_2O	CO_2
>			
CO, H_2O	CO H_2O	H_2	CO_2
>			
CO_2, H_2	H_2	CO	H_2O CO_2
>			
$^{12}CO, ^{13}CO_2$	CO	CO_2	

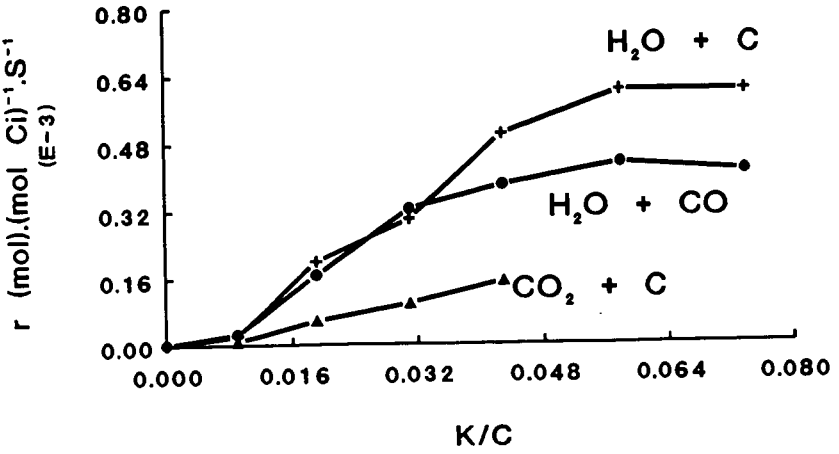

Figure 1 : Steady state reaction rates (r_n) for CO_2 (▲) and H_2O (+) gasification at 1000 K (at 25% burn−off) and r_{ox} (CO,H_2O) (●) at 833 K (after partial gasification in H_2O at 1000 K to 25% burn−off) as a function of the K/C ratio of the sample.

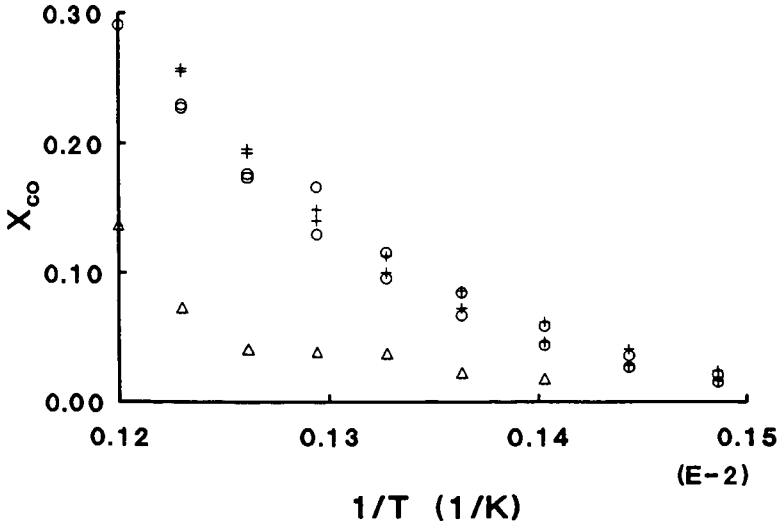

Figure 2 : CO,H_2O oxygen−exchange (○) over a 10 wt% K_2CO_3/Norit RXI sample. The CO conversion is plotted as a function of 1/T (1/K). Effect of CO_2 (△) and H_2 (+) addition to the feed.

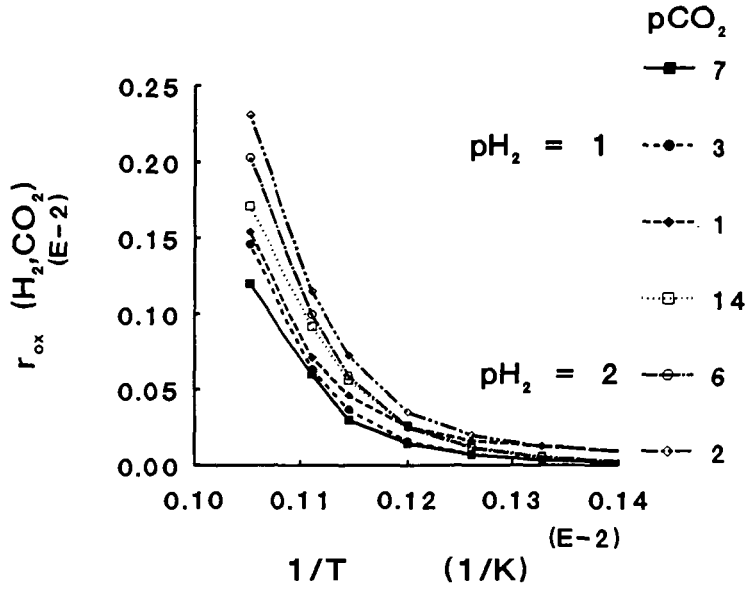

Figure 3 : $r_{ox}(H_2,CO_2)$ over a 10 wt% K_2CO_3/Norit RX1 Extra sample as a function of 1/T (1/K) for pH_2 = 1 bar (closed symbols) and pH_2 = 2 bar (open symbols) at different H_2/CO_2 feed ratio.

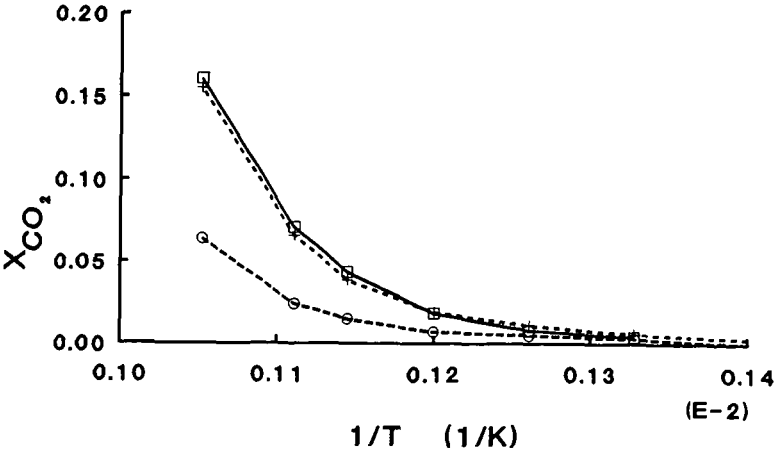

Figure 4 : CO_2,H_2 oxygen exchange (□) over a 10 wt% K_2CO_3/Norit RX1 sample. The CO_2 conversion is plotted as a function of 1/T (1/K). Effect of CO (+) and H_2O (○) addition to the feed.

CALCIUM DEACTIVATION IN CO_2 AND STEAM GASIFICATION REACTIONS

A. Linares-Solano, M. Almela-Alarcón, C. Salinas-Martínez de Lecea and D. Cazorla-Amorós.

Departamento de Química Inorgánica e Ingeniería Química. Universidad de Alicante. Alicante. Spain.

INTRODUCTION

Catalytic activity loss during the gasification reaction has a great practical importance. The factors controlling the deactivation process are difficult to study due to the difficulty of fixing all the variables related with the catalytic activity and to the lack of a simple technique able to evaluate "in situ" the changes undergone by the catalyst during the reaction.

In this sense the deactivation of a gasification catalyst has not been extensively investigated and is, without appropiate experimental support, generally related to (1,2): a) the mineral mater content of the carbon, b) the available internal surface area of the carbon, c) the catalyst addition method and d) the catalyst nature.

Currently it is well accepted that calcium is a good catalyst for the carbon-gas reactions (3) but deactivates more severely than potasium (4). These results were interpreted owing to inability of calcium species to redisperse themselves as occurs with potasium species. However results obtained in lignites with ion-exchanged calcium (3,5-7) do not seem to have so great tendency to deactivate. To interpret the different results found in the literature (mainly caused by the different experimental conditions used, as well as, by the nature of the gasification agents and of the carbon studied),it will be helpful to develop a simple experimental technique able to follow the catalyst modifications over the gasification reaction.

Recently, a "in situ" CO_2 chemisorption technique has been used to determine the active area of CaO particles in a carbon-CaO system, in order to interpret the carbon-gas reactions (8,9). This technique will be applied, together with X-ray diffraction, to analyse the calcium deactivation process during the carbon gasification reaction. The following factors have been studied: a) initial catalyst dispersion, b) reaction temperature and c) reaction agents. In order to simplify the study, the carbon used has almost no impurities and has a large surface area and a highly accesible porosity, to minimize their effects.

EXPERIMENTAL

A phenolformaldehide resin has been treated in N_2 flow (5 K/min to 1273 K, 1h) to prepare the carbon used for this study.

To increase its calcium exchange capacity, the carbon has been oxidized in 15N HNO_3 solution (1 g of carbon/10 ml solution) at 353 K to dryness and washed until free of nitrate ions.

Calcium has been loaded by ion-exchange from a 1.5M calcium acetate solution (7 g of carbon/50 ml solution); calcium loading obtained is 3.2 wt %. The contact time of the ion exchange (from 10 min to 8 h) do not significantly change the wt % calcium uptake.

Carbon reactivities (CO_2 and steam) and CO_2 chemisorption at 573 K has been studied following the thermogravimetrically (STA-780) experimental procedures described elsewhere (9,10).

RESULTS AND DISCUSSION:

Figure 1 presents CO_2 reactivities at 1073 K (0.1 MPa) of four samples with different activation degrees obtained by treatment of the original sample -0 % burn-off in the Figure- in CO_2 at 1073 K during different reaction time. Reactivity decreases noticeably with gasification time. Taking into account that reactivity increases lightly with burn-off for the uncatalized samples (8), it seems reasonable to ascribe the reactivity loss to changes ocurring in the catalyst over the gasification reaction.

X-ray diffraction patterns for these samples are shown in Fig. 2. There is no evidence of calcium species for the original sample (0 % burn-off) whereas $CaCO_3$ reflection peaks are obtained for the reacted samples in CO_2 (samples were cooled in CO_2 atmosphere before XRD study). The absence of detectable crystallites in the unreacted sample which is not caused by the small wt % calcium used ($CaCO_3$ reflection peaks has been observed in a narrow porosity carbon using lower wt % of calcium loading), is indicative of a high calcium dispersion in the carbon matrix; its particle size should be lower than the XRD technique detection limit. With increasing gasification level the peaks sharpen; there is an increase in crystallite size owing to an enlargement of the catalyst particles. This increase in particle size should be the responsible of the deactivation process observed in Figure 1.

CO_2 chemisorption technique at 573 K (8,9), during 30 min, has been applied to the calcium/carbon samples, after been heat treated in N_2 (20 K/min) up to 1173 K (10 min). Heat treatment decomposes the ion-exchanged calcium (in the case of the unreacted sample) and the $CaCO_3$ (in the reacted samples) to CaO. The amount of CO_2 chemisorbed is related to the CaO present at the surface of the CaO particles.

In Table 1 are compiled, for comparison purposes, the average size of the CaO particles obtained by X-ray diffraction and CO_2 chemisorption. Both techniques clearly show an enlargement of particle size during the gasification reaction. X-ray diffraction does not allow to deduce the particle size of the unreacted samples and gives significantly larger values than chemisorption. This happens because XRD has a non-detectable particle range <5 nm which

displaces the average particle size to higher values. Consequently XRD technique will be severely limited in a catalyzed gasification reaction, considering that the main catalytic activity is due to these very small particles. Furthermore XRD technique can not be applied "in situ" to the TG reactor, as it has been done with CO_2 chemisorption.

From Figure 3, where the CO_2 reactivity data are plotted versus the CaO average particle size, deduced by chemisorption, it is evident that reactivity is function of the catalyst particle size. Gasification reaction causes a noticeable reduction of the catalyst surface area exposed to the reaction atmosphere -by an enlargement of its particle size- and therefore a catalytic activity loss is observed with increasing the activation degree.

Effect of initial catalyst dispersion

The effect that the initial catalyst dispersion has on the reactivity and on its deactivation behaviour over the reaction time has been studied. The calcium/carbon sample has been heat treated in N_2 up to 1223 K during two hours in order to modify its initial dispersion. Figure 4 and 5 show respectively, the evolutions of the CO_2 reactivities at 1023 K and of the CaO surface areas, versus the activation degree for both the original and heat treated sample.

Reactivities have been calculated from one simple TG experiment and are expressed per gram of the initial weight of the carbon used. CaO surface areas are obtained in the TG reactor with samples partially reacted in CO_2 in the TG system.

Heat treatment causes a noticeable decrease in reactivity (comparable to that obtained during the reaction in CO_2 after a 40 % activation degree) as well as a change in the reactivity evolution profile.

Figure 5 has a very good parallelism with Figure 4 indicating the close relation between catalytic reactivity and available surface area of the catalyst. In that sence its noteworthy to point out that the heat treatment causes a 50 % reduction in both the initial reactivity and the CaO surface area.

The different reactivity behaviours, of the original and heat treated sample, versus activation degree can be related to a different sintering process caused by the heat treatment. After 20 % burn-off there is for the treated sample a much lower deactivation process than for the original sample.

Effect of reaction temperature

Figures 6 and 7 show respectively CO_2 reactivity (at 1023 and 1073 K) and CaO dispersion (obtained from CO_2 chemisorption), plotted versus the activation degree. Again it is important to recall the shape similarity of these two figures which corroborates the catalityc activity and the CaO dispersion relationship. The

reactivity loss is higher the higher is the reaction temperature used owing to a greater sintering process.

It is interesting to note in Figure 7 that the initial dispersions (for samples with 0 % burn-off) at 1023 and 1073 K, are not the same. The reason is that $CaCO_3$ formation is much favoured at 1023 K than at 1073 K, as it has been checked by XRD and TG-DTA technique (8). There is an instantaneous decrease in calcium dispersion when CO_2 is introduced in the reactor at 1023 K before the activation process starts. $CaCO_3$ favours the sintering process respect to CaO.

A closer look to Figures 6 and 7 shows that decreasing the reaction temperature reactivity decreases in a factor of 3 (burn-off degree <20 %),while CaO surface area only decreases in a factor of 1.5. These results seems to make clear that besides the importance of the catalyst dispersion there is an additional effect caused by the chemical changes in the catalyst due to the different reaction temperatures used. For a given temperature, the rate changes in reactivity, are very similar to the rate change observed in the dispersion degree as also happened in Figs. 4 and 5.

Effect of reaction atmosphere

Calcium catalytic activity has been studied in CO_2 (0.1 MPa) and in steam (19.7 KPa) at 1073 K. Figure 8 and 9 show respectively reactivity and CaO surface area results versus reaction time. Figure 8 clearly reveals that calcium activity is much higher in CO_2 than in steam under the experimental condition used. It is noteworthy that during gasification in steam the catalyst keeps a constant activity in contrast with the behaviour observed in CO_2 atmosphere. Reactivity results are confirmed and become evident from the changes observed in the catalyst surface area, as a function of the reaction atmosphere, in Figure 9. In steam no appreciable change in the catalyst surface area is observed. The burn-off degrees obtained in both reactions, after reaction time of 20 and 80 min, for CO_2 and steam respectively, are comparable.

Considering that both reactions have been studied at the same reaction temperature, it is evident that the gas phase atmospheres, as well as the different partial pressures used affect the chemical composition of the catalyst and its sintering behaviour. In CO_2 atmosphere (0.1 MPa) the catalyst is very active and the reaction mechanism involves a transformation of the active specie (probably CaO) to $CaCO_3$, as it has been proved by XRD. The $CaCO_3$ shows a promoted sintering behaviour due to the higher CO_2 partial pressure in the system. However in steam (19.7 KPa), where the catalyst activity is quite smaller, there is no evidence of a complet transformation of the active phase to carbonate because of the CO_2 partial pressure is very low. The calcium species present under the steam gasification will be: mainly CaO, some $Ca(OH)_2$ (which will decompose to CaO) and a small amount of $CaCO_3$. The lower tendency of CaO respect to $CaCO_3$ to sinter is evident from Figure 9 as it is also expected from the Tamman

Temperature (1501 and 838 K respectively).

CONCLUSIONS

A polymer carbon of high purity, high surface area and easy accesibility to the porous structure provides a simple medium to study the calcium deactivation during gasification reactions in CO_2 and steam.

XRD technique has severe limitations to be applied in the study of catalyzed carbon gasification. The range of undetected particles sizes are expected to be the most actives in the gasification reactions. CO_2 chemisorption technique is able to measure the specific surface area of the active calcium species, without need to take the sample out of the reactor.

Catalyst deactivation during the reaction is a direct consequence of a loss in active surface area (or enlargement of the particle size). Heat treatment, reaction gas and reaction temperature have a remarkable importance in the calcium deactivation process.Reactivity results for the different factors studied are closely related to CO_2 chemisorption data.

BIBLIOGRAPHY

(1) Van Heek, H.K. and Muhlen, H.J., Fuel 64 1045 (1985).
(2) Moulijn, J.A. and Kapteijn, F. "Carbon and coal gasification" Eds. J.L. Figueiredo and J.A. Moulijn, 181 (1986).
(3) Linares Solano, A., Hippo, E.H. and Walker, P.L.Jr., Fuel 65 776 (1986).
(4) Kapteijn, F., Pore, H. and Moulijn, J.A., AIChE Journal, 32 691 (1986).
(5) Radovic, L.R., Walker, P.L.Jr. and Jenkins, R.G. J. Catal. 82 382 (1983).
(6) Hippo, E.J., Jenkins, R.G. and Walker, P.L.Jr., Fuel 58 338 (1979).
(7) Walker P.L.Jr., Matsumoso, S., Hanzawa, T., Miura, T. and Ismail, I.M.K., Fuel 62 140 (1983).
(8) Alamela Alarcón, M., PhD. Thesis. University of Alicante. (1988).
(9) Linares Solano, A., Salinas Martínez de Lecea, C. and Almela Alarcón, M., ICCS 559. Elsevier Science Publishers (1987).
(10) Fernandez González, C., Linares Solano, A., McEnaney, B. and Salinas Martínez de Lecea, C., Fuel 65 991 (1986).

ACKNOWLEDGMENT

Thanks to the DGICYT for financial support (proyect no. PB86-0286).

Table 1

Average CaO particle size (nm) by XRD and CO_2 chemisorption

%burn-off	XRD	CO_2
15	9	3.3
28	13	3.6
40	18	4.6

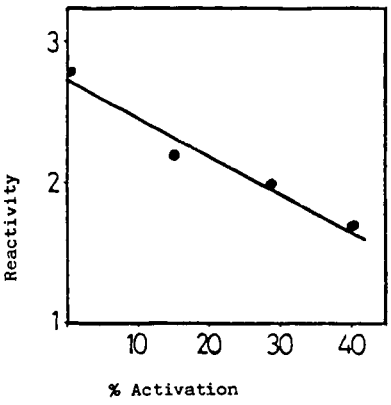

Figure 1. CO_2 Reactivity at 1073K versus degree of activation.

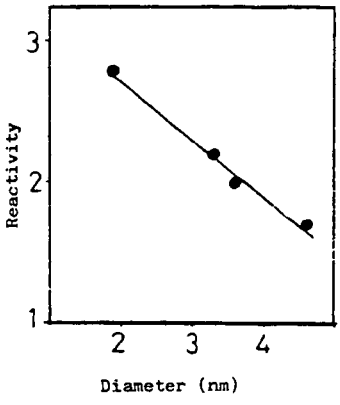

Figure 3. Reactivity versus CaO particle size.

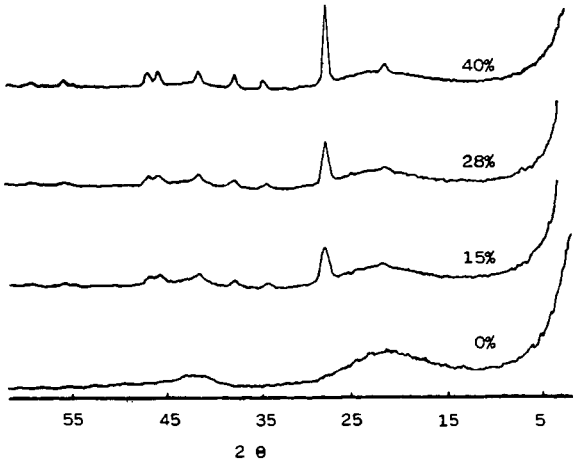

Figure 2. X-Ray diffraction profiles of samples with different degree of activation.

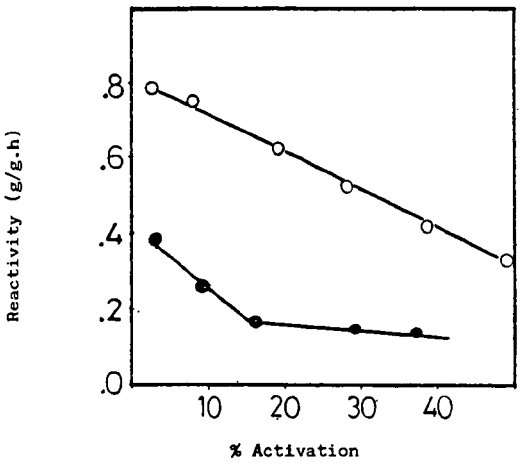

Figure 4. CO_2 Reactivity at 1023K versus degree of activation. O original sample, ● heat treated sample.

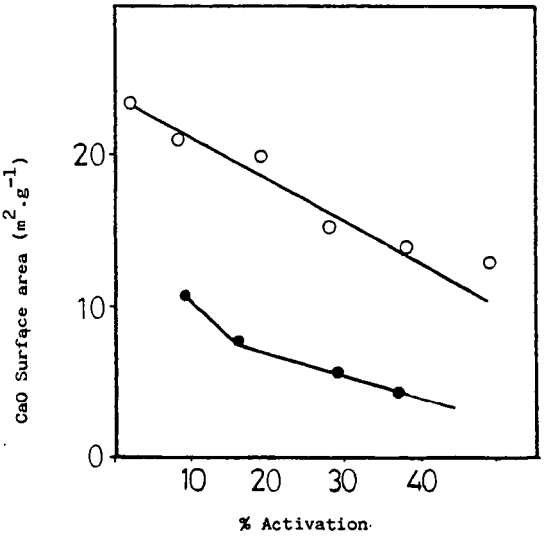

Figure 5. CaO surface area versus degree of activation.(O) original sample,(●) heat treated sample.

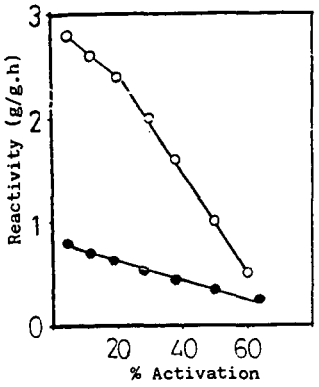

Figure 6.

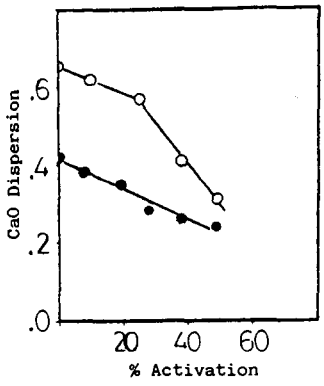

Figure 7.

Figure 6. CO_2 Reactivity versus degree of activation.
O 1073K, ● 1023K.

Figure 7. CaO Dispersion versus degree of activation.
O 1073K, ● 1023K.

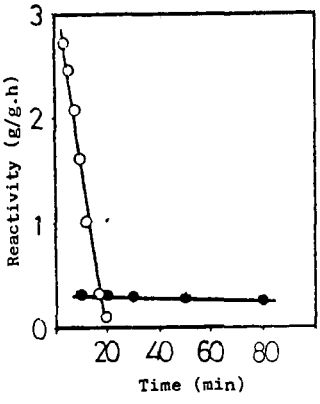

Figure 8.

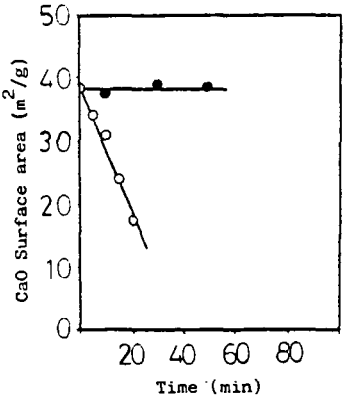

Figure 9.

Figure 8. Reactivity in CO_2 (O) and steam (●) at 1073K versus time of reaction.

Figure 9. CaO Surface area in CO_2 (O) and steam (●) versus time of reaction.

MEASUREMENT OF OXYGEN CHEMISORPTION AND GASIFICATION RATES BY A PULSE TECHNIQUE

Kouichi Miura, Kenji Hashimoto* and Peter L. Silveston
Department of Chemical Engineering, University of Waterloo
Waterloo, Ontario N2L 3G1, Canada
*)Department of Chemical Engineering, Kyoto University
Kyoto 606, Japan

INTRODUCTION

Chemisorbed oxygen on char has been investigated over several years by many researchers[1-9] in relation to the gasification mechanism or as an index of the gasification reactivity. Several methods have been developed to measure the amount of chemisorbed oxygen including volumetric, gravimetric, temperature programmed desorption (TPD), and flash desorption methods. The amount of chemisorbed oxygen, or the so called active surface area, measured by these relatively low temperature methods are sometimes far from oxygen adsorbed under reactive conditions.

The pulse method has been used to measure reaction rates and to examine reaction mechanisms of solid catalyzed reactions for many years[10-11]. Recently, this method has been applied to measure the combustion rate of chars[12] or to clarify the mechanism of catalytic gasification[13]. In this paper, the pulse technique is applied to simultaneously measure the chemisorption rate of oxygen, the amount of chemisorbed oxygen, and the gasification rate.

EXPERIMENTAL

Samples

Two different chars prepared by flash pyrolysis at 650°C from two demineralized coals (chars A and B) and a carbon produced by the pyrolysis of propylene at 600°C (char C) were used. The ultimate analyses of the chars are given in Table 1. The particle size of the chars A and B was between 62 and 210 μm. The pyrocarbon was flaky powder and was used without further modification.

Pulse Experiment

Figure 1 shows a schematic of the apparatus. The reactor was a U-tube of 6.3 mm o.d. stainless steel. A sample consisting of 2 to 150 mg of char was placed in the reactor into which a thermocouple was inserted. The sample was heated in the He flow, introduced to the reactor via 6-way valve 2 (He flow 2), up to 550°C to remove water and other gases adsorbed during storage. It was then cooled to a temperature between 200 to 550°C. The sample weight after this pretreatment was regarded as the initial weight, W_0 (d.a.f. basis). Once the temperature was constant, the He flow was changed to the main flow (He flow 1) by the 6-way valve 2. Then a pulse of oxygen was introduced to the reactor via 6-way valve 1, and the outlet gas was sent to a GC with Porapak Q (5 ft) and Carbosieve (6 ft) dual column to measure the unreacted oxygen, and CO, CO_2 and H_2O produced

by the gasification reaction. Figure 2a shows the typical separation of four gas components obtained with the GC system. For this separation, the CO_2 retention time was 30 min. To increase the number of pulses within a time period, another pulse was injected between the peaks of H_2O and CO_2. Thus, two pulses were injected in every 45 minutes. The overall conversion of oxygen, X_{O_2}, the yield of each gas, y_{CO}, y_{CO_2} and y_{H_2O}, and the oxygen uptake, Δn_O, were calculated from the analysis of gas for each pulse injection, where the yield was defined as the ratio of the moles of oxygen consumed to produce each product species to the moles of injected oxygen, and Δn_O is the moles of oxygen atom adsorbed per unit weight of initial sample. By summing Δn_O the total oxygen adsorbed by the i-th pulse can be found. The change in total weight can also be obtained from the overall mass balance. The total weight data permitted calculation of the overall conversion of char, X.

TGA Experiment

Two series of experiments were performed using a Perkin Elmer thermobalance (Model TGS2). The first series measured the weight change at constant temperatures in an air stream. Figure 3 shows the sequence of temperatures and and a typical weight change. About 2 mg of char was placed in a platinum pan (6mm i.d. and 2mm high) and heated to 550°C in a N_2 atmosphere, held there for 5 min, before cooling the char to a temperatures between 50 and 450°C. After the temperature stabilized, the gas stream was changed from N_2 to air and the weight change was continuously recorded. If the gasification rate is small, the weight increase will be due to the uptake of oxygen.

The second series of experiments measured the gasification rate. Chars were heated linearly from 350 to 600°C at the rates of 2, 5, and 10 K/min in an air stream of atmospheric pressure (Temperature Programmed Reaction, TPR). The conversion of the char, X, was obtained as a function of temperature, T, from these experiments. These data were utilized to obtain the gasification rate.

ANALYSIS

Pulse Experiments

The oxygen mass balance for an isothermal char layer through which oxygen-helium mixture passes in plug flow is given by

$$\varepsilon(\partial C_{O_2}/\partial t) + u(\partial C_{O_2}/\partial z) = \rho_b r_{O_2} \qquad (1)$$

where r_{O_2} the rate of oxygen accumulation per unit weight of char, C_{O_2} the oxygen concentration, u the superficial velocity of the gas mixture, ε the void fraction of the layer, and ρ_b the density of the char layer. The rate, $-r_{O_2}$, can be regarded as the oxygen chemisorption rate, r_a, since CO, CO_2 and H_2O are formed via chemisorption of oxygen, and physisorption should be negligible by the pulse technique. Then $-r_{O_2}$, that is r_a, can be represented as a first approximation by

$$-r_{O_2} = r_a = k_a P_{O_2} \quad (2)$$

Combining Eqs (1) and (2), k_a can be expressed as[10,11]

$$k_a = -\ln(1-X_{O_2})/(W/P_t F) \quad (3)$$

where P_t is the total pressure, F is the molar flow rate of the gas mixture, and W is the weight of the char layer. Since k_a is calculated for each pulse input, we can examine the change of k_a with the progress of reaction.

To obtain the gasification rate, the form of the rate equation, that is the pressure dependency of the rate, must be known beforehand. Here we assumed the gasification rate is proportional to the oxygen pressure to facilitate the analysis. Then, the gasification rate which was defined as the rate of weight loss per unit weight of remaining char can be written as

$$r_g = dX/dt/(1-X) = k_g P_{O_2} \quad (4)$$

Furthermore, we assumed the formation rate of each product species, r_i, is also proportional to the oxygen pressure. Then r_i is given by

$$r_i = k_i P_{O_2} \quad (5)$$

Based on the above assumptions, the gas formation rate constant, k_i, and the gasification rate constant, k_g, are represented by

$$k_i = k_a(y_i/X_{O_2}) \quad (6)$$

$$k_g = M_C(k_{CO} + k_{CO_2}) + M_{H_2} k_{H_2O} \quad (7)$$

where M_C and M_{H_2} represent the molecular weights of carbon and hydrogen, respectively.

The rate constants, k_a, k_i and k_g, are expected to depend on the conversion of char or the amount of oxygen adsorbed. If we assume the dissociative adsorption of oxygen, r_a can be written as

$$r_a = dn_O/dt = k_a P_{O_2} = k_a'(1-\theta)^2 P_{O_2} = k_a'(1-n_O/n_t)^2 P_{O_2} \quad (8)$$

where θ is the fractional coverage of active site, and n_t is the maximum amount of chemisorbed oxygen. k_a' and n_t can be estimated from a linearized plot of $\sqrt{k_a'}$ and n_O.

Analysis of TGA Data

Data from the first series of experiments were analyzed to obtain the adsorption rate constants based on Eq. (8). A plot of $1/n_O$ against $1/t$ gives the value of k_a' and n_t.

The X vs. T relationships obtained from the second series of experiments were analyzed by the Bhatia and Perlmutter model[14] to obtain the rate parameters. The model was modified so as to be applicable

to the TPR experiments by the authors[15]

RESULTS AND DISCUSSION

Changes in n_O and Total Weight with the Number of Pulse Injections

Figure 4 shows a typical result representing the change of X_{O_2}, y_i, and the amount of trapped oxygen, Δn_O, with the number of pulse injections. The abscissa is the ratio of the atoms of oxygen fed, F_O, to the initial weight of char, W_0. The total area of each rectangle gives the moles of atomic oxygen injected during each pulse. The height of each small rectangle gives $1-X_{O_2}$, y_{CO}, y_{CO_2} or y_{H_2}, and the hatched area gives Δn_O. By summing up the hatched areas, n_O can be obtained as a function of F_O/W_0. The relative change of total weight, 1-X, can also be obtained from the overall mass balance. It can be seen clearly that fairly large amount of H_2O were evolved. It is essential to analyze H_2O to achieve satisfactory oxygen and overall mass balances.

From results similar to those in Fig. 4, the changes in the total weight, 1-X, and n_O were calculated at several temperatures for every sample as a function of F_O/W_0. Figures 5 and 6 show the results of these calculations for chars A and B. For both samples, n_O tends to increase with the increase of temperature within the experimental range. On the other hand, the total weight, namely 1-X, increases monotonously at low temperatures, but it reaches a maximum at a certain F_O/W_0, and then decreases when the temperature is high. The thermogravimetric method is often employed to estimate n_O. The method assumes the weight increase is due solely to oxygen uptake. This assumption, however, is not valid at higher temperatures even if the total weight increased monotonously with time as the above discussion indicates. On the other hand, the pulse method, discussed above, is expected to give the true amount of chemisorbed oxygen.

Changes in Adsorption and Gasification Rate Constants with the Changes in n_O and X

Figures 7 and 8 show typical changes in the adsorption and gasification rate constants with the number of oxygen pulses or the progress of reaction. In these figures, the gasification rate constant is represented by the oxygen consumption rate, k'_g. At lower temperatures where the total weight increased monotonously, both $k_a(1-X)$ and $k'_g(1-X)$ decreased with increasing F_O/W_0, but seemed to reach a constant value at larger F_O/W_0 values as shown in Fig. 7. Since k_a and k'_g are the rate constants per unit weight of remaining sample, they are multiplied by (1-X) to compare the rate constants on a same basis. The n_O value increased rapidly initially, but the slope decreases gradually thereafter. No simple relations were found between $k_a(1-X)$, $k'_g(1-X)$ and n_O.

At higher temperatures where the total weight decreased with the number of oxygen pulses, $k_a(1-X)$ and $k'_g(1-X)$ changed differently depending on the sample. For char B, both rate constants decreased with the progress of gasification as shown in Fig. 8. At smaller

values of X, $k_a(1-X)$ was larger than $k'_g(1-X)$, but the latter exceeded the former at larger X values, leading to a maximum n_O value at a certain X value. This figure also shows that there are no simple relations between the rate constants and n_O.

Temperature Dependency of Adsorption and Gasification Rate Constants

Figure 9 shows the Arrhenius plot of k'_a obtained from the pulse and thermogravimetric (TGA) methods based on Eq. (8). k'_a from the TGA experiment was calculated only at temperatures lower than 300 °C, because the TGA method is not suited to measuring the oxygen chemisorption rate at higher temperatures as discussed earlier. The k'_a values estimated by the pulse technique are a little larger than those estimated from the TGA measurements at temperatures above 200 °C, even though activation energies are almost the same. This is because the contribution of gasification is not eliminated by the TGA technique. However, this technique may be employed to estimate the oxygen chemisorption rate at around 200 to 300°C, because the contribution of gasification is relatively small at these temperatures as shown in Fig. 9. The k_a values obtained at lower temperatures (100 and 150 C) show a different tendency. This is because the contribution of physisorption becomes significant at such temperatures.

Figure 10 compares the initial gasification rate constants obtained from the pulse and TGA methods. The k_g values obtained from the pulse technique showed different slopes at higher and lower temperature regions. This seems to suggest a change of controlling mechanism in gasification depending on the temperature. For char B, the k_g values obtained from both techniques almost coincide at higher temperatures. For chars A and C, on the other hand, the k_g values obtained from the pulse technique were larger than those obtained from the TGA method, though the activation energy was almost the same. This discrepancy may come from the assumption of a first order dependency of rate on P_{O_2} (Eq. 4). It is possible that the gasification rate measured by the pulse technique would larger than that measured by the TGA method, because part of the active site occupied by oxygen may be released between the adjacent oxygen pulses. We are now examining this possibility in detail.

CONCLUSION

The oxygen chemisorption rate onto the coal char, the amount of chemisorbed oxygen, and the gasification rate were simultaneously measured by the pulse technique. It was shown that the thermogravimetric method is not suitable for measurement of the chemisorption rate and the amount of chemisorbed oxygen especially at high temperatures even if weight increases continuously during the measurement. No appropriate correlations were found between the gasification rate and the amount of chemisorbed oxygen under the reactive conditions. More detailed work is necessary to clarify the role of chemisorbed oxygen during gasification.

ACKNOWLEDGMENT

This work was performed in the framework of the "Japan-Canada Joint Research Program---Developing Advanced Processes for the Efficient Use of Coal" which was sponsored by the Ministry of Education, Culture and Science of Japan. Additional support was also made available through a Strategic Grant to PLS from the Canadian Natural Sciences and Engineering Research Council.

REFERENCES

1. Laine, N.R., Vastola, F.J. and Walker, P.L., J. Phys. Chem., 67, 2030(1967).
2. Radovic, L.R., Walker, P.L. and Jenkins, R.G., Fuel, 62, 849 (1983).
3. Ahmed, S. and Back, M.H., Carbon, 23, 513(1985).
4. Takarada, T., Tamai, Y. and Tomita, A., Fuel, 64, 1438(1985).
5. Hashimoto, K., Miura, K. and Ueda, T., Fuel, 65, 1516(1986).
6. Muhlen, H.-J., van Heek, K.H. and Juntgen, H., ACS Div. Fuel Chem., vol.32, No.1, p.298(ACS 1987).
7. Cerfountain, M.B., Agalianos, D. and Moulijn, J., Carbon, 25, 357(1987).
8. Khan, R.M., Fuel, 66, 1629(1987).
9. Furimsky, E., Palmer, A., Duguay, D.G., McConnel, D.G. and Henson, D.E., Fuel, 67, 798(1988).
10. Hattori, T. and Murakami, Y., J. Catalysis, 10, 114(1968).
11. Blanton, W.A., Byers, C.H. and Merrill, R.P., Ind. Eng. Chem. Fundam., 7, 611(1968).
12. Kataoka, T. and Toyoda, K., J. Fuel Soc. Japan, 65, 1027(1986).
13. Suzuki, T., Inoue, K. and Watanabe, Y., Energy & Fuels, 2, 673(1988).
14. Bhatia, S.K. and Perlmutter, D.D., AIChE J., 26, 379(1980).
15. Miura, K. and Silveston, P.L., MS submitted to Energy & Fuels.

Table 1 Ultimate Analyses of Chars Used (d.a.f. basis)

Chars	Raw Material	C	H	N	O (by diff.)
A	Estevan Coal	93.9	3.0	0.9	2.2
B	Coronach Coal	87.4	2.6	0.8	9.2
C	Propylene	93.7	1.0	0	5.3

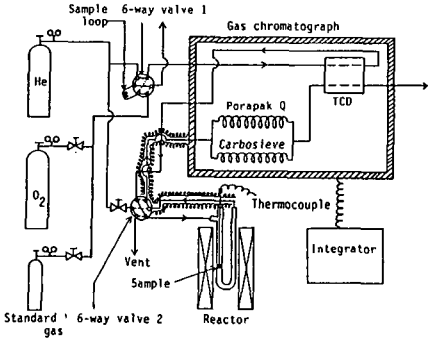

Figure 1 Schematic of the experimental apparatus

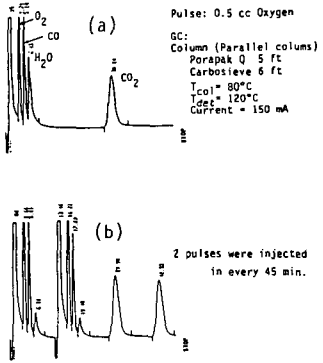

Figure 2 Typical chromatograms measured by a dual column of Porapak Q and Carbosieve

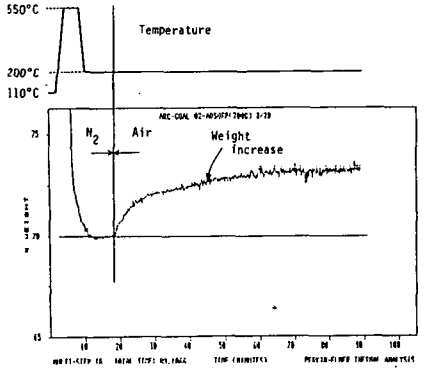

Figure 3 A typical weight change curve obtained at 200°C in an air stream by TGA

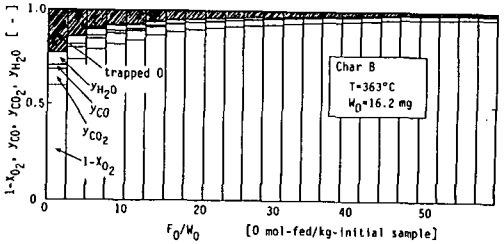

Figure 4 Mass balance of oxygen for each oxygen pulse

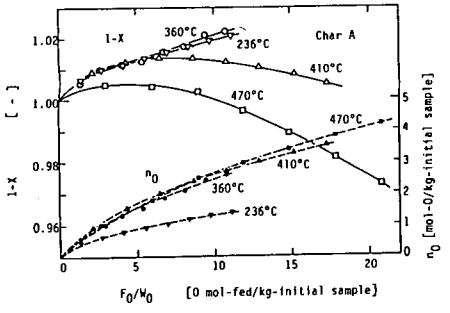

Figure 5 Changes in the total weight and the amount of chemisorbed oxygen with the number of pulse injections for char A

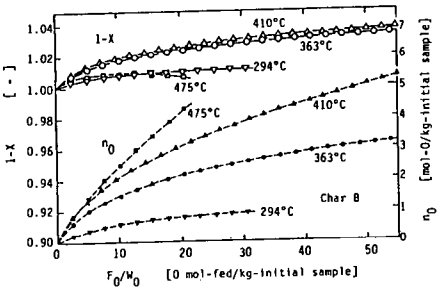

Figure 6 Changes in the total weight and the amount of chemisorbed oxygen with the number of pulse injections for char B

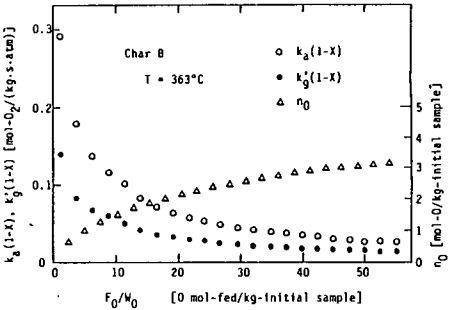

Figure 7 Changes in the adsorption and gasification rate constants and the amount of chemisorbed oxygen with the number of pulse injections

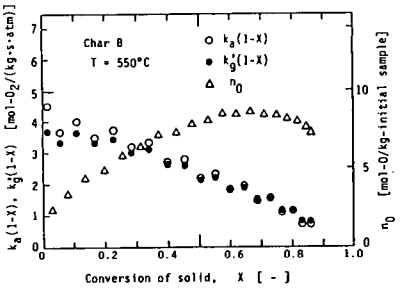

Figure 8 Changes in the adsorption and gasification rate constants and the amount of chemisorbed oxygen with the progress of reaction

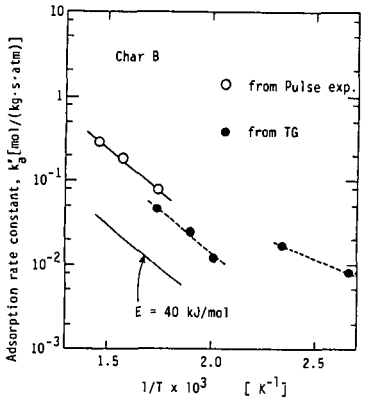

Figure 9 Arrhenius plots of adsorption rate constants measured by the pulse and TGA methods

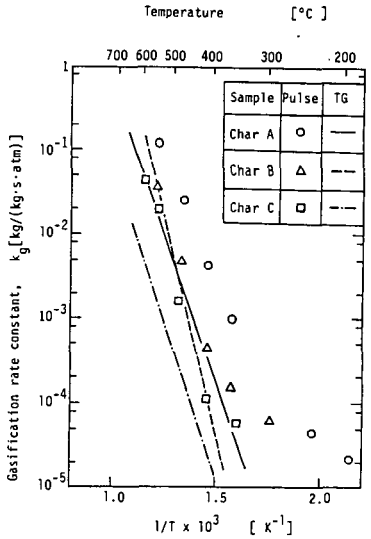

Figure 10 Comparison of gasification rate constants measured by pulse and TGA methods

ACTIVE SURFACE AREA ON CARBON REACTIVITY

K. Kuo and H. Marsh
Northern Carbon Research Laboratories, Department of Chemistry,
University of Newcastle upon Tyne, Newcastle upon Tyne, NE1 7RU, U.K.

Introduction

Carbon reactions with oxidizing gases result in carbon being selectively and continuously removed. The overall reactivity (g g-1 s-1) which is usually expressed in terms of "rate of mass burn-off" does not give a detailed understanding of these heterogeneous carbon/gas reactions and the influence of factors such as:- (a) parent material e.g. cellulose to polycyclic hydrocarbons, giving a more or less defective constituent lamellar molecule structure; (b) the heat treatment temperature (HTT) of the carbon; increasing severity of heat treatment possibly results in a reduction of defect density and hence decreased reactivity; (c) accessible or total surface area (TSA); (d) catalysis by inorganic impurities.

Measured kinetic parameters should reflect the true chemical reactivity of the carbon surface if possible. The intrinsic reactivities of carbon-gas systems usually expressed on a surface area basis (g m-2 s^{-1}) are normalized with respect to either the geometric or Total Surface Area (TSA) or Active Surface Area (ASA).

Despite numerous studies of the carbon/oxidising gas reaction, quantitative intrinsic rate data are scarce. Smith (1) collected published data of intrinsic reactivities of a large variety of carbons with the objective of comparing one with another. Values of the intrinsic reaction rate based on TSA for different types of carbons, at a given temperature and otherwise constant conditions can differ by up to four orders of magnitude. It has long been recognised that TSA is a gross indicator of carbon reactivity and does not always correlate well with reactivity. TSA which is usually measured at very low temperature e.g. N_2 at 77 K and CO_2 at 273 K could sometimes give unrealistically low surface areas due to activated diffusion effects. This is especially so with carbons having significant contents of ultra- or micro-porosity. Reactant gases at gasification temperatures which are much higher (e.g. CO_2 at 1173 K) than adsorption temperatures would have access to more surface than the adsorbates. Hence the poor correlations of TSA with reactivity especially with low TSA carbons.

The use of low temperature oxygen chemisorption technique as a measure of ASA to correlate carbon reactivity originated with the work of Laine et al. (2). Although this technique of measuring ASA is essentially empirical due to the complexity of the carbon/oxygen interaction (3-6), there has been success with correlations of ASA with carbon reactivity (7-12).

Concept of Active Surfcace Area (ASA)

The concept of ASA, which attempts to rationalise differences in carbon reactivity can be described using Figures 1, 2 and 3. These figures are plots of three reactivity functions against TSA of carbons. TSA can range from <0.1 m2 g-1 to >1000 m2 g-1. Generally, anisotropic (graphitizable) carbons e.g. cokes have low surface areas and isotropic (non-graphitizable) carbons e.g. chars have high surface areas. In Figure 1, the overall reactivity R (s-1) is plotted against the measured accessible total surface area (TSA) of the carbon. If all surfaces are comparable in terms of reactivity then there should be a linear relationship between R and TSA (solid line of Figure 1). However, most carbon surfaces could be either more or less reactive (broken lines) or could be more randomly distributed.

Figure 2 is a plot of the intrinsic reactivity R' (g m-2 s-1) based on TSA against the measured accessible total surface (TSA) of the carbon. If all surfaces are comparable in terms of reactivity then they should all have the same reactivity (solid horizontal line of Figure 2). Differences between surfaces will be indicated by deviations from this line. For example, significant catalysis or possibly inaccurate low surface area measurements give data points above the horizontal line.

Figure 3 uses the intrinsic reactivity R'' (g m-2 s-1), based on ASA plotted against the measured accessible TSA of the carbon. If all surfaces have equal densities and type of active sites (and hence reactivity) then they should have the same reactivity value (horizontal line AB of Figure 3). Again, differences between the active sites of carbons will be indicated by deviations from this line. Points D, E and F could describe carbons with contained mineral matter which is catalytic. The line BC describes solid carbon surfaces of increasing surface area but where the percentage of defects or active sites increases with increasing surface area. Position C is for carbons of high heat treatment temperature and Position B is for carbons of low heat treatment temperature.

The approach adopted in this study is: (a) to create a range of carbons of quite different structures from the same parent materials which have relatively low impurity contents; (b) to relate reactivities of these 'pure' model carbons of different structures to surface areas (TSA, ASA); (c) to relate reactivities of coal chars of the same heat treatment temperature to the standard reactivity line of the 'pure' carbons. It is not unrealistic to assume that for 'pure' model carbons, values of the intrinsic reactivity based on ASA do not change much. Hence any wide variations from the standard reactivity line would be due to catalysis.

Experimental

Carbons (cokes/chars) with different sizes of optical texture or structure were prepared by carbonization in a horizontal tube furnace under flowing nitrogen of the phenolic resin, Alnovol and by co-carbonization of Alnovol with increasing amounts of petroleum pitch, Ashland A500 (0-100 wt%). The carbons were found to have relatively low impurity contents (Table 1). Other parent materials used in this study to make cokes/ chars include a coal tar pitch (CTP 104), a commercial polymer polyvinylidene chloride (PVDC), a synthesized in-house polymer polyfurfuryl alcohol (PFA) (13) and a rank series of 6 bituminous coals from the Lower Kittaning seam supplied by Southern Illinois University, Illinois. All systems were carbonized to 1173 K, at a heating rate of 5 K min^{-1}, with a soak period of 1 h, except for the coal tar pitch which was carbonized to 1223 K at 4 K min-1 with a 0.5 h soaking period .

Carbon Reactivity Measurements

The reactivities of resultant carbons (size range 38-106 μm) to carbon dioxide at 1173 K were measured using a STA 780 Stanton Redcroft Thermal Analyser. This involves heating 10 mg ± 0.5 mg sample in a stream of dry nitrogen in the TGA apparatus to 1173 K at 50 K min-1. Once at this temperature the nitrogen is changed to carbon dioxide at the same gas flow rate (50 cm3 min-1). The sample was allowed to burn-off isothermally until less than 50 wt% of the sample remained.

Under the conditions selected, the "burn-off" plots have a rectilinear portion which is indicative of the region of maximum reactivity. The reactivity parameter, R was calculated using Equation 1:

$$R = -\frac{1}{W_o} \cdot \frac{dW}{dt} \qquad (1)$$

where R is the maximum reactivity at temperature,T K ($g\ g^{-1}\ s^{-1}$), W_o = initial mass of the carbon sample (ash free; g) and dW/dt is the maximum rectilinear weight loss ($g\ s^{-1}$).

Carbon Characterization

Elemental analyses (C,H,N) were performed on the cokes/chars to determine the extent of their devolatilization (Tables 2 and 4). The reflectance measurements (R_o%) of the raw coals were taken from Skorupska N.M. (14).. The resultant cokes/chars were mounted in resin, polished and examined for optical texture (15) to determine their degree of anisotropy (order). X-ray diffractions (XRD) were obtained from the carbons using a Phillips X-ray diffractometer (Phillips 1730) and CuKα radiation. The crystallite height, Lc, and diameters, La, were estimated from the (002) and (10) diffraction peaks, respectively, using the Scherrer equation:

$$L = \frac{K\lambda}{\beta\cos\theta} \qquad (2)$$

where λ = the wavelength of the X-rays; θ = the Bragg angle; β = the corresponding peak width at half-maximum intensity and K = 0.9 (Lc) and 1.84 (La).

The Total Surface Area (TSA) of the resultant cokes/chars apart from the coal tar pitch CTP 104 coke and petroleum pitch A500 coke were determined from the adsorption isotherms of carbon dioxide at 273 K at pressures up to 0.1 MPa (p_o = 3.4 MPa; p/p_o = 0.03) using a McBain Spring Apparatus. From Dubinin- Radushkevich (DR) plots, the TSA as well as the gradient D were calculated. The gradient D can be used as a semi-quantitative indicator of average pore size distributions. Lower or higher values of the gradient represent narrower or wider micropores, respectively. The TSA of the two cokes (CTP 104 and A500) were determined from the nitrogen adsorption (BET) at 77 K using a low surface area volumetric apparatus. The oxygen chemisorption capacities (ASA) of the carbons were determined by two methods (a) oxygen chemisorption and (b) desorption of the chemisorbed oxygen. The sample (~250 mg) in a quartz bucket was 'cleaned' by outgassing to $<10^{-2}$ Pa and heated to 1173 K for 3.1 h. Chemisorption was carried out at 423 K and 22 kPa oxygen for 24 h. Weight gains were continuously recorded and used to calculate ASA:

$$ASA = n \times \sigma \times 10^{-18}\ m^2\ g^{-1} \qquad (3)$$

where n = no. of oxygen atoms

and σ = area of chemisorbed oxygen atom = 0.083 nm^2

Extents of chemisorption can also be calculated from equivalent amounts of carbon monoxide and carbon dioxide desorbed on heating to 1173 K. A multirange micromanometer which is attached to the vacuum rig was used to monitor the partial pressure of carbon monoxide by first trapping carbon dioxide in liquid nitrogen, and then evacuating the carbon monoxide and measuring the partial pressure of the evaporated carbon dioxide.

Results and Discussion

Table 1 shows the carbons to have very low inorganic impurities. The elemental analysis and carbon yields are in Table 2. The increase in carbon yield with increasing wt % A500 was an additive effect produced by incorporating increased amounts of A500 which has a higher carbon yield compared with that of Alnovol.

Optical microscopy and Transmission Electron Microscopy (TEM) show that the Alnovol resin produced an isotropic char which has a highly disordered microstructure whereas the petroleum pitch, A500, produced an anisotropic coke which has a more ordered microstructure.

With mixtures of the two, the resultant carbons showed some anisotropic texture the percentage of which roughly reflected the percentage of resin in the sample.

Table 3 shows that both the crystallite height, Lc (0.91 to 1.49 nm) and the diameter, La (3.70 to 4.45 nm) increase with increasing amounts of A500 present in the Alnovol:A500 mixture. This provides further semi-quantitative evidence to indicate the gradual change in microstructure of the carbons from disorder to order with increasing amounts of A500 added. An increase in both Lc and La is indicative of a decrease in the ratio of edge carbon atoms to basal carbon atoms. The chemisorption capacity of the carbons which decreased significantly from 41 $m^2 g^{-1}$ for Alnovol chars to 4 $m^2 g^{-1}$ for 25% Alnovol: 75% A500 carbon (Table 3) provide further quantitative evidence to support the theory that a more ordered 'pure' carbon would have less active sites. Although the trend is similar, the ASA calculated by desorption of chemisorbed oxygen complexes (CO and CO_2) is larger. The differences between the two ASA values vary from carbon to carbon. It is possible that for certain reactive carbons there is gasification occuring during oxygen chemisorption; hence the lower ASA values calculated by oxygen chemisorption.

Changes in adsorption properties are reflected by a decrease in the TSA (570 - 1.11 $m^2 g^{-1}$) and an increase in the gradient D of the DR plot (0.1-0.2) which is indicative of an increase in the average pore size (Table 3).

Table 4 shows the % Reflectance, % Carbon yield and elemental analysis of the raw coals and their chars. The reflectance measurement (14) as well as the % carbon yield increase with increasing rank of coals (from SIU 1439 to SIU 1467). It is shown in Table 5 that the oxygen chemisorption capacity and the TSA of the coal chars decreases with increasing rank of coal. Figures 4, 5 and 6 show the reactivities (R, R' and R'') of all the carbons plotted against TSA. The observed overall reactivity, R decreased by a factor of 60 between the highest reactivity value of SIU 1439 coal char (210 x 10^{-6} s^{-1}) and the lowest reactivity value of A500 coke (3.5 x 10^{-6} s^{-1}). The calculated TSA is found not to be a relevant reactivity normalization parameter. ASA on the other hand seemed to be a good reactivity parameter; a factor in overall reactivity of 60 is reduced to only 7 (0.57 x 10^{-6} to 3.85 x 10^{-6} g m^{-2} (ASA)s^{-1}) when the reactivity is expressed in terms of ASA.

Figure 4 shows the overall reactivity, R of the Alnovol:A500 carbon increases with increasing Alnovol present (i.e. equivalent to increasing TSA) (cf Figure 1). The slightly higher overall reactivity, R of the coal tar pitch coke, CTP 104 (4.8 x 10^{-6} s^{-1}) compared to the petroleum pitch coke, A500 (3.5 x 10^{-6} s^{-1}) is to be expected since coal tar pitches are known to be more heterogeneous and contain more impurities. The coal chars which contained more catalytic impurities (Table 4) exhibit higher overall reactivities R. However, the overall reactivity, R increases with decreasing coal rank (i.e. equivalent to increasing TSA).

Figure 5 is a plot of the intrinsic reactivity R' (per unit TSA) against the TSA of the carbon (cf Figure 2). For Alnovol:A500 cokes/chars with a TSA >200 $m^2 g^{-1}$ surfaces seem to be comparable in terms of reactivity, i.e. there is little variation in the intrinsic reactivity R'. However, deviations start to occur for low TSA carbons (cokes) (<200 $m^2 g^{-1}$) which have a high intrinsic reactivity, (R') and is due to activated diffusion effects giving inaccurately low TSA. This illustrates the inadequacy of using TSA as an indicator of carbon reactivity and is especially so when one is working with low TSA carbons. However, for a 'pure' carbon with relatively large TSA e.g. PVDC and PFA (no activated diffusion problems), intrinsic reactivities, R' fall on the same line as the Alnovol:A500 carbons. The intrinsic reactivity, R' of the coal chars deviates from the model carbons which is indicative of the significant effect of catalysis.

Figure 6 is a plot of the intrinsic reactivity R" (per unit ASA) against the TSA of the carbon (cf Figure 3). For the Alnovol:A500 model carbons, there appears to be very little variation in the intrinsic reactivity, R" for carbons ranging from low TSA to high TSA. The intrinsic reactivity, R" of the other 'pure' model carbons, PFA and PVDC fall within the same region as the Alnovol:A500 carbons but the coal chars deviates from this region. This indicates that for 'pure' carbons with little or no catalytic impurities, most of their surfaces have equal densities and type of active sites and hence they have almost similar reactivity value. In contrast heterogeneous carbons like coal chars with contained catalytic mineral matter have different densities and type of active sites and hence the deviations.

Conclusions

In order to develop the concept of Active Surface Area a series of closely related but different carbons have been prepared with the same final heat treatment temperature. These carbons have been characterized in terms of optical texture, X-ray diffractions, total surface area (TSA) and Active Surface Area (ASA) as measured both by weight uptake of chemisorbed oxygen and by volume measurement of oxides of carbon desorbed from the carbon surface. The reactivities of these carbons to carbon dioxide at 1173 K and 0.1 MPa pressure have been measured. Reactivities are described as R, i.e. $g\,g^{-1}\,s^{-1}$ (weight loss data), as R',($g\,m^{-2}\,s^{-1}$) i.e. an intrinsic reactivity parameter based on total surface area (TSA) measured from adsorption isotherms, and as R" ($g\,m^{-2}\,s^{-1}$) based on active surface area (ASA) measured from chemisorption of oxygen. Differences in R are progressively reduced when R' and R" are the describing parameters. Differences in R" can be attributed to the uses of too low a value of TSA, due to activated diffusion effects operating at physisorption adsorption temperatures. The carbons of different origins of relatively low inorganic impurities do not exhibit significantly large variations in reactivity.

Acknowledgement

Acknowledgement is made to the British Coal Utilization Research Association Ltd for a grant in aid of this research, but the views expressed are those of the authors , and not necessarily those of BCURA.

References

1. W. Smith, (1978),Fuel, 57, 409.
2. N.R. Laine, F.J. Vastola and P.L. Walker Jr., (1963), J. Phys. Chem., 67, 2030.
3. J.M. Calo and M.T. Perkins (1987), Carbon, 25, 395.
4. G. Tremblay, F.J. Vastola and P.L.Walker Jr., (1978), Carbon, 16, 35.
5. P.J. Hall, J.M. Calo and W.D. Lilly, (1988), Carbon 1988, Proc of an International Conference on Carbon, Newcastle Upon Tyne, 77.
6. J.M. Calo, E.M. Suuberg and M. Wojtowicz, (1988), Carbon 1988, Proc of an International Conference on Carbon, Newcastle Upon Tyne, 319.
7. L.R. Radovic, P.L. Walker Jr., and R.G Jenkins (1983), Fuel, 62, 849.
8. P. Causton and B. McEnaney (1985), Fuel, 64, 1447.
9. E.M. Suuberg, J.M. Calo and M. Wojtowicz, (1986), ACS Div. Fuel Chem. Prepr.,31,186.
10. R.G. Jenkins and A. Piotrowski (1987), ACS Div. Fuel Chem. Prepr.,32, 4, 147.
11. M.R. Khan (1987), Fuel, 66, 1626.
12. X. Garcia and L.R. Radovic (1986), Fuel, 65, 292.
13. H. Marsh and W.F.K. Wynne-Jones, (1964), Carbon, 23, 555.
14. N.M. Skorupska (1987), Ph.D. The University of Newcastle Upon Tyne.
15. Northern Carbon Research Laboratories Optical Texture Classification System, The University of Newcastle upon Tyne.

Table 1

Neutron Activation Analysis of Parent Materials used and the Resultant Cokes/Chars.

SAMPLE	Sodium/ mg kg^{-1}	Potassium/ mg kg^{-1}	Iron/ mg kg^{-1}
Phenolic resin, Alnovol	12.1 ± 0.7	10 ± 2	19 ± 6
Petroleum pitch Ashland A500	7 ± 1	<7	23 ± 8
Coal tar pitch CTP 104	32.1 ± 0.7	8 ± 2	61 ± 6
Alnovol char (HTT 1173 K)	39 ± 2	54 ± 5	130 ± 10
75% Alnovol:25% A500 (HTT 1173 K)	182 ± 4	73 ± 7	60 ± 9
50% Alnovol:50% A500 (HTT 1173 K)	46 ± 2	130 ± 9	100 ± 10
25% Alnovol:75% A500 (HTT 1173 K)	76.1 ± 0.8	107 ± 7	101 ± 8
A500 (HTT 1173 K)	19.8 ± 0.9	33 ± 3	81 ± 9
Polyfurfuryl alcohol (HTT 1173 K)	6.6 ± 0.7	<7	25 ± 5
CTP 104 (HTT 1223 K)	101 ± 2	19 ± 2	160 ± 4

Table 2

% Carbon Yield and Elemental Analysis of Cokes/Chars prepared at 1173 K, 5 K min^{-1}, with 1 h soak.

SAMPLE	C/wt%	H/wt%	N/wt%	Atomic C/H	wt% Carbon Yield
Alnovol	95.7	0.6	0.4	13.6	56
87.5 Alnovol:12.5 A500	97.2	0.6	0.3	13.2	58
75 Alnovol:25 A500	96.7	0.6	0.1	12.7	60
62.5 Alnovol:37.5 A500	97.3	0.6	0.1	12.8	62
50 Alnovol:50 A500	96.6	0.6	0.3	12.4	63
37.5 Alnovol:62.5 A500	95.8	0.7	0.5	12.3	67
25 Alnovol:75 A500	98.3	0.6	0.1	13.1	69
12.5 Alnovol:87.5 A500	98.7	0.7	0.1*	12.6	74
A500	98.3	0.7	0.1	13.5	78
PVDC	95.1	0.6	0.8	14.5	26
PFA	96.9	0.8	0.1	13.8	49
CTP 104	97.1	0.4	1.1	20.4	46

TABLE 3

Crystallite dimensions, TSA and ASA of Alnovol:A500 carbons prepared at 1173 K, 5 K min^{-1} and 1 h soak.

SAMPLE	XRD		DR PLOT (CO_2,273K)		ADS (423K,22Pa O_2)	DESORPT. (1173K,3.1 h)			
	Lc/nm	La/nm	TSA/m^{2}g^{-1}	DX10^{-2}	ASA (ads.)* m^{2}g^{-1}	ASA/ TSA	mol CO/g X10^{-4}	mol CO_2/g X10^{-4}	ASA** m^{2}g^{-1}	ASA/TSA**
Alnovol	0.91	3.7	570	10.1	41	0.07	8.43	2.58	68	0.12
87.5% Alnovol : 12.5% A500	0.95	3.65	540	11.2	38	0.07	9.28	2.57	72	0.13
75% Alnovol : 25% A500	1	3.94	480	11.2	33	0.07	7.31	2.28	59	0.12
62.5% Alnovol : 37.5% A500	1.02	3.75	410	12.2	29	0.07	7.15	2.13	57	0.14
50% Alnovol : 50% A500	1.16	3.5	310	11.1	25	0.08	5.55	1.8	46	0.15
37.5% Alnovol : 62.5% A500	1.22	3.51	210	7.2	18	0.08	2.48	1.14	24	0.11
25% Alnovol : 75% A500	1.42	4.2	55	18.3	4	0.07	2	0.43	14	0.26
12.5% Alnovol : 87.5% A500	1.46	4.2	9	19.2			1.94	0.27	12	1.39
A500	1.49	4.45	1.1							

Table 4

% Reflectance, % Carbon Yield and Elemental Analysis of Coals and Coal Chars prepared at 1173 K, 5 K min^{-1} witb 1 h soak.

SAMPLE	*R/%	C/wt%	H/wt%	N/wt%	Atomic C/H	% Ash	% Carbon Yield
Coal							
SIU 1439	0.47	62.6	4.7	1.3	1.12	10.2	
SIU 1444	0.66	66.5	4.7	1.3	1.18	10.7	
SIU 1436	0.86	72.6	5.0	1.4	1.22	13.3	
SIU 1445	1.01	70.6	4.4	1.3	1.33	14.2	
SIU 1458	1.24	75.5	4.3	1.2	1.48	9.9	
SIU 1467	1.75	69.6	3.6	1.3	1.64	18.0	
*(Ref 14)							
Char (HTT 1173 K, 5 K min^{-1} 1 h soak)							
SIU 1439		78.0	0.4	1.3	15.97	16.4	61%
SIU 1444		80.0	0.4	1.0	14.93	17.3	66%
SIU 1436		83.0	0.5	1.2	14.21	22.7	70%
SIU 1445		77.9	0.4	1.1	15.20	17.9	72%
SIU 1458		83.3	0.4	1.1	15.54	13.6	76%
SIU 1467		78.1	0.4	1.1	15.99	34.4	85%

Table 5

Crystallite dimensions, TSA and ASA of Cokes and Chars.

SAMPLE	XRD Lc/nm	XRD La/nm	ASA / $m^2 g^{-1}$ DR PLOT (CO_2,273K) TSA/$m^2 g^{-1}$	DR PLOT (CO_2,273K) 0x10^{-2}	AOS (423K,22Pa O_2) ASA* (ads.)* $m^2 g^{-1}$	AOS (423K,22Pa O_2) ASA/TSA	DESORP (1173K,3 h) mol CO/g x10^{-4}	DESORP (1173K,3 h) mol CO_2/g x10^{-4}	DESORP (1173K,3 h) ASA** $m^2 g^{-1}$	DESORP (1173K,3 h) ASA/TSA**
CIP 104			0.75							
PFA	0.81	3.11	396	8.5	41	0.11	8.82	2.68	71	0.18
PVOC	0.84	3.19	750	12	40	0.05	7.47	1.96	56	0.07
SIU 1439			250	32.1						
SIU 1444			240	6.9	52	0.22	8.18	2.84	87	0.36
SIU 1436			160	7.7	22	0.14	4.23	1.6	50	0.32
SIU 1445			110	6.9	26	0.24	4.48	1.82	51	0.48
SIU 1458			52	9.8	11	0.22	2.44	0.72	23	0.45

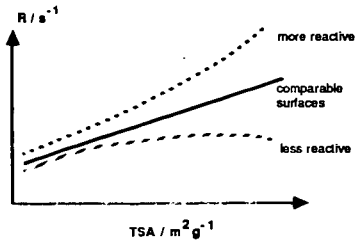

FIGURE 1 Overall Reactivity , R , vs TSA

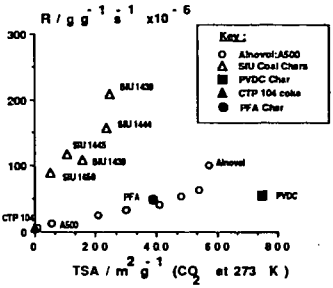

Figure 4 . Overall Reactivity, R, vs TSA.

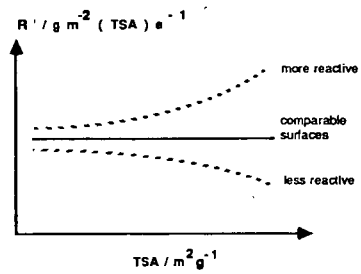

FIGURE 2 Intrinsic Reactivity, R', vs TSA

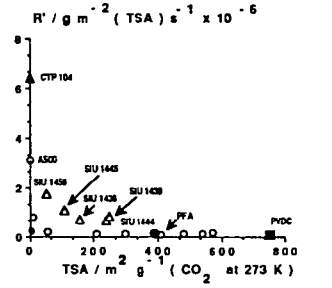

FIGURE 5 . Intrinsic Reactivity, R', vs TSA.

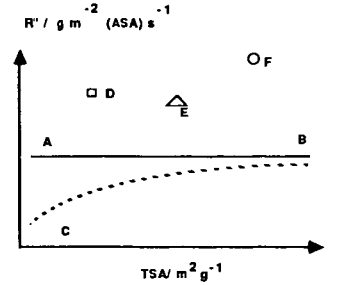

FIGURE 3. Intrinsic Reactivity, R", vs TSA

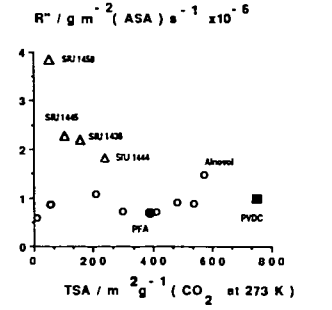

FIGURE 6. Intrinsic Reactivity, R", vs TSA.

EFFECT OF MICROTEXTURE ON COKE VAPOR GASIFICATION
A QUALITATIVE GASIFICATION MODEL

Bruno DUVAL, Jean-Noël ROUZAUD
Centre de Recherche sur les Solides à Organisation Cristalline Imparfaite
1B, rue de la Férollerie, 45071 ORLEANS CEDEX 02, (France)

Jean-Robert RICHARD
Centre de Recherche sur la Chimie de la Combustion et des Hautes Températures
1C, Avenue de la Recherche Scientifique, 45071 ORLEANS CEDEX 02 (France)

Jean-Michel GUET
Laboratoire de Cristallographie, B.P. 6759, Université d'Orléans
rue de Chartres, 45067 ORLEANS CEDEX 02 (France)

INTRODUCTION

It is generally accepted that microtexture is one of the keys to the study of many carbonaceous materials (1) and probably one of the most important characteristics of coke in order to provide for its reactivity. So the purpose of this work is to give details on the relation between microtexture and coke reactivity during vapor gasification.

According to Transmission Electron Microscopy studies (1), coke is formed by plane polyaromatic units, also called Basic Structural Units, with local parallel orientation inside a Molecular Orientation domain (M.O. domain). The size of these domains depends on the chemical nature of the precursor (1, 2, 3). As coals are chemically heterogeneous, their cokes contain M.O. domains with varied sizes and their microtexture can be represented by M.O. domains sizes histograms. Ten classes were chosen to form a logarithmic scale: the first three classes corresponding to the smallest M.O. domains (< 15 nm) and classes 9 and 10 corresponding to the largest M.O. domains (> 1 µm).

T.E.M. studies lead to a choice of model of coke microtexture made of "crumpled stacked sheets", where each pore wall is formed by a M.O. domain (1). In the case of carbonaceous materials, it is well known that only the aromatic layer edges (not the layer planes) are reactive (4). Consequently, the smaller the M.O. domain size the larger the free edge density and the more reactive should the material be.

Indeed, previous studies have shown that reactivity was connected to Active Surface Area (i.e. a parameter also connected to the free edge density) (5).

SAMPLING AND MICROTEXTURE CHARACTERIZATION

Six samples were chosen to cover the variety of M.O. domain size (five orders of magnitude from 5 nm to tens of µm) : on one hand, three homogeneous reference cokes without mineral impurities and on the other hand, three heterogeneous cokes from three coals with ashes (Table).

A study by T.E.M. (6) and Small Angle X-ray Scattering (S.A.X.S.) has

permitted to caracterize the microtexture. Some results of T.E.M. studies are given in the table (average class and average size of M.O. domains).

S.A.X.S. results presented here are qualitative in nature. Figure 1 presents the scale laws of the three homogeneous cokes and one of the three coal cokes (Vouters). The scale law corresponds to the graph Ln I/Ln $|\vec{s}|$ where I represents experimental scattered intensity and $\vec{s}$ the scattering vector (in reciprocal space) the modulus of which is given by the Bragg's law :

$|\vec{s}| = (2 \sin \theta)/\lambda$ (θ : Scattering angle, λ : wavelength of incident beam).

In the case of Marathon coke, we do not distinguish shoulders or marked peaks in the studied range (1 to 110 nm^{-1}). It appears that we have a similarity of texture at all scales, which was confirmed by previous microscopic observations. Inversely, for the coke of Saran mainly and but also for the coke of Saccharose, we notice the existence of a shoulder around 3 nm. This corresponds to the microporosity described in T.E.M. before. Between these two textural extremes, the coke of Vouters presents an intermediary curve which is not easily interpretable. It is interesting to note the cross checking of microscopic observations with S.A.X.S. data.

APPARATUS

1. Cokefaction

Standardized conditions were specified for the manufacture of the cokes. Samples are pyrolyzed in a Pyrox model oven. The sample (approximatively 5g is placed in a graphite crucible which is itself set inside a Pyrex pipe. The sample is constantly swept by a nitrogen current of 2 l/mn. The heating rate is fixed at 4 K/mn and the final temperature is 1223 K. This temperature was maintained for an hour and then the sample is cooled.

2. Gasification

The powdered coke sample is positioned on a sintered quartz plate held by a quartz tube and placed inside a furnace. The gas flow passes through the sintered plate and the sample. The gases produced by the reaction between the coke and the flowing water mixture are analysed. The main gasification experimental parameters were :
- vector gas pressure : 10^5 Pa
- gasification temperature : 1223 K
- reactive gas : H_2O
- reactive gas concentration : 80%
- vector gas (N_2 + H_2O) flow : 180 l/h (N.T.P.)
- sample weight : 1 g
- grain size : 160-500 µm

So we try to eliminate, as much as possible, parameters extraneous to the effect of microtexture on the gasification processes.

EXPERIMENTAL RESULTS

1. Study of reactivity

Figure 2 presents the evolution of instantaneous reactivity during conversion. By normalizing the integrated reactivity to 100% conversion, a global reactivity scale can be drawn up which follows the scale of increasing M.O. domains size (Figure 3). We can notice that, in our experimental conditions, mineral impurities appear to have no effects on reactivity.

Since the cokes of Vouters and Reden are more reactive than Saccharose coke at the begining of conversion, the evolution of microtexture during gasification was followed in an attempt to understand this difference.

2. Evolution of the microtexture during conversion

Dark-field technique allows one to follow the evolution of M.O. domains size histograms (Figure 4), because the size of M.O. domains does not appear us to change significantly but some M.O. domains preferentially disappear. Thus for heterogeneous cokes, the ratio of the different types of texture change. We have defined three types of texture : small (classes 1 to 3), intermediate (classes 4 to 8) and large (9 and 10) M.O. domains.

Histograms show an increase of the ratio of large M.O. domains. But it appears that intermediate M.O. domains are preferentially burned off, more than small M.O. domains.

DISCUSSION

It can be assumed that global reactivity is the product of "textural intrinsic reactivity" and accessibility to the porosity, which depends on the pore diameter and therefore on the M.O. domain size (if we are in Knudsen regime) (7, 8).

Figure 5 presents the evolution of qualitative gasification model during conversion and Figure 6 illustrates this in the case of a texturally heterogeneous coke (a particle with the three different types of texture).

In the range of large M.O. domains area, accessibility is good but the domains contain only few reactive sites.

In the range of intermediate M.O. domains area, accessibility is still good, reaction takes place inside this texture and a more important number of active sites is present.

When the M.O. domains are small, accessibility is low, reaction occurs only at the circumference of the area, although a very high number of active sites produces strong intrinsic reactivity.

With this qualitative gasification model, we are now able to explain our experimental data : histograms evolution and evolution of instantaneous reactivity during gasification.

In the case of homogeneous cokes of Saran and Saccharose which are constituted only of small M.O. domains, the reactivity increases due to the opening of the pore which increases the accessibility.

In the case of cokes of Vouters and Reden, we have intermediate M.O. domains which give higher reactivity at the begining of conversion. Consequently we have an enrichment in large M.O. domains which stabilizes reactivity.

In the case of coke of Peak-Downs, which is consituted by small and large M.O. domains, reactivity is due only to small M.O.domains, the increase of the ratio large M.O. domains over small M.O. domains also stabilizes reactivity before it decreases. The coke of Marathon, only constituted from large M.O. domains, is not reactive.

CONCLUSION

The samples chosen were representative of practically all the different types of cokes likely to be met. The microtexture of each sample is a key factor in understanding its behaviour during the gasification by water vapor. These first results will be compared to the evolution of microtexture as determined by different independent approaches such as B.E.T. area measurements, and determination of active sites.

LITERATURE CITED

(1) A. OBERLIN, Carbon, 22, 1984, 521-541.
(2) J.N. ROUZAUD, D. VOGT and A. OBERLIN, Fuel Processing Technology, 1988, in press
(3) F. BENSAID and A. OBERLIN, J. de Chim. Phys., 84, 1987, 1457-1467.
(4) F. RODRIGUEZ-REINOSO, P.A. THROWER and P.L. WALKER, Jr., Carbon, 12, 1974, 63-70.
(5) L.R. RADOVIC, P.L. WALKER and R.G. JENKINS, Fuel, 62, 1983, 849-856.
(6) B. DUVAL, J.M. GUET, J.R. RICHARD and J.N. ROUZAUD, Fuel Processing Technology, 1988, in press.
(7) J.M. DRAKE, P. LEVITZ, N.J. TURRO, K.S. NITSCHE and K.F. CASSIDY, J. Phys. Chem., 1988, in press.
(8) NORMAND M. LAURENDAU, Prog. Energy Combust. Sci., 4, 1978, 221-270.

TABLE

Coke of...	Ashes %	Weight %			M.O. domains	
		C	H	O	Average class	Average size (mm)
Saran	0	90,79	2,12	7,09	1	∿ 5
Saccharose	0	95,31	0,55	4,14	2	∿ 10
Vouters	3,6	95,70	0,56	3,73	3,2	∿ 15
Reden	4	96,92	0,44	2,64	6,5	∿ 50
Peak-Downs	15	95,85	2,80	1,36	8,9	∿ 1.000
Marathon	0	99,47	0,17	0,35	10	∿ 100.000

Ash content, weight % (normalized to 100%) and textural parameters of the cokes studied.

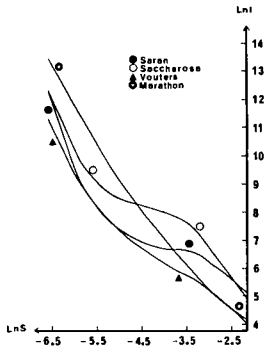

Fig. 1 - Scale laws (S.A.X.S.) of four cokes

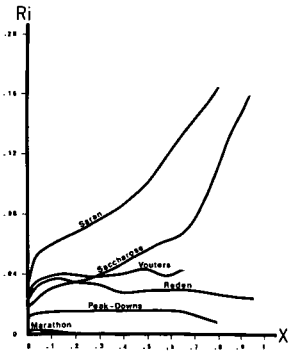

Fig. 2 - Evolution of instantaneous reactivity Ri = 1/m (dX/dt) in $g^{-1}mn^{-1}$ versus conversion (X).

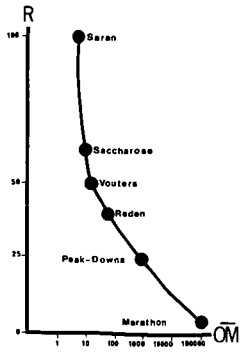

Fig. 3 - Relationship between global reactivity R in arbitrary units versus average size of M.O. domains (O.M.)

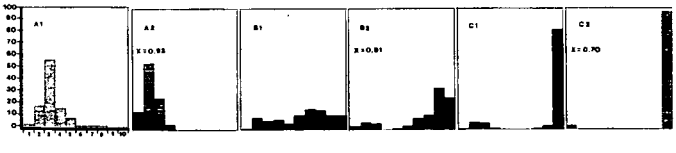

Fig. 4 - Histograms evolution of the M.O. domains size from the heterogeneous cokes of Vouters (a), Reden (b), Peak-Downs (c), before (1) and after (2) gasification, X = conversion.

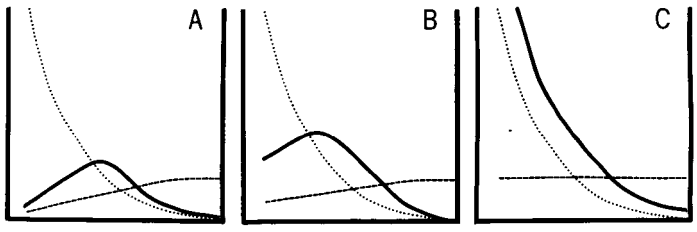

Fig. 5 - Qualitative model for the evolution of the global reactivity (___) during conversion, versus M.O. domains size. Global reactivity is assumed to be the product of the "intrinsic textural reactivity" (...) and the accessibility (---) of porosity.

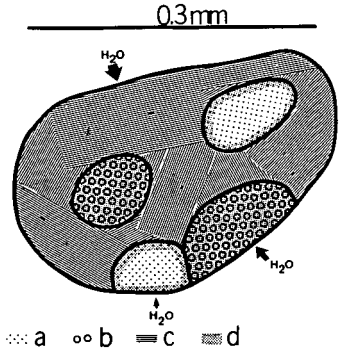

Fig. 6 - Conversion model for coke particles constituted of small (a), intermediate (b) and large (c) M.O. domains, illustrating the difference of accessibility (arrows) and the reactive area (d).

MECHANISM OF CARBON DIOXIDE GASIFICATION STUDIED BY TPD

K.J. Hüttinger, J.-S.Nill
Institut für Chemische Technik, Universität Karlsruhe
Kaiserstrasse 12, D-7500 Karlsruhe, FRG

ABSTRACT

Kinetic studies of carbon dioxide gasification are combined with TPD measurements. It is shown that this technique allows to calculate not only the concentration of surface complexes but also the true activation energies of gasification. It is followed that this procedure may be more successful than the determination of active sites by oxygen adsorption.

INTRODUCTION

The mechanism of carbon dioxide gasification was studied by applying (i) 'classical' kinetic measurements, whereby the temperature and partial pressures were varied, and (ii) TPD measurements in order to determine the concentration of surface complexes. The studies were performed by using a model coke from polyvinylchloride (HTT 900°C), which has neither cations nor heteroatoms. The TPD studies with samples which were quenched from reaction temperature allow to calculate the desorption kinetics of the C(O) and C(H) surface complexes and to determine the total concentration of these complexes. By combination of these results with the data of the kinetic studies of gasification (rate constants) it is possible to determine the concentration of occupied, free and total sites and also the true activation energies of the single steps of gasification.

EXPERIMENTAL

Gasification and TPD measurements were performed in one and the same reactor, which is described in an earlier paper (1). This also holds for the model coke made of polyvinylchloride (grain size: 0.1 mm to 0.2 mm). For the TPD measurements an argon atmosphere and a heating rate of 20 K min^{-1} were used, the final temperature was 1100°C which was held for 0.5 hours.

RESULTS AND DISCUSSION

Classical treatment of kinetics

Fig.1 shows carbon monoxide formation rates as function of carbon dioxide partial pressure after 10 h gasification. The rates vary only slightly with time and the mass loss even at 900°C at p_{CO_2} = 1 bar is below 15 %. The carbon monoxide formation rates are related on the initial amount of carbon, they only represent the formation of carbon monoxide which is produced by carbon gasification.

For evaluating kinetic data the oxygen exchange mechanism was used as basis:

$$C_f + CO_2 \underset{k_{-1}}{\overset{k_1}{\rightleftharpoons}} C(O) + CO \qquad (1)$$

$$C(O) \xrightarrow{k_2} CO + C_f \qquad (2)$$

From this mechanism the following rate equation is obtained:

$$r_s = c \cdot k_1 \cdot p_{CO_2} / [1+(k_1/k_2) \cdot p_{CO_2} + (k_{-1}/k_2) \cdot p_{CO}] \qquad (3)$$

The following rearrangement of this equation

$$r_s^{-1} = (c \cdot k_2)^{-1} + (c \cdot k_1 \cdot p_{CO_2})^{-1} \qquad (4)$$

shows that a plot of r_s^{-1} versus $p_{CO_2}^{-1}$ should give a straight line. In view of the experimental results it was assumed that the partial pressure of carbon monoxide is negligibly small. The experimental data of Fig.1 fulfill equation (4). Therefore, the values of $c \cdot k$ are directly given in Fig.2 using an ARRHENIUS plot. The following equations have been derived from Fig.2:

$$c \cdot k_1 = 5.6 \cdot 10^{12} \cdot \exp(-60000/RT), \text{mmol mol}^{-1}\text{h}^{-1}\text{bar}^{-1} \qquad (5)$$

$$c \cdot k_2 = 2.7 \cdot 10^{11} \cdot \exp(-54000/RT), \text{mmol mol}^{-1}\text{h}^{-1} \qquad (6)$$

These equations allow to calculate the ratio k_1/k_2:

$$k_1/k_2 = 20.9 \cdot \exp(-6000/RT), \text{ bar}^{-1} \qquad (7)$$

The total concentration of active sites c is unknown. It may vary with temperature. This means that the activation energies in eqs. (5) and (6) are probably not true activation energies.

TPD STUDIES

Fig.3 shows the quantity of carbon monoxide which was measured in the TPD experiments using the samples of Fig.1 (10 h gasification). In order to check the importance of these values the gasification rates were related on the quantity of desorbed carbon monoxide. The results are given in Fig.4. These related rates are constant over the entire range of carbon dioxide partial pressure at least for 800 and 850°C. The deviation at 900°C may be explained by the fact that the coke was only heattreated at this temperature.
If it is assumed that the quantity of desorbed carbon monoxide corresponds to the quantity of C(O) surface complexes it is now possible to calculate the quantity of the concentration of free sites. The derivation of eq. (3) is based on the assumption that the formation rate of the C(O) complex according to eq. (8):

$$r_{(1)} = k_1 \cdot c_{(\ )} \cdot p_{CO_2} \qquad (8)$$

is equivalent to the desorption rate of the carbon monoxide from the C(O) complex:

$$r_{(2)} = k_2 \cdot c_{(O)} \qquad (9)$$

With $r_s = r_{(1)} = r_{(2)}$ follows:

$$c_{(\ )} = (k_1/k_2) \cdot (1/p_{CO_2}) \cdot c_{(O)} \qquad (10)$$

The ratios k_1/k_2 are known from the gasification studies. Therefore, $c_{(\ )}$ can be calculated. The results are shown in Fig.5. The quantity or concentration of free sites decreases with increasing partial pressure and increases with temperature. As the concentrations of occupied and free sites are known, the concentration of total sites can additionaly be calculated:

$$c = c_{(O)} + c_{(\ )} \qquad (11)$$

The results are also given in Fig.5. The concentration of total sites is independent on the partial pressure for the gasification temperatures 800 and 850°C. The deviation at 900°C has probably the same reason as already mentioned in relation to Fig.4. On the other hand, it has to be stated that the majority of the carbon edge atoms is saturated with hydrogen (C(H) complexes). The importance or value of the presented TPD measurements suffers from the fact that a ten hour gasification at different temperatures causes not only different mass losses but also different structural changes. For elimination of this disadvantage gasification and TPD studies were performed at different temperatures and additionally by variation of the reaction time. For these studies pure carbon dioxide was used. The Figs. 6 and 7 show the carbon monoxide formation rates and the relative quantities of desorbed carbon monoxide as function of the residual amount of carbon m/m_o.
As follows from Fig.7 the amount of desorbed carbon monoxide continuously increases with progressive gasification, but only at temperatures up to 850°C. The decrease at 900 and 950°C is confirmed by many measurements. It can not be explained by the decreasing amount of residual carbon. In any case, these results confirm that the concentration of C(O) complexes increases with decreasing gasification temperature. This means that the surface is loaded with oxygen because the desorption rate is too small.

The results of Figs. 6 and 7 offer three possibilities: (1) To calculate the activation energy of the overall rate of gasification $\dot{n}_{CO}/n^o_C$. (2) To calculate the temperature dependence of the concentration of C(O) surface complexes $n^o_{CO,des}/n^o_C$ using an ARRHENIUS plot. (3) To calculate the activation energy of the gasification rate related on the quantity of C(O) surface complexes $\dot{n}_{CO}/n^o_{CO,des}$. In all cases this was done for equal degrees of carbon conversion $(1-m/m_o)$ or residual carbon m/m_o. As the gasification rates are extremely low under all conditions it is assumed that the develoment of the pore structure is not significantly influenced by the gasification temperature. In the case of the overall rate nearly identical results are received whether the carbon monoxide formation rate is related on the initial quantity of carbon or the residual quantity of carbon, because the degree of carbon conversion is very low. The same argument is valid for $n^o_{CO,des}/n^o_C$.
The activation energies which were obtained by this procedure are shown in Fig.8 as function of the residual amount of carbon. Constant values are found if m/m_o is equal to or larger than 0.95. It may be assumed that steady-state gasification conditions are achieved beyond this degree of conversion. In the steady state region of gasification the following activation energies may be taken from Fig.8:

- For the carbon monoxide desorption $n^{\circ}_{CO,des}/n^{\circ}_{C}$: -31 kcal mol-1 (positive slope in the ARRHENIUS plot)
- For the overall rate $\dot{n}_{CO}/n^{\circ}_{C}$: 54 kcal mol^{-1}
- For the rate related on the quantity of C(O) complexes $\dot{n}_{CO}/n^{\circ}_{CO,des}$: 85 kcal mol^{-1}.

The value of 85 kcal mol^{-1} corresponds to the true activation energy of the desorption step E_2 as follows from the following equations:

$$r_s = r_{(2)} = k_2 \cdot c_{(O)} \tag{12}$$

$$k_2 = r_s/c_{(O)} = \dot{n}_{CO}/n^{\circ}_{CO,des} \tag{13}$$

The rate constant of the desorption step k2 is identical to the turnover rate of the surface complex.
With the known activation energy of k_2 the activation energy of the rate constant of the dissociation step k_1 may be calculated using eq. (7):

$$k_1 = k_2 \cdot 20.9 \exp(-6000/RT) \tag{14}$$

$$E_1 = E_2 + 6 = 91 \text{ kcal mol}^{-1} \tag{15}$$

These values of the true activation energies are very near to the values presented by Walker and others (2-4) for gasification of graphitized materials.
The TPD studies also allow to determine the desorption kinetics of the C(O) complex. Typical desorption rates are shown in Fig.9 after 10 h gasification. Using non-isothermal kinetics the desorption rate (first order reaction assumed) is as follows:

$$d(n_{CO,des})/dT = (dT/dt)^{-1} \cdot k_o \cdot \exp(-E/RT) \cdot (n^{\circ}_{CO,des} - n_{CO,des}) \tag{16}$$

The application of this equation to all experimental results (reaction times from 1 to 10 h, temperatures from 750 to 950 °C) yielded an average value of the activation energy of 53 kcal mol^{-1} (Fig.10). This activation energy corresponds to the following equation:

$$r_{(2)} = k_2\,(T) \cdot c_{(O)}(T) = k_2\,(T) \cdot n^{\circ}_{CO,des}/n^{\circ}_{C}(T) \tag{17}$$

The previous results yielded a value of 54 kcal mol^{-1} for the product of eq. (17). This agreement is really satisfying.

Finally it should be mentioned that the average value of the activation energy of hydrogen desorption resulting from the same experiments amounts to 62.5 kcal mol^{-1} by assuming a second order reaction:

$$2\ C(H) \rightleftharpoons H_2 + 2\ C_f \tag{18}$$

This value is identical to the result published by Yang and Yang (5). The difference of activation energies for carbon monoxide and hydrogen desorption confirms the inhibiting effect of hydrogen.

SUMMARY

The present paper represents an attempt to measure and calculate the concentration of the intermediate surface complexes and the true activation energies of carbon dioxide gasification by combining kinetik studies of gasification with TPD measurements. This route looks promising. The true activation energies for the dissociation and desorption step are 91 or 85 kcal mol^{-1} in comparison to 60 or 54 kcal mol^{-1} for the apparent activation energies. The difference results from the change of the concentration of the surface complexes with gasification temperature in gasification of the model coke used in these studies. Therefore, it is not surprising that the obtained true values of activation energies nearly correspond to values reported by other authors for carbon dioxide gasification of graphitized materials. The meaning of this agreement still has to be explained, it probably results from more or less constant concentrations of sites in gasification of graphitized materials.

REFERENCES

(1) Hüttinger, K.J. and Hermann, G., Carbon 24, 705 (1986)
(2) Strange, J.F. and Walker, P.Jr., Carbon 14, 345 (1976)
(3) Turkdogan, E.T. et al., Carbon 6, 467 (1968)
(4) Biederman, D.L. et al., Carbon 14, 351 (1976)
(5) Yang, R.T. and Yang, K.L., Carbon, 23, 537 (1985)

ACKNOWLEDGEMENT

Financial support of this study by the German Research Foundation (DFG) is gratefully acknowledged.

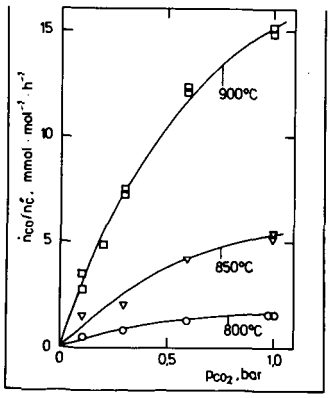

Fig.1: Carbon monoxide formation rates

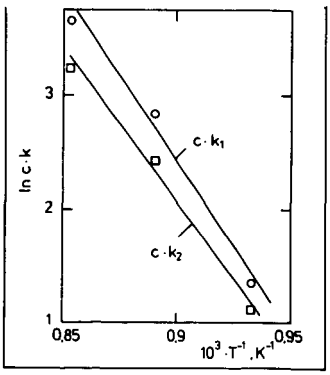

Fig.2: ARRHENIUS plot according to eq.(4)

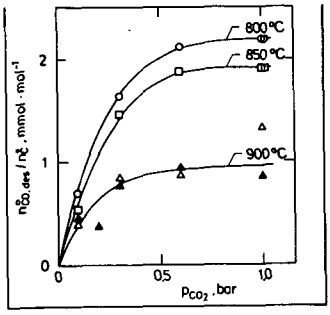

Fig.3: Concentration of C(O) complexes

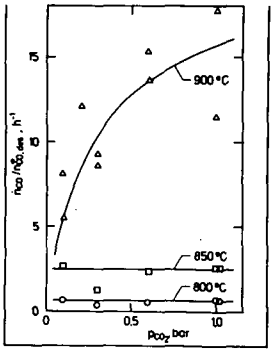

Fig. 4: Specific gasification rates acc. to eq. (11)

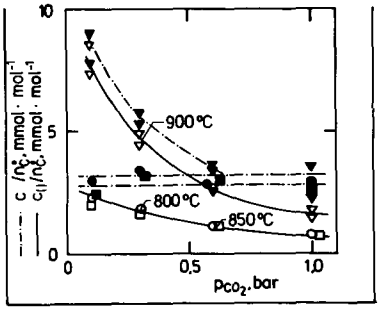

Fig.5: Concentration of free and total sites

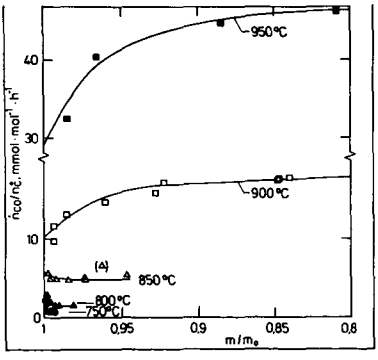

Fig. 6: Gasification rates versus residual carbon

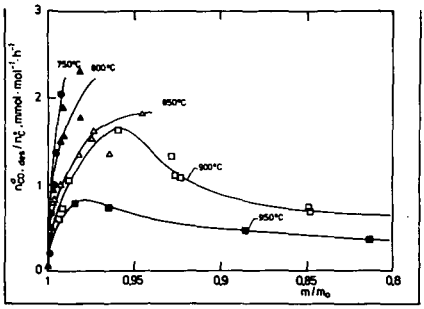

Fig.7: Concentration of C(O) complexes versus residual carbon

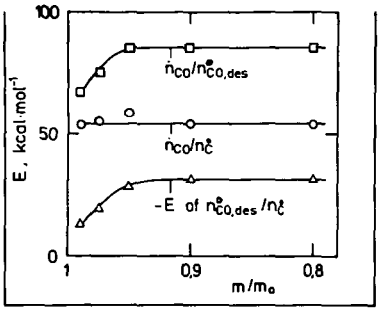

Fig.8: Activation energies versus residual carbon

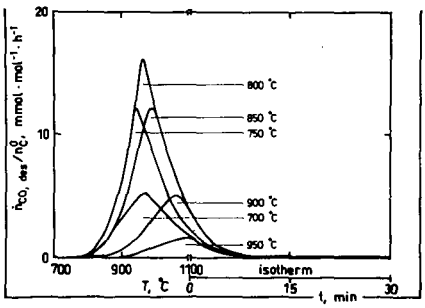

Fig. 9:
Temperature dependence of specific gasification rates according to eq. (11): ARRHENIUS plot

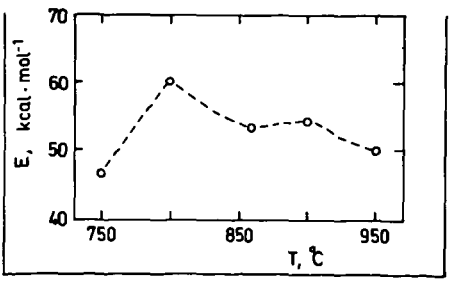

Fig. 10:
Activation energies of the desorption of the C(O) complexes

HYDROGEN GASIFICATION OF OXIDIZED CARBONS

Michael H. Treptau and Dennis J. Miller
Department of Chemical Engineering
Michigan State University
East Lansing, MI 48824-1226

INTRODUCTION

Hydrogen gasification of carbon has been studied less intensively than steam and carbon dioxide gasification over the past twenty years, although the carbon-hydrogen reaction is important in producing synthetic fuels from coal. In addition to being a direct, selective route to methane, the carbon-hydrogen reaction reduces the endothermicity of steam gasification. More importantly, hydrogen gasification can be studied as a model system to better understand fundamental aspects of steam gasification such as catalyst behavior and hydrogen inhibition. Also, gasification in pure hydrogen provides a unique environment for the accounting of oxygen present in the catalyst and carbon during gasification.

Alkali carbonates are effective catalysts for hydrogen gasification of coal chars and carbon black [1-3] but not of graphite [4]. The presence of oxygen during hydrogen gasification is also reported to accelerate methane formation. For uncatalyzed gasification of wood char, Blackwood [5] reported that rate is linearly related to oxygen content of the char. For carbon films, Cao and Back [6] reported that the addition of 0.1% oxygen to the hydrogen stream accelerated methane formation considerably.

The nature of oxygen-containing groups on carbon surfaces has been studied for many years; such surface groups can generally be categorized as acidic, neutral, basic, or inert [7]. Carboxyl, phenol, and lactone groups have been proposed [8] as acidic complexes; they are formed by oxidation at temperatures around 400°C and decompose to give CO_2 above 500°C. Carbonyl and quinone groups are neutral or weakly acidic and decompose to CO around 750°C [9]. Basic surface groups include chromene or pyrone complexes and can persist on the surface at temperatures above 1000°C [10]. Aromatic ethers are generally inert and make up the majority of surface oxygen [11].

Over the past several years we have conducted experimental studies to better understand alkali carbonate catalyst behavior in hydrogen gasification and to determine the effect of oxygen on gasification rate. We observe [12,13] that catalyst behavior in hydrogen gasification is similar to that in steam gasification, leading us to believe that catalyst-carbon interactions are of primary importance in gasification and that catalyst behavior is relatively unaffected by reactant gas. Thus hydrogen is a suitable model environment for studying catalyst behavior. One exception, however, is that higher rates of catalyst loss are observed in hydrogen [12] than in steam [14].

For uncatalyzed gasification, we have shown [15] that partial combustion of carbon black prior to exposure to hydrogen enhances methane formation rate, while high temperature pretreatment (degassing) drastically reduces reaction rate. These results, shown in Figure 1, arise from the addition or removal of active surface oxygen groups and from thermal annealing of the carbon active sites. Via pH measurements [15], we have found that partial combustion at

400°C fixes acidic groups on the carbon surface. Gasified and degassed carbons contain a predominance of basic groups.

The paper presents further studies of the role of surface oxygen and thermal treatments in both catalyzed and uncatalyzed hydrogen gasification. In this work, a second carbon substrate and oxidation by HNO_3 are investigated. Nitric acid produces a variety of groups on carbon, but does not alter the carbon structure. Comparison of results for the different carbons and two methods of oxidation provides clarification of the role of oxygen. X-ray photoelectron spectroscopy (XPS) provides further information.

EXPERIMENTS

Apparatus- Gasification experiments, including high temperature pretreatment and partial combustion, were carried out in a high-pressure fixed bed differential reactor described in detail elsewhere [12]. Reaction rates were measured by timed collection of product gas, which typically consisted only of methane in hydrogen. All gasification experiments, unless otherwise indicated, were carried out in pure hydrogen (Airco, 99.999%) at 500 psig and a flow rate of 310 ml (STP) per minute. Gasification temperatures ranged from 775°C to 865°C and typical carbon sample sizes ranged from 40-110 mg. The reactor was evacuated to 0.01 torr during initial heatup; hydrogen flow was started when sample temperature reached 500°C. For the gasification rates measured, transport resistances are negligible [16].

Surface analyses of solid reactants were carried out on a Perkin-Elmer PHI 5400 X-ray Photoelectron Spectrometer located in the Composite Materials and Structures Center at Michigan State University. To pretreat, oxidize, and gasify carbons for XPS analyses, a separate high-vacuum chamber has been constructed. The chamber is capable of attaining vacuum to 10^{-8} torr and pressure to 30 psig at room temperature, and vacuum to 10^{-7} torr at 1000°C. The chamber is equipped with a sample introduction attachment which allows samples to be transferred to the XPS without exposure to atmosphere.

Solid Reactants- The carbon black was Raven 16 furnace black (Cities Service, Co., Columbian Chemicals) produced by oxygen-deficient combustion of heavy oil. It is a graphitic carbon black with a particle size of about 60 nm. X-ray diffraction shows crystallite dimensions of L_a=3.7 nm and L_c=3.0 nm. The initial N_2-BET surface area is about 15 m^2/g; BET surface area increases almost linearly with conversion during gasification to a value of 400 m^2/g at 60% conversion. Ultimate analysis of the carbon black is given in Table 1.

The second carbon was a 50-200 mesh coconut charcoal (Fisher Sci.) which was washed in concentrated HCl at room temperature to reduce its ash content prior to gasification. The char is noncrystalline and has a N_2-BET surface area of 750 m^2/g which remains essentially constant during reaction. Ultimate analysis of the char is given in Table 1. Most noteworthy is the higher oxygen content of the char as compared to carbon black.

In all experiments, the order of treatment was degassing, oxidation, and impregnation. Degassing consisted of heating at 1273 K for 15 hours at 0.01 torr. Nitric acid oxidation was accomplished by placing the sample in 70% HNO_3 at room temperature for 24 hours, washing thoroughly with doubly-

distilled deionized water, and oven drying at 120°C. Potassium carbonate was deposited on the carbons by wet impregnation. A K/C ratio of 0.02, corresponding to about 10 wt% K_2CO_3, was used in all catalyzed experiments.

RESULTS

Gasification results are reported as reaction rate per unit total surface area (TSA) versus carbon conversion. While rates are best represented per unit active surface area, no measurement of active surface area was made in this study. Because the TSA for both carbon black and char are well characterized and depend only on conversion, this basis is equivalent, for comparative purposes, to a weight basis. Total surface area is used instead of weight to eliminate consideration of effects of TSA on gasification rate.

Carbon Black - The effect of degassing at 1273 K on carbon surface composition was determined via XPS and is shown in Figure 2. Degassing lowers oxygen surface content from over 5% to 0.26%; the residual concentration is close to that of oxygen in the bulk solid.

The effects of pretreatment and HNO_3 oxidation on uncatalyzed hydrogen gasification rate are shown in Figure 3. Oxidation of as-received (fresh) carbon black results in approximately a 30% increase in methane formation rate. Degassing reduces the rate approximately six-fold; subsequent exposure to nitric acid results in only a slight rate enhancement (5-10%) which cannot be discerned in the Figure.

These results are compared to earlier gasification rate measurements following oxidation via partial combustion in oxygen at 400°C (Figure 1). Partial combustion prior to hydrogen exposure results in approximately a two-fold increase in methane formation rate for both fresh and degassed carbon black.

Results of pretreatment and HNO_3 oxidation on catalyzed gasification rate are shown in Figure 4. K_2CO_3 strongly catalyzes hydrogen gasification of all samples; HNO_3 oxidation enhances catalyzed methane formation from fresh and degassed samples more significantly than uncatalyzed methane formation.

Coconut Char - XPS analysis of the char indicates that initial surface oxygen content is 4.1%, close to the value for bulk char of 3.4%. Uncatalyzed gasification rates for coconut char exposed to degassing and HNO_3 oxidation are shown in Figure 5. In contrast to carbon black, degassing only reduces reaction rate by a factor of two. Nitric acid oxidation significantly increases rate for both fresh and degassed samples; for the degassed sample oxidation increases rate almost to the value of that for fresh char. At high conversion the rates of all samples converge; the effects of surface treatments apparently decay as carbon is consumed.

Catalyzed gasification rates for coconut char exposed to the same degassing and oxidation are shown in Figure 6. Degassing has essentially no effect on the catalyzed hydrogen gasification rate, and HNO_3 oxidation enhances rate about two-fold for both fresh and degassed chars.

DISCUSSION

Uncatalyzed gasification - In an earlier paper [15], we postulated that acidic groups on the carbon black surface decompose to form "nascent" or active sites at which hydrogen gasification most readily occurs. These nascent sites are consumed as carbon black reacts, resulting in the observed decrease in gasification rate. Thermal degradation of nascent sites does not occur at gasification temperatures, as evidenced by an experiment in which carbon black was heated to 865°C for four hours in helium. Upon exposure to hydrogen, the reaction rate observed was the same as that of a sample directly heated to 865°C.

High temperature (1270 K) degassing desorbs CO_2 and CO from acidic groups and then thermally "anneals" the nascent sites formed, thus resulting in a much lower gasification rate. The XPS results indicate that all excess surface oxygen is removed. Gasification activity following degassing, which remains constant with carbon conversion, is attributed to basic oxygen groups in bulk carbon which are exposed as carbon is gasified. These groups must also facilitate carbon gasification although at a much slower rate. Finally, X-ray diffraction patterns are identical for fresh and degassed carbons, indicating that "annealing" is a surface process only.

Partial oxidation in oxygen at 400°C produces significant new surface area in carbon black, as about 10% of the solid is gasified by oxygen. In addition, acidic oxygen groups are fixed on the surface. Upon heating to hydrogen gasification temperatures (830-865°C), these acidic sites decompose to give nascent sites at which hydrogen gasification takes place. Thus partial combustion enhances methane formation for both fresh and degassed carbon black via the creation of active sites from acidic surface groups on newly exposed surface area.

Nitric acid oxidation produces both acidic and basic oxygen groups and gives different results than partial combustion. Oxidation of fresh carbon black somewhat enhances methane formation rate; acidic groups formed in oxidation again form nascent sites upon heating in hydrogen. Upon degassing, however, the carbon surface is no longer susceptible to nitric acid oxidation, and only slight methane rate enhancement is observed following oxidation of the degassed carbon. Little evolution of NO_2 occurred during oxidation; the degassed carbon black surface is apparently not susceptible to oxidation.

The coconut char studied has significantly different structure and oxygen content and exhibits much different gasification behavior than carbon black. The nearly constant gasification rate of the char over the conversion range studied suggests that the high bulk oxygen content and amorphous structure of the char provide new active sites for gasification as carbon is consumed.

The effect of degassing on gasification rate is much less for the char than for carbon black. We propose that this also results from the amorphous nature and high bulk oxygen content of the char. Degassing removes only surface-adsorbed groups and does not affect bulk oxygen, which is present in much higher levels than in carbon black (Table 1). Also, because the char is amorphous and thus so many carbon atoms are potential reactive sites, thermal annealing does not destroy as large a fraction of active sites in the char as in carbon black. Thus, while acidic surface groups are desorbed during

degassing and the nascent sites associated with them likely annealed, there are enough reactive sites and bulk oxygen remaining that char reactivity is only moderately reduced.

Both fresh and degassed char show significant gasification rate enhancement upon oxidation in HNO_3. The large quantity of NO_2 evolved during oxidation indicates extensive oxidation of the surface, which is directly attributable to the noncrystalline nature of the char. The increase in acidic group concentration from oxidation results in accelerated methane formation following oxidation.

Catalyzed Gasification - The results in Figures 4 and 6 for carbon black and coconut char, respectively, suggest that the neutral and basic groups (carbonyl and pyrone/chromene) interact with K_2CO_3 and result in catalytic enhancement of reaction rate. Hydrogen gasification of degassed carbon black, which contains only stable basic groups arising from bulk oxygen, is strongly catalyzed by K_2CO_3; oxidation by HNO_3 further enhances the catalyst activity. Partial combustion at 400°C does not enhance the K_2CO_3-catalyzed gasification rate of degassed carbon black [15], indicating that nascent sites formed by desorption of acidic groups do not interact with the catalyst.

For coconut char, there is essentially no difference in catalyzed gasification rate of fresh and degassed samples. This indicates that surface groups desorbed during degassing are not important for the catalytic reaction; instead it appears that basic groups arising from bulk oxygen, which are not affected by degassing, interact with the catalyst. Nitric acid oxidation, which results in a significant increase in all types of oxygen groups, also results in a significant enhancement in catalyzed rate.

The nature of interaction between surface carbonyl and basic groups and K_2CO_3 is not yet understood. It is possible that surface oxidation simply allows catalyst to better wet and disperse on the carbon during hydrogen gasification. It has been observed that surface oxygen stabilizes catalyst on the surface during gasification; catalyst loss experiments indicate that catalyst loss is more rapid for degassed samples than fresh carbon and slower for oxidized samples than for fresh. Stabilizing of catalyst, however, may not enhance gasification rate. Finally, it is possible that surface oxygen may participate in one of the M-O- surface oxides currently under investigation as possible active catalyst forms [17].

In summary, it is apparent that hydrogen gasification rate is influenced by the treatments implemented. This is not to imply, however, that other factors are not important: for instance, the observations of Yang and Duan [18], who analyzed etch pits formed in hydrogen and oxygen and found that hydrogen produces hexagonal basal plane edges while oxygen produces arm-chair edges, could explain at least some gasification behavior. Further work, including extensive XPS studies, will provide more insight into the importance of oxygen in the reaction.

CONCLUSIONS

High temperature degassing and nitric acid oxidation have significant effects on the hydrogen gasification rate. For graphitic carbon black, surface annealing of nascent sites during degassing most strongly affects gasification

activity, with oxidation having a lesser effect. This results from the fact that most oxygen and thus most active sites are initially on the carbon surface; once these sites are eliminated gasification is slowed. For uncatalyzed coconut char, degassing and nitric acid oxidation have opposite effects of about the same magnitude. The high bulk oxygen content makes initial removal of surface oxygen during degassing relatively unimportant; the amorphous char structure results in extensive oxidation which facilitates an increase in gasification rate.

Uncatalyzed hydrogen gasification is proposed to occur at nascent sites created by desorption of CO_2 from acidic surface groups, and to a much lesser extent at the basic groups formed from bulk carbon. Catalyzed gasification is proposed to occur via interaction of catalyst with basic surface groups.

REFERENCES

1. Gardner, N., E. Samuels, and K. Wilks, Adv. Chem. Ser. **131**, 217 (1974).
2. Walker, P.L. Jr., S. Matsumoto, T. Muira, and I.M.K. Ismail, Fuel **62**, 140 (1983).
3. Cypres, R., M. Ghodsi, and D. Feron, Thermochim. Acta **81**, 105 (1984).
4. Casanova, R., A.L. Cabrera, H. Heinemann, and G. Somorjai, Fuel **62**, 1138 (1983).
5. Blackwood, J.D., Aust. J. Chem. **12**, 14 (1959).
6. Cao, J.R. and M.H. Back, Carbon **23**, 141 (1982).
7. Voll, M. and H.P. Boehm, Carbon **9**, 481 (1971).
8. Barton, S.S. and B.H. Harrison, Carbon **13**, 283 (1975).
9. Marchon, B., J. Carrazza, H. Heinemann, and G.A. Somorjai, Carbon **26**, 507 (1988).
10. Papirer, E., S. Li, and J.-B. Donnet, Carbon **25**, 243 (1987).
11. Rivin, D., Rubber Chemistry and Technology **35**, 729 (1962).
12. Zoheidi, H. and D.J. Miller, Carbon **25**, 265 (1987).
13. Treptau, M.H., H. Zoheidi, and D.J. Miller, ACS Div. Fuel Chem. Prepr. **31**(3), 150 (1986).
14 Sams, D.A., T. Talverdian, and F. Shadman, Fuel 64, 1208 (1985).
15. Zoheidi, H. and D.J. Miller, Carbon **25**, 809 (1987).
16. Zoheidi, H., Ph.D. Dissertation, Michigan State University (1987).
17. Moulijn, J.A. and F. Kapteijn, Carbon and Coal Gasification, NATO ASI Series E, **105**, 181 (1986).
18. Yang, R.T. and R.Z. Duan, Carbon **23**, 325 (1985).

TABLE 1
ULTIMATE ANALYSIS OF REACTANTS

	Carbon Black	Coconut Char
Moisture, %	0.46	1.02
Carbon, %	96.92	91.82
Hydrogen, %	0.27	0.43
Nitrogen, %	0.29	1.81
Sulfur, %	1.54	0.06
Ash, %	0.31	1.48
Oxygen (diff), %	0.21	3.38

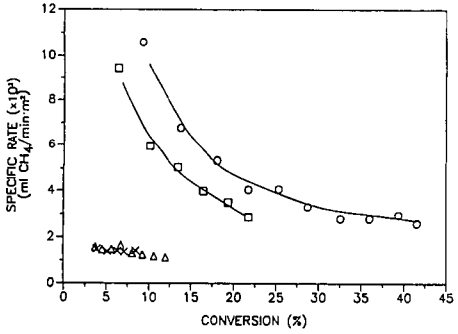

Figure 3. Uncatalyzed Carbon Black, 865°C, 500 psi H_2. (□)–Fresh; (○) HNO_3 oxidized, (△)–Degassed; (×)–Degassed, HNO_3 oxidized.

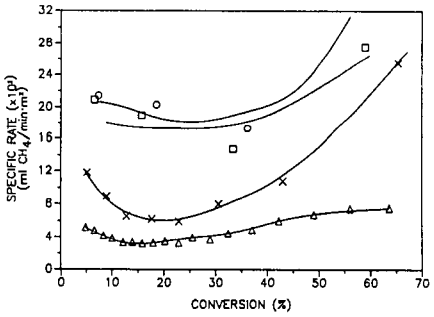

Figure 4. K_2CO_3–Catalyzed Carbon Black, 865°C, 500 psi H_2, K/C=0.02. (□)–Fresh; (○)–Oxidized, impreg.; (△)–Degassed, impreg. (×)–Degassed, oxidized, impregnated.

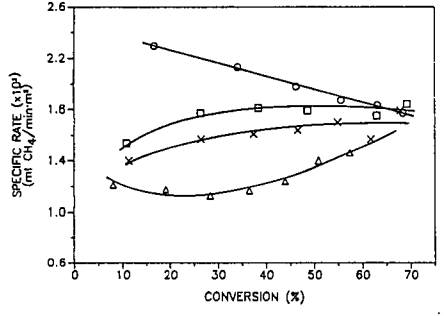

Figure 5. Uncatalyzed Caconut Charcoal, 865°C 500 psi H_2. (□)–Fresh; (○)–HNO_3 oxidized, (△)–Degassed; (×)–Degasssd, HNO_3 oxidized.

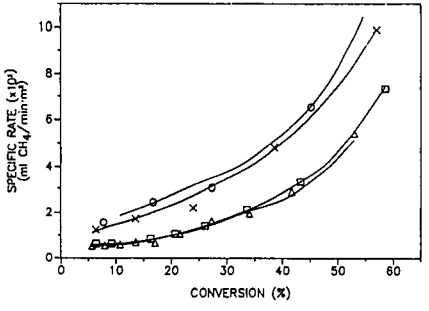

Figure 6. K_2CO_3–Catalyzed Cacanut Charcoal, 775°C, 500 psi H_2, K/C=0.02. (□)–Fresh; (○)–Oxidized, impreg.; (△)–Degassed, impreg., (×)–Degassed, oxidized, impregnated.

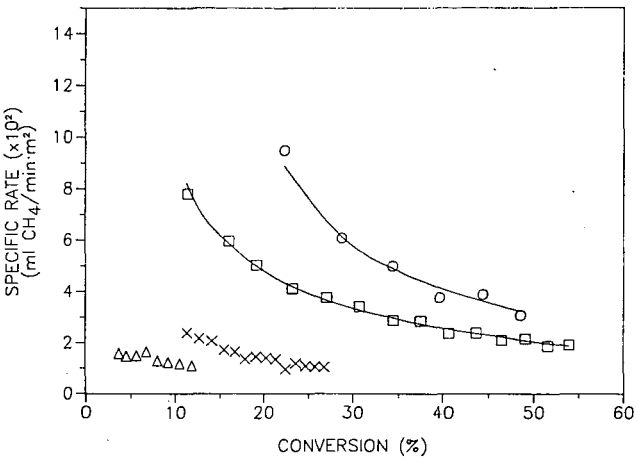

Figure 1. Uncatalyzed Carbon Black, 865°C, 500 psi H_2. (□)–Fresh; (o)–O_2 400°C; (Δ)–Degassed; (×)–Degassed, O_2 400°C.

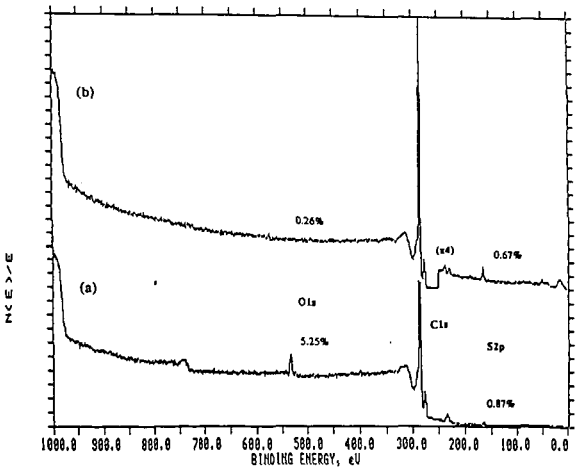

Figure 2. XPS scan of a) fresh and b) degassed carbon black.

Low Temperature Oxidation Reaction of Microporous Carbons

J. K. Floess, S. A. Oleksy, and K. J. Lee
Department of Chemical Engineering
University of Illinois at Chicago
Chicago, IL 60680

Introduction

The oxidation of carbon by different gases is a reaction of major industrial importance, which to date at least, is not adequately understood on a molecular basis. Although a number of investigators[1-4] have proposed mechanistic models involving elementary steps for the gasification of carbon by different reactants, these models are generally qualitative in nature since the assignment of values to all individual rate constants is not yet possible. Careful experimental studies, in particular with graphite have been central to the development of these models and have been important in determining the role of certain postulated steps in the mechanisms. Other studies using labeled gas species have been useful in selecting the correct reaction pathway among possible alternative steps. Transient kinetic studies, in other instances, have led to a further understanding of the role of the intermediate complexes during reaction. However, a consensus on a reaction mechanism, particularly for the oxygen reaction, has yet to be obtained, nor have adequate quantitative comparisions been made between models and data obtained with various carbons.

In this study, work has focused on three aspects of the low temperature (<850K) carbon-oxygen reaction: the relationship between oxygen partial pressure and rate, the role of the surface oxide intermediate in the reaction mechanism, and the effect of carbon structure on the kinetics.

Experimental Equipment and Procedure

Rate data for both oxygen chemisorption and carbon gasification were obtained from measurements of weight gain (or loss) using a Stanton Redcroft thermogravimetric analyzer. The instrument consists of an electronic balance and a water cooled micro-furnace having a temperature limit of 1500°C and a heating rate capability of 50°C/min. A significant feature of the instrument is the small volume of the furnace (ca. 5 cc), which makes it possible to obtain a rapid change in gas composition upon introduction of a reactant. With nominal gas flowrates of 1 to 4 cc/s, the transient time for a change in gas composition is a few seconds. The TGA was also modified for operation under vacuum, which allows a further reduction in the transient time by allowing for slightly higher gas velocities in the furnace.

Weight changes of less than 1 μg can be readily measured with this instrument, and for a sample weight of 10 mg, this gives a weight gain or loss sensitivity of ca. 100 ppm (g/g carbon) after corrections for background weight changes caused by buoyancy and drag forces on the sample pan and hang down wire have been made. The actual amount of sample used in individual runs was modulated as necessary to minimize the effects of external heat transfer between the sample pan and the furnace and mass transfer between the sample and gas on the kinetics. This required rates to be nominally

held below 0.2 mg/min.

The experimental procedure was usually as follows. The sample was heated in nitrogen to 800°C at a rate of 50°C/min and held at 800°C for 3 min. This ensured the removal of the majority of the surface oxides. After outgassing, the sample was cooled to the reaction temperature and the experiment started by switching to the reactant gas. In several experiments, however, the carbon was first partially reacted at 535°C in air to 35% conversion and then reheated to 800°C before the start of an experiment. The total weight loss of the sample after burn-out and outgassing was 48%. At the conclusion of a run, the gas was switched back to nitrogen, the sample reheated to 800°C, and again cooled to the reaction temperature, where the sample weight was measured. The amount of oxygen on the carbon surface was calculated from the weight loss during outgassing as follows:

$$w_a = w_d(8+4\lambda)/(11+7\lambda) \qquad (1)$$

where w_a is the weight of adsorbed oxygen, w_d is the measured weight loss, and λ is the CO/CO_2 mole ratio of the desorption products. The difference between the weight of oxygen in the desorption products and the total weight change in each run gives the amount of carbon gasified. This method was used in all experiments to separate the total weight change into an oxygen adsorption curve and a true carbon loss curve.

The carbon used in these experiments was Spherocarb, a molecular sieve carbon commercially available from Analabs, North Haven, CT. The elemental and physical analyses of the carbon are given in Table 1. Surface area data as a function of conversion were obtained from data reported by Hurt et al.[5] The micropore diameter was estimated in two ways. One method used isosteric heat of adsorption data[6] from physisorbed N_2 to estimate the pore size using theoretical adsorption potential models for a graphite surface[7-8]. The other technique used the random pore model[9] to determine an average pore size from the micropore surface area and volume measurements. The former value is probably characteristic of the spacing between parallel orientated lamellae in a microcrystallite, whereas the latter represents an overall average ratio of pore volume to surface area. The difference of a factor of three in the calculated pore sizes indicates that there is a distribution of micropore sizes in the char.

Results and Discussion

A. Oxygen Chemisorption and Reaction. Gravimetric measurements of the oxygen-carbon reaction rate have been made at 498, 548, 563, and 708 K with both the partially reacted and unreacted Spherocarb. Figure 1 shows the the oxygen adsorption and carbon gasification curves obtained at 563K. For each experimental point, the reaction was stopped at appropriate times by switching to nitrogen, and the carbon outgassed to determine the oxygen content. The measured weight change was separated into individual curves for carbon loss and oxygen adsorption using a value of ∞ for λ in equation (1). No appreciable weight loss occurred when the reaction was stopped by switching to nitrogen; the surface oxides are stable and remain on the carbon at temperatures below ~900K. The initial oxygen adsorption rate is rapid (the characteristic reaction time is ~10s at 548K) and is characterized by an activation energy of a few kcals. A rapid loss of carbon, which is presumably due to the gasification of labile carbon atoms[10], occurs concurrently with the initial uptake of oxygen. The initial rate of oxygen adsorption is more clearly shown by the data given in Figure 2, where adsorption data

between 3s and 300min are shown on an Elovich plot. This plot gave the best linear fit for the chemisorption data obtained in these experiments, implying that the adsorption sites are heterogeneous as would be expected.

At carbon conversions between 5 and 8%, the rate of carbon loss approaches a steady state value as shown by the carbon conversion curves presented in Figure 3 for data obtained at 708K. The oxygen content of the char (also shown in Figure 3), however, continues to increase with conversion, gradually reaching a value of ~0.18 mol O/mol C-remaining. The increase in oxygen content with conversion is more clearly shown in Figure 4, in which the oxygen to carbon ratio of the char is plotted as a function of carbon conversion for different reaction conditions. The amount adsorbed at equivalent conversions is practically the same for all reaction conditions, implying that the formation of the secondary oxides (as compared to those oxides formed initially) is a consequence of the removal of carbon from the solid substrate. Carbon reactivity was found to correlate with the initial amount of oxygen adsorbed but did not correlate with the variation in oxide concentration with conversion. A turn-over number (ton) based on the initial amount of oxygen adsorbed of 6.1×10^{-3} sec^{-1} was calculated for (unreacted) Spherocarb at 773K and 0.1 atm pressure. This value is in good agreement with the t.o.n. reported by Ahmed and Back[11] for a pyrolytic carbon.

B. Reaction Mechanism. Figure 5 shows the variation in rate with oxygen partial pressure. A value of 0.75 ± 0.06 was calculated for the reaction order with respect to oxygen from these data. The significant feature of these measurements, though, is the insensitivity of both the reaction order as well as the overall activation energy (not shown) to variations in oxygen partial pressure of almost two orders of magnitude and to variations in temperature of almost 150 C, implying that the rate controlling step of the reaction remains the same for the range of conditions investigated. Langmuir-Hinshelwood mechanisms, which could account for the observed non-elementary reaction order, however, typically would predict a change in the rate controlling step for such a range of conditions, and thus a shift in the observed order and overall activation energy. An appropriate mechanism for these data, therefore, requires an explanation of the reaction order (and activation energy) that remains largely invariant over a broad range of conditions. The observed reaction order is near enough to unity that the rate determining step in the reaction mechanism presumably involves oxygen adsorption at an active site. We propose a kinetic model that can be described in terms of the following steps:

$$2\,C_i + O_2 \rightarrow 2\,C(O)_i \qquad (2)$$

$$C_i + C(O)_i + O_2 \rightarrow C(O)_i + C_i' + CO_2\ (+CO) \qquad (3)$$

$$C(O)_i \rightarrow CO + C_i \qquad (4)$$

where C_i is a free site with energy i; $C(O)_i$ is an occupied site of energy i; and CO_2 and CO the reaction products. Equation (3) is representative of reactions occuring at various edge sites. Oleksy[12] has specified the appropriate stoichiometry for edge sites of arm-chair, zig-zag, or mixed configurations[13] for different surface complex coverages. Both CO and CO_2 are possible reaction products in these reactions However, it is not possible at present to identify individual kinetic parameters for the various types of sites, and as a

result, we have chosen to represent these parallel reactions in terms of a continuous energy distribution function[14]. This approach decreases the number of parameters necessary to characterize the parallel set of reactions represented by (3). Reactions (2) and (4) are also assumed to occur at sites of different energies, and it is assumed that the rate equation for these reactions can also be expressed in terms of a continuous site energy distribution. However, it is assumed in the analysis that the parameter relating the site energy distribution to the activation energy for reaction at a site (i.e., the Polanyi relationship between the activation energy and the site energy) is not the same for each elementary reaction since each reaction step does not involve a common reaction intermediate (i.e., transition state).

At low temperatures (<850K) reaction (3) is assumed to be the rate controlling step in the mechanism. Transient kinetic measurements show that neither reaction (2) or (4) have activation energies or rates comparable to that of the gasification reaction. The rate controlling Eley-Rideal step proposed here for this reaction is in agreement with the work of Chen and Back[15] and more recently Ahmed and Back[11], who have previously proposed this to be the principal rate controlling step in the low temperature oxidation mechanism. Ahmed and Back provided some direct evidence for this mechanism by showing that carbon gasification occurred only subsequent to the formation of surface oxides. In this study, the gasification of labile carbon atoms during the initial formation of the surface oxides made it impossible to separate the steady state carbon gasification rate from the measured carbon weight loss. However, we argue in favor of this mechanism as follows. The formation of CO from a surface complex requires approximately 70 kcal (in our calculations we have attributed ca. 20 kcal to a carbon surface energy, and have assumed the formation of a ketone bond between the oxygen atom and edge carbon), which is some 30 kcal greater than the measured overall activation energy of 40 kcal for the oxygen-Spherocarb reaction. The additional energy needed for desorption can only be obtained from the energy released when oxygen is adsorbed on the carbon surface. Bond rearrangements and energy transfer leading to the desorption of a surface complex would most likely occur if adsorption occured at or adjacent to the surface complex. Secondly, the nearly first order dependence of the rate on oxygen partial pressure clearly suggests that reactions such as (2) to be the rate controlling. At present, the 0.75 reaction order must be taken as an empirical value. The non-integer reaction order could possibly be explained as the result of interaction between the oxygen molecule and a surface complex.

Conclusions

1. The initial rate of oxygen chemisorption on a microporous carbon is rapid and characterized by an activation energy of a few kcals. The adsorption data can be linearized when plotted as amount adsorbed vs. ln(t). The surface oxides are stable and remain on the carbon at temperatures below ~900K.

2. Char reactivity appears to correlate with the initial amount of oxygen chemisorbed. For the unreacted Spherocarb, a turn-over number of 0.0061 sec^{-1} at 773K and 0.1 atm oxygen was obtained.

3. The oxygen to carbon ratio increases dramatically with carbon conversion; however, no comparable increase in the steady state reactivity of the carbon is observed. The

secondary O/C ratio is a function of carbon conversion alone and independent of the particular reaction conditions.

3. The reaction order with respect to oxygen for Spherocarb is 0.75 and remains invariant over a broad range of oxygen partial pressure and temperature, implying that the rate controlling step in the reaction remains the same. Because the reaction order is near unity, it is proposed that the principal rate controlling step of the reaction involves the reaction of an oxygen molecule with a free site at a surface complex. It is proposed that the non-integer reaction order can be explained as the result of induced heterogeniety at a surface complex.

Acknowledgement

Acknowlegdement is made to the donors of the Petroleum Research Fund, administered by the ACS, and to the University of Illinois for support of this research.

References

1. Marsh, H., in "Oxygen in the Metals and Gaseous Fuels Industries", Chemical Society, London (1978).
2. Essenhigh, R.H., in "Chemistry of Coal Utilization," Second Supplementary Volume, M. A. Elliott, ed., Wiley, New York (1981).
3. Laurendeau, N. M. Prog. Energy Combust. Sci. 4, 221 (1978)
4. Ahmed, S., Back, M.H., and Roscoe, J. M., Comb. and Flame 70,1 (1987).
5. Hurt, R. H., Dudek, D. R., Longwell, J. P., and Sarofim, A.F., "The Phenomenon of Gasification Induced Carbon Densification and its Influence on Pore Structure Evolution", to appear in Carbon, 1988.
6. Floess, J. K., Eden, G., and Luberda, J., "Reaction-Diffusion Model of Microporous Carbon", Final report submitted to the Campus Research Board, University of Illinois at Chicago (1987).
7. Chihara, K., Suzuki, M., and Kawazoe, K., J. Colloid Interface Sci., 64, 584 (1976).
8. Everett, D. H. and Powl, J. C., J. Chem Soc., Faraday Trans. I, 619 (1976).
9. Gavalas, G., AIChE J. 26 577(1980).
10. Tucker, B. G. and Mulcahy, M. F. R., Trans. Faraday Soc. 65 274 (1969).
11. Ahmed, S. and Back, M.H., Carbon 23, 513 (1985).
12. Oleksy, S. A., MS Thesis, Department of Chemical Engineering, University of Illinois at Chicago (1988).
13. Ben-Aim, R. I., Int. Chem. Eng., 27, 70 (1987).
14. Boudart, M. and Djega-Mariadassou, G.,"Kinetics of Heterogeneous Catalytic Reactions", Princeton University Press, Princeton, NJ (1984).
15. Chen, C-J. and Back, M. H., Carbon 17 495 (1979).

Table 1. Physical Properties and Chemical Composition of Spherocarb.

Elemental Analysis		Surface area	$1020\ m^2/g$
C	96.8 wt%	Micropore volume	$0.39\ cm^3/g$
H	0.73 wt%	Pore radius[a]	6.7Å
O	2.43 wt%	Pore radius[b]	2.2Å
ash	~200 ppm		

Conversion (%)	0	20	40	60	80
Surface area (m^2/g-remaining)	1020	870	765	670	570

a. by application of the random pore model
b. from isosteric heat of adsorption

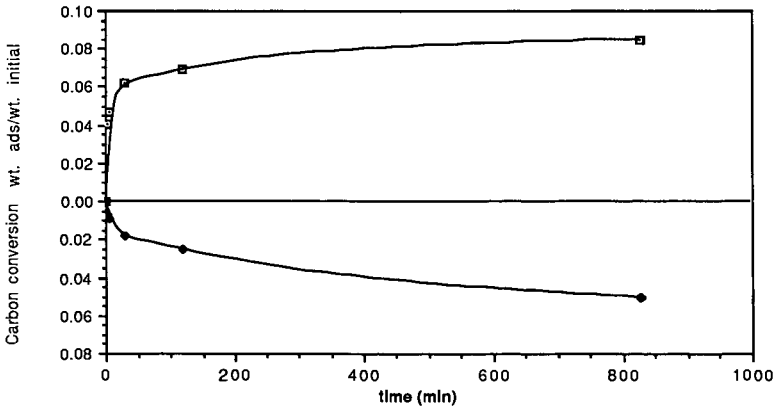

Figure 1. Adsorption and conversion curves at 563K and 0.5 atm; partially reacted Spherocarb.

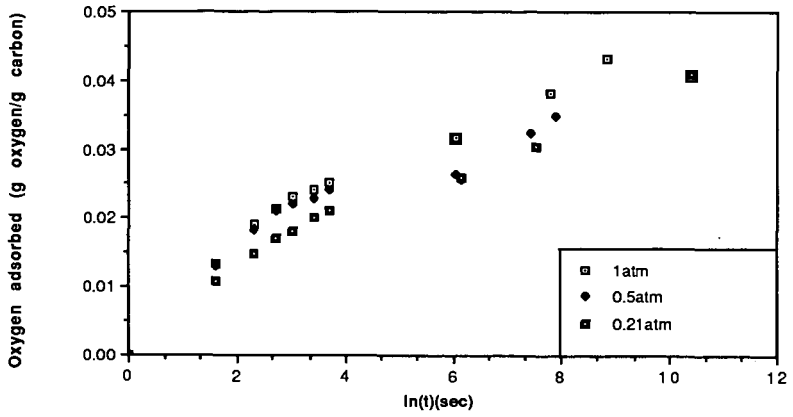

Figure 2. Oxygen adsorption vs ln(time) at 498K; partially reacted Spherocarb

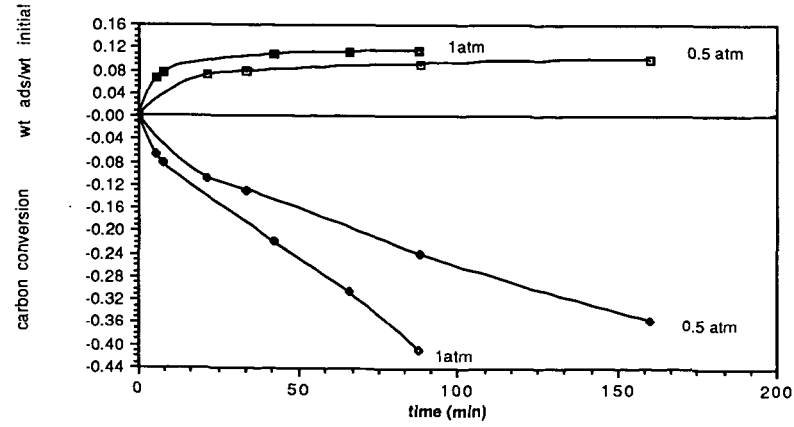

Figure 3. Adsorption and conversion curves at 708K for partially reacted Spherocarb (0.5 and1 atm oxygen)

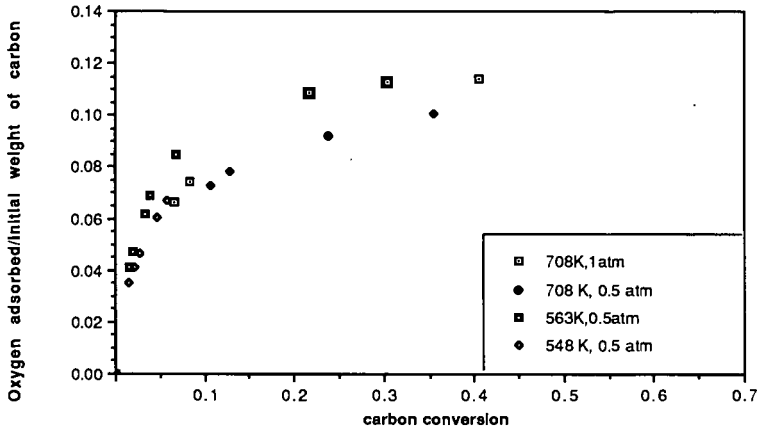

Figure 4. Amount of chemisorbed oxygen vs carbon conversion for the partially reacted Spherocarb.

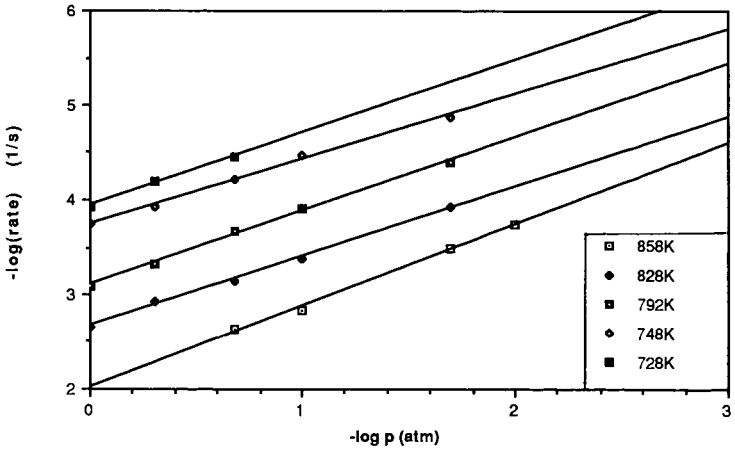

Figure 5. Variation of reactivity of Spherocarb with pressure.

VARIATIONS IN THE OXYGEN CHEMISORPTION CAPACITY OF MILD GASIFICATION CHAR AT VARIOUS LEVELS OF BURNOFF

M. Rashid Khan
U.S. Department of Energy
Morgantown Energy Technology Center
Morgantown, WV 26507-0880

INTRODUCTION AND BACKGROUND

Our results demonstrated that by careful selection of coal devolatilization conditions, it is possible to produce high quality (but, perhaps, low yield) liquid fuels (1). However, the overall economics of a devolatilization process is strongly influenced by the commercial use of char which constitutes as the major portion of the devolatilization products, regardless of pyrolysis scheme utilized. Coal chars prepared by low-temperature devolatilization have a higher degree of crystallinity than the starting coal. However, the crystalline structure of coal char is significantly less ordered than graphite. The lower the coal pyrolysis temperature, the greater the disorder. In graphite, the building blocks are lamellar in structure held together by van der Waals forces. At the edge, crystallites have unpaired sigma electrons which are susceptible to attack by oxidants. The edge carbon atoms are more reactive than basal carbon atoms. Active carbon sites are considered as dislocations or imperfections in the crystallite edges of carbon (2). It was demonstrated (1) that chars prepared at mild conditions (i.e., 500°C) had higher active surface areas, and thus had higher reactivity than those prepared at severe conditions (i.e., 950°C). Numerous studies have been reported on the reactivity of chars generated at different operating conditions, (e.g., different char formation temperatures, burnoff temperatures, oxygen partial pressures, and particle sizes) (1-4). The factors which influence the reactivity of coal char include the following: (a) concentration of carbon active sites, (b) catalysis by the inherently present minerals, and (c) the diffusion of the reactant and product gases within the pores of the devolatilized char (3). Coal chars are heterogeneous materials that can contain significant amounts of heteroatoms such as hydrogen, oxygen, nitrogen, and sulfur, which may also influence the reactivity. While oxygen sites influence reactivity by electron exchange, nitrogen and sulfur sites encourage ring attack due to concentration of the electrons (2). It was demonstrated that the char's hydrogen content can play a significant role in reactivity perhaps by providing a source of nascent-carbon sites (1).

Numerous studies considered the significance of active surface area for investigating the reactivity of coal char or carbon (9-14). The technique used to determine the concentration of carbon active sites is oxygen chemisorption. Laine et al. (4) investigated the role of the active surface area in the carbon-oxygen reaction, and observed that the unoccupied (i.e., available) active surface area was the major factor that determines the rate constant, rather than the conventional Brunauer-Emmett-Teller (B.E.T.) surface area. Although carbon-oxygen reactions have widely been investigated (2-18) and several mechanisms postulated, the exact mechanisms are not well understood. Several elementary reactions (shown below) have been used (2) to describe the reaction mechanisms:

$$2C_f + O_2 \rightleftarrows 2C_f(O) \quad (1)$$

$$C_f(O) \rightleftarrows C_{fs} \quad (2)$$

$$C_f(O) \rightleftarrows CO \quad (3)$$

$$C_f(O) + C_f(O) \rightleftarrows CO_2 + C_f \quad (4)$$

where,

C_f = Free active site.

$C_{fs}(O)$ = Stable carbon-oxygen complex.

$C_f(O)$ = Transient oxygen-surface complex.

On the basis of active surface area, the rate constants of carbon-oxygen reactions were calculated using an equation of the form:

$$\frac{dP_{O_2}}{dt} = k\,(P_{O_2})\,(UASA) \quad \text{where, } UASA = ASA(1-\theta) \qquad (5)$$

ASA is the active surface area for the char, and (1-θ) is the fraction of the ASA which is unoccupied (UASA). Laine et al (4) calculated rate constants based on both UASA as well as total surface area (TSA), determined by BET measurements. On the basis of UASA, the calculated rate constants were essentially constant over the burnoff and time range studied. According to this theory, available active surface, as determined by oxygen chemisorption capacity is a fundamental property of a coal char which influences its reactivity.

From a gasification or combustion standpoint, the sites participating in gasification can be significantly different from those measured initially, *i.e.*, before any burnoff occurs. Chornet et al. (15) assumed that the char-oxygen reaction system undergoes three sequential phases: (a) initially, the reaction proceeds slowly because the inventory of "active sites" is rather limited at the onset of the reaction; (b) acceleration of the reaction rate occurs because the concentration of active sites increases significantly due to pore growth and opening, and a maximum rate reflects a balance between generation and depletion of these active sites; and (c) beyond this maximum point, the total number of active sites and thus, the reaction rate, decrease due to the consumption of active sites during burnoff. However, no experimental work was performed to validate this model. Mahajan et al. (16) suggested that the availability of active sites might be controlled by the opening and loss of the pores during oxidation in a complex way.

The normalized burnoff rate has been extensively used in the literature for studying coal char combustion. Arbitrarily defined reference times such as 10-, 15-, or 50-percent conversion for maximum reactivity have been used by various investigators (1,9,18,21). For example, while Mahajan et al. (16) normalized reactivity results based on the time needed for 50 percent burnoff, Solomon et al. (17) developed a new approach for normalizing the reaction rate based on 10 percent burnoff, implying that various reference times used may have fundamental significance. The significance of various reference times on normalization of char reactivity is not well understood. The objectives of this study are: (a) to investigate the variation in ASA as a function of burnoff, and (b) to study the influence of various reference times (from 10- to 70-percent burnoff) on a normalized reaction rate.

EXPERIMENTAL

As described elsewhere (1), a Pittsburgh No. 8 (high-volatile bituminous) coal was pyrolyzed in a thermogravimetric analysis (TGA) system heated at 20°C/min in an inert atmosphere. Low-temperature char was prepared at 500°C while the high-temperature char was prepared at 950°C. Operating conditions for oxidation as well as the technique that was used to monitor the isothermal burnoff rate have been described in detail (1). Selected chars were then subjected to oxidation in a TGA system at burnoff temperatures of 400 to 474°C. Char weight loss was monitored continuously during the reaction period and was converted to the fractional char burnoff at various times (Figure 1). The reactive gas had a flowrate of 120 mL/min oxygen. The oxygen chemisorption capacity (OCC) was determined by measuring the oxygen uptake by the coal char at approximately 200°C and 0.1 MPa of oxygen for about 15 hours in a TGA system. The oxygen chemisorption capacity for the low- and high-temperature chars are 203 and 70 m^2/g, respectively. Obviously, the results demonstrate that the low-temperature chars have a significantly higher OCC than the high-temperature chars. These and other related results have been discussed elsewhere (10) in detail.

RESULTS AND DISCUSSION

Normalization of Burnoff Curves Using Various Reference Times

The instantaneous weight of char in a typical TGA run is monitored continuously during the reaction period. The fractional char conversion (f) is generally used to represent the characteristic of char burnoff. The values of f at any time during char burnoff can be calculated from the TGA weight-loss curve using the following expression:

$$f = \frac{M(0) - M(t)}{M(0) - Mash}$$

where M_0 is the initial weight of char, M_t is the instantaneous weight of char, and M_{ash} is the ash content in the original char sample. The time scale can also be normalized to the dimensionless time τ, based on the reference time $t_{0.5}$. Figure 1 compares the fractional burnoff curves for chars prepared at 500° and 950°C. For the 500°C char, there is a maximum burnoff rate at about 10 percent of char burnoff. The shape of the combustion curve (i.e., changing slopes) possibly reflects the competing events of pore growth and pore depletion as proposed by others (3,16). Lizzio et al. (19), suggested that this observed maximum rate is not caused by decreasing intraparticle diffusional limitations, but rather is a result of competing mechanisms as described by other investigators (15,16) in the kinetically controlled regime.

Upon normalization of the burnoff rate, there is only one characteristic burnoff curve for any burnoff temperature. For example, Figure 2 (a,b) shows some of the burnoff curves for the 500°C char oxidized at burnoff temperatures of 400 to 474°C. These burnoff curves have been normalized with the time required for 10- to 70-percent char burnoff corresponding to each T_b. The curves are very similar to each other and can be considered as a single characteristic curve. Also, similar results were obtained for the 950°C char oxidized at T_b = 400, 430, and 450 as shown in Figure 2 (c,d).

The data for 50 percent burnoff cases is not shown. The unique characteristic burnoff curve for each char preparation temperature facilitates analysis of data at different temperatures. However, these data demonstrate that there is little fundamental significance of the burnoff time used for normalized reactivity data.

Oxygen Chemisorption Capacity (OCC) of a Low-Temperature Char Measured at Various Levels of Burnoff

The variation of OCC with fractional burnoff was monitored in a TGA system for the 500°C char. The char was heated to 400°C in helium before pure oxygen was introduced into the reactor at the same temperature. At each level of burnoff, the burned char was subjected to measurement of OCC by oxygen chemisorption at 200°C. The level of burnoff measured in this study ranged from zero to 85 percent (dry-ash-free char basis). Results of the OCC measurement at different burnoff levels are shown in Figure 3. Several interesting observations can be made about this data. First of all, the measured OCC in this study are very high compared to those generally reported in the literature for coal chars. The ASA was calculated assuming that chemisorption is dissociative and each oxygen atom occupies one carbon atom with a cross sectional area of 8Å A^2. Such assumption, though reasonable for pure graphite, may not be strictly valid for highly amorphous char where oxygen may sorb on surface without dissociation. This high-surface area perhaps reflects that the low-temperature chars (500°C) are indeed highly amorphous and, therefore, have the highest concentration of reactive sites. Second, the measured peak in OCC does not necessarily coincide with the peak in reactivity. In fact, the maximum reactivity as a function of burnoff occurs at 10 percent burnoff where the OCC is much lower. The maximum OCC occurs at about 60 percent burnoff. Therefore, the changes in OCC does not correlate with the reactivity as a function of burnoff. Several other researchers also faced difficulties in correlating rate constant with active surface area. Using the same procedure as Laine et al. (4), Taylor and Walker (23) measured ASA for partially oxidized samples of Saran char. Their attempts to measure UASA led to the conclusion that there was no correlation between ASA and reactivity.

An alternative approach to the ones taken by Laine et al. (4) can be considered (18). One can argue that in addition to gaseous products generated by the "transient" carbon-oxygen surface intermediates, the decomposition of the "stable" carbon-oxygen complex also contributes to gasification. The reaction rate of the samples with oxygen can be described by:

$$\frac{-dP_{O_2}}{dt} = k_e (P_{O_2}) (UASA) + k_b (P_{O_2})(TSA) \qquad (7)$$

Where k_e and k_b represent the reaction rate constants for attack at the edge and basal plane carbon atoms, respectively. If $k_e >> k_b$, upon some activation by carbon to produce a large amount of ASA, the first term of the above equation dominates.

Su and Perlmutter (18) considered that the rate constants for char oxidation cannot be described based solely on UASA. According to these authors, all surface (stable or transient oxygen-complex) sites are important for coal char. Coal chars are more disordered than the graphon studied by Laine

(whose surface is composed mainly of unreactive basal planes with very few edge sites). While Laine et al. (4) proposed that deposited oxygen tend to retard reaction, we note in this study that the reactivity was highest when OCC (unoccupied active surface area) was very low. This suggests that the stable complexes may play an important role for char oxidation, especially the chars that are highly amorphous. Keeping this in mind, Su and Perlmutter (18) proposed the following elementary reactions:

$$2C + O_2 \underset{k_{a'}}{\overset{k_a}{\rightleftarrows}} 2C(O) \quad (8)$$

$$C(O) + O_2 \xrightarrow{k_d} CO, CO_2 \quad (9)$$

$$C + O_2 \xrightarrow{k_b} CO, CO_2 \quad (10)$$

k_a = rate constant for oxygen adsorption on carbon.
$k_{a'}$ = rate constant for reversible desorption.
k_d = rate constant for oxygen decomposition on char.
k_b = rate constant for direct burnoff.

The mechanism proposed by Su and Perlmutter (18) emphasizes the importance of stable sites in determining the reactivity of carbon-oxygen reaction. The present study suggests that the mechanism developed by Laine, et al., is not directly applicable for the low-temperature char used in this investigation.

The results shown in Figure 3 suggest that there may be three competing phenomena related to the change of OCC during char burnoff. During the early stage of char burnoff, the only active sites available for chemisorption are those that present on the char surface. These char active sites form stable C-O complexes by chemisorption, but not all sites undergo decomposition at the reaction temperature of 400°C. Thus, the inventory of unoccupied active sites, is greatly reduced during the initial stages of char oxidation by the formation of stable carbon-oxygen complexes. Our unpublished results showed that as oxygen was introduced at 400°C, the sample showed a significantly rapid weight gain. Nonisothermal heating in air of coal chars, which were prepared from coals of various ranks, also showed the significant increase in sample weight at various temperature ranges, depending on the coal rank. These results suggest the formation of stable C-O surface complexes that would occupy a significant amount of active sites. Guerin et al. (22), Floess et al. (20), and Lizzio et al. (19) have recently made similar observations. As the char continues to burn, a competing process, the opening of fresh sites previously closed that reside on micropore walls, plays the dominant role in increasing the amount of active sites. For a char burnoff between 35 and 65 percent, micropores in the inner core of the char may open up to expose more chemisorption sites to the bulk gas phase. At 55-percent burnoff, the active surface area reaches its maximum, indicating that the accessibility of unoccupied active surface area caused by opening of previously closed pore also reaches its maximum. As the walls between existing pores are burned away, the total number of open pores, as well as active sites, start to decrease. Beyond 65-percent burnoff, the

total availability of active sites decreases. At still higher burnoff (e.g., 85-percent burnoff) the amount of OCC is reduced to its initial amount of about 200 m^2/g.

In summary, the measured oxygen chemisorption capacity can be explained by three competing mechanisms. This study provides credence to the hypothesis proposed by Chornet et al (15) (at least the second and third stages of the proposed reaction schemes seem to follow the events observed in this study). The competing events proposed in this study, however, require additional validation perhaps by measurements of the total surface area of the char at various levels of burnoff. Furthermore, significance of measured oxygen chemisorption capacity and the role of stable and unstable oxygen-carbon complexes on the reactivity of char at various burnoff levels warrants further investigation.

SUMMARY AND CONCLUSIONS

The results of this study demonstrate that the conventionally defined unoccupied active surface area, as determined by oxygen chemisorption capacity at various levels of burnoff, does not seem to strictly correlate with the reactivity rate at various levels of burnoffs. This study suggests that stable sites may play a key role in reactivity, but their exact role at this stage of investigating is only speculative. The observed phenomenological changes in the measured OCC (active surface area not occupied by stable sites), as determined by oxygen chemisorption, at various levels of burnoff have been explained in terms of three competing mechanisms: (a) depletion of active sites available on the char surface caused by formation of a stable C-O complex, (b) increase of nascent active sites because of pore opening, and (c) decrease of OCC in the final stage of burnoff because of pore wall burnoff. The normalized reaction rate, based on a 10- to 70-percent burnoff time for different reaction temperatures, resulted in a single characteristic curve for a given type of char that was reacted at any reaction temperature. This finding suggests that the different reference times used widely in the literature do not necessarily signify parameters of fundamental importance.

ACKNOWLEDGEMENTS

The author thanks Dr. P. Weiber of METC for his comments in this study. A. Lui of EG&G helped plotting the data shown in Figure 2. Funding for this work was provided by the U.S. Department of Energy, Assistant Secretary for Fossil Energy, Office of Coal Utilization, Advanced Conversion, and Gasification.

REFERENCES

1a. Khan, M. R. "Significance of Char Active Surface Area for Appraising the Reactivity of Low- and High-Temperature Chars," Fuel, 1987, 66, (12), 1626.

1b. Khan, M. R. Fuel Science and Technology International, Vol. 5, No. 2. pp. 185-231.

2a. Laurendeau, N. Proj. Energy Comb. Sci. Vol. 4, pp. 221-270.

2b. Ismail, I. M. K. Carbon, 1987, 25, (5), 653-662.

3. Walker, Jr., P. L. Fuel, 1981, 60, (9), 801.

4. Laine, N. R., Vastola, F. J., and Walker, P. L., Jr. J. Phys. Chem., 1963, 67, 2030.

5. Radovic, L. R., Walker, P. L., Jr., and Jenkins, R. G. Fuel, 1983, 62, (7), 849.

6. Tong, S. B., Pareja, P., and Back, M. H. Carbon, 1982, 20, (3), 191.

7. Causton, P., and McEnaney, B. Fuel, 1985, 64, (10), 1447.

8. Ranish, J. M., and Walker, P. L., Jr. Preprints of Papers Presented at the 194th National Meeting, New Orleans, Louisiana, August 31-September 4, 1987, Div. Fuel Chem., ACS, 1987, 32, (4), 132.

9. Jenkins, R. G., and Piotrowski, A. Preprints of Papers Presented at the 194th National Meeting, New Orleans, Louisiana, August 31-September 4, 1987, Div. Fuel Chem., ACS, 1987, 32, (4), 147.

10. Vastola, F. J., Hart, P. J., and Walker, P. L., Jr. Carbon, 1964, 2, 65.

11. Hart, P. J., Vastola, F. J., and Walker, P. L., Jr. Carbon, 1967, 5, 363.

12. Lussow, R. O., Vastola, F. J., and Walker, P. L., Jr. Carbon, 1967, 5, 591.

13. Bansal, R. C., Vastola, F. J., and Walker, P. L., Jr. J. Colloid Interface Sci., 1970, 32, (2), 187.

14. Phillips, R., Vastola, F. J., and Walker, P. L., Jr. Carbon, 1970, 8, 197.

15. Chornet, E., Baldasano, J. M., and Tarki, H. T. Fuel, 1979, 58, (5), 385.

16. Mahajan, O. P., Yarzab, R., and Walker, P. L., Jr. Fuel, 1978, 57, (10), 643.

17. Solomon, P. R., Serio, M. A., and Heninger, S. G. ACS Div. Chem. Prepr., 1986, 31, (3), 200.

18. Su, J-L., and Perlmutter, D. D. AIChE J., 1985, 31, (6), 973.

19. Lizzio, A. A., Piotrowski, A., and Radovic, L. R. submitted to Fuel, 1988.

20. Floess, J. K., Longwell, J. P., and Sarofim, A. F. Energy and Fuels, 1988, 2, 18-26.

21a. Simons, G. A. Fuel, 1980, 59, (2), 143.

21b. Simons, G. A. Combustion Science and Technology, 1979, 19, 227.

22. Guerin, H., Siemieniewska, T., Grillet, Y., and Francois, M. Carbon, 1970, 8, 727.

23. Taylor, R. L., and Walker, P. L., Jr. Extended Abstracts, 15th Biennial Conference on Carbon, Philadelphia, Pennsylvania, 1981, 437.

19B:10-19-87:ds:5a

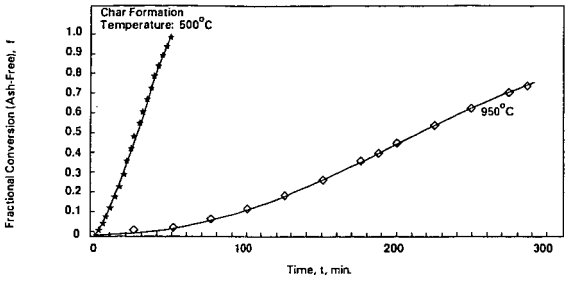

Figure 1. Fractional Burnoff Curves for Chars Prepared from Pittsburgh No. 8 Coal at 500° and 950°C; Burnoff Temperature 400°C

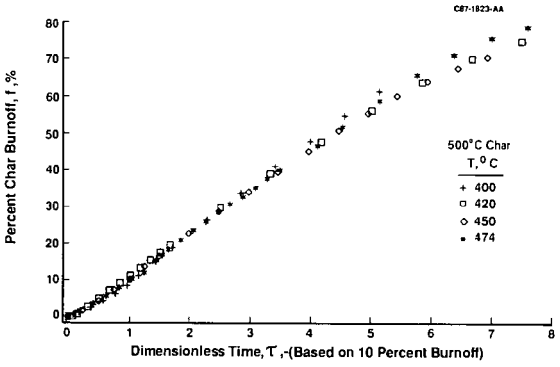

Figure 2a. Normalized Burnoff Curves for 500°C Char Oxidized at 400°, 420°, 450°, and 474°C

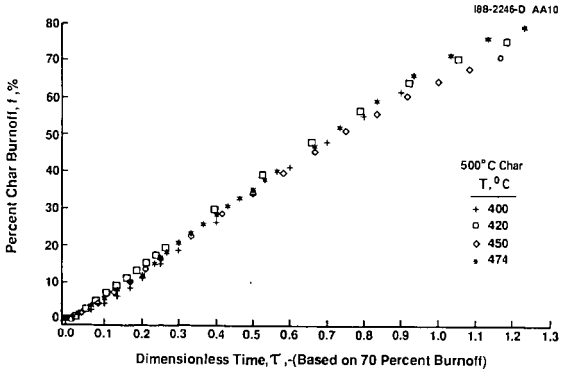

Figure 2b. Normalized Burnoff Curves for 500°C Char Oxidized at 400°, 420°, 450°, and 474°C

I88-2246-A AA10

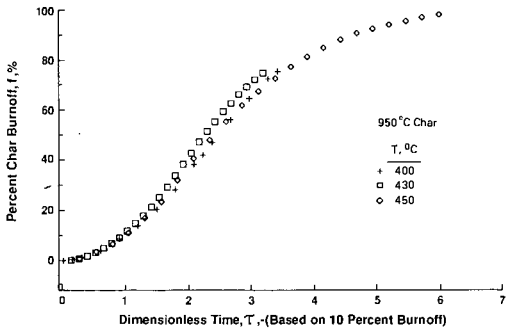

Figure 2c. Normalized Burnoff Curves for 950°C Char Oxidized at 400°, 430°, and 450°C

I88-2246-C AA10

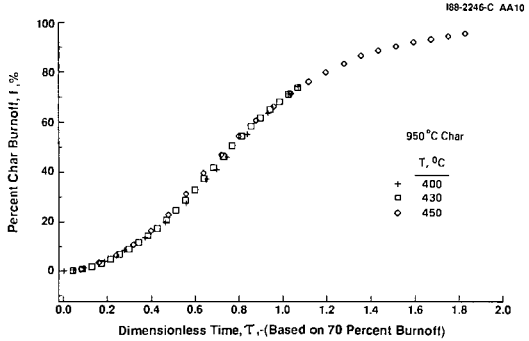

Figure 2d. Normalized Burnoff Curves for 950°C Char Oxidized at 400°, 430°, and 450°C

I88-2246-B AA10

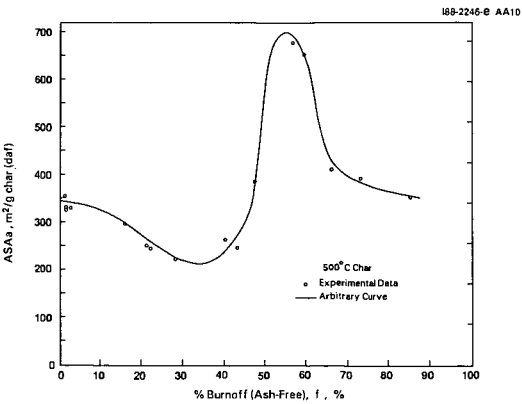

Figure 3. Changes in the Measured Active Surface Area (ASA) as Determined by Oxygen Chemisorption at Different Burnoff Levels of 500° C Char (Oxidized at 400° C)

C87-1823-HH

A NEW DISCRETE SIMULATION METHOD FOR MODELING CHAR GASIFICATION IN THE DIFFUSION-CONTROLLED REGIME

Kyriacos Zygourakis
Department of Chemical Engineering
Rice University
Houston, TX 77251-1892

ABSTRACT

Cellular automata and discrete iterations are employed to develop a new simulation method for gas-solid reactions. This approach overcomes many of the limitations of earlier models since it can handle heterogeneous systems with multiple porous reactants and arbitrary pore/solid geometries. The new models are used to simulate the gasification of porous char particles under conditions leading to strong intraparticle diffusional limitations and to low utilization of the micropores. In order to accurately account for the effects of the macropore structure on char reactivity, the new models employ computational grids obtained by digitizing images of actual char particle cross-sections using an optical microscope equipped with a video camera and an image processing computer. Simulation results are presented from multiple runs performed on several char samples that were prepared in our laboratory by pyrolyzing two parent coals under various operating conditions. Model predictions are compared and analyzed in order to elucidate the effects of the macropore structure on the gasification rates and particle burn-out times.

MODEL DEVELOPMENT

This study will consider a porous solid that reacts with one or more gaseous reactants to produce one or more gaseous products. Thus, the developed model can be applied to all the important coal gasification and combustion reactions.

Discrete models employ rectangular arrays of usually square cells to simulate the temporal evolution of pore structures in reacting systems. Our earlier discrete models (Sandmann and Zygourakis, 1986) defined the pores of a solid reactant (char) by randomly distributing on the grid overlapping *regular geometrical entities* (circles, spheres or cylinders) of a given size distribution. Direct microscopic measurements, however, revealed that char particles exhibit highly irregular pore structures (Zygourakis and Glass, 1988; Zygourakis, 1988).

Cellular Arrays and Reaction Rules

A new discrete simulation approach was developed to overcome the computational complexities introduced when considering heterogeneous reactions in system with arbitrary pore/solid geometries and multiple porous reactants. The new approach is based on ***cellular automata*** and ***discrete iterations***. The evolving pore structure of multicomponent systems is again modeled on rectangular arrays of cells. Each cell can exist in one of several possible states. It can represent, for example, a small volume element of either solid reactant, a pore that is accessible to the gaseous reactants etc.

The important thing to notice about our simulations approach is that the initial configurations of the cellular arrays are obtained ***directly from the digitized images of actual char particle cross-sections***. For example, Fig. 1A is a 1024x1040 binary image of a char particle cross-section. Black pixels correspond to the char matrix, while the particle exterior and the interior macropores are denoted by white.

The number of possible states for each cell depends on the assumed reaction

regime. This study will consider the following two limiting cases of reaction regimes.

Regime A: When there are no diffusional limitations in the macropores, the entire surface area associated with the macropores is available for reaction. Then each cell of our computational grid can exist in one of two possible states: it can represent a small volume element of either solid reactant or pore void. An initial computational grid for this regime is shown in Fig. 1A. The evolution of the pore structure is modeled by updating the initial cellular array at equally spaced time instants $t^1, t^2, \ldots, t^r, t^{r+1}, \ldots$ as follows: *If at time t^r a solid reactant (black) cell is adjacent to one or more gaseous reactant (white) cells, then this solid cell may be changed to a pore void cell or* ***reacted*** at the next *time level $t^{r+1} = t^r + \Delta t$*. The solid cells are reacted according to a probabilistic algorithm that guarantees isotropic consumption of the solid reactant. This algorithm erodes a single layer of pixels from the entire surface area exposed to gaseous reactants during each iteration step Δt. Figs. 1B and 1C show the computational grid of Fig. 1A after 10 and 16 iteration steps that correspond to solid conversions of 24.9% and 38.4%. Fig. 1D shows the temporal evolution of the predicted reaction rate as a function of the number of iterations.

Regime B: In this regime, only the surface area directly accessible to reactants from the irregular particle exterior participates in the reaction. Internal macropores are not initially accessible to the gaseous reactants. When the reaction front "opens" these interior pores, however, their surface area becomes available for reaction. These rules are implemented by allowing each cell of the computational grid to exist in one of three possible states (see Fig. 2A): it can be a solid reactant cell (black), a cell occupied by gaseous reactants or "open pore cell" (white) or a cell belonging to a "closed macropore" (grey). The initial cellular array is updated according to the following rules: ***(1)*** A solid reactant (black) cell may "react" (changing its state to white), if its immediate neighborhood contains one or more gaseous reactant (white) cells; ***(2)*** A solid reactant (black) cell will not change its state, if it is surrounded only by solid (black) or "closed pore" (grey) cells; ***(3)*** If "closed pore" (grey) cells get exposed to gaseous reactant (white) cells, their state may change to gaseous reactant (white). Figs. 2B and 2C show the configuration of the cellular array at two different iteration steps and Fig. 2D again shows the evolution of the predicted reaction rate. In general, gaseous reactant cells "consume" solid or closed pore cells at different rates. These rates can be appropriately adjusted to account for different degrees of diffusional limitations in the macropores opening up for reaction.

Estimating Reaction Rates from Discrete Simulations

The simulation results can be related to experimental gasification data as follows. If m(t) is the mass of solid remaining at time t, the specific rate R_m of the heterogeneous reaction can be expressed as

$$R_m \equiv \frac{1}{m(t)} \frac{dm}{dt} = S_g(X)\ \mathcal{R}_s(c,T;a) \qquad (1)$$

where S_g is the ***specific pore surface area available for reaction*** (expressed in m^2 of surface area per kg of solid), $\mathcal{R}_s(c,T;a)$ is the intrinsic reaction rate expressed in (kg of solid)/(s)(m^2 of surface area), c denotes the gaseous reactant concentrations, T is the temperature and a(X) is a measure of the surface activity. Since the porous solid is consumed during the reaction, the surface area S_g changes drastically with the solid conversion X defined by

$$X = \frac{m_o - m(t)}{m_o} \qquad (2)$$

where m_o is the mass of the unreacted solid. Intraparticle diffusional limitations are accounted by Eq. (2), since such limitations (in the micropores, for

example) may dramatically decrease the total surface area S_g available for reaction.

Let dV be the volume of solid consumed by the heterogeneous reaction over a time period equal to dt. Then

$$\rho_s \frac{dV}{dt} = m(t)\ S_g\ \Re_s(c,T;a) \tag{3}$$

where ρ_s is the density of the solid reactant. If the reaction rate is uniform over the entire surface area S_g, a layer of solid with uniform thickness dz will be consumed over the time period dt. Thus, $dV = S_g\ m(t)\ dz$ and Eq. (3) becomes

$$\frac{dz}{dt} = \frac{\Re_s(c,T;a)}{\rho_s} \tag{4}$$

The previous equations can be used to normalize the reaction rates predicted by the discrete models. At every simulation step, we erode a single layer of pixels from the solid surface area available for reaction. Thus, every erosion step corresponds to a time interval Δt that equals the time required to convert a solid layer of uniform thickness Δz, where Δz is the pixel size. From Eq. (4)

$$\frac{\Delta z}{\Delta t} = \frac{\Re_s(c,T;a)}{\rho_s} \tag{5}$$

and if two simulations are carried out on images with different pixel sizes Δz and Δz^*, their time steps will be related according to the formula

$$\frac{\Delta z}{\Delta t} = \frac{\Delta z^*}{\Delta t^*} \tag{6}$$

The measured reaction rates are most often normalized with respect to the mass m_o of the unreacted solid or

$$R_o \equiv \frac{1}{m_o}\frac{dm}{dt} = (1-X)\ R_m \tag{7}$$

Let now N_o be the number of solid reactant pixels on the initial computational grid and let $(\Delta N)^r$ be the number of solid pixels that react in the time interval $[t^r, t^{r+1}]$. The specific rate R_o^r for this step can be computed as

$$R_o^r\ \Delta t = \frac{(\Delta N)^r}{N_o} \tag{8}$$

Let Δz be the pixel size (in μm) for this image and let Δt^* be the time required to react a layer of solid with uniform thickness equal to $\Delta z^* = 1$ μm. Eqs. (8) and (6) yield

$$R_o^r\ \Delta t^* = \frac{(\Delta N)^r}{N_o}\ \frac{\Delta z^*}{\Delta z} \tag{9}$$

Thus, Eq. (9) provides specific reaction rates that are independent of the pixel size of the digitized images used in the simulations.

Using Eq. (5), the value of Δt^* can be computed from the value of the intrinsic rate $\Re_s(c,T;a)$ at the appropriate conditions. Most often, however, the reactivity data obtained at various temperatures and reactant concentrations are normalized so as to obtain **master curves** that yield (within experimental error) the dependence of the active surface area on conversion. Such master curves can be obtained directly from the simulations by plotting the dimensionless rate $R_e^r \equiv R_o^r\ \Delta t^*$ vs. either the conversion or a dimensionless time θ where

$$\theta = \frac{t}{\Delta t^*} = \frac{t\ \Re_s(c,T;a)}{\Delta z^*\ \rho_s} \tag{10}$$

The predictions of observed reaction rates assume, of course, that the surface activity and the intrinsic reaction rate $\Re_s$ do not change appreciably with conversion. Since several simulations are performed for each char sample, the

average rate R_e^r is computed by the formula

$$R_e^r = \frac{\sum (\Delta N)^r}{\sum N_o} \frac{\Delta x^*}{\Delta x} \qquad (11)$$

where the summations are taken over all simulation runs performed for different particle cross-sections from the same char sample. The reaction rates computed according to Eq. (11) can be directly compared regardless of the amount of solid in each sample or the magnification used when acquiring the digitized images.

The simulations described here are performed on two-dimensional cellular arrays that are discrete approximations of cross-sections of actual char particles. At each iteration step, heterogeneous reactions occur at the boundaries (perimeter) of the two-dimensional pore profiles (see Figs. 1 and 2). Results from ***two-dimensional simulations***, however, can be used to obtain accurate ***estimates*** of reaction rates occurring on our ***three-dimensional structures***. If we assume that the cross-sections used for our simulations form a "random plane section" through our population of char particles, unbiased estimators of the macroporosity ε and of the macropore surface density S_v (in (cm^2 pore surface)/(cm^3 particle)) are given (Weibel, 1980) by

$$\varepsilon = \frac{A_a}{A_c} \qquad S_v = \frac{1}{4\pi} \frac{B_a}{A_c} \qquad (12)$$

where A_a is the total area of pore profiles, B_a is the total pore profile boundary length and A_c is the total area of particle cross-sections. Note that S_v can be estimated from two-dimensional sections ***without any restricting assumptions concerning the geometrical shape of the pores*** (DeHoff, 1983). The three primary quantities A_a, A_c and B_a can be easily obtained from the particle cross-sections via image processing techniques, and the total specific macropore surface area S_t (expressed in m^2 per kg of solid) can be easily computed as

$$S_t = \frac{S_v}{(1-\varepsilon)\ \rho_s} \qquad (14)$$

When reaction takes place in Regime A, there are no diffusional limitations in the macropores and the entire macropore surface area reacts at the same rate ($S_g = S_t$). If we assume that the evolving cross-sections continue to constitute "random sections" for our char particle population, the discrete simulations provide accurate ***estimates*** of the changing surface area of the ***three-dimensional macropores*** and, consequently, of the temporal evolution of reaction rates in Regime A (see Eqs. 1 or 7). Although these arguments do not hold in the general case of reaction in Regime B (where the internal macropores are assumed to be "closed" and $S_g \neq S_t$), approximate estimates of reaction rates can be obtained if we assume that the internal pores for any cross-section do not become available for reaction due to burn-through occurring at planes above or below the studied one. Although this assumption can be easily relaxed in our discrete models, such an extension of the models would require information about the connectivity of the three-dimensional macropores. Such structural information is not currently available.

RESULTS AND DISCUSSION

An earlier study (Zygourakis, 1988) presented the results from microscopic investigations on the macropore structure of coal chars prepared under different pyrolysis conditions. Char particles collected from several runs at each set of conditions were embedded in an epoxy-resin block, and one side of the block was polished to reveal random cross-sections. Digitized images of particle cross-sections were then acquired and segmented on an image processing computer to identify the char matrix and macropores with diameter greater than 1 μm.

The original binary images had a resolution of 640x480 pixels. Many char samples, however, exhibited macropores with very thin walls that were consumed in only a few iterations. In order to increase the accuracy of the simulations, each 640x480 image was first magnified by a factor of 4. The magnified 2560x1920 images were smoothed to remove the edge "jaggedness" that is introduced by simple magnification operations. Several runs were also carried out by magnifying the original images by a factor of 8 and smoothing them. Results obtained from simulations with 5120x3840 images showed only small differences from those obtained from simulations with 2560x1920 images. For each char sample, 48 runs were performed with different particle cross-sections and the results were averaged as previously discussed.

We simulated first a gas-solid reaction taking place in Regime A, where there are no diffusional limitations in the macropores and the entire macropore surface area reacts at the same rate. Fig. 3 presents the reactivity patterns predicted for 4 chars produced from an Illinois #6 coal at different pyrolysis heating rates. The model predictions reflect the wide differences in the pore structure of these chars (Zygourakis, 1988). All chars exhibit an initial increase in reactivity caused by macropore growth. Such a behavior cannot be predicted by shrinking-core models. Since the chars produced at high heating rates (10 and 1000 °C/s) have almost exclusively large thin-walled cavities (ibid.), the predicted rates drop dramatically when the thin walls separating the macropores are consumed. The rate vs. conversion patterns exhibit a small maximum that is shifted towards higher conversion levels for the chars produced at high heating rates. Fig. 4 shows the predicted reactivity behavior for three chars produced from different size fractions of Illinois #6 coal particles at a pyrolysis heating rate of 10 °C/s. Small coal particle sizes lead to chars with larger macropore surface areas and, hence, with higher reactivity. These high reaction rates fall rapidly, however, and the maximum in the rate vs. conversion pattern shifts towards lower conversions. Fig. 5 shows the predicted reactivity behavior for two chars produced from a lignite coal at 0.1 and 1000 °C/s. Small differences in char reactivity can be seen from these graphs, an observation consistent with the pyrolysis mechanism and the pore structure of these chars.

Fig. 6 presents simulation results obtained when 4 Illinois #6 chars (see Fig. 3) react in Regime B, where the internal macropores are not initially accessible to the gaseous reactants. Due to the progressive opening of internal macropores, the reactivity of chars produced at low pyrolysis heating rates (e.g. 0.1 °C/s) remains high even at fairly large values of conversion. The reactivity patterns of chars produced at high pyrolysis rates (e.g. 1000 °C/s) show several local maxima that correspond to the opening up of internal large macropores and of the smaller secondary vesicles formed in the walls separating the larger macropores (see Zygourakis, 1988). Such jumps in the reaction rate have been observed during single-particle gasification experiments (Sundback et. al., 1984).

ACKNOWLEDGMENT

This work was partially supported by the Department of Energy under the contract DE-FG22-87PC79930.

REFERENCES

DeHoff, R.T., *J. Microscopy*, ***131***, 259 (1983).
Sandmann, C.W. and Zygourakis, K., *Chem. Eng. Sci.*, ***41***, 733 (1986).
Sundback, C.A., Beer, J.M. and Sarofim, A.F., *Procs. 20th International Symposium on Combustion*, p. 1495, Ann Arbor, Michigan, August 12-17 (1984).
Weibel, E.R., *Stereological Methods*, vol. ***2***, Academic Press (1980).
Zygourakis, K. and Glass, M.W., *Chem. Eng. Commun.*, ***70***, 39 (1988).
Zygourakis, K., *ACS Div. Fuel Chem. Preprints*, ***33(4)***, 951 (1988).

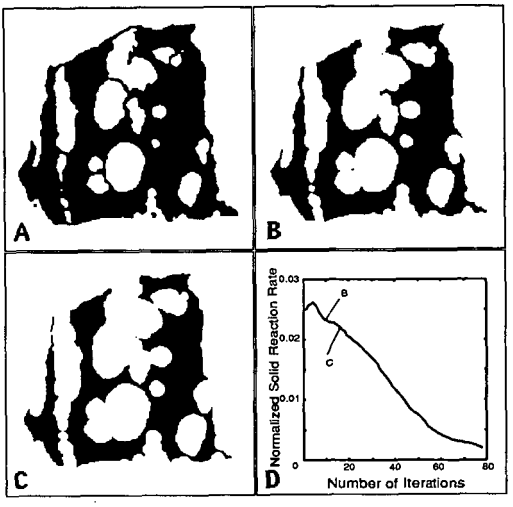

Figure 1: Binary images showing the computational grids at three conversion levels (A: X=0.00, B: X=24.9%, C: X=38.4%) and the evolution of normalized reaction rates for a simulation in reaction Regime A (two-state computational cells).

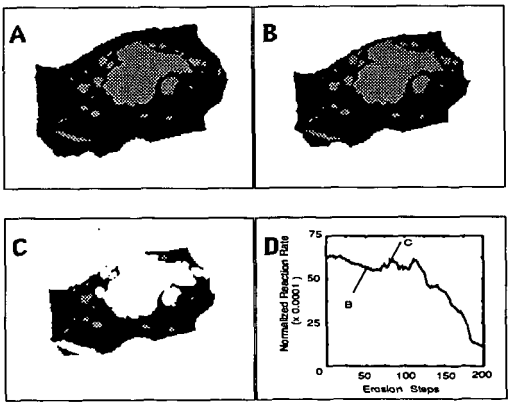

Figure 2: Binary images showing the computational grids at three conversion levels (A: X=0.00, B: X=30.9%, C: X=49.1%) and the evolution of normalized reaction rates for a simulation in reaction Regime B (three-state computational cells).

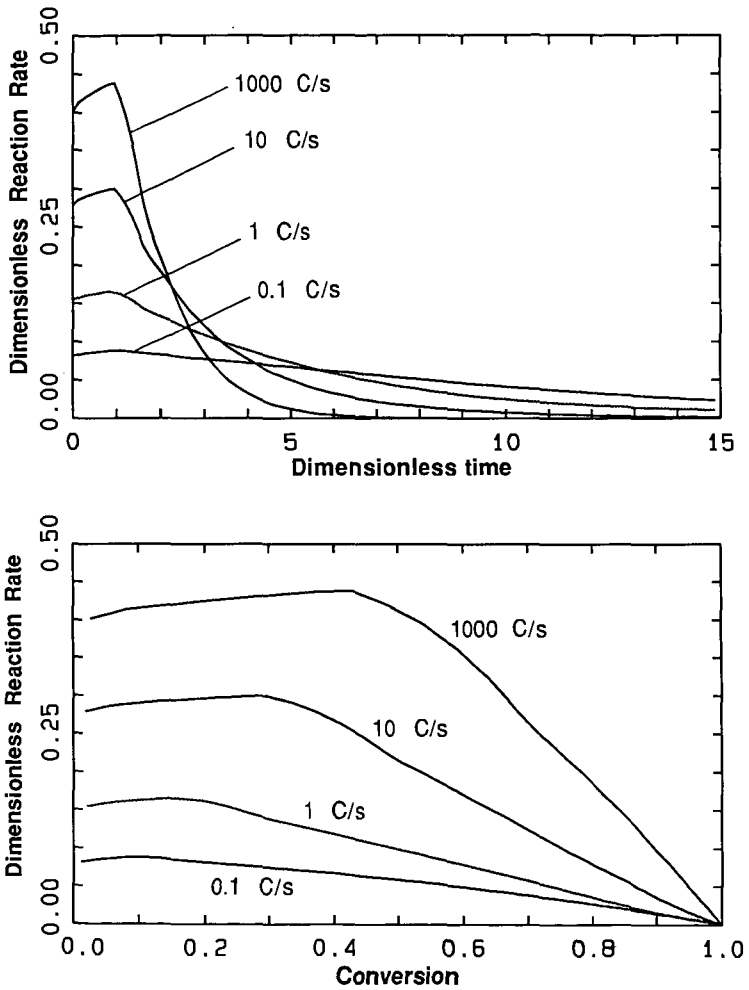

Figure 3: Reactivity patterns predicted for reaction in Regime A of four Illinois #6 chars produced at different pyrolysis heating rates (Coal particle size: 50-60 mesh). Each curve is the average computed from 48 runs with different particle cross-sections.

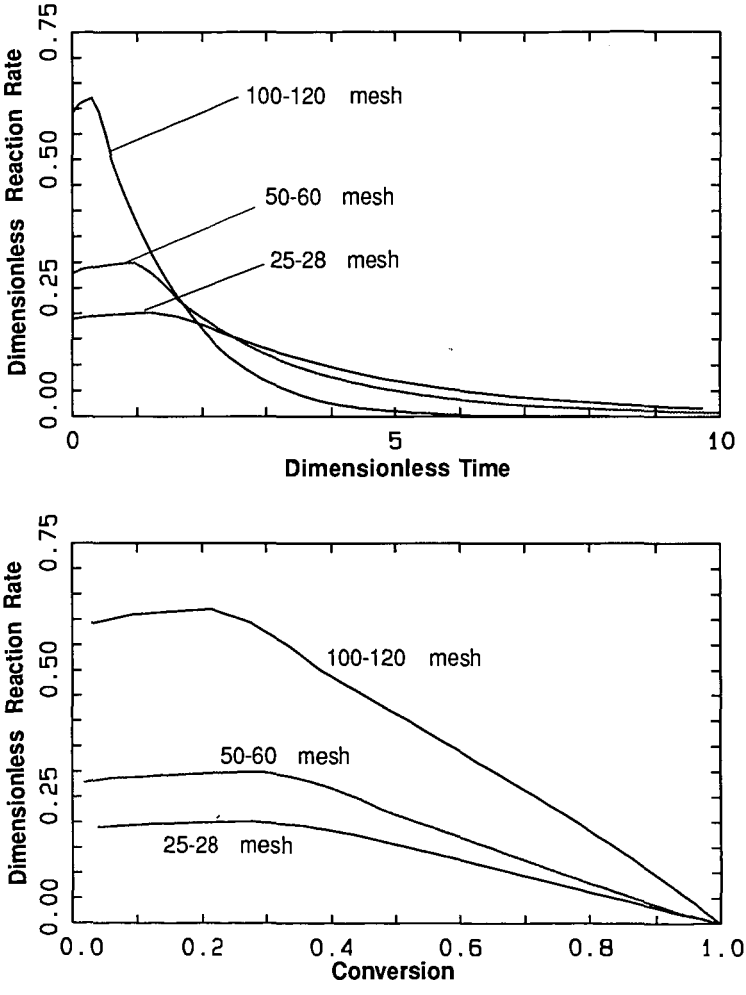

Figure 4: Reactivity patterns predicted for reaction in Regime A of three Illinois #6 chars produced from different coal particle size fractions (Pyrolysis heating rate: 10 °C/s). Each curve is the average computed from 48 runs with different particle cross-sections.

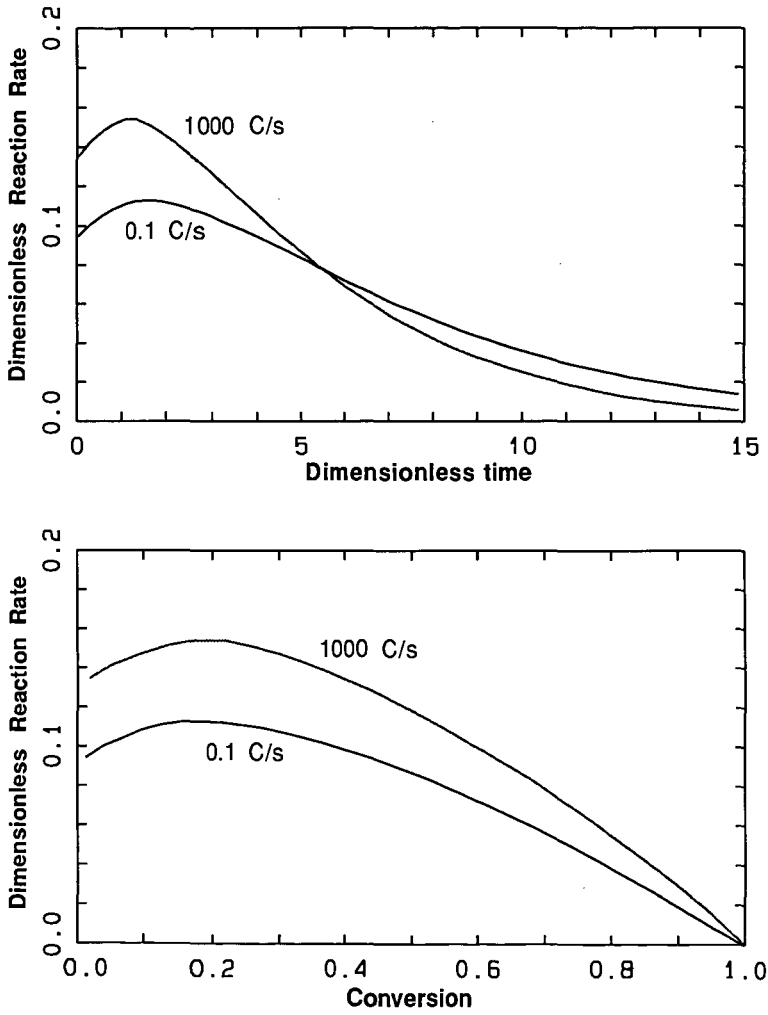

Figure 5: Reactivity patterns predicted for reaction in Regime A of two lignite chars produced at different pyrolysis heating rates (Coal particle size: 50-60 mesh). Each curve is the average computed from 48 runs with different particle cross-sections.

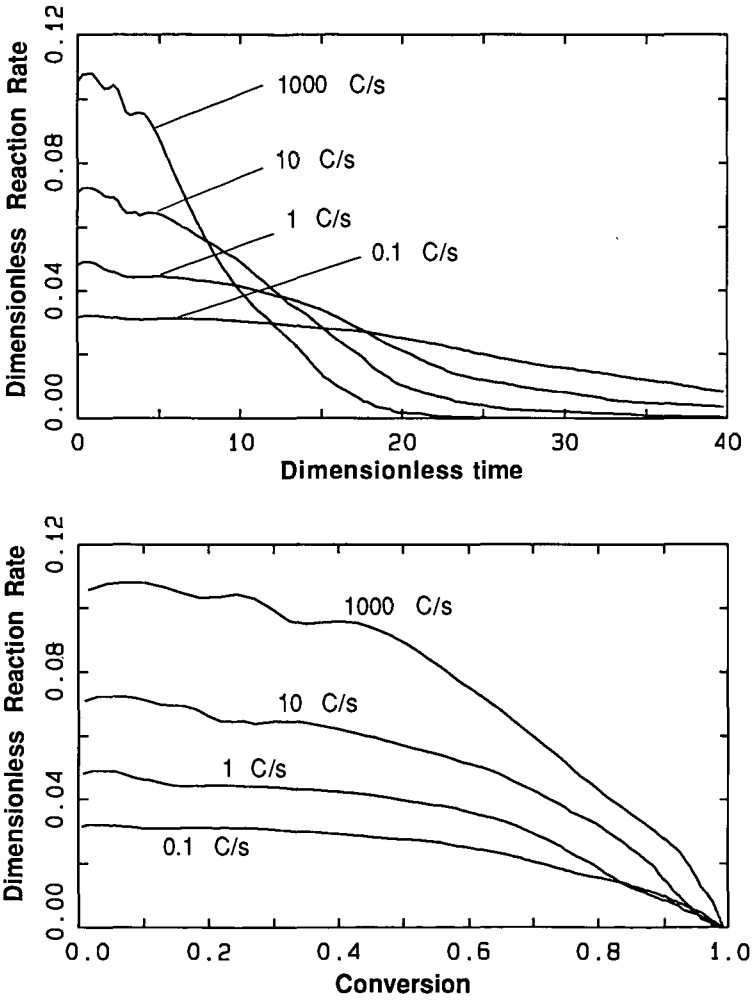

Figure 6: Reactivity patterns predicted for reaction in Regime B of four Illinois #6 chars produced at different pyrolysis heating rates (Coal particle size: 50-60 mesh). Each curve is the average computed from 48 runs with different particle cross-sections.

EFFECT OF THE POROUS STRUCTURE OF CHAR ON THE RATE OF GASIFICATION

E. Hampartsoumian, M. Pourkashanian, D.T. Trangmar and A. Williams
Department of Fuel and Energy, Leeds University
Leeds, LS2 9JT

INTRODUCTION

A detailed understanding of the reactions kinetic of coal/char gasification is required for the successful design and construction of coal gasifiers. The reactor design criteria are largely dependent on the coal/char reactivity with reactant gases, such as carbon dioxide, steam and hydrogen. Extensive studies(1-3) have been carried out to determine this for different experimental conditions (eg. pressure, temperature or reactant gases concentration). However most of these studies have concentrated either on the variation of overall reaction rate and for different feedstocks or on establishing the fundamental mechanisms of the reaction(4).

The experimental and theoretical analysis of solid/gas reaction rate is further complicated by shrinkage, mass transfer and changing surface area and porosity of the solid during reaction. The influence of the progressive evolution of the solid pore structure on the overall reactivity depends on whether the reaction rate is controlled by external diffusion only, by chemical kinetics, or by a combination of these two limits. Because of the continuous changes in the pore structure, simultaneous reactivity and pore structure studies are needed to obtain a realistic solid/gas reaction rate. In addition, the estimation of the effective diffusivity of the porous solid can provide information on the evaluation and importance of the intra particle diffusion limitation and therefore the influence of mass transfer on the overall reaction rate can be obtained.

The major objective of this work is to utilize the effectiveness factor as a tool in the analysis of the kinetics of gasification of char with carbon dioxide using both an experimental and theoretical approach. This was accomplished by investigating the relationship between the effectiveness factor and the physical properties of coal/char (eg. porosity and density) during the gasification process. The overall reaction rates of two U.K coal derived chars were measured gravimetrically and the progressive changes in pore structure and the subsequent implications for the controlling mechanism investigated.

2. EXPERIMENTAL PROCEDURE

Two coals were sized to <90 μm and pyrolysed by passing through a rich methane/air flame (ϕ = 0.72). The coal particles were pyrolysed under rapid heating conditions ranging from 10^4-10^5 K/s and with temperatures approaching 2000 K. The char particles produced were collected after a total residence time of 180 - 200 ms. The proximate and ultimate analysis and the physical properties of the parent coals and chars used are shown in Table 1.

The N_2 and CO_2 surface areas of the samples were determined using a Quantisorb continuous flow analyser working with He/N_2 and He/CO_2 mixtures at 77 K. The percentage porosity of the samples were obtained from the measured apparent and

true densities of the chars. The values of true and apparent densities were obtained by He and Hg displacement techniques respectively.

Gasification experiments with CO_2 as a reactant gas were conducted over the temperature range 1023-1273 K following the experimental procedures outlined previously(5). A thermogravimetric reactor system was used to monitor the changes in the char mass by recording the sample weight and reaction temperature. In each run, a reactant gas mixture comprising of CO_2/N_2 was passed into the reactor containing around 3 mg of char particles placed as a single layer held on a screen pan. The reactivity experiments consisted of initially heating the char to the target temperature at a rate of 50°C/min in flowing nitrogen. The sample was then held at this temperature for 10 minutes and, after thermal equilibrium was established, the gas flow was switched to the reactant gases. In addition some reactant gas mixtures containing known concentrations of CO were also used in order to investigate CO inhibition of the char/carbon dioxide gasification reaction. The total gas flow rate was kept high enough so that the role of external mass transfer could be discounted as a possible rate limiting step.

Changes in physical properties of the char at different conversions were obtained by allowing the sample to react to target conversion and, at that point, replacing the flow of reactant gases by the nitrogen and allowing the reactor to cool to room temperature.

3. EXPERIMENTAL RESULTS AND DISCUSSION

(a) Reaction Kinetics:

The reaction of carbon with carbon dioxide can be expressed as:

$$CO_2 + C \underset{j_1}{\overset{i_1}{\rightleftharpoons}} CO + C_{(o)} \qquad (1)$$

where C_f and $C_{(o)}$ represent active site and a site possessing an oxygen atom. This reaction takes place at the surface of the carbon where carbon dioxide dissociates at an active site of the carbon surface releasing a molecule of carbon monoxide. This reaction is followed by the gasification of solid carbon to form a gas phase

$$C_{(o)} \xrightarrow{j_2} CO + n\,C_f \qquad (2)$$

The above chemical reactions are based on an oxygen exchange reaction mechanism. Previous studies(6-8) have shown that Langmuir-Hinshelwood theory can be used to treat the kinetics of C - CO_2 reaction. By applying a steady state assumption to $C_{(o)}$ and assuming that the number of free sites remain constant with burn off (n = 1), the overall rate of gasification can be shown as:

$$\text{Rate} = \frac{1}{w_o}\frac{dw}{dt} = \frac{k_1 P_{CO_2}}{1 + k_2 P_{CO} + k_3 P_{CO_2}} \qquad (3)$$

where the k's are generally a function of the rate constants for the elementary steps of reaction 1 and 2 and $k_1 = i_1$, $k_2 = j_1/j_2$ and $k_3 = i_1/j_2$. The initial

weight of the dry-ash free char is given by w_o and dw/dt is the average rate of weight loss. Equation 3 indicates that the presence of CO produced by the reactions 1 and 2 has the effect of retarding it (i.e. reaction j_1), therefore the retarding effect of CO was also investigated.

The equation 3 was solved by keeping the ratio of P_{CO}/P_{CO2} constant and varying P_{CO2}, i.e.

$$\frac{1}{R} = \frac{1}{k_1}\left(\frac{1}{P_{CO_2}}\right) + \left(\frac{k_2}{k_3}\right) \qquad (4)$$

From a plot of 1/R vs $1/P_{CO2}$ at a fixed temperature, values of k_1 and k_3 were obtained. The values of k_2 were evaluated by rearranging equation 3 and using the experimental data at varying CO - CO_2 concentrations. The calculated rate constants, k_1, k_2 and k_3 were plotted against 1/T as shown in Fig.1 for five of the reaction temperatures investigated. The experimental results indicate that the rate of oxygen exchange and carbon gasification increases with temperature in accordance with the change in their rate constant. Values for the activation energies (E) and pre-exponential factors (A) for the rate coefficient ratios are listed in Table 2. The equilibrium constant (K_{eq}) for the reaction (1) can be calculated from values of i and j, which is obtained from experimentally determined values of k_1, k_2 and k_3(7). The value of ΔH for reaction (1) obtained from thermochemical calculation is of order of 104 kJ. On the basis of an oxygen exchange mechanism, the heat of reaction for the first step of C - CO_2 reaction (i.e. reaction 1), was found to be 109 kJ/mole for char A and 120 kJ/mole for char B (endothermic). These values are larger than the calculated values, therefore indicating that the carbon oxygen bonded surface complex is an intermediate between single and double π bond but closer to that of double π bond.

From the values of activation energies (E_i, E_j) it can be concluded that the reaction leading to the presence of oxygen atom from CO_2 on the carbon surface requires more energy than its removal by CO.

In theory the values of k_2 and k_3, which are the intrinsic reaction rate ratios, should be independent of the char type at a given temperature. Similarly the values of E_{i1}, E_{j1} and E_{i2} should be independent of the type of char used. However, it is noted that the values of E_{i1}, E_{i1} and E_{i2} determined from equation 3 are influenced by the char type. This variation in the activation energies can be related to few factors such as (i) the presence of the inorganic impurities in the char which will influence the reaction rate by acting as a catalyst and (ii) the variation in the pore growth and coalescence during the gasification process which will influence the intraparticle diffusional limitations.

(b) Effects of pore diffusion:

The overall rate of reaction on a porous char depends upon the extent of the internal surface and the size of the pores comprising this surface. In addition the pore structure of the char particles change during the gasification process. The quantitative analysis of the problem of pore diffusion of reactant gases coupled with the pore surface reaction was carried out by Thiele(9), where he introduced the concept of effectiveness factor (η). The effectiveness factor is a useful indicator of the amount of limitation due to boundary layer and in pore

diffusion. The effectiveness factor at any instant during the reaction is defined as

$$\eta = \frac{\text{overall reaction rate of particle}}{\text{reaction rate when reactant concentration throughout the particle were equal to that in free stream.}} \quad (5)$$

Solving equation 5 for spherical geometries which is modified to include overall fractional solid conversion term (x) gives:

$$\eta = (1\text{-}X) \left[\frac{3}{\phi_m} \right] \left[\frac{1}{\tanh \phi_m} - \frac{1}{\phi_m} \right] \quad (6)$$

where ϕ_m is the modified Thiele modulus. From the experimental results the initial modified Thiele modulus was calculated and the contribution of pore diffusion effect during the gasification process obtained. In order to investigate the influence of the pore diffusion, the observed fractional rate (dx/dt) for char B was plotted against 1/T at 30% carbon conversion as shown in Fig. 2. The results indicate that for the temperature range 1023-1173 K the plot is reasonably linear over the experimental points but at higher temperature the experimental values are below the line. The intraparticle diffusional limitation effect over the chemical reaction rate can be determined by calculation of the intrinsic chemical reaction rate [(dx/dt)/η] using the calculated effectiveness factor. Fig. 3 shows the plot of intrinsic chemical reaction rate against 1/T for the char B. Results indicate that all experimental points are on the straight line and therefore the effectiveness factor is used as a correction factor to eliminate the effect of the intraparticle diffusion at a region where the reaction rate is controlled by both chemical and mass diffusion.

The effectiveness factor at different carbon conversions can be predicted(10) from the values of relative physical and structural properties of char using the equation below:

$$\eta = (1\text{-}X)^{n/2} \; a^{-X/2} \left[\frac{(\rho_T^X/\rho_T^o)\, D_e}{(\rho_a^X/\rho_a^o)\, \theta^X/\theta^o} \right]^{0.5} \quad (7)$$

where ρ_a^o, ρ_T^o, ρ_a^X, ρ_T^X and θ are the initial apparent and true densities and apparent and true densities at different carbon conversion and porosity of char respectively. Note that n is proportional to the number of active sites and a is a constant related to the ratio of adsorption constant and an effective diffusivity of CO_2 (D_e). The predicted effectiveness factor was based on isothermal reaction with no fluid film diffusion resistance.

The predicted η values for char A were first plotted against carbon conversion as shown in Fig. 4. and then compared with the calculated values and the influence of a and n investigated. The limiting case (i.e. $a = 1$ and $n = 1$), assuming that all the active sites remain available for gasification process, are also shown in Fig. 4 as well as the the variation of porosity with carbon conversion. The best prediction of η was obtained when $a = 1$ and $n = 1.5$.

CONCLUSIONS

From the rate of reaction between porous chars and carbon dioxide, it can be concluded that two stage oxygen exchange mechanism holds. The L - H type rate expression are capable of representing the data in a temperature range of 1023 - 1223 K.

The effect of mass transfer on the rate of carbon-carbon dioxide reaction occurring in a porous char was analysed. Results indicate that intraparticle diffusional limitation becomes significant at $T \geq 1173$ K. The estimated effectiveness factor based on the variation of physical properties of char during the gasification process can be used to investigate the influence of the pore diffusion limiting of reactant gases at different experimental conditions.

REFERENCES

1. Laurendeau, N.M., Prog. Energy Combust. Sci., 4, p 221, 1978.

2. Mühlen, H.J., van Heek, K.H., and Juntgen, H., Fuel, 64, p 944, 1985.

3. Gadsby, J., Long, F.J., Sleightholm, P. and Sykes, K.W., Proc. R. Soc. A193, p 357, 1948.

4. Essenhigh, R.H., Chemistry of Coal Utilization, 2nd Suppl. Vol., (Ed. M.A. Elliott), Wiley, New York, p. 1153, 1980.

5. Hampartsoumian, E., Pourkashanian, M., Trangmar, D.T., Proceedings of the First Int. Conference on Gasification Status and Prospects, Institute of Energy, Harrogate U.K. 1988.

6. Freund, H., Fuel, 64, p 657, 1985.

7. Hampartsoumian, E., Pourkashanian, M., Trangmar, D.T. and Williams, A., paper submitted to Combustion and Flame, 1988.

8. Hampartsoumian, E., Pourkashanian, M., Trangmar, D.T. and Williams, A, Proceedings of the Carbon '88 Conference, Newcastle, UK, 1988.

9. Aris, R., Chem. Eng. Sci., 6, p 262, 1957.

10. Hampartsoumian, E., Pourkashanian, M. and Williams, A., Department of Fuel and Energy, University of Leeds, paper in preparation.

Table 1: Proximate, ultimate and physical properties of parent coals and produced chars.

	Coal A Markham-Main NCB Rank 702	Coal B Linby NCB Rank 800	Char A	Char B
Proximate Analysis (%)				
Moisture	5.88	8.4	2.67	4.02
Volatile matter	34.09	31.0	5.36	5.70
Ash	2.47	9.4	8.95	18.97
Fixed carbon	57.56	51.2	83.02	71.31
Ultimate Analysis (%)				
Carbon	81.12	79.80	89.38	89.14
Hydrogen	4.48	5.40	0.96	0.74
Nitrogen	1.67	1.61	1.62	1.85
Physical Properties				
True density (g/cm^3)	1.35	1.28	1.511	1.382
N_2 surface area (m^2/g)	11.94	14.07	34.56	28.13
Porosity %	18.50	16.80	57.	51.

Table 2: Arrhenius constants for the C - CO_2 reaction.

$k = A \exp(-E/RT)$ E = kJ/mole	Char A	Char B
k_1 ($g\ g^{-1}\ s^{-1}\ atm^{-1}$)	$4.26 \times 10^4 \exp(-187.1/RT)$	$8.32 \times 10^4 \exp(-177.7/RT)$
k_2 (atm^{-1})	$7.24 \times 10^{-6} \exp(138.2/RT)$	$2.91 \times 10^{-6} \exp(150.2/RT)$
k_3 (atm^{-1})	$6.45 \times 10^{-2} \exp(28.4/RT)$	$8.39 \times 10^{-2} \exp(30.1/RT)$
A_i ($g\ g^{-1}\ s^{-1}\ atm^{-1}$)	4.26×10^4	8.32×10^4
E_i (kJ mole)	187.1	177.7
A_{j1} ($g\ g^{-1}\ s^{-1}\ atm^{-1}$)	4.78	2.88
E_{j1} ($kJ\ mole^{-1}$)	77.3	57.6
A_{j2} ($g\ g^{-1}\ s^{-1}$)	6.45×10^5	9.91×10^5
E_{j2} ($kJ\ mole^{-1}$)	216.4	207.8
K_{eq}	$8.91 \times 10^3 \exp(-109.8/RT)$	$2.89 \times 10^4 \exp(-120.1/RT)$
ΔH ($kJ\ mole^{-1}$)	109.8	120.1

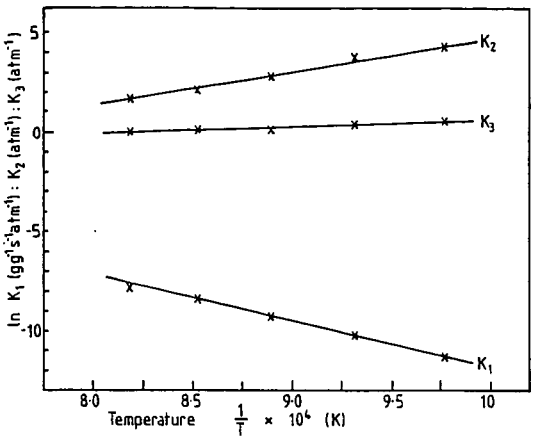

Fig. 1 Arrhenius plot of L-H equation constants for char A.

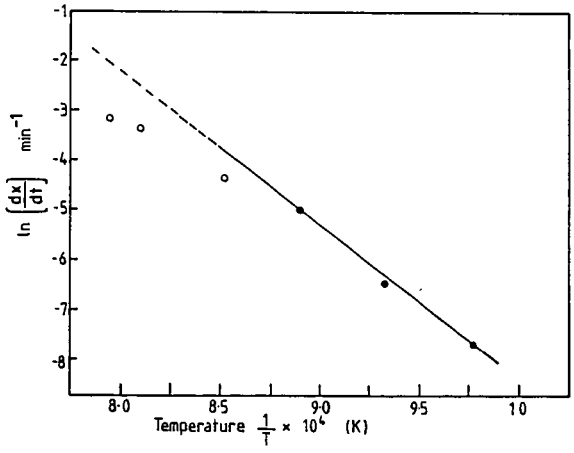

Fig.2 Variation of observed reaction rate with temperature for char B at X = 0.3.
● chemical reaction control, O intra-particle diffusion effect on overall rate.

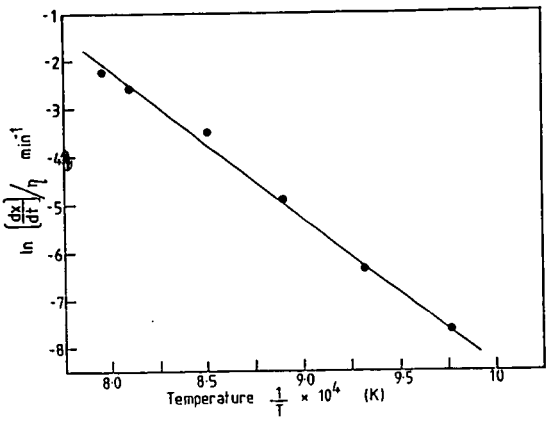

Fig.3 Variation of intrinsic chemical reaction rate with temperature for char B at X = 0.3.

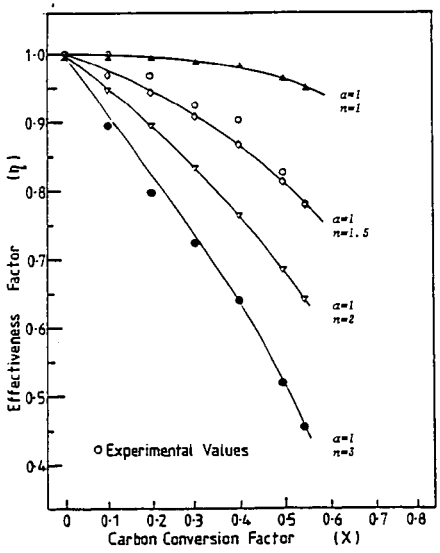

Fig.4 Comparison of predicted and experimentally obtained values of effectiveness factor for char A.

POROUS STRUCTURE AND REACTIVITY OF BROWN COAL HUMIC ACIDS CHARS OF DIFFERENT DEGREES OF DEMINERALIZATION

T.Siemieniewska, K.Tomków, A.Jankowska, M.Jasieńko, E.Broniek, J.Kaczmarczyk and A.Albiniak

Institute of Chemistry and Technology of Petroleum and Coal, Technical University, Gdańska 7/9, 50-344 Wrocław, POLAND

INTRODUCTION

Humic acids are the main constituent of brown coals and can be regarded as a model substance representing the organic matter of coals of low degree of coalification. Humic acids can be obtained with a much lower mineral matter content than that in the parent coals. They seem to be a suitable material for fundamental studies on pyrolysis and gasification of coals of low rank.

It is troublesome to obtain humic acids in a state of high purity. This research was carried out to evaluate the influence of the degree of demineralization of brown coal humic acids on their behaviour in the processes of carbonization and steam gasification, with particular attention to the development of their capillary structure.

EXPERIMENTAL

A Polish humodetrinitic brown coal (moisture=52.1%,raw; ash=9.5%, dry; carbon=70.8%,dry,ash-free; hydrogen=6.0%,dry,ash-free) was demineralized with dilute HCl. The demineralized brown coal contained 5.8,dry, of ash. Humic acids (HA) were obtained from this coal by alkaline extraction with 1% NaOH followed by precipitation with dilute HCl. The obtained HA gel contained 1.4%,dry, of ash. Further demineralization with HCl and mixtures of HCl and HF permitted to obtain HA with following ash contents (A^{d}_{HA}%,dry): 0.4, 0.18 and 0.07%. The obtained HA were designed, respectively, as $HA_{1.4}$, $HA_{0.4}$, $HA_{0.18}$ and $HA_{0.07}$. To the $HA_{0.18}$ gel calcium acetate was added to introduce 1 mmol of Ca per 1 g of organic substance of this HA. The obtained sample was designed as $HA_{0.18}$(Ca). The above mentioned HA were carbonized in a thermogravimetric apparatus (TG) at a heating rate of 5°C/min, in a stream of argon, to the desired heat treatment temperature (HTT). Example of designation of chars: $HA_{1.4}$ carbonized to HTT 900°C was designed as $HA_{1.4}$900. The gasification of chars was carried out in the same TG apparatus in one heating run, to obtain a burn-off of 50%, dry,ash-free. Sorption measurements of benzene and carbon dioxide at 25 were carried out using a gravimetric vacuum apparatus (McBain springs).

An additional suite of $HA_{1.4}$ and $HA_{1.4}$(Ca) samples (1), carbonized to HTT of 800°, 900° and 1100°C, at two heating runs, was included into the sorption measurements.

RESULTS AND DISCUSSION

TG measurements of the HA differing in ash content from 1.4 to 0.07%, indicate a close similarity in the course of their carbonization (loss of mass versus HTT). However, significant differences were observed during gasification of their chars (Figure 1, Table I). This is accompanied by profound differences in the shapes of respective iso-

therms of benzene sorption on the gasified chars (Figure 2) and the slopes of the derived γ -plots (2) shown in Figure 3, analogical in their meaning to the frequently presented α-plots or t-plots(3).

Figure 4 illustrates, for the $HA_{1.4}$...$HA_{0.07}$ and their carbonized and gasified at 900°C chars, the changes in the respective capillary structures caused by demineralization. The influence of lowering of ash content is visible already on the level of the initial HA: a successive decrease of the micropore volume can be noted. This tendency is more accentuated for the non-gasified chars. On gasification, the influence of demineralization with regard to micropores becomes reversed: chars with lowest ash content indicate the highest development of micropore volumes.

The addition of Ca to $HA_{0.18}$ caused an important increase in the rate of gasification and reactivities of the chars (Figure 5, Table I), although the carbon dioxide accessible micropore volumes (V^{DR}_{oCO2}) of the chars, corresponding to different HTTs ,calculated according to the Dubinin-Radushkevich (DR) equation (4), were not very much influenced (Figure 6). It was only for the gasified chars that the influence of calcium on the capillary structure became visible (Figures 7-9, Table I).Catalytic gasification, occuring in the proximity of the calcium compounds ($CaCO_3$ or CaO), favours the development of mesoporosity.

This phenomenon is also clearly visible in case of a different suite of TG gasified chars from $HA_{1.4}$, carbonized previously in a laboratory furnace (two heating runs). The reactivities R^{daf} of these chars, presented in Table II, have been already published (1). As can be noted in Figure 10, the addition of Ca caused, in all cases, a very distinct increase of mesoporosity and a decrease of the micropore volume. A further influence of Ca addition is manifested by diminishing the differences between the capillary structures of the gasified chars from different HTTs (lower part of Figure 10), strongly pronounced in case of the gasified chars without Ca addition (upper part of Figure 10).

An attempt was made to recalculate the reactivities related to 1g of the gasified chars into reactivities related to 1 m^2 of the surface area S_t of these chars. The values of R^{daf}/S_t^{daf} of samples 1-8 in Table I, mark more strongly the influence of demineralization of the HA then do the respective values of R^{daf}. Comparing, in Table II, the values of R^{daf}/S_t^{daf} for samples gasified at the same temperatures but corresponding to different HTTs (e.g. sample 12 with 13 or sample 14 with 18) , it seems that the calculated values of S_t for samples corresponding to higher HTTs are too low (or those corresponding to lower HTTs too high) in relation to the surface areas really partaking in the reaction of gasification (because the respective values of R^{daf}/S_t^{daf} increase with increasing HTT, what does not seem probable).

The values of S_t were calculated as the sum of the surface area of the mesopores (S^{γ}_{mes} calculated from the slopes of the γ-plots) and the geometrical surface area of the micropores. It seems that in case of gasification, it is rather the geometrical surface area of the micropores which should be considered, than their effective (5) surface area (S_{eff} - amount of adsorbate filling volumetrically the micropores, expressed in a formal manner in terms of surface area, representative for the sorptive properties of chars).

These geometrical surface areas of micropores were calculated from the micropore volumes, assuming their slit-like shape (6). In case of all chars without Ca addition, the micropore volumes and the characteristic energies of adsorption E_o (to enable the calculation of χ -the half widths of the slits) were taken from the DR equation. For all chars with Ca addition, the micropore volumes were assumed to be equal to V_o^{γ} from the γ-plots (in Tables I and II, the values of V_{mic} - calculated on the basis of the Gurvitsch rule and the size distribution of the mesopores - V_o^{DR} and V_o^{γ} do not differ significantly) and the values of χ were taken, arbitrary, as 0.5 nm, because the application of the DR equation appeared impossible. For these chars the correction of the experimental isotherms for adsorption in the mesopores (based on a standard benzene isotherm on a non-porous carbon black: Spheron 6-2700) rendered ,not a horizontal, but a decreasing line of the corrected isotherm. This phenomenon was reflected in the γ-plots, an example of which is shown in Figure 8. In the region of lower relative pressures, the experimental points, which usually deviate downwards from the straight line (the micropore filling is not yet completed), are, in case of samples with Ca addition, placed near, or even above, this line. This might point to an enhanced specific adsorption of benzene on the chars with Ca addition.

CONCLUSIONS

1. Successive demineralization of the HA from ash content of 1.4% to 0.4, 0.18 and 0.07%, lowered the reactivity R^{daf} of the HA900 chars at steam gasification: at 800°C by a factor of 6,and at 900°C by a factor of about 3.5. For chars from $HA_{0.18}$ and $HA_{0.07}$ the reactivities were almost identical. In this range of gasification temperatures the energy of activation for the chars from $HA_{1.4}$ was 110 kJ/mol and increased for the more demineralized chars to about 170-180 kJ/mol, with respective frequency factors of the order of 10^5 and 10^8 g/g.h.

2. As a result of demineralization, in the capillary structure of the steam gasified chars (e.g. at 800°C), a successive increase of the volume of benzene accessible micropores is noted, from c.0.15 to c.0.4 cm^3/g. This is accompanied by a decrease of the volume of mesopores from c.0.5 to below 0.1 cm^3/g. The respective effective benzene surface areas S_{eff} increase from 700 to 1400 m^2/g.

3. The strong increase of reactivity of the demineralized HA chars after Ca addition (a 30-fold increase of reactivity was observed after addition of 1 mmol to 1 g of $HA_{0.18}$) was accompanied by a very strong development of the volume of mesopores, with the volume of micropores becoming very small .

4.For the gasified chars obtained from HA with Ca addition, an enhanced adsorption of benzene at low relative pressures was observed. As a result, the evaluation of microporosity using the Dubinin approach was impossible. In these cases the application of the α-plots (γ-plots) appeared very useful.

ACKNOWLEDGEMENTS

This work was sponsored by the Polish Academy of Sciences (Scientific Program CPBP 0.1 16).

REFERENCES

1. Tomków,K.; Siemieniewska,T.; Jankowska,A.; Broniek,E.; Jasieńko,M. Fuel 1986, 65,1423-1428.
2. Dubinin,M.M. in Characterization of Porous Solids, Proceedings of the IUPAC Symposium, Bad Soden F.R.G., April 26-29,1987 (K.K. Unger et al.Editors);Elsevier:Amsterdam,1988;Vol.39,pp 127-137.
3. Gregg,S.J.; Sing,K.S.W., Adsorption,Surface Area and Porosity; Academic:London 1982.
4. Dubinin,M.M.in Chemistry and Physics of Carbon (P.L.Walker, Jr. Ed.); Dekker: New York ,1966;Vol.2.pp.51-120.
5. Marsh,H.Carbon 1987,25,49-58.
6. Dubinin,M.M. Carbon 1981,19,321-324.

Table I. Steam gasified HA900 and HA(Ca)900 chars (one heating run)

Sample No	A_{HA} % dry	Gasif. at: °C	Based on benzene adsorption: V_{mic} cm³/g	V^{γ}_{o} cm³/g	V^{DR}_{o} cm³/g	E_o kJ/mol	S^{γ}_{mes} m²/g	S_{eff} m²/g	S_t m²/g	R^{daf} g/g.h	R^{daf}/S^{daf}_t g/m².h·10³
			Chars from HA								
1	1.4	800	0.159	0.172	0.146	24.0	290	723	582	1.98	3.21
2	0.4	800	0.388	0.424	0.410	17.7	131	1346	704	0.40	0.56
3	0.18	800	0.431	0.463	0.450	19.2	68	1401	756	0.38	0.50
4	0.07	800	0.442	0.452	0.459	21.8	51	1411	865	0.34	0.39
5	1.4	900	0.179	0.172	0.147	36.5	236	672	671	5.72	8.06
6	0.4	900	0.268	0.294	0.246	19.7	187	916	574	2.28	3.91
7	0.18	900	0.360	0.385	0.351	19.5	117	1157	664	2.04	3.05
8	0.07	900	0.399	0.433	0.437	19.2	53	1348	721	1.66	2.30
			Chars from HA(Ca)								
9	0.18	660	0.124	0.100	-	-	279	575	479	0.68	1.10
10	0.18	700	0.074	0.075	-	-	285	507	435	1.60	2.81
11	0.18	800	0.064	0.023	-	-	209	277	255	5.22	15.60

Table II Steam gasified chars from $HA_{1.4}$ and $HA_{1.4}(Ca)$ (two heating runs)

Sample No	HTT °C	Gasif. at: °C	Based on benzene adsorption: V_{mic} cm³/g	V^{γ}_{o} cm³/g	V^{DR}_{o} cm³/g	E_o kJ/mol	S^{γ}_{mes} m²/g	S_{eff} m²/g	S_t m²/g	R^{daf} g/g.h	R^{daf}/S^{daf}_t g/m².h·10³
			Chars from $HA_{1.4}$								
12	800	800	0.281	0.274	0.251	32.2	215	959	959	0.84	0.83
13	800	800	0.200	0.188	0.178	18.1	176	703	431	0.71	1.56
14	900	850	0.202	0.211	0.195	19.1	141	719	437	1.50	3.43
15	900	900	0.187	0.194	0.179	17.5	127	657	374	2.64	7.06
16	1100	850	0.044	0.028	0.026	17.3	70	147	105	0.85	8.10
17	1100	900	0.054	0.052	0.054	13.2	40	200	95	1.39	14.60
			Chars from $HA_{1.4}(Ca)$								
18	800	800	0.064	0.032	-	-	262	357	326	3.12	7.68
19	900	725	0.077	0.021	-	-	358	420	400	0.54	1.03
20	900	750	0.076	0.041	-	-	294	415	376	1.08	2.20
21	900	800	0.049	0.005	-	-	316	331	326	1.92	4.42
22	1100	800	0.037	0.016	-	-	251	298	283	1.38	3.70
23	1100	850	0.037	0.028	-	-	218	301	274	2.16	6.00
24	1100	900	0.045	0.002	-	-	270	276	274	3.00	8.24

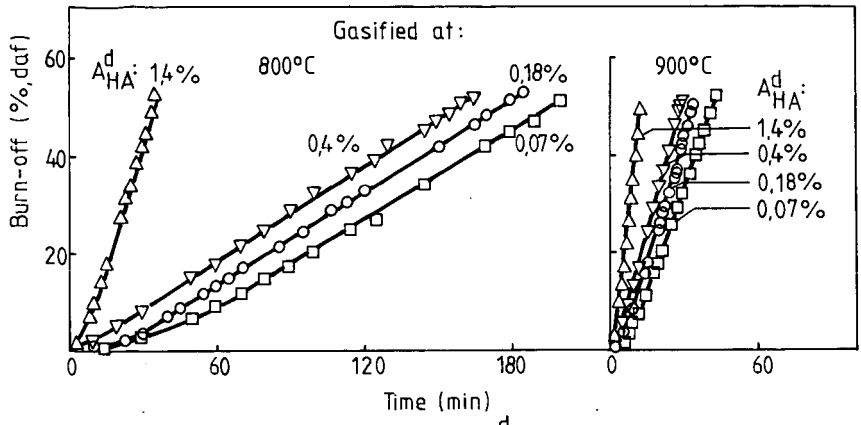

Figure 1. Infuence of ash (%, dry) in initial HA - A^d_{HA} on the course of steam gasification of the HA900 chars.

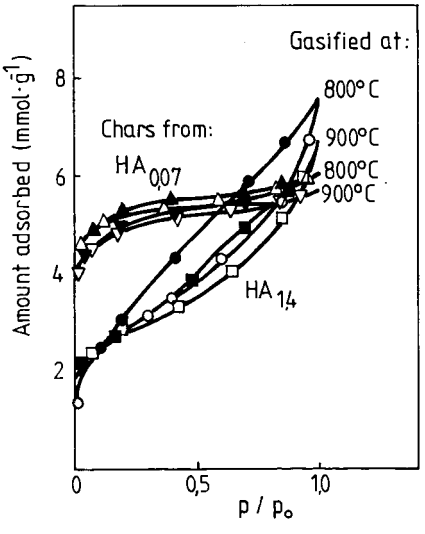

Figure 2. Changes in the shape of isotherms of benzene sorption (25°C) on steam gasified (burn-off 50%, daf) HA900 chars, caused by demineralization of the HA.

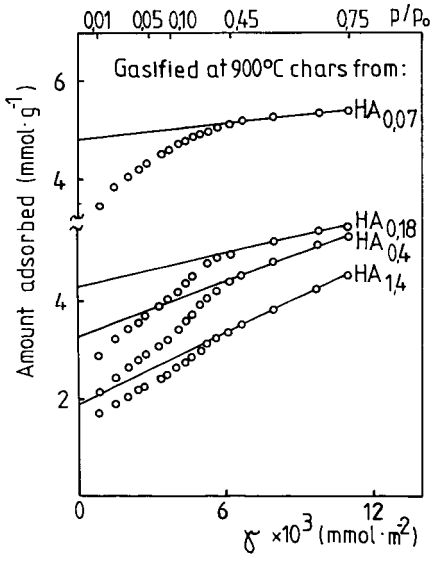

Figure 3. γ-plots for benzene adsorption (25°C) on steam gasified (burn-off 50%, daf) HA900 chars obtained from HA of different degrees of demineralization.

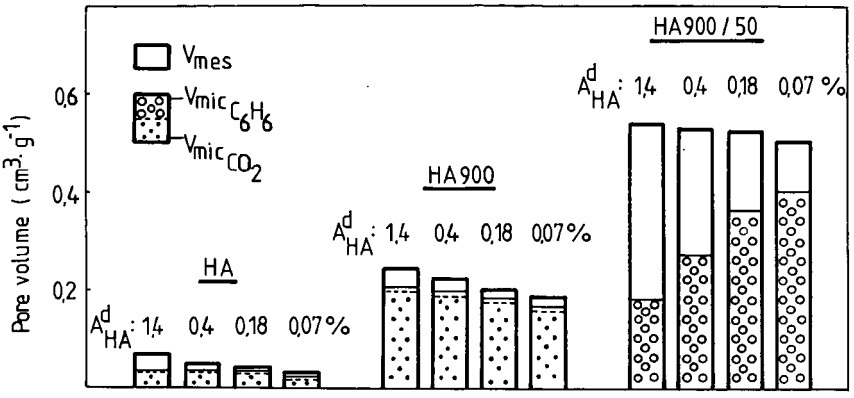

Figure 4. Influence of A^d_{HA} (%, dry) on the development of porosity in humic acids: initial (HA), carbonized (HA900) and steam gasified at 900°C to 50% burn-off, daf (HA900/50).

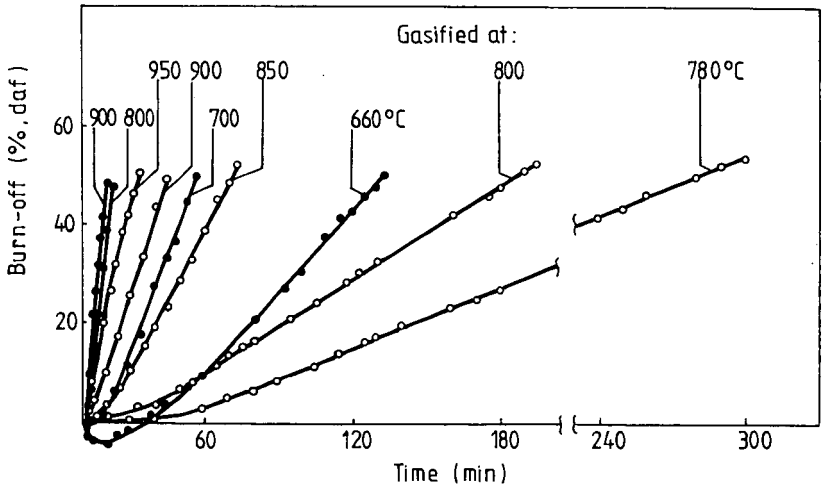

Figure 5. Course of steam gasification of the $HA^{900}_{0,18}$ chars (∘) and $HA(Ca)^{900}_{0,18}$ chars (•).

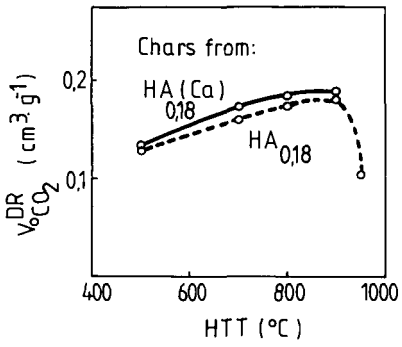

Figure 6. Variations of $V_{\infty CO_2}^{DR}$ during carbonization of $HA_{0,18}$ and $HA_{0,18}$ (Ca).

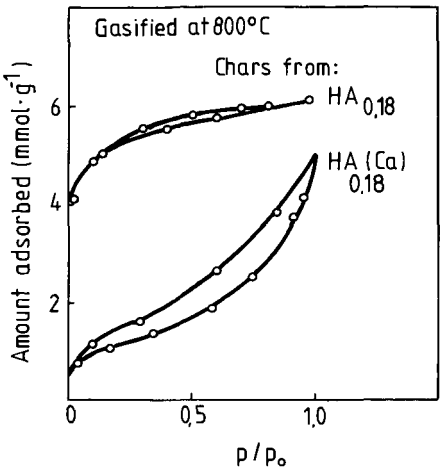

Figure 7. Isotherms of benzene sorption (25°C) on steam gasified (burn-off 50%, daf) $HA_{0,18}900$ and $HA_{0,18}$ (Ca) 900 chars.

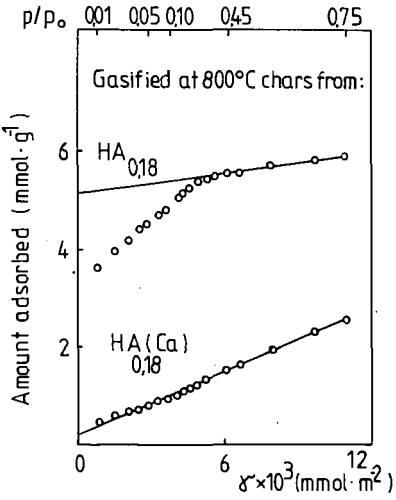

Figure 8. γ-plots for benzene adsorption (25°C) on steam gasified (burn-off 50%, daf) $HA_{0,18}900$ and $HA_{0,18}$ (Ca) 900 chars.

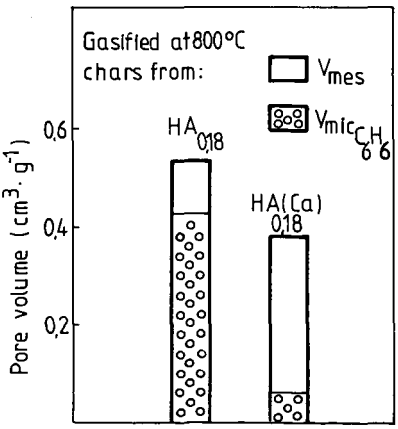

Figure 9. Decrease in microporosity and increase in mesoporosity of steam gasified (burn-off 50%, daf) chars (HTT 900°C), caused by Ca addition to $HA_{0,18}$.

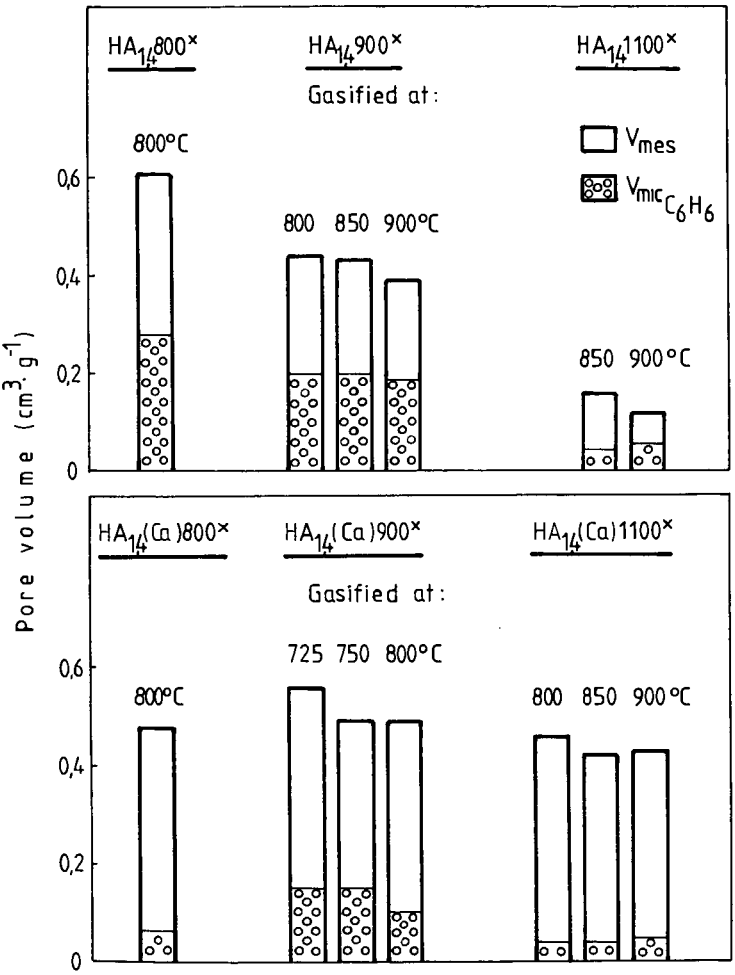

Figure 10. Development of porosity in steam gasified (burn-off 50%, daf) chars obtained from HA_{14} and $HA_{14}(Ca)$.
×) Carbonization was carried out at two heating runs.

THERMODYNAMIC ANALYSIS OF COAL GASIFIER PERFORMANCE

T. FURUSAWA, T. ADSCHIRI and V. BOONAMNUAYVITAYA
Department of Chemical Engineering
The University of Tokyo
7-3-1, Hongo, Bunkyo-ku, Tokyo 113, JAPAN

ABSTRACT

Performance data of large scale fluidized bed gasifier which were operated at the temperature ranging from 1000 to 1200 °C were reviewed and the optimum steam/oxygen ratio were demonstrated.The extents of four basic reactions evaluated on the basis of mass and enthalpy balances were effectively used to explain the relation between the coal gas efficiency and the steam/oxygen ratio. A thermodynamic model was developed to analyse the effect of operating condition on the gasifier performance. The simulation model can explain not only the performance data of fluidized bed gasifier but also estimate the performance under various operating conditions.

INTRODUCTION

It is not uncommon that the temperature of fluidized bed gasifier can not be raised high enough to achieve the high conversion of coal and the excess steam has to be introduced , because of problems of hot spot and ash agglomerates. Thus the improvement of fluidized bed gasifier efficiency requires the technological development to reduce the consumption of excess steam and the understanding of the optimum operating condition.

The gasification performance is controlled by both of kinetic and thermodynamic factors. If the retention time of gases and solids as well as the temperature in the reactors are almost the same, kinetically determined factors such as carbon conversion and the gas conversion can be assumed to be the same. Thus by the selection of reactor scale and gasification temperature, the effect of kinetic parameters on the cold gas efficiency can be eliminated in the thermodynamic analysis of gasifier performance. Consequently the present authors analysed only large scale fluidized bed gasifiers which operated at the temperature ranging from 1000 to 1200 °C. The simulation model was developed on the assumption that heat loss is 5% of the heat of combustion of coal, temperatures of steam and oxygen fed are 300 °C , the carbon conversion is 0.9 and product gases reach the shift equilibrium. The effect of the steam/oxygen ratio on the cold gas efficiency was simulated covering various gasification conditions.

ANALYSES OF GASIFICATION PERFORMANCE

In the present analyses, data in which gasifier scale larger than 4.5 [t/d] were selected. Considering a coal with a

composition CHaOb, the overall equation for coal gasification is expressed as follows.

$$CHaOb + xO_2+yH_2O=pCO+qCO_2+rH_2+sCH_4+uH_2O+(1-m_c)C \quad (1)$$

This equation can be divided into four independent basic reaction equations as follows.

e_1:	$C+O_2 = CO_2$	$Hr_1= -94050$ [kcal/kmol]	(2)
e_2:	$C+H_2O = CO+H_2$	$Hr_2= 31380$ [kcal/kmol]	(3)
e_3:	$C+2H_2 = CH_4$	$Hr_3= -17880$ [kcal/kmol]	(4)
e_4:	$CO+H_2O= CO_2+H_2$	$Hr_4= -9840$ [kcal/kmol]	(5)

The extents of four reactions (e_i) can be evaluated by the mass and heat balances. Three independent equations of mass balance can be given for carbon, hydrogen and oxygen respectively.

$$C : e_1+e_2+e_3 = m_c \quad (6)$$
$$H : 2e_2+4e_3+2e_4 = a+2(y-u) \quad (7)$$
$$O : 2e_1+e_2+e_4 = b+2x+y-u \quad (8)$$

Enthalpy balance is formulated as follows.
Summation of heat of reaction in Eqs.(2) to (5)
= (heat of combustion of coal)
-(heat of combustion of product gases) (9)

$$= HHV- Hc[pCO+rH_2+sCH_4-(1-m_c)C] \quad (10)$$

SIMULATION MODEL DEVELOPMENT

A simulation model was developed to analyse the effects of various operating conditions on the cold gas efficiency. This model was formulated based on the following assumptions:

1) No external heat is supplied.
2) Heat loss is 5% of HHV.
3) Coal composition is $CH_{0.8}O_{0.1}$.
4) Temperature of coal fed is 25°C.
5) Temperatures of steam and oxygen fed are 300°C.
6) The carbon conversion is 0.9.
7) Pressure is atmospheric.
8) The gas composition of CO, CO_2, H_2, H_2O, is determined by the shift reaction of which equilibrium constant is given as follows.

$$K_S= \exp[1/8.31431(41568/T_a-2.151n(T_a)+0.013T_a -3.678*10^{-6}T_a^2)-4.19149] \quad (11)$$

9) The formation of CH_4 is determined by the equilibrium of hydrogasification of which equilibrium constant is given as

$$K_h= \exp[1/8.31431(56680/T_a-61.141n(T_a)+.03645T_a -3.678*10^{-6}T_a^2+439320/T_a^2)+37.6711] \quad (12)$$

Thus the model is composed of three mass balance equations(6)-(8), one enthalpy balance equation (13) and two equilibrium equations(14) and (15).

Summation of heat of reaction in (2) to (5)
= (enthalpy of exist gas stream)+(heat loss)
-(enthalpy of feed stock)-(enthalpy of gasifying agents) (12)

$$\cdot\Sigma Hri\cdot ei = Hog+Hl-(Hif+Hig+His) \quad (13)$$

$$Ks = (qr)/(pu) \quad (14)$$

$$e3 = 0.5(1-1/\sqrt{(4KhP)+1}\,)(e2+e4) \quad (15)$$

By choosing "x" and "y" as variable parameters, T_a could be obtained by solving the above equations. Therefore the cold gas efficiency can be estimated only from steam and oxygen feed rates.

RESULTS AND DISCUSSION

The cold gas efficiency of gasification temperature 1000-1100 °C increases to the maximum where steam/oxygen ratio is around 2-4, and then decreases with the increased steam/oxygen ratio. In the cases of higher or lower temperature than this, the tendency is not clear owing to the shortage of data.

The extents of reaction could be used to explain the correlation between the cold gas efficiency and steam/oxygen ratio. As shown in Fig. 2 the extent of reaction (e_2) also increases to the maximum and then decreases with increased steam/oxygen ratio. Fig. 3 shows the extent of reaction (e_4) first increases rapidly from negative to positive value and then slowed down with the increased steam/oxygen ratio. When the value of e_4 is negative, the shift reaction proceeds reversely and endothermically to produce H_2O and CO. Thus the heat of reaction is carried out with the produced steam. While the larger steam/oxygen ratio is employed, the amount of unconverted steam is increased. As a result, the cold gas efficiency attains the maximum when steam/oxygen ratio is around 3.

The simulation model could describe the above results. The analyses of the data proved that the gasification temperature is 100-200 °C higher than the shift equilibrium temperature owing to the heat loss. The temperature indicated in Fig.4 is the shift equilibrium temperature while the temperature in Fig. 1 is that of gasification. Consequently, it is reasonable to consider that the curve of 1000-1100 °C in Fig.1 is corresponding to the curve of 800 °C in Fig.4. Also in Fig. 4 increase of temperature resulted in reducing the cold gas efficiency. In practical the coal conversion increases with increased temperature, thus the higher cold gas efficiency will be obtained.

It is demonstrated that this simulation model can also estimate the extents of reactions fairly well. The extent of reaction (e_2) significantly affects the entire efficiency but the steam/oxygen ratio of the peak in Fig. 5 does not give the maximum of the cold gas efficiency. Because of the effect of the exothermic heat of shift reaction, the steam/oxygen ratio of the peak in Fig.4 is larger than that in Fig. 5.
Further analyses of gasification performance will be given in the forth coming paper.

CONCLUSIONS

Performance data of large scale fluidized bed gasifiers were analysed. The optimum molar ratio of steam to oxygen feed proved to be around three. The extents of four basic reactions introduced were effectively used to explain the relationship between the cold gas efficiency and the steam/oxygen molar ratio. The extents of steam gasification and shift reaction significantly affect the cold efficiency. A thermodynamic model was developed to evaluate the effects of various conditions on the gasifier performance . This model can describe the performance data of fluidized bed gasifiers as well as the extents of the reactions.

NOMENCLATURE

a : atom ratio of hydrogen to carbon [-]
b : atom ratio of oxygen to carbon [-]
ei : extent of reaction [-]
Ha : heat supply [kcal/kmol of CHaOb]
HHV : higher heating value of coal [kcal/kmol of CHaOb]
Hif : amount of preheat of coal feed [kcal/kmol of CHaOb]
Hig : amount of preheat of gasifying agents [kmol/kmol of CHaOb]
His : amount of preheat of steam [kcal/kmol of CHaOb]
Hl : heat loss [kcal/kmol of CHaOb]
Hog : enthalpy of exist gas stream [kcal/kmol of CHaOb]
mc : coal conversion [-]
p : molar production rate of CO [kmol/kmol of CHaOb]
P : pressure [atm]
q : molar production rate of CO_2 [kmol/kmol of CHaOb]
r : molar production rate of H_2 [kmol/kmol of CHaOb]
s : molar production rate of CH_4 [kmol/kmol of CHaOb]
Ta : shift equilibrium approaching temperature [°C]
u : molar unconverted steam [kmol/kmol of CHaOb]
x : molar feed of oxygen [kmol/kmol of CHaOb]
y : molar feed of steam [kmol/kmol of CHaOb]

REFERENCES

1. Patel, J.G., Energy Research 1980,4,149-165
2. Elliot, M.A. (Editor), "Chemistry of Coal Utilization", Second Supplementary Volumn, 1981, 166-1663
3. Yagi, S., D. Kunii, Nenryo-kyokai-shi, 1955, 34,426

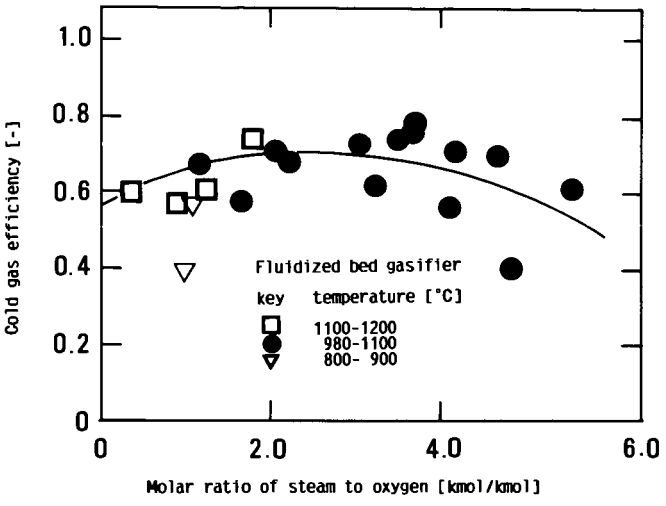

Fig. 1 The relation between the cold gas efficiency and molar ratio of steam to oxygen.

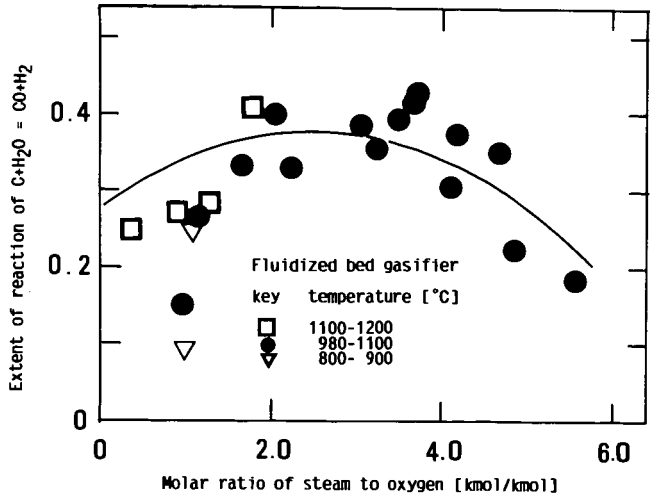

Fig. 2 The extent of steam gasification reaction vs molar ratio of steam to oxygen.

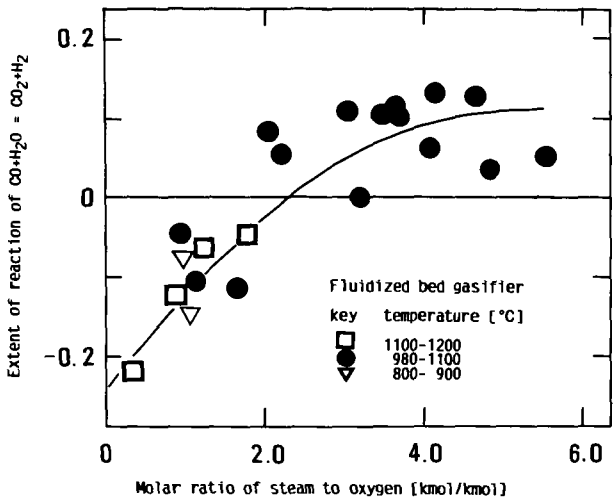

Fig. 3 The extent of shift reaction vs molar ratio of steam to oxygen.

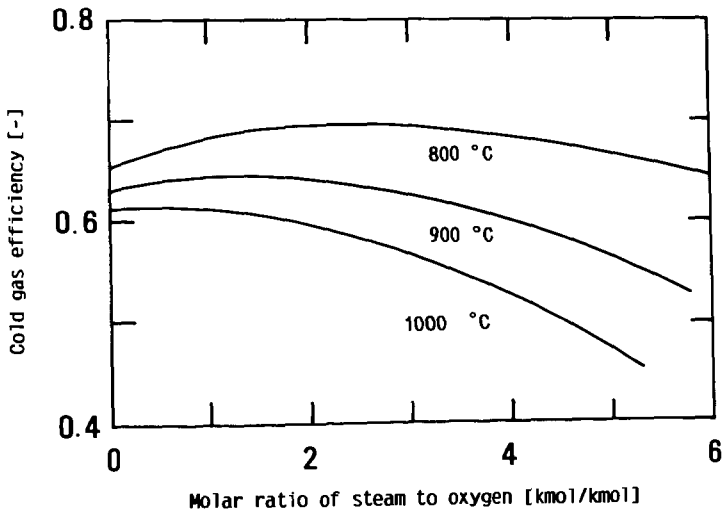

Fig. 4 The relation between the cold gas efficiency and molar ratio of steam to oxygen obtained from the simulation.

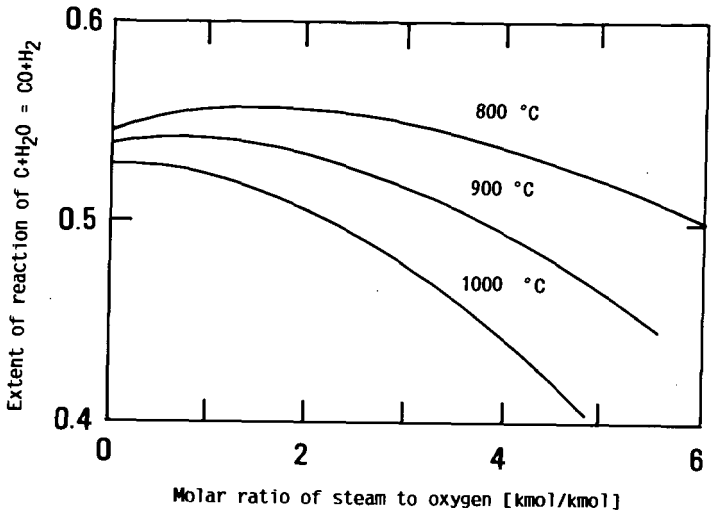

Fig. 5 The extent of steam gasification reaction vs molar ratio of steam to oxygen obtained from the simulation.

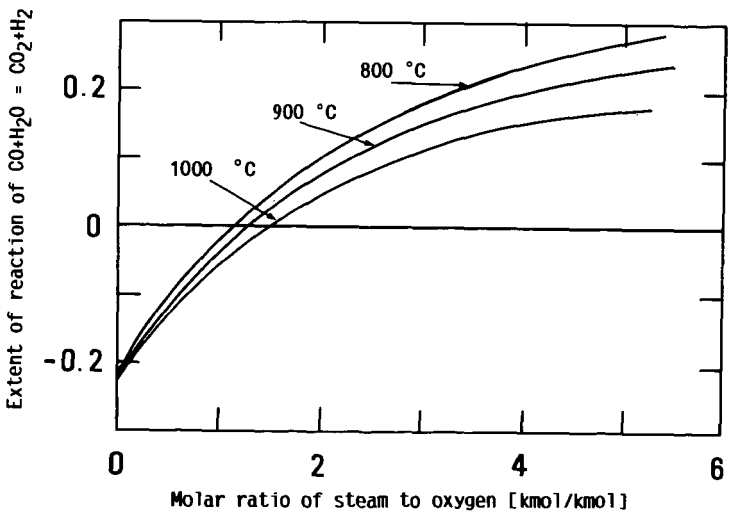

Fig. 6 The extent of shift reaction vs molar ratio of steam to oxygen obtain from the simulation.

REGENERATION KINETICS OF COKED SILICA-ALUMINA CATALYST

R. Hughes
M. Parvinian

Department of Chemical Engineering
University of Salford
Salford M5 4WT
England

INTRODUCTION

The regeneration of coked catalysts be means of a gas stream containing a few per cent of oxygen is a well established process. The main problem is to limit the temperature rise caused by the exothermic combustion of the deposited coke so as to prevent sintering of the catalyst. Coke contains appreciable amounts of hydrogen as well as carbon and its composition may be represented as CH_n, where n usually lies between about 0.2 to 1.5.

Earlier studies (1,2,3) considered coke to be composed of carbon only and neglected the hydrogen component. Haldeman and Botty (4), however, studied the deposition and subsequent oxidation of the coke and suggested that the hydrogen-rich part of the coke is attacked preferentially in the first stages of reaction. Following this Massoth (5), proposed a double reaction model with the hydrogen reacting at a retracting interface leaving a carbon rich residue for subsequent oxidation. This concept was extended by Ramachandran et al (6) who were able to predict temperature rises in catalyst particles for the early stages of combustion for varying values of n in CH_n. Hashimoto et al (7) proposed a multiple reaction model based on separate oxidations of hydrogen and carbon in the coke from which rate constants for either reaction could be obtained.

The aim of the present work is to obtain kinetic constants for both the hydrogen and carbon components of the coke as well as determining the variation of the oxidation products CO, CO_2 and H_2O with temperature.

EXPERIMENTAL

Materials. The catalyst employed was a commercial silica-13% alumina bead catalyst, crushed and sieved to give 80-100 mesh particles. The catalyst surface area was 328 m^2/g, with a total pore volume of 0.3×10^{-3} m^3/kg and an average pore radius of 2 nm.

Xylene, which was used for coking the catalyst was of standard laboratory grade (low sulphur). Gases employed were obtained from cylinders and dried with silica gel; any traces of carbon dioxide were removed by soda-lime.

Apparatus. Both coking and the subsequent regeneration were carried out in a stainless steel reactor operating under differential conditions. Xylene was vaporised in a heated tube and mixed with preheated nitrogen as carrier before entering the reactor in order to coke the catalyst. The preheater used to heat the nitrogen also served to preheat the oxygen/nitrogen gas mixtures during the regeneration experiments. The stainless steel reactor was heated by a resistance furnace controlled to $\pm$ 1°C and the catalyst bed was contained by a stainless steel gauze supported on a 5 mm bore stainless steel tube which contained two thermocouples, the junctions of which were placed within the catalyst bed.

The product gas was analysed for CO, CO_2 and water vapour. Infra-red analysers were used for analysing the former, while water vapour was determined using a recording dewpoint meter. The range of the dew point meter was from 0-1000 ppm water vapour, which covered the range of interest.

Procedure. The catalyst in the reactor was brought up to a temperature of 400°C and was then coked for an appropriate time using a xylene flow of 2 x 10^{-5} kg/s and a nitrogen flow fo 5 x 10^{-6} m^3/s. After coking, the xylene flow was stopped and the reactor heated to the temperature required for regeneration in the nitrogen stream. Approximately 7% of coke was deposited on the catalyst in all the experiments to ensure that measurable amounts of combustion products were obtained. The required oxygen/nitrogen mixture at the appropriate flow rate was then substituted when a steady temperature had been obtained. Water vapour, CO and CO_2 were monitored continuously during the regeneration and after sufficient time had elapsed the final traces of coke were removed by changing the gas mixture to air and raising the reactor temperature to 580°C.

RESULTS AND DISCUSSION

Preliminary experiments in which the total gas flow rate was varied from 3 to 10 x 10^{-6} m^3/s gave only small random variations in rate, indicating that external mass transfer resistances were negligible. Similarly variation of the average catalyst particle size from 20 to 100 mesh showed only slight random variations in the rate constant and therefore intraparticle diffusion could be neglected with the 100 mesh particles used in this work.

An example of the results obtained in a typical regeneration run is shown in Fig. 1. Cumulative amounts of CO_2, CO and H_2O released were obtained by measuring the areas under the appropriate curves. Both CO_2 and CO were observed to be present as products in all experiments, the amount of CO_2 always being greater than CO. Water vapour arises from the oxidation of hydrogen in the coke and decays more rapidly than the oxides of carbon. A plot of the mole fractions of elemental carbon and hydrogen in the coke which are converted are plotted against time in Fig. 2., and it can be seen that removal of hydrogen is much more rapid than carbon, in agreement with the results of Massoth[5]. All experiments were conducted at 1.05 bars.

Kinetics of carbon oxidation. Because the carbon constituent of the coke reacts more slowly than the hydrogen constituent, two separate and parallel gas-solid reactions were considered. The overall order of reaction in oxygen (to yield both CO and CO_2 products) was determined by varying the partial pressure of oxygen in the nitrogen stream from .06 to .2 bar. The oxidation rate was measured at each partial pressure value and a log-log plot (Fig. 3) of the oxidation rate against partial pressure of oxygen for two levels of coke conversion gave slopes of 1.05 (X_c = 0) and 0.953 (X_c = 0.5). These are sufficiently close to unity to regard the reaction in oxygen as being first order, in agreement with most previous work [1,2]. The order of reaction in oxygen for individual production of CO_2 and CO was also found to be unity.

The order of reaction with respect to deposited carbon was determined by fitting the experimental data to standard kinetic expressions. The data were found to give a best fit to a first order dependency in carbon. Therefore, the rate equation for the reaction may be written as

$$-\frac{dC_c}{dt} = k_c\, C_{Ag}\, C_c \qquad (1)$$

where C_{Ag} is the gas phase concentration of oxygen, C_c is the concentration of carbon and k_c is the overall second order rate constant for the reaction of carbon. Since the oxygen is in excess, its concentration will be only very slightly diminished in a differential reactor, so that the concentration C_{Ag} may be considered as constant and lumped with the rate constant. Therefore eqn. (1) may be written as a pseudo first order reaction

$$-\frac{dC_c}{dt} = (k_c\, C_{Ag}) \qquad (2)$$

Integrating

$$-\ln (1 - X_c) = (k_c\, C_{Ag})\, t \qquad (4)$$

and a plot of $-\ln (1 - X_c)$ against time should be a straight line with a negative slope equal to $k_c\, C_{Ag}$. Plots for experimental data at various temperatures and a constant oxygen partial pressure of 0.21 bar are given in Fig. 4 and good straight line fits for the data were obtained. Thus the reaction is first order in the concentration of deposited carbon.

The temperature dependence of the carbon oxidation was determined using first order kinetic expressions with respect to both carbon and oxygen. An Arrhenius plot of the data gave a value of 151,640 ± 9900 kJ/kmol for the activation energy. This compares with values of 156,000 kJ/kmol obtained by Hughes & Shettigar (2) and 156,200 kJ/kmol obtained by Hashimoto et al (7) from their analysis of a model based on experimental measurements after all the hydrogen in the coke has been consumed. The comparable value of the activation energy observed in this work plus the absence of any discernable curvature in the Arrhenius plot confirms that the kinetica results were obtained under conditions of chemical control.

The overall rate constant for the oxidation of carbon may therefore be written as

$$k_c = \frac{1.914 \times 10^8}{C_{Ag}} \exp\left[\frac{151{,}640 \pm 9900}{RT}\right]$$

Kinetics of hydrogen oxidation. The order of reaction in oxygen was determined by varying the partial pressure of this gas in the nitrogen stream from 0.07 to 0.21 bar. A log–log plot of the hydrogen oxidation rate against oxygen partial pressure for two values of the fraction hydrogen conversion is shown in fig. 5. The slopes of the lines were close to unity (0.93 at $X_H = 0$, 0.98 at $X_H = 0.5$) confirming the first order kinetic behaviour for oxygen.

An integral method of analysis of the data was attemped in order to determine the order of reaction with respect to the hydrogen component of the coke. Nor correlation was found over the complete range of experimental points for zero order, first order or second order kinetics. Only when the first 10 minutes of reaction were considered, was a reasonable fit obtained to any of these integral rate expressions.

It appeared therefore that the reaction was not kinetically elementary and could not be

satisfactorily represented by any of the simple rate expressions produced by the integral method of analysis. The differential method of analysing the data was therefore adopted to obtain an empirical order of reaction for the hydrogen in the coke. The order of reaction in hydrogen, at different temperatures in the range 430°C to 550°C were found by plotting the rates ($-dC_H/dt$) against the corresponding hydrogen concentration values (C_H) on a log-log scale (Fig. 6). The slope of the lines represents the order of reaction in hydrogen at different temperatures. The orders obtained varied from 1.57 to 1.86 and showed no trend with respect to temperature. This result indicates that the apparent kinetics of the hydrogen oxidation reaction is more complex than that of carbon.

The temperature dependence of the hydrogen oxidation was obtained by first obtaining values of the rate constant at each temperature from the intercepts of the lines in Fig. 6. An Arrhenius plot gave an activation energy for the hydrogen oxidation of 97,800 ± 8000 kJ/kmol, a value significantly less than that for carbon oxidation, and confirming the easier removal of hydrogen from the coke.

The lower value of the activation energy for hydrogen oxidation in the coke has been confirmed by the results of Hashimoto et al[7]. However, they found the hydrogen activation energy to be 140,300 kJ/kmol compared with their value for carbon oxidation of 156,200 kJ/kmol, and thus the effect of early hydrogen oxidation would be less prounounced than that obtained from our results.

It is of some interest to compare the variation of the CO/CO_2 and the H/C ratios with temperature. Some results given in Table 1 for an oxygen partial pressure of 0.21 bars and a gas flow rate of 6.0×10^{-4} m^3/min. It can be seen that the CO/CO_2 ratio increases with temperature from 0.31 at 430°C to 0.50 at 550°C. This is in general agreement with previous investigations. The hydrogen to carbon ratio, however, changes only slightly decreasing from 0.55 at 430°C to 0.49 at 550°C. This indicates that the hydrogen content is important at all effeective regeneration temperatures and must be considered in all regeneration procedures.

The final expression obtained for the rate constant for the oxidation of the hydrogen in the coke in the present work was

$$k_H = 3.56 \times 10^5 \exp\left[\frac{96,140 \pm 8,000}{RT}\right]$$

CONCLUSIONS

The kinetics of both carbon and oxidation of coke deposited on a silica-alumina catalyst from

xylene vapour have been investigated. The effects of oxygen partial pressure, temperature and gas velocity have been evalued. The reaction products consisted of carbon dioxide, carbon monoxide, water vapour and unreacted regeneration gas. It was observed that the carbon associated with the coke reacted more slowly than the hydrogen fraction in the coke. Hence the water vapour arising from the hydrogen oxidation decays more rapidly than the carbon oxides concentrations. Consequently two separate and parallel gas–solid reactions have to be considered. Both carbon monoxide and carbon dioxide are primary products of carbon oxidation and were observed to form throughout the range of oxidation conditions. Carbon dioxide was also the major product but the CO/CO_2 ratio increased with reaction temperature. First order dependency on oxygen concentration was observed for both carbon and hydrogen. The order of reaction with respect to the carbon in the coke was unity but the order in hydrogen was not elementary indicating a complex mechanism. The activation energy for hydrogen was much less than that for carbon, confirming the initial nature of hydrogen oxidation.

References

1) Weisz, P.B., Goodwin, R.D., J. Catal. (1966) 6, 227.
2) Hughes, R., Shettigar, U.R., J. Appl. Chem. Biotechnol. (1971) 21, 35.
3) Mickley, H.S., Nestor, J.W. Jr., Gould, L.A., Can. J. Chem. Engng, (1965) 43, 61.
4) Haldeman, R.G., Botty, M.C., J. Phys. Chem. (1959) 63, 489.
5) Massoth, F.E., Ind. Eng. Chem. Process. Des. Dev. (1967) 6, 200.
6) Ramachandran, P.A., Rashid, M.H., Hughes, R., Chem. Eng. Sci. (1975) 30, 1391.
7) Hashimoto, K., Takatani, K., Iwosa, H., Masuda, T., Chem. Engng. J. (1983) 27, 177.

TABLE 1. EFFECT OF TEMPERATURE ON PRODUCT COMPOSITIONS

Partial pressure of oxygen = 0.21×10^5 N/m^2

Gas flow rate = 6.0×10^{-4} m^3/Min

Coke weight 1%	Weight of the sample (g)	TEMP. °C	$\frac{CO}{CO_2}$	$\frac{H}{C}$
7.2	0.301	430	0.31	0.55
7.2	0.370	460	0.33	0.56
7.2	0.310	490	0.38	0.55
7.6	0.350	520	0.45	0.49
7.6	0.340	550	0.50	0.49

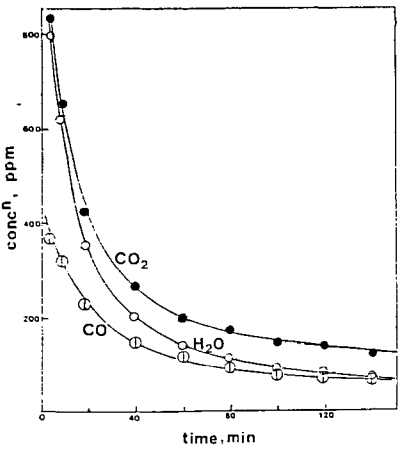

Fig.1. Typical oxidation product concentrations as a function of time.

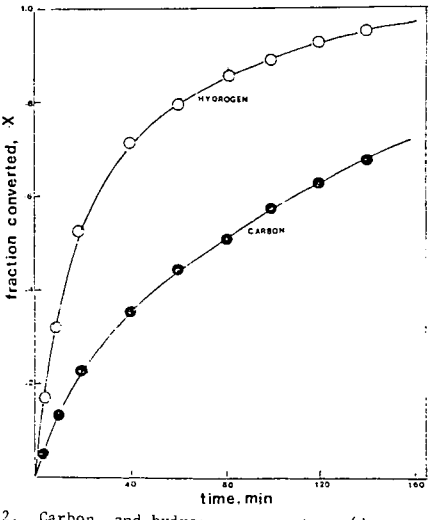

Fig.2. Carbon and hydrogen conversions (data as for Fig.1).

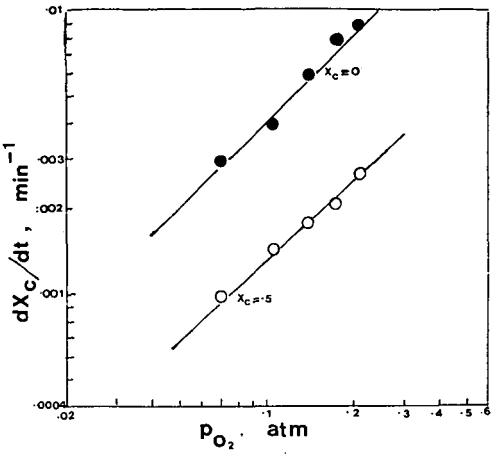

Fig.3. Effect of oxygen partial pressure on carbon burning rate.

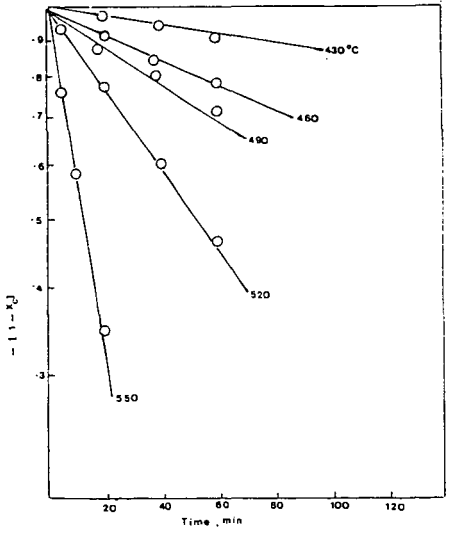

Fig. 4. First order correlation for carbon oxidation.

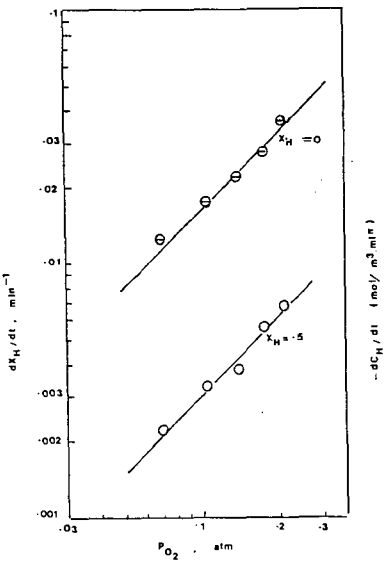

Fig. 5. Effect of oxygen partial pressure on hydrogen burning rate.

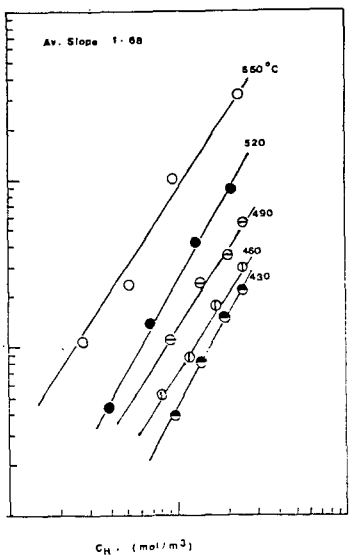

Fig. 6. Differential analysis plot for hydrogen oxidation.

Biothermochemical Conversion of a Bituminous Coal

by

Muthu S. Sundaram,[1] Shanthi K. Sundaram,[2] Mow Lin[2] and Eugene T. Premuzic[2]
[1]Process Sciences Division
Department of Applied Science
[2]Division of Environmental Biotechnology
Brookhaven National Laboratory
Upton, New York 11973

Microbial degradation of organic compounds, in general, and of aliphatic/aromatic hydrocarbons, in particular, is well documented.[1-5] Microorganisms already have been utilized in the degradation of petroleum hydrocarbons and oil spill clean up.[6] Some of the microbial degradation work has been applied to coal. However, most of the research on bioprocessing of coal is limited to desulfurization. A sulfur oxidizing acidophilic bacterium, Thiobacillus ferrooxidans[7-12] and an acidophilic thermophilic organism, Sulfolobus[13-15] were used in several biodesulfurization studies and were found to be effective in the removal of pyritic sulfur. Limited success has also been achieved in the removal of organic sulfur from coal using S. acidocaldarius[15,16] and cultures containing dibenzothiophene.[18,19]

Recently, various organisms were tested for their ability to solubilize coal. The type of "liquid" products obtained from microbial interaction with various coals are listed in Table 1. These liquid products were very aromatic and contained polycondensed aromatic ring structures with many hydroxyl groups and very low volatility.[19] Extremely complex nature of these products precluded any characterization at molecular level.

Considering the complexity of the coal "structure" compounded by the presence of appreciable quantities of mineral matter, it is doubtful that the microorganisms can successfully degrade coal directly into end products. Furthermore, it has not been proven that the micoorganisms act specifically in attacking particular functional groups.

Table 1. Liquid Products From Microbial Interaction with Various Types of Coal[19]

Type of coal	Microorganism	Liquid product*
Mississippi lignite	Aspergillus sp., Candida sp. ML13, P. waksmanii, T. versicolor ATCC 12679	Clear, amber, and black, inconsistent and generally in moderate Clear; moderate amounts
North Dakota I lignite	Aspergillus sp., Candida sp. ML13, Paecilomyces sp., P. waksmanii ML20, Sporothrix sp.	Clear; moderate amounts
North Dakota II	Aspergillus sp., Candida sp. ML13, Paecilomyces sp., P. monticola ATCC 11538 Sporothrix sp. T. versicolor ATCC 12679	Brown to black; moderate to profuse amounts; some clear initially, turning brown to black after two weeks
Texas lignite	Aspergillus sp., Candida sp. ML13, Paecilomyces sp., Sporothrix sp.	Clear; trace to moderate amounts
Vermont lignite	Candida sp. ML13, Sporothrix sp. Paecilomyces sp.,	Brown to black; trace amounts Clear; trace amounts
Wyodak	Aspergillus sp., Candida sp. Sporothrix sp. T. versicolor	Clear; trace amounts Clear to black; trace amounts

*Trace amounts - less than 10% of the coal surface covered with liquid moderate amounts - 10% to 50% of the coal surface covered with liquid; and profuse amounts - >50% of the coal surface covered with liquid.

(1.10)

While there are organisms that attack thiophenic group or pyrite inclusions, they may be capable of attacking other structural units in the coal as well. Many such organisms, could be somewhat non-specific in attacking various functional groups when they interact with coal, and may prove more beneficial in a process point of view.

Keeping this in mind, some exploratory experiments were conducted using Wellmore Kentucky No. 8 bituminous coal, (carbon 77.2%, hydrogen 4.9%, nitrogen 1.5%, sulfur 1.3%, oxygen 6.4% and ash 8.7%), and a microorganism, from the BNL collection, BNL-2-46 strain. The product of interaction of the "as-received" coal and BNL-2-46 strain, a solid, powdery material, after drying, was then pyrolyzed in an inert nitrogen atmosphere to 850°C at a heating rate of 100°C/min in a thermogravimetric apparatus. The microbial treatment with BNL-2-46 strain caused a positive enhancement in total yield of volatiles as shown in Figures 1 and 2. At the same time, another organism, BNL-3-25 strain, caused only a minor change in the volatiles yield.

This experiment has demonstrated that the microorganisms play a role in enhancing the production of volatile materials from coal. Microbial treatment alone can produce a cleaner starting material with less sulfur content, less ash content, less mutagenicity, and above all, a product that is more amenable for further thermal degradation. By itself, gasification can produce smaller molecules from coal and a variety of desirable products, the slate of which can be easily altered by changing the processing conditions. The integration of the developing biotechnology of bacterial treatment using different microorganisms, different strains of the same microorganism and/or combination of all in conjunction with the already well developed gasification technology is an interesting and desirable concept which should be pursued further.

ACKNOWLEDGMENTS

This work was performed under the auspices of the U.S. Department of Energy, Washington, DC under Contract No. DE-AC02-76CH00016.

REFERENCES

1. Davis, J. I. and Evans, W. W. Biochem. J., 91, 251 (1964).

2. Gibson, D. T. CRC crit. Rev. Microbio., 1, 79 (1971).

3. Patt, T. E., Cole, G. C., Bland, J., and Hanson, R. S. J. Bacteriol., 120, 955 (1974).

4. Norris, D. M. Appl. Environ. Microbio., 40, 376 (1980).

5. Berry, D. F., Francis, A. J., and Bollag, J. M. Microbio. Rev., 51, 43 (1987).

6. Atlas, R. M. Microbio. Rev., 45, 180 (1981) and References therein.

7. Regerson, A. and Berger, J. J. Gen. Microbio., 124, 53 (1981).

8. Chandra, D., Roy, P., Mishra, A. K., Chakrabarti, J., Prasad, N. K., Chandhri, S. G. Fuel, 59, 250 (1980).

9. Kargi, F and Weissman, J. G. Biotechn. Bioenergy, 26, 604 (1984).

10. Gokcay, C. and Yrteri, R. N. Fuel, 62, 1223 (1983).

11. Rai, C. Biotech. Prog., 1, 200 (1985).

12. Doddemma, H. J., Huber, T. F., Kos, C. H., and Bos, P. European Coal Utilization Conference, 3, 183 (1983).

13. Detz, C. M. and Barvinchark, G. Mining Cong. J., p. 75 (1979).

14. Kargi, F. and Robinson, J. M. Environ. Microbio. 44, 878 (1982).

15. Kargi, F. Biotech. Bioenergy, 24, 2115 (1982)..

16. Krawiec, S. Proc. Biological Treatment of Coal Workshop, Herridon, VA, June 23-25, 1985, p. 52.

17. Hatcher, H. ibid, p. 38.

18. Isbister, J. ibid, p. 18.

19. Scott, C. D., Strandberg, G. W., and Lewis, S. N. Biotech. Prog., 2, 131 (1986).

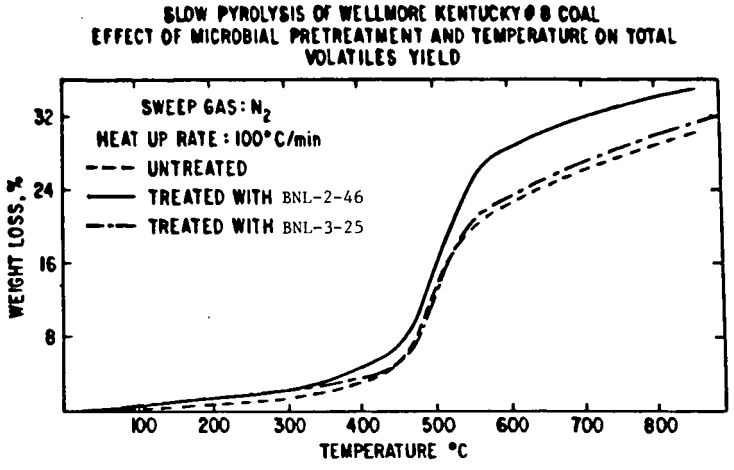

FIGURE 1

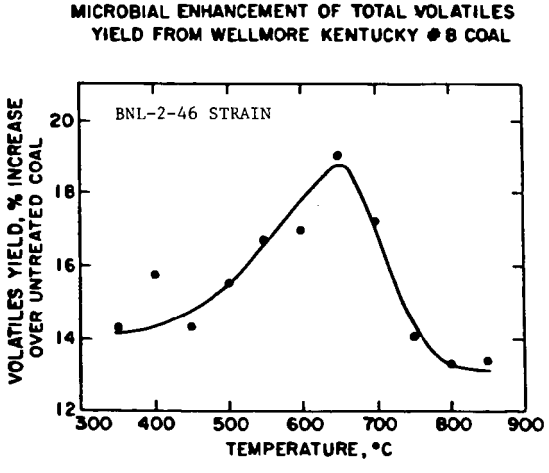

FIGURE 2

COAL COMBUSTION - OLD AND NEW CHALLENGES*

Alan W. Scaroni
The Combustion Laboratory
The Pennsylvania State University
404 Academic Activities Building
University Park, PA 16802

The burning of coal has been practised for centuries and misunderstood for centuries. Therefore, the challenges facing the coal combustion community are as diverse and heterogeneous as coal itself. They range from overcoming the institutional resistance and social unacceptability of coal to understanding the exact nature of an active site on a char surface. The path to expanded and acceptable coal use, and this surely has to be the ultimate objective of coal combustion research, leads through a maze of interrelated conceptions and misconceptions regarding what coal is, what it is not and how it behaves.

From a combustion viewpoint coal's legacy is most assuredly that it is not natural gas and therein lies the essence of the problem. It is an unfortunate fact for expanded coal utilization that, in nature, conventional fossil fuels occur as gases, liquids, and solids. The ease with which these fuels can be recovered, handled, processed, analyzed, characterized, and burned decreases in the order listed. This translates directly into the ease of extraction of energy in a useful form, usually as heat. Notice that solid coal is at the end of the list. Therefore, in order to understand the problems facing the coal combustion community it is not only appropriate but essential to compare and contrast aspects of the preparation and combustion of coal's chief competitors, natural gas and petroleum-based liquids.

The Competition

Natural gas occurs in a form convenient to transport over long distances in pipelines and short distances through pipes. In general, onsite storage capacity at the user station is neither required nor desirable. A continuous supply of fuel from a pressurized pipeline is but a valve turn away. As a fuel, natural gas is relatively easy to ignite with a spark or, more commonly in industrial practice, with a pilot flame and requires a burner of relatively simple construction. Once ignited, it burns rapidly and cleanly. High combustion intensity translates into small, hence inexpensive, combustion chambers. Clean combustion depicts the absence of significant quantities of solid and gaseous pollutants in the products of combustion, which avoids the need for complicated firing strategies and expensive pollution control equipment. In short, natural gas is by any measure of evaluation a premium fossil fuel for energy production.

Unlike natural gas which is composed predominantly of the single simple molecule methane, petroleum-based liquid fuels are available in a range of molecular compositions. The size and structural features of the constituent molecules determine to a large extent the quality of the liquid as a fuel. In general, quality decreases from light, low boiling distillate to heavy, high boiling residual oils. Heavy fuel oils are, for example, too viscous to flow under normal conditions and must be heated prior to pumping. Whereas transportation through pipes and pipelines is possible, transfer lines often require heat tracing to keep the liquid flowing and prevent clogging. This is particularly the case in cold climates, since viscosity is strongly temperature dependent. Liquid fuels, which generally emanate from petroleum refineries, require on-site storage capacity to ensure that a limited continuous supply in both a valve turn and pump switch away.

---

* Revision of an article appearing in Earth and Mineral Sciences, 53 (2), 1, 1984 by the same author. Earth and Mineral Sciences is a publication of The Pennsylvania State University.

Ignition of liquid distillates is a relatively straight forward procedure and subsequent combustion is intense. Ignition is more difficult for heavy oils but is still a routine procedure with current technology. Often, startup on natural gas or distillate oil to raise the combustion chamber temperature precedes firing of heavy oils. The phenomenon of ignition is related to the rates of heat generation in, and heat loss from, the flame and less heat is lost to a hot combustion chamber than to a cold one. Of course, heat generation derives from the reaction kinetics and mechanisms, subjects of significant scientific debate. Liquid fuel burners have some degree of complexity associated with the need to atomize the liquid prior to combustion. The principal role of the atomizer is to produce liquid droplets of small size to aid ignition and increase combustion intensity. Liquids combust by first vaporizing, then the fuel vapors ignite and burn in a stable envelope around the shrinking liquid droplet. Combustion occurs essentially homogeneously in the gas phase, hence, intensity is high and combustion chambers are only marginally larger than those into which natural gas is fired. Fuel oils, particularly the heavier grades, do not burn as pollutant free as natural gas but as considerably less troublesome than coal. In general, most petroleum-based liquid fuels are categorized also as premium fossil fuels for energy generation.

Coal's Legacy

By comparison, coal has unique handling and combustion problems. Because of lingering opposition to coal-slurry pipelines, transportation of coal is restricted currently to road, rail and barge. Over short distances, coal is transferred by belt conveyors or moved pneumatically. Unless the user plant is located in close proximity to the mine mouth, extensive on-site storage capacity is a necessity. Moreover, a complex coal preparation plant is required to produce fuel in a form commensurate with the mode of combustion. Most of the preparation involves regulating particle size and mineral matter, both of which affect combustion behavior. In general, coal preparation and handling systems are costly and cumbersome. In short, a continuous supply of coal requires a complicated, integrated preparation process containing a multitude of valves and pump switches.

The term coal is used generically here to describe what is, in fact, a vast array of rank and types of coal. There is general familiarity with the concept of classifying coals according to rank, for example, lignites compared to bituminous coals or anthracites. Within a given rank of coal, however, constituent molecules can vary widely in shape and composition depending to a large extent on the biological and geological history of the coal's formation. That is, coals of a given rank can vary widely in type. A consequence of these variations is that it is tenuous at best to make blanket statements about combustion behavior, there always being an exception to the rule. Therein lies one of the major problems facing the coal combustion community. It is being asked to describe, in detail, the chemical and physical transformations occurring in a material that is, at best, ill-defined. Predictive capabilities will never be fully established without an adequate model of coal constitution. With this in mind, some gross generalizations are now provided.

Coal is a relatively difficult fuel to ignite. Preceding combustion is some degree of devolatilization, a well studied but rather nebulous process whereby gases, vapors, and liquids are released from the heating coal particle. To what extent the volatiles are actually produced prior to release (as distinct from preexisting in the coal matrix) and what fraction of the total volatiles escapes the coal particle are just two of the multitude of still unanswered questions. Furthermore, the kinetics of the pyrolysis processes have eluded even the most fervent researchers for a number of good reasons. Firstly, without knowing the constitution of the starting material it is rather difficult to write anything other than the most simple chemical equations to describe the transformation. Furthermore, despite a plethora of claims and counterclaims, the temperatures of rapidly devolatilizing (and combusting) coal particles have not yet been established unequivocally.

It is often assumed, but by no means proven as being applicable to all situations, that the released volatiles ignite and burn in the gas phase thereby providing heat to ignite the residual char. The char then burns heterogeneously as a solid. It is to the detriment of coal as a fuel that solids combustion is

an order of magnitude or more slower than homogeneous gas phase combustion. That is, once ignited, coal particles are relatively slow to burn, and slowness translates directly into size and expense.

It is probably true that a little more is known about the fundamentals of char combustion than of the pyrolysis behavior. Several decades of study on relatively pure carbons has produced a clearer picture of the high temperature interactions between carbon and oxygen. What has not been established, however, is a definitive theory with predictive capability of what constitutes an active site for carbon oxidation, how this relates to structural features and the role of inorganics in determining the reactivity of a coal char.

Generally, it is not possible to start up a combustor on coal. Combustion of natural gas or light liquids usually precedes switching to coal which is fed through a burner that requires both complexity and ruggedness to handle abrasive air-entrained solids. Ignition temperatures are coal and combustor specific and cannot yet be predicted a priori. Since particle combustion times are long, large and expensive combustion chambers are required. This is the principal reason that retrofitting combustors designed for oil or natural gas to fire coal requires capacity downrating, or, more often, cannot be achieved at all. Obviously, conversion in the other direction from coal to oil or gas firing presents less difficulty and has been performed extensively in the past.

One troublesome product of pulverized coal combustion is ash, mostly micron and submicron sized fly ash. Efficient collection and disposal of this potential pollutant by baghouses and precipitators is an expensive operation. The properties of fly ash that affect collection capacity are only partially understood. Gaseous pollutants, in particular sulfur oxides and nitrogen oxides, abound from the combustion of all but premium and therefore expensive coals. Mechanisms and kinetics of sulfur and nitrogen release from the coal and their conversion to SO_x and NO_x, respectively, need to be established definitively. In short, coal in its naturally occurring form is a long way from fitting the bill as a premium fossil fuel as far as convenience and cost of energy extraction is concerned.

Convenience Reigns Supreme

Needless to say, convenience has reigned supreme in the history of energy generation, at least in the U.S. Hence, although up to 80 percent of the nation's fossil fuel resources are solids (mainly coal), resources of premium gaseous and liquid fuels have persistently been depleted even in cases where solid fuels would serve as well. Take the case of steam generation in industrial boilers as an example. Installation of new capacity or reconversion of existing equipment has not been directed en masse towards coal firing. Despite persistent price hikes and intermittent interruptions in the supply of natural gas and petroleum-based liquids, convenience dictates continued reliance on these fuels.

Much of the opposition to coal is institutional in nature. It is not always sufficient to justify the use of coal combustion on economic considerations alone. The perception lingers, for example, that coal is dirty to look at, dirty to handle, and dirty to burn. While no combustion technology can overcome the first two, emerging technologies can and will help to cast the third aspersion aside.

In this context, it is not difficult to follow the argument in favor of, say, fluidized-bed combustion of coal. It alleviates many of the problems associated with conventional coal combustion technologies, in particular those related to fuel quality and pollution control. Fluidized-bed combustors can handle without difficulty materials so low in heating value that they have been discarded or disregarded as fuels in the past. This decreases the extent of expensive coal processing in order to meet fuel specifications. In addition, fluidized-bed combustors can be operated in a mode so that acid gas emissions are not of regulatory concern. The net effect of fluidized-bed combustion technology is to narrow the so-called ease-of-combustion gap between natural gas and coal, thereby making coal combustion a more acceptable and attractive proposition.

Current Combustion Technologies

Coal-burning equipment has been available to the industrial market for close to a hundred years. Historically, combustors have been equipped with mechanical stokers. These are multi-purpose devices which feed coal on to a grate within a combustor and remove the ash residue. In addition, the grate acts as the support structure for the burning bed of coal. The concept of continuous and automatic stoker firing is attributed to James Watt who patented it in 1785. He was concerned with smoke emissions, imperfect combustion, and capacity limitations associated with hand firing or manual stoking. Concerns have not changed much in the last 200 years.

About sixty years ago, a revolutionary development occurred in coal combustion technology. To overcome problems of boiler capacity versus size restrictions associated with stokers, pulverized coal-firing technology was developed for steam locomotives. The technology was quickly adapted to stationary utility boilers and today, stoker firing is no longer a serious competitor in the utility market. Pulverized coal firing offers greater flexibility in furnace design and has been embraced in the trend toward large units. The present market for small stoker-fired units is quite poor.

Coal combustion rates are determined to a large extent by the size of the particles fed to the combustor. Pulverized coal particles are typically less than 75 μm in diameter, that is, they are relatively small. In contrast, stokers normally feed a size range between 0.5 and 1.5 centimeters, relatively coarse particles. As a consequence, efficiency loss due to unburned fuel in a pulverized coal combustor is typically less than 1 percent compared to about 5 percent for a spreader stoker.

Pulverized coal combustors do have limitations, however. In particular, a high-grade fuel (high heating value and low mineral matter content) is generally required. Moreover, pulverized coal combustors have, in general, high levels of solid and gaseous pollutants in their products of combustion.

Emissions from Coal Combustors

Three principal classes of emissions from coal combustors have been judged significant from an air quality standpoint: particulate matter, sulfur oxides (SO_x) and nitrogen oxides (NO_x). Historically, particulate matter has been the focus of attention since it can be easily seen and therefore is easy to label as a public nuisance. It is comprised of fly ash and unburned carbon. Particulate matter release is controlled to some extent by either electrostatic precipitation or fabric filtration. Oxides of sulfur and nitrogen are of concern because they are precursors to acid rain and can cause ill health effects in humans. In addition, oxides of nitrogen participate in atmospheric reactions that produce photochemical smog.

Acid rain has emerged as one of the top environmental issues of the 1980s. According to the experts, it is caused by the atmospheric conversion of gaseous SO_x and NO_x into sulfuric and nitric acids. In the eastern United States where most attention is focused, man-made emissions of acid gases are said to dwarf natural emissions. In the case of SO_x, emissions are said to be dominated by a relative handful of sources. Coal-fired power plants are being labeled as the prime culprits, with the 20 largest plants producing about a quarter of all SO_x emissions in the region. NO_x emissions, on the other hand, are attributed to both power plants, not necessarily those firing coal, and motor vehicles.

All fossil fuels are being blamed for releasing CO_2 into the atmosphere, a fact which will get no dispute from combustion scientists. What will stir debate, however, is whether or not such release of CO_2 is causing global warming. This debate and the associated research effort in the next decade is likely to dwarf the current preoccupation with the causes and effects of acid rain.

The sulfur content of different coals varies widely. It is unfortunate but a fact of life that many of the high-sulfur coals are located in the eastern half of the U.S. The east is also the region that is under scrutiny for the effects of acid rain. Furthermore, it is the region of the country that is most intensive in the use of fossil fuels. All these factors work against utilization of local, inexpensive, and abundant coal and drive users toward transported (and often imported) natural gas or petroleum-derived liquids.

Sulfur atoms are either chemically bound to the organic fraction of coal or found in mineral constituents such as pyrite. Coal preparation plants can reduce mineral matter content, hence, inorganic sulfur content. They can do little, however, to reduce organic sulfur content. There is some renewal of interest in the concept of superclean coal and coal water slurry fuels produced either by chemical and/or biological treatment methods. The concept here is to add cost to the fuel thereby producing a so-called premium fuel and reduce the burden on the combustor and down stream cleanup devices. This is likely to continue to receive attention, particularly for gas turbine and diesel engine applications.

As coal burns, most (often 90 percent or more) of the sulfur is converted into SO_x. Historically, gaseous SO_x emissions have been "controlled" by either dispersion or reduction. Dispersion of pollutants through tall stacks is an old-slight-of-hand which is no longer acceptable. Reduction by flue-gas desulfurization (FGD) is a band-aid solution, according to some, often creating as many problems as it solves. There is a general movement towards alternative ways to combat acid rain, and it is not difficult to understand why. According to industry figures, maintenance costs for FGD systems are 20 times higher than those for the rest of the power plant, and this has lead some to call FGDs the most costly and least reliable pieces of equipment in the utility industry. Operational problems aside, there is the challenge of what to do with the sludge produced. In fact, disposal of all residues associated with coal combustion systems is likely to be the focus of significant regulatory attention.

While SO_x emissions can be related directly to fuel sulfur content, NO_x emissions originate from two different sources. During combustion, NO_x forms in high-temperature regions in and around the flame zone. Oxidation of both atmospheric nitrogen (thermal NO_x) and fuel-bound nitrogen (fuel NO_x) occurs. The rate of thermal NO_x formation is influenced by temperature and the oxygen concentration. Reducing flame temperature and excess air, therefore, can help control thermal NO_x formation. This is achieved in practice by performing combustion in stages, appropriately called staged combustion, and recirculating some of the products of combustion. Fuel NO_x formation is related to fuel nitrogen concentration and is most significantly influenced by the oxygen concentration in the combustion zone. In an oxygen-deficient atmosphere, fuel nitrogen can be converted to N_2 rather than NO_x, particularly the nitrogen contained in the volatiles. Details of reactions kinetics and mechanisms are still sketchy.

Fluidized Bed Combustion

Debate is currently raging over the issue of whether or not the effects of acid rain are serious enough to warrant costly emissions control programs. When the ayes prevail, the question will be reduced to what control strategy should be implemented. While the current preferred technology may still be FGD or some form of limestone injection, a promising alternative technology for new construction and retrofit applications is fluidized-bed combustion.

Burning coal in fluidized-beds usually involves injecting the fuel into a bubbling or circulating bed of calcined limestone or dolomite and ash. Combustion occurs both within and above the bed and the gaseous pollutants produced can be captured by the bed material. Until recently, this technology was aglow with praise, but it has now been relegated by some for "supported implementation" until economic and political circumstances change. What this means, in essence, is a time delay until petroleum supplies are again interrupted or prices hiked.

The principle of fluidization is conceptually simple and mathematically complex. To state the obvious, solid particles can be moved by a fast-flowing stream of air or other gas and it is this simple principle upon which fluidized beds operate. Consider a chamber open at the top with a wire mesh at the bottom. On the mesh is a bed of inert granular particles. From beneath, a stream of air is being blown up through the mesh. If the air flow rate is low, air will percolate between particles in the bed without disturbing them to any great extent. If the air velocity is increased, a point will be reached when the particles move upward in unison and the bed will occupy an expanded, yet still well-defined, space. The particles, in essence, are now being supported by the air rather than the grate. At still higher air velocities, the particles begin to mix violently within the envelope of the bed and adopt the appearance, and some of the properties, of a boiling liquid. The bed is then said to be fluidized in a conventional bubbling mode.

Were the air velocity to be increased even further, granular particles of bed material would become entrained in the air and be blown or carried from the bed. The bed would then lose its integrity. In practice, granular particles come in a range of sizes intimately mixed. Fluidizing velocity depends, among other things, on particle size. Hence, operating limits for a boiling bed are set, on the one hand, by the minimum velocity needed to keep the largest particles fluidized and, on the other hand, by the maximum velocity that can be tolerated before an excessive number of small particles are blown from the bed.

This highlights not only the principles of fluidized bed operation but also those of fixed bed (stokers) and entrained-flow (pulverized) combustors. In fixed beds, coal particles are large and the grate-supported bed is relatively undisturbed by the percolation of combustion air through it. In entrained-flow combustors, small pulverized coal particles are carried at high velocities into a turbulent fireball in a combustion chamber. In fluidized-bed combustors, medium-sized coal particles are injected into a turbulent bed, and burn within and above the bed in intimate contact with the bed material.

Fluidized-bed combustion affords some advantages over other modes. When operated at atmospheric pressure, however, and this is the current state of the art, boilers employing fluidized beds have no particular thermodynamic advantages over conventional boilers. Their attractiveness and potential for success lie in their ability to meet air pollution standards at a lower cost than conventional systems, particularly those equipped with FGDs. The development of pressurized fluidized bed combustion of coal, on the other hand, is being driven by improved cycle efficiencies, particularly in connection with gas turbines.

Low emissions levels in fluidized beds are inextricably linked to low bed temperatures, 700 to 900 C, compared to flame temperatures of 1600 to 1800 C in pulverized coal boilers. The lower temperatures are a prerequisite for efficient sulfur capture by the bed material, normally calcined limestone, by the endothermic reactions:

$$CaO + SO_2 + 1/2\ O_2 \rightarrow CaSO_4 \qquad (1)$$

$$CaO + SO_3 \rightarrow CaSO_4 \qquad (2)$$

Calcium oxide particles are porous with sulfation occurring to some extent over much of the surface. SO_2 is the predominant sulfur oxide in combustion gases, usually accounting for 80% or more of the sulfur-containing species, hence, equation 1 predominates. Calcium sulfate does form preferentially on outer particle surfaces, however, eventually creating an impervious skin which stops further reaction. The relationship between sorbent composition, combustor operating conditions and sorbent performance is the subject of considerable enquiry at the moment.

A second major pollutant that suffers retarded production at temperatures less than 900 C is thermal NO_x . Thermal NO_x is a term coined to specify those nitrogen oxides, mainly NO, formed in

combustion systems in which the original fuel contained no chemically bonded nitrogen atoms. Generally, it is thought that the NO is formed from N_2 in air by the following overall equation:

$$N_2 + O_2 \rightarrow 2NO.$$

According to equilibrium considerations, significant NO would be found only at temperatures considerably in excess of 900 C. However, the route to NO formation involves several radical species including O and N atoms and OH radicals. Consequently, equilibrium calculations provide only a conservative estimate of actual NO concentrations as a function of temperature. Nevertheless, it is generally recognized that thermal NO_x formation is not of great consequence at the operating temperatures of fluidized-bed combustors.

Although not directly temperature-related, reactions destroying NO_x, which does manage to form in fluidized-bed combustors, are quantitatively significant. Most of the NO_x formed originates from nitrogen contained in the fuel. Once formed, it can be converted to N_2 by heterogeneous reactions with bed char and sorbent. There is some evidence that these reactions are catalyzed by CO, one of the major gaseous products of carbon combustion. In summary, the consequence of having a limestone- and char-containing bed at low temperatures is the elimination of regulatory concern about NO_x and SO_x emissions. This is the feature that may control the destiny of atmospheric fluidized-bed combustors.

Some combustion experts try to sell the concept of fluidized beds on the basis of high heat transfer rates to in-bed water tubes. From an economic point of view, this is offset to a large extent by high tube erosion rates, and some now question the wisdom of inserting tubes into the bed at all.

An additional advantage of low-temperature coal combustion is suppression of slag and deposit formation. Both are attributed to the presence of various inorganic constituents in coal which undergo physical and/or chemical transformations at high temperatures. The presence of slag and deposits causes capacity downrating of the boiler and operational problems. The behavior of inorganics during combustion may be the single most important operational issue in the coal combustion community at the present time.

The current trend in medium size units is circulating fluidized beds. In circulating fluidized-beds, gas velocities are much higher and a consequence is that coal and bed material are elutriated from the bed and recirculated through the combustor back to the bed via a hot primary cyclone. Combustion of the coal occurs throughout its passage, hence, combustion efficiencies are high and SO_2 removal is more efficient. Fluidized bed technology is undergoing the inevitable growing pains associated with commercialization, particularly with respect to tube failures and bed agglomeration. Materials handling problems have also surfaced in units firing low grade fuels. The problems are not insurmountable and should be overcome with further research and development. Fluidized bed combustion will then take its place alongside existing technologies, and will then face the common enemy, a lack of knowledge of the fuel being burned in the combustor.

The Challenge

Coal combustion research is and should be driven by necessity. A thorough knowledge of how coal burns is predicated on the desire to mitigate the environmental impact of coal combustion, overcome operational difficulties and develop predictive capabilities. This will only be achieved once a detailed understanding of coal constitution has been obtained. Then the task of describing, in detail, the transformations that occur when coal is burned can be launched in earnest. Applications may have changed over the decades but the challenge has not. It is, indeed, a formidable one.

COAL CARBONIZATION: CURRENT AND FUTURE APPLICATIONS

R. Menendez and R. Alvarez.
Instituto Nacional del Carbon y sus Derivados,
"Francisco Pintado Fe" (CSIC), Apartado 73, 33080 Oviedo, Spain.

INTRODUCTION

Carbonization is defined as "The destructive distillation of organic substances in the absence of air, accompanied by the production of carbon and liquid and gaseous products". The coke produced by carbonization of coal is used in the iron and steel industry and as a domestic smokeless fuel.

Only a limited range of coals produces acceptable metallurgical cokes. These coals are in the bituminous rank range but not all bituminous coals are caking coals. Prime coking coals are expensive and not always available nationally. It is predicted that remaining indigenous coals available for coke making are poorer in coking quality (1). In addition, coke ovens need to be rebuilt and , in most parts of the world, profits from the steel and iron business are insufficient to provide the necessary capital. In future years , we will have to extend our technology even further and find new blends or raw materials and optimum operating conditions in order to reduce costs. This will only be possible with a better understanding of the fundamental aspects of the coking process, i.e. properties of coals and their functions in the coal-to-coke conversion. This understanding is also necessary because of the gradually increasing stringency of requirements made on coke by modern industrial practices, i.e. maximum output with maximum efficiency.

In this paper, the authors attempt a preview of the future of coal carbonization from the viewpoint of past and current experience.

COAL PETROLOGY

Greatest use of coal petrology has been made in the area of coke making. Most steel companies have adopted petrographic relationships, based on coal rank (reflectance) and type (maceral composition), for use them for preliminary evaluation of coals and for coal-blend design. Coal macerals have their own carbonization behaviour, some of them, e.g. part of semifusinite and most of the micrinite and fusinite, remain relatively inert whilst others, e.g. vitrinite, resinite and part of semifusinite, gasify, soften and become porous, hardening ultimately into coke (2, 3). However, maceral behaviour is more complex than originally thought and as Kaegi et al. (4) showed, they behave quite differently depending on what other macerals are in contact with them. Quick et al. (5) proposed the use of a tandem system of fluorescence and reflectance microscopy for the recognition of reactive vitrinite and inertinite to provide a better assessment of carbonization behaviour.

RHEOLOGICAL PROPERTIES OF COAL

Several tests are available to evaluate the suitability of coals for coke production (6). Coking coals become plastic when heated; consequently, a wide variety of tests have been introduced to measure the plastic and swelling properties of coal (7). The most common are the free-swelling index test to determine the agglomerating and swelling characteristics of heated coal, the Gieseler plastometer for assessing the plastic properties and the Audibert-Arnu dilatometer to record volume change as a function of time.

CHEMISTRY OF COAL CARBONIZATION

A significant development in understanding carbonization processes was made with the discovery of mesophase in the plastic stage of carbonization leading to graphitizable carbons, as observed by optical microscopy (8). The development of spherical mesophase particles (Figure 1) from an isotropic mass and their progressive growth and coalescence eventually to form anisotropic structures is well established for pitch-like precursors (9-11). Essentially, during the carbonization process, dehydrogenative polymerization of aromatic molecules occurs, with a consequential increase in average molecular weight (12). The final coke structure (Figure 2) is related to the properties of mesophase at the time of solidification and these, in turn, are dominantly dependent upon the chemical properties of the parent material. Coke quality improvements are dictated by the quality of the parent feedstock which predetermines the optical texture of the resultant coke.

In contrast to pitch-like materials, carbonization of coal produces mesophase in the form of very distorted spheres which do not show observable coalescence because of their high viscosity. These differences in behaviour could be attributed to inhibiting effects of elements such as nitrogen, oxygen and sulphur and to the influence of particulate inert matter in the coal (13).

COMMERCIAL CARBONIZATION

The coals selected for blending for blast furnace coke give the highest coke physical strength with acceptable chemistry, acceptable reactivity and at a competitive cost. The coke must contract sufficiently for easy removal from the oven and swelling pressures must be acceptable.

Strength and reactivity

The chemical composition of coke can be controlled within desirable limits by coal selection and control of carbonizing and quenching conditions (14). The desirable physical properties of coke are less defined in that furnace operation is still not completely understood. The physical quality of coke is usually defined in terms of its size and by empirical parameters representative of its resistance to breakage and abrasion. The classical strength tests (shatter test or drum tests, Micum, Irsid) are size dependent and it is difficult to derive relationships linking the results of one test to another (15).

Conventional strength indices are being supplemented by new coke heating procedures which provide a better simulation of the behaviour of coke in the blast furnace. These include various "solution loss" reaction tests and hot strength tests (16). A major objective of modern coke making is to improve the properties of coke at high temperatures, especially its strength after reaction with CO_2 and its reactivity (17, 18). Table 1 shows the BSC coke specifications for large blast furnaces. Many tests have been developed to measure coke reactivity and a large and diffuse amount of literature is available on this subject. A synoptic report describing the high temperature properties of coke has been published by the Commission of the European Communities (19).

Coking pressure

It is established that some coals can damage coke oven walls because of either excessive pressure developed during carbonization or insufficient coke contraction at the end of the coking process. This problem has lately become a matter of importance due to coal preheating and the widespread acceptance of tall batteries which increase the bulk density of the coal charge, so affecting coking pressure, contraction and coke oven life. The Spanish National Coal Institute (INCAR) has

developed (20) a laboratory method of predicting expansion and contraction behaviour during carbonization, based on a modification of the early Koppers laboratory test.

Prediction of coking properties

Much effort has been made to predict coke strength based mainly on measurements of vitrinite reflectance and maceral analysis. These predictive techniques have two common premises: i) for any given coal there is an optimum blend of reactives and inerts which will give the best coke, ii) percentages representing this optimum blend or ratio vary with rank. Different approaches have been followed in terms of analysis and treatment of coke conditions and of the particular index of coke strength determined (21-23). The Japanese assessed the suitability of a single coal to be used in a blend from maximum fluidity values and Ro (24). CRM Belgium developed a new prediction method (25) applicable only to the conventional wet charge process which relates coke strength indices to inert content of coal, caking ability of the reactive components and the maximum Gieseler fluidity of the blend.

Predictions for volume charge and carbonization pressures based on petrographic data have also been formulated.

CURRENT COKING TECHNIQUES

As mentioned before, producers of metallurgical coke are experiencing a shortage of prime coking coals and suitable high volatile coals at a time when more stringent coke quality demands are being made as iron is being produced in larger, faster-driven blast furnaces. The conventional wet charging process of making good quality coke is very dependent on coal quality. To solve this problem several techniques have been tested.

Additions of caking substances

The aim of this process is to produce metallurgical coke of good quality by adding reformed non-coking coal or petroleum heavy residue to coal. This technical approach does not produce any particular problems in the coking process itself and its success depends upon making inexpensive binders. Major binder manufacturing processes that have already been industrialised or are in the pilot plant stage are in Japan. Coal tar pitch has been found to be a satisfactory substitute for medium volatile coking coal in blends in coke oven tests conducted in West Germany (26).

Selective crushing

It is known that selective crushing of many types of coal and blends can produce an improvement of coke quality (27) but commercial development has been obstructed by the non-availability of suitable equipment to screen wet fine coal with large throughput. Nippon Steel Corporation has developed a large wet coal screening equipment (110 t wet coal/hour) which is efficient and commercially available (28). The process minimizes the production of very fine coal particles and, at the same time, selectively crushes inertinite-rich particles into smaller sizes than the vitrinite-rich particles. In this way, the inertinite-rich particles are evenly distributed in the coking blend, the bulk density is increased and coke quality is improved (29).

Partial briquetting

Briquette blend coking process (BBCP) is most commonly used in Japan as a technique to use low grade coals (30). Non-caking and poorly caking coals can replace coking coal giving coke with a suitable strength. However, blending conditions must still be optimized and briquette manufacturing costs reduced.

Stamp charging

This technology is applied in China, Czechoslovakia, Poland, East Germany, Rumania, France and West Germany. In India a plant is being built and the USSR recently decided to implement it. This process has been used for many years in Europe to produce coke from high volatile coals and, at the present time it has been successfully incorporated into the new high ovens (31). The coke oven feed is compacted in a stamping machine and is charged into the ovens horizontally. Stamping increases bulk density of the charge and improves coke strength, especially resistance to abrasion.

Formed coke

Formed coke processes (32-33) consist of manufacturing briquettes from non-caking or weakly caking coals which, after suitable carbonization, can be fed directly into blast furnaces. This avoids the construction and maintenance of expensive coke oven batteries. The briquetting may be hot or cold and the binder is usually a pitch. Several tests have been carried out in the blast furnaces with formed coke replacing conventional coke but , at the present time, the process does not have significant application.

Preheating

Preheating is a technique which substantially improves coke quality from low rank coals. It also produces an increase in oven and battery throughput (as much as 50% for the lower rank coals). Other advantages derived from the elimination of the water from the charge include more uniform heating and a reduction in the thermal shock. Applications of preheating also provide more effective smokeless charging, elimination of routine mechanical levelling and a decrease of pollution during the pushing operation. These effects of preheating may be due to modifications of the plastic properties or possibly to a permeable plastic layer which allows tar and other pyrolysis products to react with the coal (34).

The disadvantages of the preheating process are related to the difficulties of handling fine hot coal and the increased carryover of fines. Coking pressure during carbonization must also be closely controlled and, in general, coking batteries charged with preheated coals have more technical problems (35).

DEVELOPMENT OF MODERN COKE MAKING TECHNOLOGY

In recent years, the productivity of coke ovens has been increased by using higher coking temperatures, silica bricks with higher thermal conductivity and coking chambers of larger volume. In past decades, the use of wide ovens was controversial because the correlation between coking time and chamber width was not clear. In this respect, Bergbau-Forschung (BBF) carried out a large scale testing operation (36) in oven chambers of 450, 600 and 750 mm width in the range of temperature of 1300-1350°C. It was assumed that the increase in residence time, at these temperatures, was not significant and in any case it could be compensated for by increasing bulk density. As a result, an increase in productivity could be achieved by building wider oven chambers. From this research, such plants were built in Germany and operational experiences indicated that the operation of coke ovens with an effective volume of $80m^3$ and more, and a coke production of about 50 t per charge is possible without too much risk.

However the controversy about coke ovens width still continues. Recently, Centre de Recherches Metallurgiques (Belgium) carried out coking tests in its experimental oven in order to determine

the effect of chamber width on coke quality and on coke oven productivity (37). It was concluded that it is mainly dependent upon coal blends used. With wider chambers, good coking blends showed an improvement in fissuring resistance, significant improvements in the abrasion resistance indices and an increase in the mean diameter of coke pieces. With poorly coking blends, the mechanical strength indices and coke piece mean diameter decreased.

FUTURE OF COAL CARBONIZATION

From the above discussions it is evident that, despite considerable effort, there is as yet no practical alternative to traditional coke making. Three different approaches to coal carbonization may be adopted in the future: i) improvement of coke production by introducing modifications, ii) the building of a new coking system, iii) the development of new carbon materials with different specifications and new functions.

Improvement in existing technology includes the construction of new heating systems which reduce NOx formation, the automation of the coke oven battery and the use of computers to control the working schedule. Automation could be extended to the characterization of coking coal blends in order to save time, i.e. techniques such as neutron activation elemental analysis are being assessed (38).

The second approach, to build a new coking system, was taken into consideration by the German coking industry, in collaboration with Ruhrkohle AG and BBF GmbH. They developed a new concept in coke making technology on the basis of ecological problems, cost-effective production of coke with high productivity and specific output. To achieve this, some constraints must be considered (39): maintenance of the present coke structure, establishment of independence from the raw materials, minimization of the energy consumption, reasonable solutions to problems of environmental protection, improvement of process control and monitoring and production of by-products adapted to prevailing conditions. Noting these constraints, a research programme called "Jumbo Coking Reactor" was developed (39).

From the studies carried out, the productivity would be higher than those currently operating. The operation of only 55 reactors will be of major benefit to the environment. The length of the sealing surfaces that require daily cleaning is 60% less than those for the large capacity ovens that are now in service. The number of opening processes is reduced to only 110, against 1200 in one of the new German plants (Prosper). From the economical standpoint, this plant will reduce the total coke costs by between 10 and 20%.

ALTERNATIVES TO COAL CARBONIZATION

One of the functions of coke in the blast furnace is to provide heat in the hearth of the furnace for melting the reduced ore. In the mid-fifties oil was injected at the furnace tuyeres to provide heat to the hearth and reduce the coke rate. When oil prices rose, a number of systems were developed to inject pulverised coal. At least 16 countries have blast furnace coal injection systems. This has been one of the most rapidly expanding iron-making developments world-wide (Figure 3) (40).

Ironmakers are now considering coal injection to reduce the coke rate of blast furnaces. Reasons given are: coal is cheaper than purchased coke; for those ironmaking plants which are considering building or rebuilding coke ovens, the capital cost of coal injection equipment is less than coke oven plant; a wide range of coal types can be injected including non-coking coals. Coal

injection results in smoother blast furnace operation with less hanging and slipping than the comparable all-coke operations.

Injected coal can reduce the fuel and reductant roles of coke in the blast furnace but the provision by coke of a solid permeable bed from stockline to the hearth cannot be replaced by coal injection. As coke rate reduces, the pressure drop across the furnace increases and it is thought that the gas and liquid flow will decrease and, consequently, the iron production rate.

SPANISH APPROACH

The availability of coking coals in Spain is limited. ENSIDESA, the most important Spanish iron and steel industry has a coking coal consumption of about 3 x 10^6 t/year. 70-80% is foreign coal and only 20-30% Spanish coal. The wide diversity of Spanish coal mines and the need to import coking coal from all over the world causes major difficulties in coal blending.

ENSIDESA is using a very sophisticated blend of 15 to 20 different coals and owns a large yard for coal blending and homogenizing with a handling capacity of 8.5 Mt/year and a stockpiling facility of 800,000 tons. To predict the coke strength and to optimize the blending from an economical stand-point, a mathematical model has been developed and successfully applied by ENSIDESA (41). The Spanish Research Council (CSIC) has two Institutes for coal research. One of them, the National Coal Institute (INCAR) has an Experimental Coking Test Plant (Figure 4). The battery contains four ovens. The oven dimensions are 2.8 m in height, 6.5 m in length and 300, 350, 400 and 450 mm, respectively, in width. The heating system is independent for each and their capacity is 4-6 tons. INCAR co-operates very closely with ENSIDESA.

Some of the research carried out by INCAR is related to coking pressure, preheating, coal weathering effects on coke quality, coal blending and the use of different additives to improve coke quality. INCAR has developed and patented (20) a laboratory method for predicting expansion and contraction behaviour during carbonization, based on the Koppers laboratory test. The Koppers-INCAR laboratory test was successfully applied to the problem of Spanish coals which have dangerous swelling behaviour during coking. The contraction behaviour data obtained are related to the chemical properties of coal, i.e. volatile matter, mean vitrinite reflectance and softening point. A 2 t/h preheating pilot plant, Precarbon process, owned by ENSIDESA and built on line with the INCAR Coking Test Plant, is being used for preheating research. It has been used to study effects of adding a high volatile coal and semi-anthracite to an industrial base blend which had given good quality coke by the conventional wet coking process (42). Studies were also carried out on the effect of petroleum coke addition to coals with high and low volatile matter content and the effect on the productivity and the pressure exerted during the coking process. The improvement of coke quality from coals with a high volatile matter content by using different additives is also being studied. It was observed that aluminium additions up to 3.0 wt% of aluminium considerably improved coke strength (43).

ACKNOWLEDGEMENTS

R.M. is grateful for support from the American Chemical Society to attend the April 1989 meetings.

REFERENCES

1. Elliot D.R. (1971), Coke Oven Managers' Year-book, Mexborough, U.K. p. 196.
2. Schapiro N., Peters J.T. and Gray R.J., (1962), Transactions of AIME, p. 1.
3. Schapiro N. and Gray R.J. (1966), A Guidebook for the Geological Society of America and Associated Societies, Utah Geology and Mining Survey, Salt Lake City, Utah, Bulletin 80, p. 55.
4. Kaegi D.D., Valia H.S. and Harrison C.H. (1988), 47th Ironmaking Conference Proceedings, 47, p. 339.
5. Quick J.C. Davis A. and Lin R. (1988), 47th Ironmaking Conference Proceedings, 47, p. 331.
6. Zimmerman R.E. (1979). Evaluating and Testing the Coking Properties of Coal. Miller Freeman, San Francisco.
7. Brewer R.E. (1945). Utilization of Coal, vol. 1, p. 170.
8. Taylor G.H. (1961), Fuel, 40, 465.
9. Davis A., Hoover D.S., Wakely L.D. and Mitchell, G.D. (1983), J. of Microscopy, 132, 315.
10. Menendez R. and Marsh H. (1987), Pyrolysis of Pitch Materials, Colloque International du C.N.R.S., Metz (France) Fuel Procesing Technology. To be published.
11. Marsh H. (1973), Fuel 52, 205.
12. Greinke R. A., (1986), Carbon 24, 677.
13. Patrick J.W. (1975), The Coke Oven Managers' Year Book, Mexborough, U.K. p. 201.
14. Graham J.P. and Wilkinson H.C. (1978), AIME 37th Ironmaking Conference, Chicago, p. 421.
15. BCRA, Investigation Report, 27, 1976.
16. Nakamura N. Togino Y. and Tateoka T. (1977), "Coal, Coke and the Blast Furnace, The Metals, Society, London, p. 1.
17. Nakamura N., Togino Y. and Adachi T., (1977), ibid, p. 93.
18. BCRA. Annual Report 1978, p. 17.
19. Wilkinson H.C. (1986), Commission of the Euopean Communities,Technical Coal Research EUR 10430 EN.
20. Procedimiento o sistema para evaluar el empuje de los carbones. Patente No. 524.258, 1983.
21. Schapiro N., Gray R.J. and Eusuer G.R. (1961), AIME Proceedings, Blast Furnace, Coke Oven and Raw Materials Conference, Vol. 20, p. 89.
22. Simonis W., Gnuschke G. and Beck K.G. (1966), Gluckauf Forsch.-H. 27, p. 105.
23. Steyn J.G.D. and Smith W.H. (1977), Coal, Gold and Base Minerals, September.
24. Miyazu T., Okuyama Y., Suzuki N., Fukuyama T. and Mori T. (1975), Nippon Kokan Technical Report-Overseas, December, p. 1.
25. Munnix R. (1984), Ironmaking Proceedings 43, p. 19
26. Rohde W. (1983), Gluckauf 119, no. 18, Trans. p. 25.
27. Burstlein E. (1971), Revue de Metallurgie, Janvier, p. 39.
28. Yamaguchi T. (1980), 68th Tech. Meeting on Coke Making, The Fuel Society of Japan, April.
29. Matsouka H. (1980), Seminar Rourkela Steel Plant and Indian Institute of Metals, September.
30. Yoshinaga M. (1976), Ironmaking Proceedings, Vol. 35, p. 256.
31. Leibrock K. and Petak H. (1983), Fuel Processing Technology, 7, 91.

32. Warren I.H. (1980), CIM Bulletin, January, p. 147.
33. United Nations, Economic Commission for Europe. Coal Committee ECE/Coal/32, 12 April,, 1978.
34 Gray R.J. (1988), Short Course: Introduction to Carbon Science, Newcastle upon Tyne, September 12-16th, To be published by Butterworths.
35. Guerin J.P. and Bowness M.M. (1984), Ironmaking and Steelmaking, Vol. 11, no. 4, p.186.
36. Rohde W. (1986), Ironmaking Proceedings, 45, 113.
37. Munnix R., Steyls D. and Vidal R. (1988), 47th Ironmaking Conference Proceedings, 47, 145.
38. Taylor R. and Massey W. (1988), Coke Oven Managers' Year Book, Mexborough U.K. p. 152.
39. Nasham G. (1987), 1st International Cokemaking Congress, Essen, Vol. 1, A2.
40. International Iron and Steel Institute Committee on Technology, Techco-20, April 26, 1988.
41. Sirgado M. and Verduras J.L. (1978), International Iron and Steel Congress, Chicago, p. 404.
42. Alvarez R. (1987), 1st International Cokemaking Congress, Essen, vol. 1, E5.
43. Menendez R., Alvarez R., Miyar E.A., Canga C.S. and Marsh H. (1988), Carbon 88, Institute of Physics, Bristol p. 522.

Figure 1. Mesophase development from isotropic pitch material.

Figure 2. Optical micrograph of polished surface of a metallurgical coke.

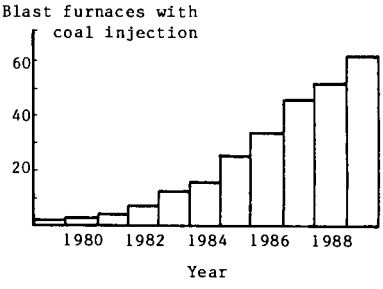

Figure 3. Development of coal injection.

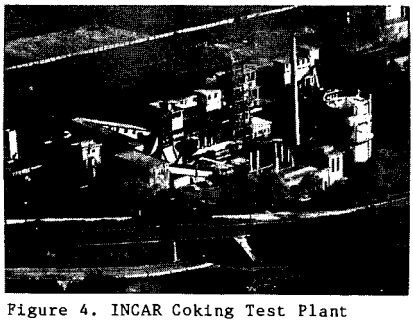

Figure 4. INCAR Coking Test Plant (Oviedo, Spain).

Table 1. The new BSC specification for large blast furnaces (18).

Mean size	50 mm
Size range	30-75 mm
Japanese DI $^{150}_{15}$	≥82
Japanese reactivity	≤30%
Japanese post-reaction strength	≥53%
Ash, d.b.	≤10%
Sulphur, d.b.	≤1.1%
M40 micum index	≥80
M10 micum index	≤7
Extended-micum slope	≤0.8

COAL IN A MODERN WORLD

Harry Marsh

Northern Carbon Research Laboratories
University of Newcastle upon Tyne,
Newcastle upon Tyne.
NE1 7RU, U.K.

INTRODUCTION

This Henry H. Storch Award review summarizes the research programme of the author during his professional career in the subject area of coal and carbon science. Marsh is a native of North East England well known for its coal-fields and for the massive transportation of coal into Newcastle upon Tyne for shipment to the open-fires of the City of London. Marsh as a schoolboy grew up within a quarter mile of one of the largest collieries in Co. Durham. The noise and dirt of coal mining became part of his life. On leaving school and entering University he had no intention at all of continuing this association with coal. But the British Association for the Advancement of Science held its annual meeting at the University and organized works visits. Marsh, as an undergraduate, was asked to lead one of these visits, yes to a coal mine, and so he became the "expert" of the graduate year in matters of coal. After graduating, Professor H. L. Riley was asked to undertake a study of dangerous swelling coals so modified by an igneous dyke. Marsh was offered the research contract, he accepted, and so inevitably commenced a career in coal.

IGNEOUS DYKE INTRUSIONS

This study of a Durham coal formed the basis of the PhD Thesis (1948) but was not published until 1971 (1) . The Hutton seam (32.7 wt.% volatile (daf) and 86.3 wt.% C (daf)) had been penetrated by a whinstone dyke, 30 m thick and coals had been modified to about 65 m away from the dyke interface. Simulations by very slow carbonizations gave indications of maximum temperatures of <500 ^{o}C reached by coal during this thermal metamorphosis. The dangerous swelling properties in coke ovens appear to be associated with a mild softening of the coal involving breakage of the hydrogen-bonding with some release of small molecules, followed by cooling with the re-establishment of a higher branch-point density, this maintaining a high coal viscosity and creating swelling dangers.

MICROPOROSITY

Following some years of research into microporosity of carbon, attention was directed to coal materials which were obviously much more difficult to characterize. Microporosity in coals exhibits three aspects of study (a) effective surface area (b) pore shape and size distributions and (c) variations in surface functionality. Coal is not of course a rigid structure. In an initial paper Marsh (2) reviewed the methods of surface chemistry then available, of heats of wetting, neon adsorption and adsorption of nitrogen and carbon dioxide. The use of nitrogen at 77 K is unsatisfactory because of slow activated diffusion effects, isotherms of this gas not describing thermodynamic equilibria. Heats of wetting by methanol had to be adjusted because of different polarities of coal surfaces. The need was to obtain isotherms of molecules such as carbon dioxide at temperatures above 273 K. If adsorbate pressures were < .01 MPa then the maximum p/p^{o} values were only of the order of 0.02 and clearly Langmuir or BET equations could not be applied.

Two events changed the course of this research. First the Russian literature describing the use of the Dubinin-Polanyi (D-P) and later the Dubinin-Radushkevich (D-R) equations was filtering into the laboratories of Western Europe. Second, Dr. Teresa Siemienieswka of Poland came to the NCRL for a period of study financed by the British Council. Together we were able to interpret adsorption isotherms , 0 to 0.02 p/p^o, of carbon dioxide, 273 K and 293 K and compare with isotherms at 195 K (3). It was concluded that this method of adsorption of carbon dioxide gave surface area values agreeing with accepted values for low rank coals but which with increasing rank became progressively greater, rising to 300 m^2g^{-1} for the high rank anthracites. Here the replacement of hydrogen-bonding in the bituminous coking coals by carbon-carbon covalent bonding had reduced the sizes of the microporosity into the range of ultramicroporosity which is accessible to small molecules only at 273 K and above. Marsh and O'Hair (4) took the subject somewhat further by adsorbing nitrous oxide and carbon dioxide on coals and comparable microporous carbons. The D-R plots of log n^a (n^a = amount adsorbed in mmol g^{-1}) against $\log^2 (p/p^o)$ are sensitive to non-equilibriated sections of the isotherm, usually at the low relative pressure end. The point was made of the futility of attempting to accommodate such isotherms mathematically to provide "correct" surface area data. Working now with French colleagues (5), studies were extended to cokes from coals where the gradients of the D-R plots were related to an average pore size.

Even to those working in the subject area, the reasons for the general acceptability of the D-R equation were not always apparent. Using carbonized anthracite as a material from which to obtain isotherm data, Marsh and Siemieniewska (6) attempted to explain the applicability of this equation. The linearity of the D-R equation is the direct result of the frequency distribution of free energies of adsorption obeying, e.g. a Rayleigh or Gaussian form of distribution. It is difficult to know from the Russian literature if this was their starting point in the development of the D-R theory. With the arrival of new students, Freeman, Rand and Campbell (7-12), the interpretations and uses of the D-R approach were explored. In more recent times, the pragmatic use of the D-R equations has been set out (13,14) in a simplified form to explain how gradients of D-R plots, intercepts and deviations from linearity are interpretative devices to characterize and distinguish porosities. Rodriguez and Marsh (15) compared adsorption isotherms of iodine and carbon dioxide. Iodine induces swelling of coals without solubilization. FTIR spectra of iodinated coals indicate changes in hydrogen-bonding within the macromolecular network (16). Thus the adsorption of iodine is indicative of flexibility in the walls of the microporosity in coals. Jackson (17) and Butler (18) in their Theses describe studies of a rank range of coals by the polar NH_3 and SO_2 adsorbates in attempts to characterize surface functionalities in fresh and oxidized coals. Amounts of NH_3 adsorbed by coals are used to calculate contents of carboxylic acid, phenolic, total hydroxyl and carboxyl groups on coal surfaces. Bromine (18) induces swelling of coals and measurements of cross-link densities indicate a minimum in coals of 80-85 wt.% C.

COAL CARBONIZATIONS

Coking principle

During coal pyrolyses the lignites, sub-bituminous and anthracites do not pass through a fluid phase. Resultant chars are pseudo-morphs of parent coal. The caking and coking coals form a plastic/fluid stage on carbonization out of which develop anisotropic components which eventually constitute structure in the resultant cokes (most often metallurgical cokes). The study of the growth of these anisotropic components (later called the mesophase) became a major contribution to coal science. It began with a study in Penn. State University U.S.A. (19) of carbonizations of anthracene and biphenyl under pressure of 300 MPa. Instead of formation of a compact coke, SEM revealed clusters of spheres, the botryoidal structures, now called mesocarbon beads. These were later identified as spheres of mesophase, ie. the discotic, aromatic, nematic liquid crystal systems, by Brooks and Taylor (20). The next stage was to examine the chemistry of formation of other graphitizable carbons, i.e. from Gilsonite pitch and polyvinylchloride (21). At the same time, Evans and Marsh (22) initiated studies of the mass spectrometry of formation of anisotropic carbons from model organic compounds. The role of heteroatoms in cyclic systems and enhancement of graphitizability were published by Marsh et al. (23) followed shortly by the first of a major series of papers describing the role of mesophase during the carbonization of coking coals (24). Earlier workers (25,26) had long recognized the need to explain the coking principle. Whereas in pitch and model compound carbonizations, when the process of dehydrogenative polymerization established mesogen systems, molecular weights > 800 amu, it was the fragmentation of the macromolecular system of coking coals in a fluid matrix which established comparable molecular mesogen systems. Thus the concepts of liquid crystal chemistry were related to coke formation from coals (24).

Optical textures

Inter-relating with this approach to coal chemistry were discussions taking place into the chemistry of the delayed coker, needle coke versus shot coke (27,28), the development of mesophases for carbon fibre manufacture and the explanation of the Dominant Partner Effect (DPE) in terms of hydrogen donor facility. In the late "70s, I. Mochida and A. Grint took up senior positions in the NCRL and together with Marsh made significant contributions to understanding the chemistry controlling size, shape, viscosity and coalescence behaviour of the wide range of liquid crystal systems. Several reviews were prepared (30-37). The findings of the liquid crystal study were published over several years (38). In the final stages of coal or pitch carbonizations, the size, shape and ability to coalesce dictate the resultant optical texture of the cokes. By optical texture is meant the characterization by optical microscopy of the isochromatic units within the overall anisotropic appearance of polished coke samples. The growth of liquid crystals is a function of the size and shape of mesogen molecules in the fluid pitch matrix, the viscosity of both the fluid and liquid crystals and the time/temperature dependance of viscosity of the liquid crystals. Chemical cross-linking continues to develop between molecules in the liquid crystals. Dominantly, the relative reactivities of mesogen molecules are all important. The presence of functionality and heteroatoms enhances reactivity so promoting increases in average molecular weight of pitch constituent molecules at that stage of carbonization processes where the overall viscosity of the fluid matrix is too high to allow effective growth. Thus the growth process is restricted. The molecular reactivity persists within the liquid crystals which rapidly increase in viscosity within themselves. Coalescence is severely restricted and surface fusion results to establish the fine-grained mosaics, < 5 μm, of optical textures often

found in metallurgical cokes. The absence of functionality, (sub-bituminous to bituminous coals) enhances the stability of polycyclic aromatics which now dominate pitch chemistry. Much lower viscosities are attainable, the liquid crystals are more stable and can undergo coalescence resulting in larger sizes of optical texture, about 20 µm, within coke structure.

Blending

Effective up-grading of rank of coal can be achieved by co-carbonization of weakly caking coals with suitable additives, petroleum or coal- based. The Dominant Partner Effect, ie. where small quantities of additives can disproportionally up-grade sizes of optical texture of cokes, essentially is the introduction of hydrogen transfer compounds which stabilize free radical intermediates so promoting stable mesophase to the higher temperatures of lower viscosities.

The chemistry of stabilization of pyrolysis products of coal (to form anisotropic carbon ultimately) is essentially similar to that of coal-derived liquids where early coking in the process is to be avoided (39). Advances made in the understanding of coal carbonization techniques benefited from the simultaneous and related studies of coal liquefaction, delayed coking and mesophase fibre production.

A major thrust in coal carbonization is towards the use of cheaper coals of lower rank than the coking coals. Hence coal blending has been introduced into coke making for many years. The use of pitch as an additive, added directly or as pellets to improve coke quality, is now industrial practice. Coals are a heterogeneous composite of macerals and mineral matter. The wide variation in coal genesis, origin of plant, swamp conditions, tectonic disturbance, etc. have created very specific chemistry within macerals. This complexity requires empirical searches for suitable coal blends which may contain from 10 to 20 coals. The purpose of coal blending is to create a "coal soup" in the fluid phase with just sufficient aromaticity, hydrogen transfer facility, etc. to form an anisotropic coke with minimum size of optical texture, i.e. about 1 µm in size. The interlocking interfaces of these small mosaics of isochromatic units of mesophase create the required toughness in the cokes to resist degradation caused by pressure, attritional forces and chemical attack (40). The additions of pitches are essentially equivalent to adding coking coals to blends, coking coals having excess coking capacity and hence can be considerably diluted without loss of coke properties. Here this available hydrogen donating capacity promotes stability in the system and a larger size of optical texture. Totally isotropic cokes, without anisotropic constituent units derived from mesophase, tend to be glass-like and fracture similarly.

Oxidation

Oxidation of coals involves removal of hydrogen and chemisorption of oxygen. On initial heating the surface oxygen complexes can interact to establish a cross-linkage. This enhances branch-point density in the macromolecular structure of coal and the reduced ability for radical capping by mobile hydrogen transforms a coking coal into a non-coking coal.

The co-carbonization of oxidised coals with pitches and decacyclene, one of the strongest of hydrogen transfer model compounds, restores, to some extent, the coking properties of an oxidized coking coal. Fluidity is restored, reduction of oxygen groupings probably occurs and stability is re-introduced to the radical systems from the hydrogen donating additive (41). However although coal-tar pitches are all good blending agents, not all petroleum pitches are as effective (42). Structural components, fractionations and elemental analyses cannot predict hydrogen donating facility in pitches. So it is necessary to carry out tests involving, e.g. co-carbonizations with anthracene or phenanthrene and using ^{1}H NMR to monitor hydrogenated derivatives.

STRUCTURE, GASIFICATION, COMBUSTION.

Working with Stadler, Marsh (43) reviewed critically the methodolgy of structural analyses of coal carbonizations, with special reference to interpretations based on the X-ray a- and c- dimensions of the hypothetical "crystallite ". Later with Crawford (44) the powerful technique of phase contrast fringe imaging by TEM provided a more satisfactory explanation, in terms of lattice distortion, of the increase and decrease in c-dimensions of crystallites of X-ray diffraction data, with increasing carbonization temperature.

Marsh maintained a simultaneous interest into mechanisms of coke gasification, in 1978 reviewing the carbon-oxygen reaction (45), and in 1979 reviewing how reactivities of cokes may be enhanced by co-carbonizating coals with alkali salts (46). The development of structure in cokes and coals and effects on resultant coke properties were set out by Marsh and Clarke in 1986 (47). Aspects of gasification kinetics and hydrogasification are more recent studies (48,49) . During this period collaborative studies with Japanese laboratories examined coal carbonizations by ^{1}H NMR and esr techniques looking at the macromolecular structure of coals and the effects of iodine uptake (50). Most recently, interests have moved towards maceral analysis of coals, with rank, on combustion behaviour of pulverized coals in power stations. Crelling is a most supportive collaborator (51,52) . Correlations are being sort between detailed petrographic analyses of coals and reactivity of coal chars (53). A brief excursion was made into coal genesis because of the enthusiasm of Butler and Goodarzi (54) and we are having another look into solvent swelling of coals to relate to physical adsorption behaviour and peculiarities in carbonizations (55).

COAL IN A MODERN WORLD

Without doubt, coal as a combustible material will remain the principal source of industrial and domestic energy. But this energy conversion process is not without problems. Globally, the greenhouse effect is a catastrophic potential problem; acid rain, although a major problem can be resolved. Major thrusts for coal utilization in a modern world are towards more efficient and pollution free combustion. Other routes, e.g. combined cycle using say pressurized fluidized bed gasification, will utilize coals as feedstocks. The carbonization and gasification behaviour of coals and cokes therefore needs precise study. Although the future of metallurgical coke appears limited, the blast furnace will remain for the immediate future with coal providing energy and a reducing atmosphere by tuyere injection. Coal liquefaction and conversion should remain in research schools not only as an insurance for the chemical industry and for liquid fuels but also for the knowledge it provides of coal material.

ACKNOWLEDGEMENTS

The support of a great many students, post-doc. collaborators and colleagues, internationally, is immensely appreciated together with Exxon Research and Engineering Company and the A.C.S. who made this presentation possible in such a gracious way.

REFERENCES

1. Marsh H., The effect of an igneous intrusion upon the properties of a Durham coal, Fuel 1971 50 280.
2. Marsh H., The determination of surface areas of coals - some physicochemical considerations, Fuel 1965 44 253
3. Marsh H. and Siemieniewska T., The surface areas of coals as evaluated from the adsorption isotherms of carbon dioxide using the Dubinin-Polanyi equation, Fuel 1965 44 355.
4. Marsh H. and O'Hair T.E., The adsorption of nitrous oxide on coals and carbons - considerations of surface areas and microporosity, Fuel 1966 45 301.
5. Chiche P., Marsh H. and Pregermain S., Adsorption of carbon dioxide, methanol and water vapour on cokes - determination of micropore volume. Fuel 1967 46 341-350.
6. Marsh H. and Siemieniewska T., Adsorption of carbon dioxide on carbonized anthracites: Interpretation by Dubinin theory, Fuel 1967 46 441.
7. Siemieniewska T., Freeman E.M. and Marsh H., The development and closure of microporosity, Proc 7th Coal Science Conf., Prague, 1968, pp.1-15.
8. Freeman E.M., Siemieniewska T., Marsh H., and Rand B., A critique and experimental observations of the applicability to microporosity of the Dubinin equation of adsorption, Carbon 1970 8 7.
9. Marsh H. and Rand B., The characterisation of microporous carbons by means of the D-R equation. J. Colloid and Interface Science, 1970 33 101.
10. Marsh H. and Rand B., Changes in slope of the D-R adsorption isotherms of coals, Fuel 1971 50 328.
11. Marsh and Rand B., Microporosity in carbonaceous materials, Proc. 3rd Conf. on Ind. Carbons and Graphites, London (1970), S.C.I., 1971, pp. 172-183.
12. Marsh H. and Campbell H.G., The characterization of microporous carbons by adsorption from liquid and vapour phases, Carbon 1971 9 489.
13. Marsh H., Adsorption methods to study microporosity in coals and carbons - a critique, Carbon 1987 25 49.
14. Marsh H. and Butler J., Microporosity in carbonaceous materials; Studies in Surface Science and Catalysis: Characterization of Porous Solids; Vol. 39., Eds. K.K. Unger, J. Rouquerol, K.S.W. Sing and H. Kral, Elsevier, Amsterdam (1988), pp. 139-150.
15. Rodriguez N.M. and Marsh H., Structure of coals studied by iodine and water adsorption, Fuel 1987 66 1727.
16. Byrne J.F. and Marsh H., Unpublished results (1988)
17. Jackson P., PhD Thesis, University of Newcastle upon Tyne, 1985, Porosity and Surfaces of Coals.
18. Butler J., PhD Thesis, University of Newcastle upon Tyne, 1987, Coal Structure.
19. Marsh H., Dachille F., Melvin J. and Walker P.L. Jr., The carbonization of anthracene and biphenyl under pressures of 300 MNm^{-2}, Carbon 1971 9 159.
20. Brooks J.D. and Taylor G.H., The formation of some graphitizing carbons, Chemistry and Physics Of Carbon, Ed. P.L. Walker Jr., Marcel Dekker, N.Y., 1968 4 243.

21. Marsh H., Akitt J.W., Hurley J.M., Melvin J. and Warburton A.P., Formation of graphitizable carbons from Gibsonite pitch and polyvinylchloride - A mass spectrometry and NMR study, J. Applied Chemistry 1971 21 251.
22. Evans S. and Marsh H., The chemistry of formation of semi-cokes from aromatic systems using mass spectroscopy, Part 1, Carbon 1971 9 733 and Part 2, Carbon 1971 9 747.
23. Marsh H., Foster J.M. and Hermon G., The enhanced graphitization of fluorene and carbazole, Carbon 1973 11 424.
24. Marsh H., Carbonization and liquid crystal development, Part 1, The significance of the mesophase during carbonization of coking coals, Fuel 1973 52 205.
25. Blayden H.E., Gibson J. and Riley H.L., Proc Conf. Ultrafine Structure of Coals and Cokes, BCURA, London, 1944 176.
26. Kipley J.J. and Shooter P.V., Factors affecting the graphitization of carbon : Evidence from polarized light microscopy. Carbon 1966 4 1.
27. Markovic V., Ragan S. and Marsh H., Structural components in needle-cokes, J. Mat. Sci., 1984 19 3287- 3301.
28. Marsh H., Calvert C. and Bacha J., Structures and formation of shot coke - a microscopy study. J. Mat. Sci., 1985 20 289.
29. Mochida I., Takeshita K. and Marsh H., Mechanistic considerations of the Dominant Partner Effect, 14th Biennial Conf. on Carbon, Univ. Park Pa, A. Carb Soc., 1979 401.
30. Marsh H. and Cornford C., Mesophase: The precursor to graphitizable carbon, Petroleum Derived Carbons, A.C.S. Symposium Series No. 21, A.C.S. Washington D.C., 1976, pp. 266-281.
31. Marsh H., A review of the growth and coalescence of mesophase (nematic liquid crystals) to form anisotropic carbon, and its relevance to coking and graphitization, Proc. 4th Conf. Ind. Carbon and Graphites, S.C.I. London, 1976, pp. 1-38.
32. Marsh H. and Smith J., The formation and properties of anisotropic cokes from coals and coal derivatives studied by optical and scanning electron microscopy, Analytical Methods for Coal and Coal Products, Ed. Clarence Karr Jr., Vol 2, Academic Press, N.Y., 1978, pp. 371-414.
33. Marsh H. and Walker P.L. Jr., The formation of graphitizable carbons via mesophase; Chemical and kinetic considerations, Chemistry and Physics of Carbon, Eds. P.L. Walker Jr. and P.A. Thrower, Marcel Dekker, N.Y., 1979 15 pp. 229-286.
34. Marsh H., Coal structure; formation, properties and relevance of microstructure in resultant cokes, Coke Oven Techniques, Commission of European Communities Symposium, Sept. 1981, Luxembourg, pp. 50-67.
35. Forrest M. and Marsh H., Theroretical and experimental approaches to the carbonization of coals and coal blends, Coal and Coal products, Analytical Characterization Techniques, Ed. E.L. Fuller Jr., A.C.S. Symposium Series, No. 205, A.C.S Washington D.C., 1982, pp. 1-26.
36. Marsh H. and Latham C.S., The chemistry of mesophase formation, Petroleum Derived Carbons, A.C.S. Symposium Series, No. 303, A.C.S. Washington D.C. 1986, pp. 1-28.
37. Marsh H. and Menendez R., Carbons from pyrolysis of coals, pitches and their blends, Fuel Processing Technology (To be published).

38. Marsh and co workers : Carbonization and liquid crystal (mesophase) development, Fuel 1973 52 205 ; 1973 52 234; 1973 52 243; 1973 52 253; 1974 53 168; 1975 54 105; 1979 58 482; 1979 58 626; 1979 58 633; 1979 58 642; 1979 58 651; 1979 58 691; 1979 58 790; 1979 58 797; 1979 58 803; 1979 58 809; 1980 59 339; 1980 59 343; 1980 59 349; 1980 59 362; 1980 59 511; 1980 59 514; 1980 59 517; 1980 59 520; 1981 60 418; 1981 60 429; 1981 60 434; 1981 60 507; 1981 60 513; 1981 60 519; 1981 60 522; 1981 60 607;1981 60 1115; 1983 62 612; 1983 62 1084; 1983 62 1355; 1984 63 875; 1984 63 1588; 1984 63 1594; 1987 66 1544.
39. Marsh H. and Neavel R.C., Carbonization and liquid crystal development; A common stage in mechanisms of coal liquefaction and of carbonization of coal blends for coke making, Fuel 1980 59 511.
40. Ragan S. and Marsh H., Microstrength and optical textures of cokes from coal-pitch carbonizations, Fuel 1981 60 522.
41. Qian Z. and Marsh H., The co-carbonization of oxidised coals with pitches and decacyclene, Fuel 1984 63 1588.
42. Grint A., Marsh H. and Clarke K., Co-carbonization of oxidised coal with petroleum pitches, Fuel 1983 62 1355.
43. Marsh H. and Stadler H.P., A review of structural studies of the carbonization of coals, Fuel 1967 46 351.
44. Marsh H. and Crawford D., Structure in graphitizable carbons from coal-tar pitch using high resolution electron microscopy, Carbon 1984 22 413.
45. Marsh H., How oxygen molecules gasify carbons. Special publication, Chemical Society, London, No. 32, 1978 133-174.
46. Marsh H. and Walker P.L. Jr., The effects of impregnation of coal by alkali salts upon carbonization properties, Fuel Processing Technology, 1979 2 61.
47. Marsh H. and Clarke D.E., Erdol und Kohle, Mechanisms of formation of structure within metallurgical coke and effects on coke properties 1986 39 113-122.
48. Osafune K. and Marsh H., Gasification kinetics of coal chars in carbon dioxide, Fuel 1988 67 384.
49. Green P.D., Edwards I.A.S., Marsh H., Thomas K.M. and Watson R.F., Coal thermoplasticity and coke structure as related to gasification, Fuel 1980 67 384.
50. Fuel 1981 60 598, 603 and 607; 1987 66 866 and 1743.
51. Skorupska N.M. PhD Thesis, University of Newcastle upon Tyne, 1987 , Coal combustibility.
52. Crelling J.C., Skorupska N.M. and Marsh H., Reactivity of coal macerals and lithotypes, Fuel 1988 67 781.
53. Bend S. and Marsh H., Unpublished results (1988).
54. Butler J., Marsh H. and Goodarzi F., World coals: Genesis of the world's major coal-fields in relation to plate tectonics, Fuel 1988 67 269.
55. Hall P.J., Marsh H. and Thomas K.M., Solvent induced swelling of coals to study macromolecular structure, Fuel 1988 67 863.